

**Synthesis and applications of some upper and lower rim
functionalized calix[4]arenes and calix[4]naphthalene
derivatives**

by

© Gopikishore Valluru

A thesis submitted to the School of Graduate Studies
in partial fulfillment of the requirements for the degree of
Doctor of Philosophy

Department of Chemistry
Memorial University of Newfoundland

August 2015

St. John's

Newfoundland and Labrador

Dedication

To my Mother and Father

To my wife Swathi Valluru

To my friend Kranthi Danda

To my Sisters and Parents-in-law

And to all my family members and friends

Abstract

The work described in this thesis is concerned mainly with the synthesis and characterization of bimodal calix[4]arene and calix[4]naphthalene derivatives. Their complexation properties with some Group 1, Group 2 and transition metal cation guests were studied.

Chapter 1 provides an overview of supramolecular chemistry, calixarenes and calixnaphthalenes and the methods employed herein.

In Chapter 2, the synthesis of some selected upper- and lower-rim functionalized calix[4]arene derivatives and their complexation studies are described. The lower rim of the calix[4]arene derivatives are modified with *O*-methyl, *O*-ethyl esters and crown ether moieties which selectively bind to Group 1 and 2 metal ions. Current studies on the development of a microcantilever (MCL)-based real-time device employing modified calix[4]arene-derived sensing layers are on-going in collaborative work with Dr. L.Y. Beaulieu's group in the Department of Physics and Physical Oceanography at Memorial University.

In order to test the selectivity for different metal ions with the sensing layers needed for the different MCLs envisioned in the MCL instrument; the work described in Chapter 3 concerns the synthesis and applications of new triazole-bridged anthracene/pyrene-appended calix[4]arene derivatives. The synthetic strategy involved a "click" reaction as the key step. In the study reported herein, their complexation properties with various

metal ions were investigated by fluorescence, UV-vis and $^1\text{H-NMR}$ spectroscopic analyses.

Chapter 4, describes the synthesis and applications towards selective metal ion recognition by a calix[4]arene-NHC (*N*-heterocyclic carbene) derivative. The lower rim of the calix[4]arene was functionalized with two different groups, one of which consists of a 1,3 bridged “crown-5” and the other 1,3 positions with imidazole groups. The resulting NHC enables the calix[4]arene to potentially form a stable self-assembled monolayer (SAM) on the Au surface of a microcantilever.

In Chapter 5, the synthesis of some sulfonated calix[4]naphthalene derivatives and their complexation studies are described. In another collaborative project with Prof. A. Coleman’s group at the University of Lyon, these naphthalene derivatives were shown to be capable of capping and stabilizing silver nanoparticles. Along with these properties, cyclotetrachromotropyene (“CTCT”) was characterized and shown to be capable of selectively dispersing SWNTs into water. The resulting supramolecular complexes in a collaborative project with Y. Zhao’s group at Memorial University and A. Adronov’s group at McMaster University were characterized by Atomic Force Microscopy (AFM), Raman spectroscopy and UV-Vis-NIR analysis.

Acknowledgments

I would like to extend my sincere admiration and immeasurable thanks to my supervisor, Prof. Paris E. Georghiou, for his guidance, valuable advice and encouragement during the course of my research and the writing of this thesis. I am truly grateful to you from the bottom of my heart.

I am also grateful to Dr. Shofiur Rahman for his advice, helpful discussions and guidance. My appreciation is also extended to my supervisory committee, Prof. Graham Bodwell, and Prof. Francesca Kerton, for their encouragement, proofreading, and valuable suggestions during my research work. My sincere thanks to all our collaborators, Prof. Luc Beaulieu's group in the Department of Physics and Physical Oceanography at Memorial University, Prof. Bodwell's group and Prof. Zhao's group in the Department of Chemistry at Memorial University. I am also grateful to Prof. A. Coleman's group at the University of Lyon and Prof. A. Adronov's group at McMaster University.

I would like to thank Prof. Sunil Pansare and all other professors in the Chemistry Department. I am also grateful to Dr. Louise Dawe for X-ray crystal structure determinations and Tim Strange for training and support with fluorescence spectroscopy. My appreciation is also extended to Linda Winsor, for training and support with mass spectroscopy and Dr. Celine Schneider for training and support with NMR spectroscopy. Ms. Julie Collins and Dr. Brent Myron are also thanked for training and support with C-CART. Also thanks to people who work in the physical sciences stores.

Thanks are also due to the members of the Georghiou group, both past and present, other group members and the staff in the Chemistry Department for their support, and friendship. It has been a great joy to me to work together with you all.

Special thanks are also extended to my mother, my father, my wife, my sisters, my brothers, my In-laws and my friends (Kranthi, Nagesh, Rakesh, Ramana, Ranjith, Kiran and others). The financial support from RDC, VALE Company, school of graduate studies, and department of Chemistry at Memorial University of Newfoundland is gratefully acknowledged.

Table of Contents

Title.....	i
Dedication	ii
Abstract.....	iii
Acknowledgments	v
Table of Contents	vii
List of Figures.....	xv
List of Schemes	xviii
List of Tables	xxx
List of Abbreviations	xxxii
Appendix.....	xxxv

Chapter 1	1
1.1 Supramolecular chemistry.....	1
1.2 Non-covalent interactions.....	4
1.2.1 Hydrogen bonding.....	4
1.2.2 π -interactions	6
1.2.3 Electrostatic interactions	9
1.2.4 van der Waals interactions.....	11
1.2.5 Hydrophobic effect	12
1.3 Host-Guest Complexation studies	12
1.3.1 Nuclear magnetic resonance (NMR) spectroscopy	13
1.3.2 UV-visible spectroscopy	13
1.3.3 Fluorescence spectroscopy	14
1.3.4 Mass spectrometry	16
1.3.5 Single-crystal X-ray diffraction	17
1.3.6 Scanning probe microscopy (SPM)	17
1.4 Calixarenes	18
1.4.1 Nomenclature of calixarenes	19
1.4.2 Conformational properties of calixarenes	21

1.4.3 Examples of <i>lower</i> and <i>upper</i> rim-modified calixarenes.....	25
1.4.3.1 <i>Lower</i> rim functionalized calixarenes.....	25
1.4.3.2 <i>Upper</i> rim functionalized calixarenes.....	29
1.5 Calix[4]naphthalenes	33
1.5.1 Homocalixarenes	37
1.5.2 Homooxacalixnaphthalenes	38
1.6 Outline of the thesis	39
1.7 References.....	42
Chapter 2	50
2.1 Introduction	50
2.2 Self-assembled monolayers of thiols on gold surfaces.....	51
2.2.1 Cation sensors	53
2.2.2 Anion sensors	55
2.2.3 Biomolecule sensors.....	58
2.2.4 Other sensors	61
2.3 Gold-coated microcantilever sensors.....	63
2.4 Determination of the association constant (K_{assoc}) values	67
2.5 Objectives of the work reported in this Chapter.....	69
2.6 Results and discussions.....	70

2.6.1 Attempts at the synthesis of thioacetate-bearing calix[4]arenes 73 and 74	70
2.6.2 Synthesis of thioacetate-bearing calix[4]arenes 70 and 71	73
2.6.3 X-ray crystallography of 70	76
2.6.4 Study of a SAMs of 70 on a Au-coated microcantilever	77
2.6.4.1 Detection of cations and their selectivity	79
2.6.4.2 Effect of anions	80
2.6.5 Solution-phase complexation studies of 70 and 71	82
2.6.6 Possible mechanism for thioacetate binding to gold surfaces	84
2.7 Synthesis of a <i>cone</i> -conformer bimodal calix[4]arene-crown-5 derivative 72	85
2.7.1 X-ray crystallography of 72	89
2.7.2 Study of a SAMs of 72 on a Au-coated microcantilever	89
2.7.3 Solution-phase complexation studies of 72	92
2.7.3.1 ¹ H-NMR titration experiments of 72 with NaI.....	93
2.7.3.2 ¹ H-NMR titration experiments of 72 with KI.....	98
2.7.3.3 ¹ H-NMR titration experiments of 72 with RbI.....	102
2.8 Computational studies	106
2.9 Synthesis of calix[4]arene-crown-5 derivative 90	110
2.10 Conclusions.....	111
2.11 Experimental section.....	112

2.11.1 Experimental	112
2.12 References	124
Chapter 3	131
3.1 Introduction	131
3.1.1 Metal ion receptors.....	132
3.1.2 Triazole bridge-based calixarene chemosensors	134
3.2 Objectives of the research work conducted by the author and reported in this Chapter.....	140
3.3 Results and discussion.....	141
3.3.1 Synthesis of a new bimodal anthracene-appended triazole-based calix[4]arene derivative 98	143
3.3.2 Characterization of bimodal calix[4]arene 98	145
3.4 Complexation studies	146
3.4.1 Complexation studies using fluorescence spectroscopy	147
3.4.1.1 Calculation of association constants.....	147
3.4.1.2 Fluorescence complexation studies of 98 with various metal ions	148
3.4.1.3 Job plot analysis for 98 with Hg ²⁺ and Fe ³⁺ ions.....	153
3.4.1.4 Comparison of the association constants of receptor 98 with metal ions.....	154
3.4.2 Metal competitive experiments	156

3.4.3	Complexation studies of 98 using $^1\text{H-NMR}$ spectroscopy.....	158
3.4.4	Computational studies.....	159
3.5	Synthesis and complexation properties of triazole-based pyrene-appended calix[4]arene 99	161
3.5.1	Synthesis of triazole-based pyrene-appended calix[4]arene 99	162
3.5.2	Characterization of bimodal calix[4]arene 99	164
3.6	Complexation studies with 99	165
3.6.1	Complexation studies using fluorescence spectroscopy	165
3.6.1.1	Comparison of the association constants of receptor 99 with metal ions.....	174
3.6.2	Complexation studies of 99 using $^1\text{H-NMR}$ spectroscopy.....	176
3.7	Conclusions	179
3.8	Experimental section	181
3.8.1	Experimental.....	181
3.9	References.....	187
Chapter 4	193
4.1	Introduction	193
4.2	<i>N</i> -Heterocyclic Carbenes (NHCs)	194
4.2.1	<i>N</i> -Heterocyclic Carbenes (NHCs) on gold surfaces.....	196
4.3	Objectives of the work reported in this Chapter.....	200

4.4 Results and discussion	201
4.4.1 Synthesis and applications towards a new bimodal calix[4]arene-NHC derivative 113	202
4.4.1.1 Attempted generation of dicarbene from calix[4]arene 117	205
4.4.2 Preparation of Gold Nanoparticles (AuNPs).....	207
4.5 Conclusions	209
4.6 Experimental section.....	209
4.6.1 Experimental.....	210
4.7 References.....	213
Chapter 5	218
5.1 Introduction	218
5.2 Silver nanoparticles and their applications.....	221
5.3 Single-walled carbon nanotubes (SWNTs).....	224
5.3.1 Covalent functionalization of SWNTs	227
5.3.2 Noncovalent functionalization of SWNTs.....	231
5.4 Objectives of the work reported in this Chapter	234
5.5 Results and discussion.....	235
5.5.1 Synthesis of sulfonated calix[4]naphthalene derivatives 124 , 125 and 137	236
5.5.1.1 Characterization of cyclotetrachromotropyrene (–CTCT” or 125).....	239

5.5.2 Complexation studies of calix[4]naphthalenes 124 , 125 and 137	240
5.5.2.1 Molecular recognition studies.....	242
5.5.2.1.1 With nucleobases	242
5.5.2.1.2 With amino acids	245
5.5.3 Dispersion of SWNTs into aqueous solutions using –CTCT” or 125	250
5.5.4 Complexation studies of –CTCT” or 125 with C ₆₀	256
5.6 Conclusions	258
5.7 Experimental section.....	259
5.7.1 Experimental.....	260
5.8 References.....	263
Chapter 6	271
6.1 Summary and conclusions.....	271

List of Figures

Figure 1.01 Examples of supramolecular complexes 1 , 2 and 3	3
Figure 1.02 Different types of hydrogen bonding geometries	5
Figure 1.03 Hydrogen bond interactions between guanine and cytosine base pairs in DNA.	6
Figure 1.04 <i>Left</i> : Schematic representation of a cation- π interaction of K^+ ion and benzene. <i>Right</i> : Schematic representation of the quadrupole moment of benzene.	7
Figure 1.05 Neutral organic π acceptors	8
Figure 1.06 (a) Two types of π - π stacking interactions: face-to-face and edge-to-face. (b) The repulsion between negatively charged π - electron clouds of aromatic rings.....	9
Figure 1.07 An example of organic cation 7a with various anions showing ion-ion interactions.....	10
Figure 1.08 Ion-dipole interactions of Na^+ in a crown ether complex.....	10
Figure 1.09 Dipole-dipole interactions between two carbonyl groups	11
Figure 1.10 The crystal structure of a typical van der Waals inclusion complex <i>p-tert-butylcalix[4]arene-toluene</i>	12
Figure 1.11 Molecular orbital energy diagrams of the relative energy dispositions of the frontier orbitals of fluorophore and receptor in (a) the analyte-free state, and (b) the analyte-bound state.	15
Figure 1.12 (a) Macrocycle 8 (b) X-ray structure of complex 8:KCl	17
Figure 1.13 <i>Cone</i> conformer of 9 (left) and a calix krater (right).....	20
Figure 1.14 Rims defined in calixarenes, shown here for calix[4]arene.....	20

Figure 1.15 Nomenclature system used for calixarenes	21
Figure 1.16 Four possible conformers of calix[4]arene	22
Figure 1.17 ¹ H- and ¹³ C-NMR spectral patterns of the methylene groups in the calix[4]arene conformers.	23
Figure 1.18 Triazole-linked quinoline appended calix[4]arene 14	26
Figure 1.19 Biscalix[4]arene derivative 21	29
Figure 1.20 Bew and co-workers' hybrid calix[4]arenes	30
Figure 1.21 Hof and co-workers' trisulfonated calix[4]arene derivatives.	31
Figure 1.22 Guanidinocalix[4]arene derivatives 33-36	32
Figure 1.23 General-acid/base catalytic mechanism of HPNP transesterification in <i>N</i> -(4-methoxyphenyl) guanidine.....	32
Figure 1.24 Regioisomeric calix[4]naphthalene derivatives 37-39	33
Figure 1.25 Some examples of homocalix[4]arene and calix[4]naphthalenes.	38
Figure 1.26 Homooxacalix[4]naphthalene 58	39
Figure 2.01 Representation of a self-assembled monolayer (SAM) structure.	52
Figure 2.02 (A) A sensor chip configuration. (B) SPR angle shifts with respect to various concentrations of several metal ions. Solid line is the linear fit ($r^2 = 0.9928$)	54
Figure 2.03 Calix[4]crown-6 derivatives 59 and 60	55
Figure 2.04 Calix[6]crown-4 derivative 61	57
Figure 2.05 A) Scheme of a receptor adsorbed at a gold electrode binding anions cooperatively. B) Scheme of the preorganization of receptor at a gold electrode	58

Figure 2.06 A schematic representation of the amino acid-induced aggregation of <i>p</i> -sulfonatocalix[4]arene thiol 62 -capped gold nanoparticles	60
Figure 2.07 Self-assembled monolayer of a calix[6]arene 67 on gold surface with an aniline guest	61
Figure 2.08 Gold-supported calix[8]arene 68	63
Figure 2.09 Schematic representation of cantilever changes before and after the interaction between probe and target molecules shown in a) and b). The bending occurs due to the surface stress	64
Figure 2.10 (A) Molecular structure of modified calix[4]arene 69 co-absorbed with decane-1-thiol on the gold surface of a microcantilever via the SAM technique. (B) Bending deflection response of the SAM-coated microcantilever as a function of the change in the concentration of Cs ⁺ and K ⁺ ions.....	66
Figure 2.11 PLUTO stereoview of the single-crystal X-ray structure (hydrogen atoms and minor disorder components omitted for clarity) showing calixarene 70 in a <i>pinched cone</i> -conformation.	76
Figure 2.12 STM images of SAM of the bimodal calix[4]arene 70 on a gold surface.....	77
Figure 2.13 Response to different concentrations of CaCl ₂ (in water) for microcantilevers functionalized with the bimodal calix[4]arene 70	78
Figure 2.14 a) Microcantilever sensor response to aqueous solutions of CaCl ₂ , MgCl ₂ and SrCl ₂ . b) The microcantilever deflection is plotted as a function of the different cations.....	79

Figure 2.15 (a) Microcantilever sensor response to 10^{-6} M aqueous solutions of CaCl_2 , CaBr_2 , CaI_2 and $\text{Ca}(\text{NO}_3)_2$. (b) The response of the functionalized microcantilevers to the variation in the counterion	81
Figure 2.16 Sulfidization of Au(111) from thioacetic acid.....	84
Figure 2.17 Scheme for two possible mechanisms (a and b) proposed to explain the <i>S</i> adlayer formation	85
Figure 2.18 Possible mechanism to explain how the thioacetate binds to gold surfaces..	85
Figure 2.19 2D NOESY spectrum for calix[4]arene 72	88
Figure 2.20 A single molecule of 72 , represented as capped sticks, showing the <i>cone</i> conformation. H-atoms and minor disorder components were omitted for clarity.....	89
Figure 2.21 STM images of calix[4]arene–crown-5” compound 72 which forms a self-assembled monolayer on the gold surface.....	90
Figure 2.22 a) Response to the different metal ions of a microcantilever sensor functionalized with calixarene–crown-5” compound 72 . b) Microcantilever deflection plotted as a function of different metal ions... ..	91
Figure 2.23a $^1\text{H-NMR}$ (300 MHz) titration spectra for SCOCH_3 of 72 (1.5×10^{-3} M) with NaI (2.0×10^{-2} M) solution.....	94
Figure 2.23b $^1\text{H-NMR}$ (300 MHz) titration spectra for Ar- <i>H</i> of 72 (1.5×10^{-3} M) with NaI (2.0×10^{-2} M) solution.....	95
Figure 2.23c $^1\text{H-NMR}$ (300 MHz) titration spectra for Ar- CH_2 of 72 (1.5×10^{-3} M) with NaI (2.0×10^{-2} M) solution.....	95

Figure 2.23d ^1H NMR (300 MHz) titration spectra for <i>t</i> -butyl of 72 (1.5×10^{-3} M) with NaI (2.0×10^{-2} M) solution.....	96
Figure 2.24 Binding constant (K_{assoc}) were determined by ^1H -NMR titration experiments using the <i>OriginPro 6.0</i> ” program.....	96
Figure 2.25 The output from the calculation from the 1:1 ^1H -NMR global analysis binding isotherm.....	98
Figure 2.26a ^1H NMR (300 MHz) titration spectra for Ar- <i>H</i> of 72 (1.5×10^{-3} M) with KI (2.0×10^{-2} M) solution.....	100
Figure 2.26b ^1H NMR (300 MHz) titration spectra for Ar- <i>CH</i> ₂ of 72 (1.5×10^{-3} M) with KI (2.0×10^{-2} M) solution.....	100
Figure 2.26c ^1H NMR (300 MHz) titration spectra for - <i>SCOCH</i> ₃ of 72 (1.5×10^{-3} M) with KI (2.0×10^{-2} M) solution.....	101
Figure 2.26d ^1H NMR (300 MHz) titration spectra for <i>t</i> -butyl of 72 (1.5×10^{-3} M) with KI (2.0×10^{-2} M) solution.....	101
Figure 2.27a ^1H NMR (300 MHz) titration spectra for Ar- <i>H</i> of 72 (1.5×10^{-3} M) with RbI (2.0×10^{-2} M) solution.....	103
Figure 2.27b ^1H NMR (300 MHz) titration spectra for Ar- <i>CH</i> ₂ of 72 (1.5×10^{-3} M) with RbI (2×10^{-2} M) solution.....	103
Figure 2.27c ^1H NMR (300 MHz) titration spectra for - <i>SCOCH</i> ₃ of 72 (1.5×10^{-3} M) with RbI (2.0×10^{-2} M) solution.....	104

Figure 2.27d ^1H NMR (300 MHz) titration spectra for <i>t</i> -butyl of 72 (1.5×10^{-3} M) with RbI (2.0×10^{-2} M) solution.....	104
Figure 2.28 ^1H -NMR (300 MHz) titration curves for Ar- <i>H</i> , Ar- <i>CH</i> ₂ , <i>SCOCH</i> ₃ and <i>t</i> -butyl, respectively of 72 (1.5×10^{-3} M) with RbI (2.0×10^{-2} M) solution.....	105
Figure 2.29 The output from the calculation from the 1:1 ^1H -NMR global analysis binding isotherm.....	105
Figure 2.30 Geometry-optimized structures of: <i>Left</i> : Free calix-crown 72 and <i>Right</i> : 72:Cs ⁺ complex. Colour code: Cs ⁺ = purple, sulphur = yellow, hydrogen = white, carbon = dark grey, and oxygen atom = red.....	107
Figure 2.31 Geometry-optimized structures of: <i>Left</i> : 72:Rb ⁺ complex and <i>Right</i> : 72:K ⁺ complex. Colour code: Rb ⁺ = magenta, K ⁺ = blue, sulphur = yellow, hydrogen = white, carbon = dark grey, and oxygen atom = red.....	108
Figure 2.32 Geometry-optimized structures of: <i>Left</i> : 72:Na ⁺ complex and <i>Right</i> : 72:Li ⁺ complex. Colour code: Na ⁺ = orange, Li ⁺ = green, sulphur = yellow, hydrogen = white, carbon = dark grey, and oxygen atom = red.....	108
Figure 2.33 Structure of 72 with oxygen atoms labelled.....	110
Figure 3.01 Triazole-modified calix[4]crown-5 as a novel fluorescent on-off switchable sensor	135
Figure 3.02 Pyrene-linked triazole-modified hexahomotrioxacalix[3]arenes 92 and 93	137
Figure 3.03 Structure of pyrenyl-appended calix[2]triazole[2]arene 97	140
Figure 3.04 Structure of anthracene-appended triazole based calix[4]arene 98	142

Figure 3.05a Fluorescence spectra of 98 upon addition of Hg^{2+} (0.18-6.8 eq) in acetonitrile/chloroform (v/v= 9:1) solutions. $\lambda_{exc} = 350$ nm.....	149
Figure 3.05b Benesi-Hildebrand plots of $1/(F_o-F)$ versus $1/[\text{Hg}(\text{ClO}_4)_2]$ for 98 upon titration with Hg^{2+} . The linear fits showed 1:1 complexation between 98 and Hg^{2+} . The association constants were calculated for the changes at the 393 nm, 414 nm and 438 nm wavelengths.....	150
Figure 3.06 Screen-capture output showing 1:1 binding model for 98 with Hg^{2+} , using Thordarson's method.....	151
Figure 3.07a Fluorescence spectra of 98 upon addition of Fe^{3+} (0.20-11 eq) in acetonitrile/chloroform (v/v= 9:1) solutions. $\lambda_{exc} = 350$ nm.....	152
Figure 3.07b Benesi-Hildebrand plots of $1/(F_o-F)$ versus $1/[\text{Fe}(\text{ClO}_4)_3]$ for 98 upon titration with Fe^{3+} ion. The linear fits showed 1:1 complexation between 98 and Fe^{3+} . The association constants were calculated for the changes at the 393 nm, 414 nm and 438 nm wavelengths.....	152
Figure 3.08 Screen-capture output showing 1:1 binding model for 98 with Fe^{3+} , using Thordarson's method.....	153
Figure 3.09 Job plot curves showing 1:1 complexation for 98 with $\text{Hg}(\text{ClO}_4)_2$	153
Figure 3.10 Job plot curves showing 1:1 complexation for 98 with $\text{Fe}(\text{ClO}_4)_3$	154
Figure 3.11 Histogram showing the association constants (K_{assoc}) values calculated by using two different methods for the fluorescence titrations of 98 with different metal ions.....	154
Figure 3.12 Metal competitive studies for receptor 98 with different metal ions.....	156

Figure 3.13 Metal competitive studies for receptor 98 with Co^{2+} and Ag^+ metal ions...	157
Figure 3.14 Metal competitive studies for receptor 98 with Cd^{2+} and Zn^{2+}	157
Figure 3.15 Partial $^1\text{H-NMR}$ (300 MHz) spectra of 98 with $\text{Hg}(\text{ClO}_4)_2$ in a $\text{CD}_3\text{CN}:\text{CD}_2\text{Cl}_2$ (4:1, v/v) at 298K; *, \blacklozenge , \circ , \triangle , and \blacklozenge denoted the anthracene- <i>H</i> , triazole- <i>H</i> , triazole- CH_2 -anthracene, and Ar- <i>H</i> protons respectively.....	159
Figure 3.16 <i>Left</i> : the geometry-optimized (ball-and-stick) structure of free receptor 98 ; <i>right</i> : the geometry-optimized (ball-and-stick) structure of 98 : Hg^{2+} complex. receptor 98	160
Figure 3.17 Structures of receptors 103a/b	161
Figure 3.18 Fluorescence spectrum of 99 . The excitation wavelength is $\lambda_{exc} = 330$ nm.....	166
Figure 3.19 Fluorescence spectra of 99 upon addition of 1 molar equivalents of various metal ions. The excitation wavelength is $\lambda_{exc} = 330$ nm.....	167
Figure 3.20 Fluorescence spectra of 99 upon addition of Zn^{2+} (0.30-21 eq) in acetonitrile/chloroform (v/v= 9:1) solutions. $\lambda_{exc} = 330$ nm.....	168
Figure 3.21 Benesi-Hildebrand plots of $1/(\text{F}_o-\text{F})$ versus $1/[\text{Zn}(\text{ClO}_4)_2]$ for 99 upon titration with Zn^{2+} . The linear fits showed 1:1 complexation between 99 and Zn^{2+} . The association constants were calculated for the changes at the 376 nm, 396 nm, 419 nm and 454 nm wavelengths.....	169
Figure 3.22 Screen-capture output showing 1:1 binding model for 99 with Zn^{2+} , using Thordarson's method.....	169

Figure 3.23 Fluorescence spectra of 99 upon addition of Cd^{2+} (0.30-21 eq) in acetonitrile/chloroform (v/v= 9:1) solutions. $\lambda_{exc} = 330$ nm.....	170
Figure 3.24 Benesi-Hildebrand plots of $1/(F_0-F)$ versus $1/[\text{Cd}(\text{ClO}_4)_2]$ for 99 upon titration with Cd^{2+} . The linear fits showed 1:1 complexation between 99 and Cd^{2+} . The individual association constants were calculated for the changes at the 376 nm, 396 nm, 419 nm and 454 nm wavelengths.....	171
Figure 3.25 Screen-capture output showing 1:1 binding model for 99 with Cd^{2+} , using Thordarson's method.....	172
Figure 3.26 Fluorescence spectra of 99 upon addition of Fe^{3+} (0.057-1.7 eq) in acetonitrile/chloroform (v/v= 9:1) solutions. $\lambda_{exc} = 330$ nm.....	173
Figure 3.27 Benesi-Hildebrand plots of $1/(F_0-F)$ versus $1/[\text{Fe}(\text{ClO}_4)_3]$ for 99 upon titration with Fe^{3+} . The linear fits showed 1:1 complexation between 99 and Fe^{3+} . The individual association constants were calculated for the changes at the 376 nm, 396 nm, 419 nm and 454 nm wavelengths.....	173
Figure 3.28 Screen-capture output showing 1:1 binding model for 99 with Fe^{3+} , using Thordarson's method.....	174
Figure 3.29 Histogram showing the association constant (K_{assoc}) values for receptor 99 with different metal ions determined by the two different methods.....	175
Figure 3.30 Partial $^1\text{H-NMR}$ (300 MHz) spectra of 99 with $\text{Cd}(\text{ClO}_4)_2$ in a $\text{CD}_3\text{CN}:\text{CD}_2\text{Cl}_2$ (4:1, v/v) at 298K; *, Δ , \blacklozenge , \blacklozenge , * and \bigcirc denoted the triazole- <i>H</i> , Ar- <i>H</i> protons, pyrene- CH_2 -triazole, - OCH_2 -triazole and AB pair of doublets respectively....	178

Figure 3.31 Partial $^1\text{H-NMR}$ (300 MHz) spectra of 99 with $\text{Zn}(\text{ClO}_4)_2$ in a $\text{CD}_3\text{CN}:\text{CD}_2\text{Cl}_2$ (4:1, v/v) at 298K; *, Δ , \blacklozenge , \blacklozenge , * and \circ denoted the triazole- <i>H</i> , Ar- <i>H</i> protons, pyrene- CH_2 -triazole, $-\text{OCH}_2$ -triazole and AB pair of doublets respectively....	179
Figure 4.01 Schematic representation of carbenes.....	194
Figure 4.02 Schematic representation of NHC.....	195
Figure 4.03 Functionalization of gold with ANHCs.....	197
Figure 4.04 a) Bonding geometry of NHC on Au(III) surface. b) An STM image of SAMs of NHC on gold surface.....	198
Figure 4.05 Structures of the molecules and Au(I) complexes studied by Richeter.....	199
Figure 4.06 Structures of targeted new calix[4]arene-NHC derivative 113	202
Figure 4.07 Schematic representation of gold MPCs functionalized with calix[4]arenes 120a ($n = 1$) and 120b ($n = 6$),.....	207
Figure 4.08 Schematic representation of the stabilization and functionalization of AuNPs with 121b and 121c	208
Figure 5.01 The structures of <i>p</i> -sulfonatocalix[<i>n</i>]arenes 122 and 123 ($n = 4, 6$).....	219
Figure 5.02 Structure of <i>peri</i> -tetrasulfonatotetrahydroxycalix[4]naphthalene 124	220
Figure 5.03 Structure of cyclotetrachromotropyrene 125	221
Figure 5.04 Schematic representation of the optunal-induced aggregation of <i>p</i> -sulfonatocalix[4]arene modified AgNPs.....	224
Figure 5.05 Schematic representation of SWNTs and MWNTs.....	225

Figure 5.06 Schematic representation of three different types of SWNTs based on the angle of chiral vector of graphene lattice.....	226
Figure 5.07 Structures of SWNTs functionalized with zinc-porphyrin conjugates 134 and 135	230
Figure 5.08 Solution process for dispersion and release of SWNTs by <i>m</i> PE-13.....	232
Figure 5.09 <i>Top</i> : Molecular structure of polymer 136 . <i>Bottom</i> : Reversible wrapping and unwrapping of SWNTs by a TTFV polymer.....	233
Figure 5.10 Structure of oxalix[4]naphthalenesultone 137	236
Figure 5.11 ¹ H-NMR diffusion spectroscopic curve ($r^2 = 0.999$) based upon the analysis of the chemical shift changes for the naphthalene ring $-C_{Naphth}H$ protons.....	240
Figure 5.12 UV-vis spectra of the three nanoparticles. <i>Left</i> : after 1 h; <i>right</i> : after 24 h, red curve (-) is 124:AgNP , blue curve (-) is 137:AgNP and green curve (-) is 125:AgNP	241
Figure 5.13 UV-vis spectra of 124:Ag NP mixed with nucleobases: red (-) with thymine; blue (-) with adenine; green (-) with cytosine; purple with guanine; yellow (-) with uracil. <i>Left</i> : after 1 h; <i>right</i> : after 24 h. Black (-) is 124:Ag NP in de-ionised water.....	243
Figure 5.14 UV-vis spectra of 137:Ag NP mixed with nucleobases: red (-) with thymine; blue (-) with adenine; green (-) with cytosine; purple (-) with guanine; yellow (-) with uracil. <i>Left</i> : after 1 h; <i>right</i> : after 24 h. Black (-) is 137:Ag NP in de-ionised water.....	244

Figure 5.15 UV-vis spectra of 125:Ag NP mixed with nucleobases: red (–) with thymine; blue (–) with adenine; green (–) with cytosine; purple (–) with guanine; yellow (–) with uracil. <i>Left</i> : after 1 h; <i>right</i> : after 24 h. Black (–) is 125:Ag NP in de-ionised water.....	244
Figure 5.16 UV-vis spectra of 124:Ag NP mixed with amino acids: red (–) with tryptophan; blue (–) with arginine; green (–) with lysine; purple (–) with alanine; yellow (–) with aspartate; fuchsia (–) with asparagine; brown (–) with phenylalanine; grey (–) with histidine. <i>Left</i> : after 1 h; <i>right</i> : after 24 h. Black (–) is 124:Ag NP in de-ionised water.....	249
Figure 5.17 UV-vis spectra of 137:Ag NP mixed with amino acids: red (–) with tryptophan; blue (–) with arginine; green (–) with lysine; purple (–) with alanine; yellow (–) with aspartate; fuchsia (–) with asparagine; brown (–) with phenylalanine; grey(–) with histidine. <i>Left</i> , after 1 h; <i>right</i> , after 24 h. Black (–) is 137:Ag NP in de-ionised water.....	249
Figure 5.18 UV-vis spectra of 125:Ag NP mixed with amino acids: red (–) with tryptophan; blue (–) with arginine; green (–) with lysine; purple (–) with alanine; yellow (–) with aspartate; fuchsia (–) with asparagine; brown (–) with phenylalanine; grey (–) with histidine. <i>Left</i> , after 1 h; <i>right</i> , after 24 h. Black (–) is 125:Ag NP in de-ionised water.....	250
Figure 5.19 Photographic image of the solutions of (A) Free 125 (B) 125 was mixed with CoMoCAT SWNTs after sonication for 30 min.....	251

Figure 5.20 UV-Vis-NIR spectra: (A) CoMoCAT and (B) HiPCO nanotubes diffusion dispersed by 125 in aqueous solutions.....	252
Figure 5.21 Raman spectra comparing the SWNTs before and after being dispersed with 125 in water. (A) CoMoCAT nanotubes (B) HiPCO nanotubes. Excitation wavelength: 785 nm.....	254
Figure 5.22 AFM image showing the supramolecular assemblies of 125 and CoMoCAT SWNT drop-cast onto mica.....	255
Figure 5.23 Spartan'10-generated molecular modeling (MMFF) showing a putative mode of binding between 125 molecules and two SWNTs. Water molecules are not shown for simplicity.....	256
Figure 5.24 ^{13}C -NMR (75.4 MHz) spectra of 125 and complex with C_{60} in D_2O at 298K; \blacklozenge denoted the C-13 signal of C_{60}	258

List of Schemes

Scheme 1.01 Gutsche's synthesis of 9-11	19
Scheme 1.02 Synthetic route to 15	27
Scheme 1.03 Water-soluble calix[4]arenes.....	28
Scheme 1.04 Synthesis of calix[4]naphthalene 40 using a [2+2] condensation approach...	34
Scheme 1.05 Synthesis of calix[4]naphthalene 37 and 38 using a [3+1] condensation approach.....	34
Scheme 1.06 Synthesis of calix[4]naphthalene 45a and 45b self-condensation approach..	35
Scheme 1.07 Synthesis of "3,5-linked" calix[4]naphthalene 48	36
Scheme 1.08 Synthesis of "3,6-linked" calix[4]naphthalene 50	36
Scheme 1.09 Synthesis of "3,6-linked" calix[4]naphthalene 53	37
Scheme 2.01 Synthesis of <i>p</i> -sulfonatocalix[4]arene thiol ligand 62	60
Scheme 2.02 Synthesis of calix[4]arenes 79 and 80	71
Scheme 2.03 Synthesis of tetrabromocalix[4]arenes 81 and 82	71
Scheme 2.04 Alternative approach for tetrabromocalix[4]arenes 81 and 82	72
Scheme 2.05 Attempts to synthesis of thioacetate-bearing calix[4]arenes 73 and 74	73
Scheme 2.06 Synthesis of thioacetate-bearing calix[4]arenes 70 and 71	74
Scheme 2.07 Attempts to synthesis of thiol-bearing calix[4]arenes 75 and 76	75
Scheme 2.08 Synthesis of calix[4]arene--crown" derivative 72	87

Scheme 2.09 Synthesis of calix[4]arene-crown derivative 90	110
Scheme 3.01 Synthesis of triazole-linked calix[4]arene 94 and its cadmium complex..	139
Scheme 3.02 Synthesis of azide intermediate 101	143
Scheme 3.03 Synthesis of a new bimodal calix[4]arene 98	144
Scheme 3.04 Synthesis of bis(azidomethyl) intermediate 105	163
Scheme 3.05 Synthesis of a new bimodal calix[4]arene 99	163
Scheme 4.01 Synthesis of first stable reported NHC	195
Scheme 4.02 Synthesis of NHC-protected AuNPs.....	200
Scheme 4.03 Synthesis of dibromo intermediate 115	203
Scheme 4.04 Synthesis of imidazole compound 117	205
Scheme 4.05 Proposed synthesis of calix[4]arene-NHC derivative 119	206
Scheme 5.01 Synthesis of amino-functionalized SWNT 129	228
Scheme 5.02 Synthesis of polystyrene-functionalized SWNT 133	229
Scheme 5.03 Synthesis of <i>peri</i> -sulfonatocalix[4]naphthalene 124	237
Scheme 5.04 Synthesis of diacetoxyoxacalix[4]naphthalenesultone 137	238
Scheme 5.05 Synthesis of cyclotetrachromotropyrene 125	239

List of Tables

Table 1.01 Classification and properties of hydrogen bonded interactions.....	6
Table 2.01 Attempted conditions for conversion of thioacetate to thiol group.....	76
Table 2.02 Average K_{assoc} values for representative salts.....	83
Table 2.03 ^1H NMR (300 MHz) titration chemical shift data for Ar- <i>H</i> , Ar- <i>CH</i> ₂ , <i>SCOCH</i> ₃ and <i>t</i> -Bu of 72 (1.5×10^{-3} M) upon the addition of NaI (0.53-22.31 eq) solution.....	97
Table 2.04 ^1H -NMR (300 MHz) titration chemical shift data for Ar- <i>H</i> , Ar- <i>CH</i> ₂ , <i>SCOCH</i> ₃ and <i>t</i> -Bu of 72 (1.5×10^{-3} M) upon the addition of RbI (0.07-2.21 eq) solution	106
Table 2.05 Calculated binding energies for the receptor 72 with metal ions.....	107
Table 2.06 Selected interatomic distances between M^+ (Cs^+ , Rb^+ , K^+ , Na^+ and Li^+) and oxygen atoms of polyether fragments in the complexes 72 : M^+ optimized at B3LYP/Def2SVP Level (distances in Å).....	109
Table 3.01 Comparison of calculated binding constants for 98 with selected metal perchlorate salts in 9:1 $\text{CH}_3\text{CN}:\text{CHCl}_3$ using the Thordarson and Benesi-Hildebrand (B-H) methods.....	155
Table 3.02 Selected interatomic distances of triazole nitrogen atoms and hydrogen atoms in the complex of 98 : Hg^{2+} optimized at B3LYP/lanl2dz Level (Distance in Å).....	160

Table 3.03 Comparison of calculated binding constants for 99 with selected metal perchlorate salts in 9:1 CH ₃ CN:CHCl ₃ using the Thordarson and Benesi-Hildebrand (B-H) methods.....	176
Table 5.01 The wavelengths and intensities of the plasmon resonance band after 1 and 24 h for the three nanoparticle systems.....	242
Table 5.02 Summary of plasmon resonance and aggregation spectral data for the nucleobase-hybrid nanoparticle interactions after 1 h	245
Table 5.03 Summary of plasmon resonance and aggregation spectral data for the nucleobase-hybrid nanoparticle interactions after 24 h	246
Table 5.04 Summary of plasmon resonance and aggregation spectral data for the amino acid-hybrid nanoparticle interactions after 1 h.	247
Table 5.05 Summary of plasmon resonance and aggregation spectral data for the amino acid-hybrid nanoparticle interactions after 24 h.	248

List of Abbreviations

Å	Angstrom
AgNPs	Silver nanoparticles
APCI-MS	Atmospheric Pressure Chemical Ionization Mass Spectrometry
Aq	Aqueous
Ar	Aromatic
AuNPs	Gold nanoparticles
br.	Broad (in NMR)
Bu	Butyl
<i>t</i> -BuLi	<i>t</i> -butyllithium
B3LYP	Becke, 3-parameter, Lee-Yang-Parr
CuI	Copper Iodide
CT	Charge-transfer
CCl ₄	Carbon tetrachloride
δ	Chemical shift in ppm down-field from tetramethylsilane
DFT	Density functional theory
DMF	<i>N,N</i> -dimethylformamide
DMSO	Dimethyl sulfoxide
DNA	Deoxyribonucleic acid
HOMO	Highest occupied molecular orbital
Hz	Hertz
<i>J</i>	Coupling constant

K_{assoc}	Association constant
kJ	Kilojoule
Lit.	Literature
LUMO	Lowest unoccupied molecular orbital
MS	Mass spectroscopy
MMFF	Merck molecular force field
Me	Methyl
mp	Melting point
min	minute(s)
MW	Microwave
NMR	Nuclear magnetic resonance
NR	No reaction
NBS	<i>N</i> -bromosuccinimide
<i>p</i>	Para-
Ph	Phenyl
ppm	parts per million
PET	Photoinduced electron transfer
PTI	Photon Technology International
PMT	photomultiplier tube
PCT	Photoinduced charge transfer
q	Quartet (in NMR)
rt	Room temperature

SAM	Self-assembled monolayer
SPR	Surface plasmon resonance
STM	Scanning Tunneling Microscopy
SEM	Scanning Electron Microscopy
<i>s</i>	Singlet (in NMR)
TMS	Tetramethylsilane (in NMR)
THF	Tetrahydrofuran
TLC	Thin-layer chromatography
<i>t</i>	Triplet (in NMR)
<i>tert</i>	Tertiary
UV-Vis	UV-visible spectroscopy

Appendix

- Figure 2.34** 2D NOESY spectrum for calix[4]arene **89**.....290
- Figure 2.35a** The asymmetric unit, represented with capped sticks, containing three chemically identical, but crystallographically independent molecules ($Z' = 3$). H-atoms and minor disorder component omitted for clarity.....293
- Figure 2.35b** Packed unit cell, represented with 30% displacement ellipsoids, looking down the c-axis, showing the discrete chain-like arrangement of molecules in the structure.....294
- Figure 2.35c** One molecule, represented with 30% displacement ellipsoids, showing the cone conformation. H-atoms and minor disorder components omitted for clarity.....294
- Figure 3.32** *Left*: Fluorescence spectra of **98** upon addition of Cd^{2+} (1.1-15 eq) in acetonitrile/ chloroform (v/v= 9:1) solutions. $\lambda_{exc} = 350$ nm. *Middle*: Benesi-Hildebrand plot of $1/(F_0-F)$ versus $1/[\text{Cd}(\text{ClO}_4)_2]$ for **98** upon titration with $\text{Cd}(\text{ClO}_4)_2$. The linear fit showed a 1:1 complexation between **98** and Cd^{2+} ions. *Right*: Screen-capture output showing 1:1 binding model for **98** with Cd^{2+} , using Thordarson's method.306
- Figure 3.33** *Left*: Fluorescence spectra of **98** upon addition of Co^{2+} (1.7-8.2 eq) in acetonitrile/ chloroform (v/v= 9:1) solutions. $\lambda_{exc} = 350$ nm. *Middle*: Benesi-Hildebrand plot of $1/(F_0-F)$ versus $1/[\text{Co}(\text{ClO}_4)_2]$ for **98** upon titration with $\text{Co}(\text{ClO}_4)_2$. The linear fit showed a 1:1 complexation between **98** and Co^{2+} ions. *Right*: Screen-capture output showing 1:1 binding model for **98** with Co^{2+} , using Thordarson's method.....306

Figure 3.34 *Left:* Fluorescence spectra of **98** upon addition of Pb^{2+} (0.30-16 eq) in acetonitrile/ chloroform (v/v= 9:1) solutions. $\lambda_{exc} = 350$ nm. *Middle:* Benesi-Hildebrand plot of $1/(F_o-F)$ versus $1/[\text{Pb}(\text{ClO}_4)_2]$ for **98** upon titration with $\text{Pb}(\text{ClO}_4)_2$. The linear fit showed a 1:1 complexation between **98** and Pb^{2+} ions. *Right:* Screen-capture output showing 1:1 binding model for **98** with Pb^{2+} , using Thordarson's method.....307

Figure 3.35 *Left:* Fluorescence spectra of **98** upon addition of Zn^{2+} (0.90-36 eq) in acetonitrile/ chloroform (v/v= 9:1) solutions. $\lambda_{exc} = 350$ nm. *Middle:* Benesi-Hildebrand plot of $1/(F_o-F)$ versus $1/[\text{Zn}(\text{ClO}_4)_2]$ for **98** upon titration with $\text{Zn}(\text{ClO}_4)_2$. The linear fit showed a 1:1 complexation between **98** and Zn^{2+} ions. *Right:* Screen-capture output showing 1:1 binding model for **98** with Zn^{2+} , using Thordarson's method.....307

Figure 3.36 *Left:* Fluorescence spectra of **98** upon addition of Cu^{2+} (1.1-36 eq) in acetonitrile/ chloroform (v/v= 9:1) solutions. $\lambda_{exc} = 350$ nm. *Middle:* Benesi-Hildebrand plot of $1/(F_o-F)$ versus $1/[\text{Cu}(\text{ClO}_4)_2]$ for **98** upon titration with $\text{Cu}(\text{ClO}_4)_2$. The linear fit showed a 1:1 complexation between **98** and Cu^{2+} ions. *Right:* Screen-capture output showing 1:1 binding model for **98** with Cu^{2+} , using Thordarson's method.....308

Figure 3.37 *Left:* Fluorescence spectra of **98** upon addition of Fe^{2+} (0.80-68 eq) in acetonitrile/ chloroform (v/v= 9:1) solutions. $\lambda_{exc} = 350$ nm. *Middle:* Benesi-Hildebrand plot of $1/(F_o-F)$ versus $1/[\text{Fe}(\text{ClO}_4)_2]$ for **98** upon titration with $\text{Fe}(\text{ClO}_4)_2$. The linear fit showed a 1:1 complexation between **98** and Fe^{2+} ions. *Right:* Screen-capture output showing 1:1 binding model for **98** with Fe^{2+} , using Thordarson's method.....308

Figure 3.38 *Left:* Fluorescence spectra of **98** upon addition of Ni^{2+} (0.38-60 eq) in acetonitrile/ chloroform (v/v= 9:1) solutions. $\lambda_{exc} = 350$ nm. *Middle:* Benesi-Hildebrand

plot of $1/(F_0-F)$ versus $1/[\text{Ni}(\text{ClO}_4)_2]$ for **98** upon titration with $\text{Ni}(\text{ClO}_4)_2$. The linear fit showed a 1:1 complexation between **98** and Ni^{2+} ions. *Right*: Screen-capture output showing 1:1 binding model for **98** with Ni^{2+} , using Thordarson's method.....309

Figure 3.39 *Left*: Fluorescence spectra of **99** upon addition of Mn^{2+} (1.4-27 eq) in acetonitrile/ chloroform (v/v= 9:1) solutions. $\lambda_{exc} = 330$ nm. *Middle*: Benesi-Hildebrand plot of $1/(F_0-F)$ versus $1/[\text{Mn}(\text{ClO}_4)_2]$ for **99** upon titration with $\text{Mn}(\text{ClO}_4)_2$. The linear fit showed a 1:1 complexation between **99** and Mn^{2+} ions. *Right*: Screen-capture output showing 1:1 binding model for **99** with Mn^{2+} , using Thordarson's method.....309

Figure 3.40 *Left*: Fluorescence spectra of **99** upon addition of Ni^{2+} (0.57-53 eq) in acetonitrile/ chloroform (v/v= 9:1) solutions. $\lambda_{exc} = 330$ nm. *Middle*: Benesi-Hildebrand plot of $1/(F_0-F)$ versus $1/[\text{Ni}(\text{ClO}_4)_2]$ for **99** upon titration with $\text{Ni}(\text{ClO}_4)_2$. The linear fit showed a 1:1 complexation between **99** and Ni^{2+} ions. *Right*: Screen-capture output showing 1:1 binding model for **99** with Ni^{2+} , using Thordarson's method.....310

Figure 3.41 *Left*: Fluorescence spectra of **99** upon addition of Pb^{2+} (0.85-21 eq) in acetonitrile/ chloroform (v/v= 9:1) solutions. $\lambda_{exc} = 330$ nm. *Middle*: Benesi-Hildebrand plot of $1/(F_0-F)$ versus $1/[\text{Pb}(\text{ClO}_4)_2]$ for **99** upon titration with $\text{Pb}(\text{ClO}_4)_2$. The linear fit showed a 1:1 complexation between **99** and Pb^{2+} ions. *Right*: Screen-capture output showing 1:1 binding model for **99** with Pb^{2+} , using Thordarson's method.....310

Figure 3.42 *Left*: Fluorescence spectra of **99** upon addition of Fe^{2+} (0.30-10 eq) in acetonitrile/ chloroform (v/v= 9:1) solutions. $\lambda_{exc} = 330$ nm. *Middle*: Benesi-Hildebrand plot of $1/(F_0-F)$ versus $1/[\text{Fe}(\text{ClO}_4)_2]$ for **99** upon titration with $\text{Fe}(\text{ClO}_4)_2$. The linear fit

showed a 1:1 complexation between **99** and Fe^{2+} ions. *Right*: Screen-capture output showing 1:1 binding model for **99** with Fe^{2+} , using Thordarson's method.....311

Figure 3.43 *Left*: Fluorescence spectra of **99** upon addition of Hg^{2+} (0.0080-0.56 eq) in acetonitrile/ chloroform (v/v= 9:1) solutions. $\lambda_{exc} = 330$ nm. *Middle*: Benesi-Hildebrand plot of $1/(F_0-F)$ versus $1/[\text{Hg}(\text{ClO}_4)_2]$ for **99** upon titration with $\text{Hg}(\text{ClO}_4)_2$. The linear fit showed a 1:1 complexation between **99** and Hg^{2+} ions. *Right*: Screen-capture output showing 1:1 binding model for **99** with Hg^{2+} , using Thordarson's method.....311

Figure 3.44 *Left*: Fluorescence spectra of **99** upon addition of Cu^{2+} (0.84-11 eq) in acetonitrile/ chloroform (v/v= 9:1) solutions. $\lambda_{exc} = 330$ nm. *Middle*: Benesi-Hildebrand plot of $1/(F_0-F)$ versus $1/[\text{Cu}(\text{ClO}_4)_2]$ for **99** upon titration with $\text{Cu}(\text{ClO}_4)_2$. The linear fit showed a 1:1 complexation between **99** and Cu^{2+} ions. *Right*: Screen-capture output showing 1:1 binding model for **99** with Cu^{2+} , using Thordarson's method.....312

Figure 3.45 *Left*: Fluorescence spectra of **99** upon addition of Co^{2+} (0.57-40 eq) in acetonitrile/ chloroform (v/v= 9:1) solutions. $\lambda_{exc} = 330$ nm. *Middle*: Benesi-Hildebrand plot of $1/(F_0-F)$ versus $1/[\text{Co}(\text{ClO}_4)_2]$ for **99** upon titration with $\text{Co}(\text{ClO}_4)_2$. The linear fit showed a 1:1 complexation between **99** and Co^{2+} ions. *Right*: Screen-capture output showing 1:1 binding model for **99** with Co^{2+} , using Thordarson's method.....312

Figure 3.46 *Left*: Fluorescence spectra of **99** upon addition of Ag^+ (0.71-27 eq) in acetonitrile/ chloroform (v/v= 9:1) solutions. $\lambda_{exc} = 330$ nm. *Middle*: Benesi-Hildebrand plot of $1/(F_0-F)$ versus $1/[\text{Ag}(\text{ClO}_4)]$ for **99** upon titration with $\text{Ag}(\text{ClO}_4)$. The linear fit showed a 1:1 complexation between **99** and Ag^+ ions. *Right*: Screen-capture output showing 1:1 binding model for **99** with Ag^+ , using Thordarson's method.....313

Chapter 1

Introduction

1.1 Supramolecular chemistry

In 1978 J.-M. Lehn introduced the term “Supramolecular Chemistry” with the statement: *“Just as there is a field of molecular chemistry based on the covalent bond, there is a field of supramolecular chemistry, the chemistry of molecular assemblies and of the intermolecular bond. Supramolecular chemistry is chemistry ‘beyond the molecule’, the science of non-covalent, intermolecular interactions”*.¹ Traditional or “classical” chemistry is concerned with ionic and also covalent bonds, whereas supramolecular chemistry examines the reversible and weaker noncovalent interactions between molecules.¹ The forces responsible for these interactions include hydrogen bonding, van der Waals forces, metal coordination, π - π interactions, hydrophobic effects and electrostatic forces. The concepts that have been demonstrated by supramolecular chemistry studies include molecular recognition, molecular self-assembly, host-guest chemistry and mechanically-interlocked molecular architectures.² A major driving force for studying supramolecular chemistry is to mimic biological systems.³

A brief historical note on supramolecular chemistry follows. In 1891, A. Villiers first described “cellulosine”, which today is known as cyclodextrin.⁴ Later, F. Schardinger identified the three naturally-occurring α -, β -, and γ -cyclodextrins. In 1893, Alfred Werner (Nobel Prize in Chemistry, 1913) was the first to propose the structure of coordination compounds containing complex ions.⁵ In biological systems there are

different types of receptors which can selectively supramolecularly bind to a specific molecule or ionic species. Such processes are called “molecular recognition”.³ In 1894 Emil Fischer proposed the “Lock and Key” principle to explain enzyme-substrate interactions.⁶ In such interactions binding must be selective and this requires size and shape complementarity. The concept of receptors was introduced by Paul Ehrlich who stated that molecules do not react if they are not bound (“*Corpora non agunt nisi fixata*”).⁷ Wolf and co-workers introduced the term “Übermoleküle” i.e. “supermolecules” (e.g. carboxylic acid gas phase dimers) in 1937.⁸ In the early twentieth century studies on noncovalent bonds increased gradually and the use of these principles led to an increasing understanding of protein structures and biological processes. Eventually, chemists were able to take these concepts and apply them to synthetic systems. A breakthrough came in 1967 when the first synthetic molecular receptor dibenzo[18]crown-6 (**1**) (Figure 1.01) was synthesized by C. J. Pedersen.⁹ He found that the macrocyclic ether formed a complex with potassium ion and called the macrocycle a *crown ether*. In 1969 J.-M. Lehn and co-workers reported a different and new class of crown ether receptors which they called “*cryptands*”, e.g. the cryptand:K⁺ complex **2** also referred to as a “*cryptate*” (Figure 1.01).¹⁰ These types of 3-D receptors are more selective than the analogous crown ethers. D. J. Cram synthesized a third class of macrocycle, which he called “*spherands*” (Figure 1.01) and which have rigid structures and specific binding sites.¹¹ In 1987 the Nobel Prize for chemistry was awarded to Pedersen, Cram and Lehn “for their development and use of molecules with structure-specific interactions of high selectivity”.

In general, intermolecular forces are weaker than covalent bonds. Therefore supramolecular species are thermodynamically less stable and kinetically more labile. In a supramolecular species a host molecule binds with a guest molecule to form a “host-guest complex” or “supramolecular complex”.¹ In most cases, the host molecule is a large molecule such as an enzyme or macrocyclic compound having a specific cavity that possesses binding sites which can be Lewis base donor atoms, hydrogen bond donors or Lewis acid donor atoms. On the other hand, the guest species is either a cation, an anion or a neutral molecule and these guest species can be hydrogen bond acceptors, halide anions, and Lewis acidic metal cations or molecules.

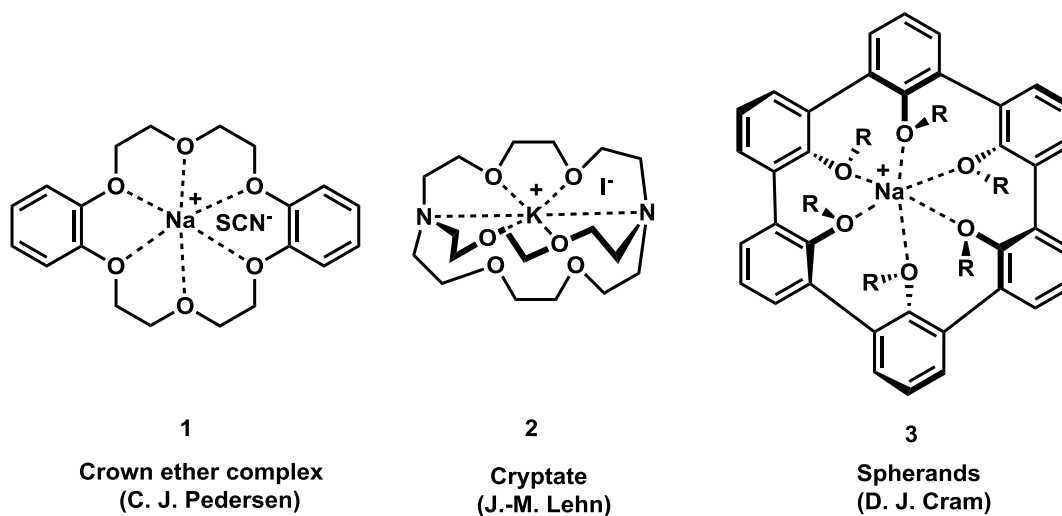


Figure 1.01 Examples of supramolecular complexes 1, 2 and 3.

Since the initial discoveries, supramolecular chemistry has become more sophisticated; for example, J. Fraser Stoddart demonstrated that weak intermolecular forces (e.g. hydrogen bonding and π - π interactions) could be used in the synthesis of catenanes and rotaxanes.¹² C. David Gutsche developed a new strategy for the synthesis

of artificial receptors by using calix[*n*]arenes. Fullerenes,^{13c} dendrimers and nanoparticles are now heavily involved in supramolecular chemistry, which indicates that the emerging science of nanotechnology has also had a strong influence on the field.^{1,13}

1.2 Non-covalent interactions

Non-covalent interactions play very important roles in holding supramolecular systems together. The term non-covalent can include a wide range of repulsive and attractive forces. As described earlier the different types of non-covalent interactions involved in host-guest chemistry include hydrogen bonding, π - π interactions, electrostatic forces, van der Waals forces and hydrophobic effects.¹ A more detailed description of these interactions is presented below.

1.2.1 Hydrogen bonding

Hydrogen bonding is one of the most important types of non-covalent interactions in supramolecular chemistry. Hydrogen bonding can be defined as the intermolecular attraction between the hydrogen atom attached to an electronegative atom or electron withdrawing group (e.g. H-F, H-O and H-N) and a neighbouring dipole on an adjacent molecule (electronegative atoms like F, O, N). A hydrogen bond can be represented as **D-H**··**A** with **D** and **A** representing the hydrogen bond donor and acceptor, respectively. The strength of a hydrogen bond has been reported to depend upon the **D-H**··**A** bond angle and also on the distance between **A** and **H**. The different types of hydrogen bonding geometries are defined by the angle of interactions as shown in Figure 1.02. Type (a) shows linear geometry with a bond angle of 180°, and Type (b) shows a nearly linear

geometry. Types (c), (d), (e) and (f) are called donating bifurcated, bifurcated, accepting bifurcated and three center bifurcated, respectively.¹³

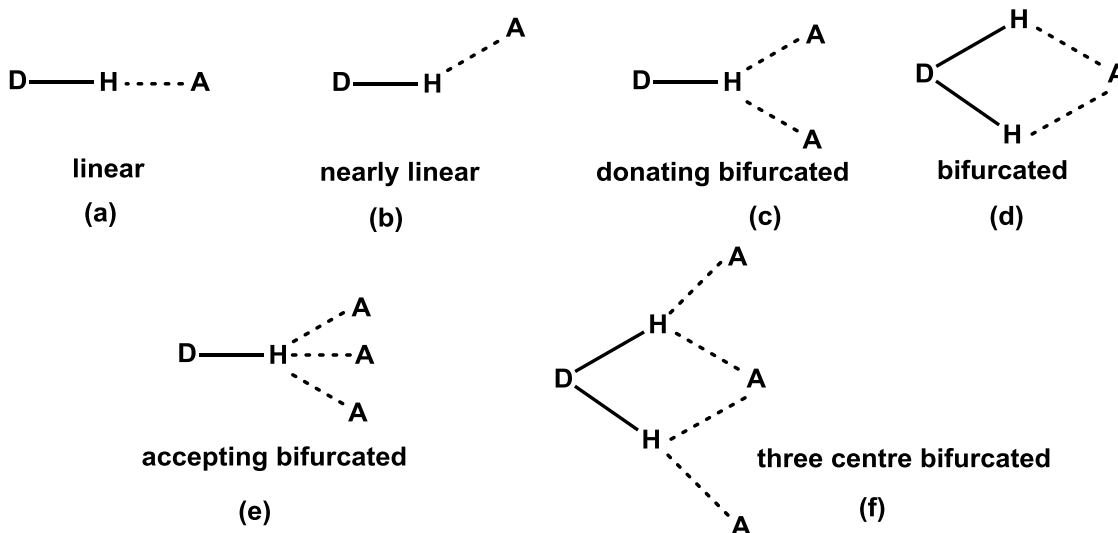


Figure 1.02 Different types of hydrogen bonding geometries.¹³

The common classification of hydrogen bonds based on their strengths and as well as properties are listed in Table 1.01.

Some molecules having many hydrogen bond donor and acceptor groups hold the components together, leading to an increase in the stability of the structure. The best example of hydrogen bonding is shown in the double helix of DNA. Multiple hydrogen bonding interactions between guanine and cytosine base pairs in DNA for example are shown in Figure 1.03.¹³

Table 1.01 Classification and properties of hydrogen bonded interactions.^{13a}

Interaction D--H···A	Strong Mainly Covalent	Moderate, Mainly Electrostatic	Weak, Electrostatic
Bond energy (kJ mol ⁻¹)	60-120	16-60	< 16
Bond lengths: H---A	1.2-1.5	1.5-2.2	2.2-3.2
Bond lengths: D---A	2.2-2.5	2.5-3.2	3.2-4.0
Bond angle	175-180°	130-180°	90-150°
Examples	HF complexes Proton sponge	Acids, Biological molecules, Alcohols	C-H hydrogen bonds, O—H---π bonds

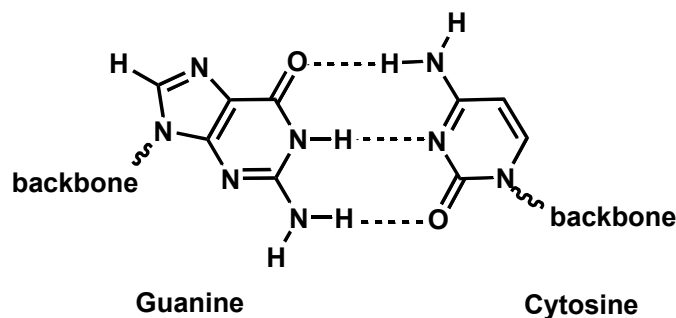


Figure 1.03 Hydrogen bond interactions between guanine and cytosine base pairs in DNA.

1.2.2 π -Interactions

π -Interactions occur between delocalized electrons, or double bonds, with aromatic rings or cations (alkaline and alkaline earth metals). π -Interactions can be divided into the following three types:

a. Cation- π interactions

The interaction of Group 1 and 2 cations with carbon-carbon double bonds is a strong non-covalent interaction which plays an important role in biological systems. Cation- π interactions are strong forces between a cation and the π -face of an aromatic structure. In this regard polarizability, induced dipoles, electrostatic forces and charge transfer all play an important role.¹⁴ A schematic representation of a typical cation- π interaction of K^+ ion and benzene is shown in Figure 1.04.

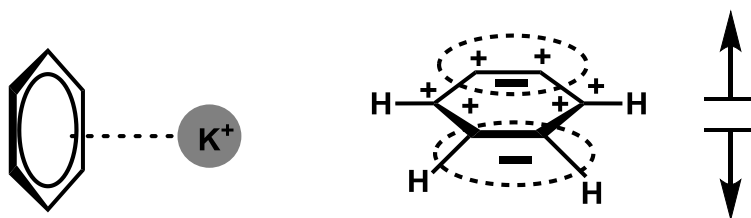


Figure 1.04 *Left:* Schematic representation of a cation- π interaction of K^+ ion and benzene. *Right:* Schematic representation of the quadrupole moment of benzene.

b. Anion- π interactions

Although cation- π interactions have been reported for many years, anion- π interactions have only most recently attracted attention.¹⁵ Such interactions occur between electron-deficient arenes and e.g. halide anions in which the negatively charged species is attracted to the centre of the electron-deficient aromatic ring. Based on theoretical calculations the strength of anion- π interactions typically ranges from 10 to 20 kcal mol⁻¹. Kochi's group^{15b} reported that halides (Cl^- , Br^- , I^-) form stable charge-transfer complexes with different electron-deficient aromatic compounds such as **4-6** (Figure 1.05).

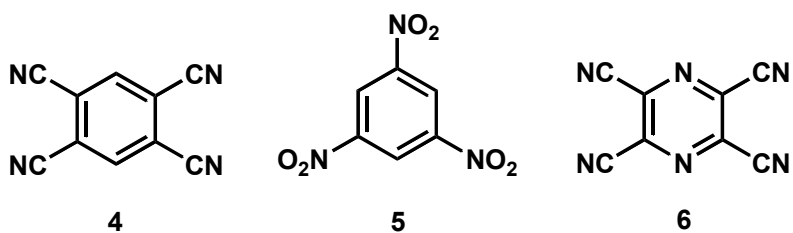


Figure 1.05 Neutral organic π -acceptors.

c. π - π Interactions

The interactions which exist between two aromatic rings are known as π - π interactions, and are also called π - π stacking interactions.^{13a} These types of interactions occur between two aromatic rings and induced dipoles and dispersion contributions play an important role in the stabilizing effect of these π - π interactions. There are two types of π - π interactions: face-to-face and edge-to-face (Figure 1.06). The face-to-face interaction is due to the attraction of the negatively-charged π -electron cloud of one aromatic ring with the positive corner of another aromatic ring. The arrangement of face-to-face orientation is due to the electrostatic repulsions existing between the two negatively charged π -systems which would disfavor a “sandwich”-type of arrangement (Figure 1.06b). The layered-structure of graphite is the best example of this type of interaction.¹⁶

Edge-to-face interactions exist between the electron-deficient edge of one aromatic ring with the negatively-charged π -electron cloud of the other aromatic ring. This type of interaction is responsible for the characteristic herringbone packing in the crystal structures of a range of small aromatic hydrocarbons including benzene.^{13a}

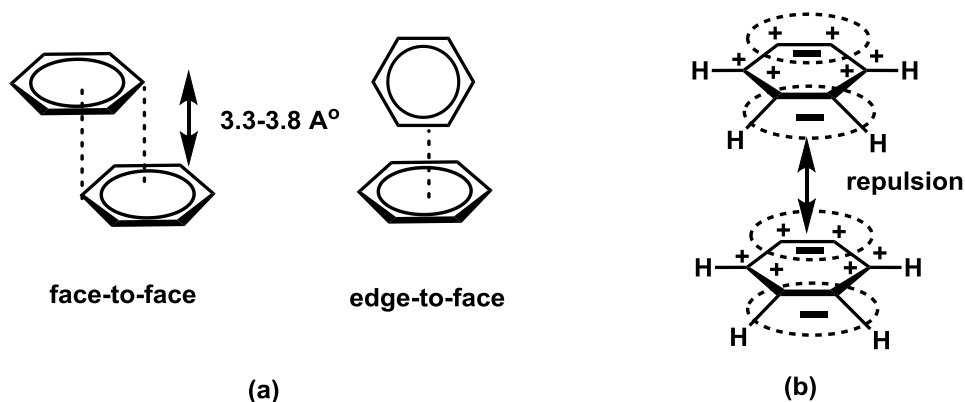


Figure 1.06 (a) Two types of π - π stacking interactions: face-to-face and edge-to-face. (b) The repulsion between negatively charged π -electron clouds of aromatic rings.

1.2.3 Electrostatic interactions

Electrostatic interactions play an important role in supramolecular and natural systems. In general, these interactions are due to the Coulombic interaction between two opposite charges.^{13a} Three different types of electrostatic interactions are discussed below.

a. Ion-ion Interactions

Ion-ion interactions are electrostatic interactions between oppositely-charged ions and are comparable in strength to covalent bonds (bond energy = 100-350 kJ mol⁻¹). A typical example of an ion-ion interaction is shown by solid NaCl. Another example showing ion-ion interactions is the salt formation of an organic cation (2,4,6-tris[1,4-diazabicyclo[2.2.2]octane-*N*-methyl]mesitylene) with the various anions such as Cl⁻, Br⁻, PF₆⁻, and [Fe(CN)₆]³⁻ (Figure 1.07).¹⁷

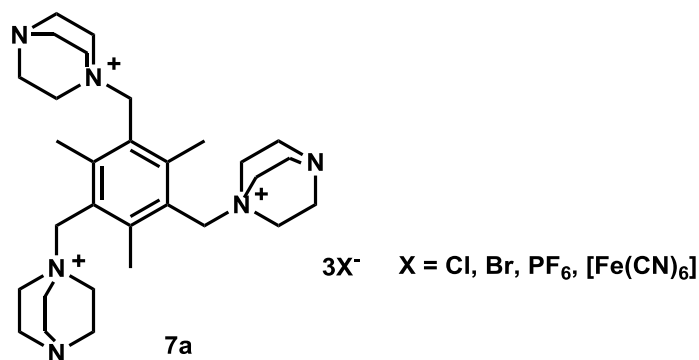


Figure 1.07 An example of organic cation **7a** with various anions showing ion-ion interactions.

b. Ion-Dipole Interactions

These interactions are the bonding of ions to polar molecules containing an oxygen or a nitrogen atom. The bond energy of these types of interactions ranges from 50-200 kJ mol⁻¹. The interactions are observed both in solution and in the solid state. The complexation of Na⁺ with [15]crown-5 occurs because of ion-dipole interactions (Figure 1.08).^{13a}

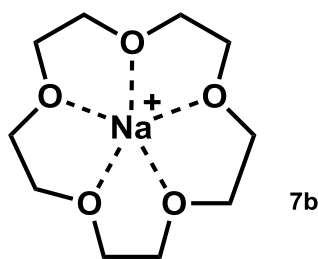


Figure 1.08 Ion-dipole interactions of Na⁺ with a crown ether.

c. Dipole-Dipole Interactions

These interactions are those which exist between polar molecules, or groups, which have permanent dipoles. The alignment of one dipole with another can occur giving rise

to significant interactions due to the matching of a single pair of poles on adjacent molecules (–Type I”) or opposing alignment of one dipole with other (–Type II”). The bond energies of these types of interactions range from 5-50 kJ mol⁻¹. Dipole-dipole interactions between carbonyl groups are shown in Figure 1.09.^{13a}

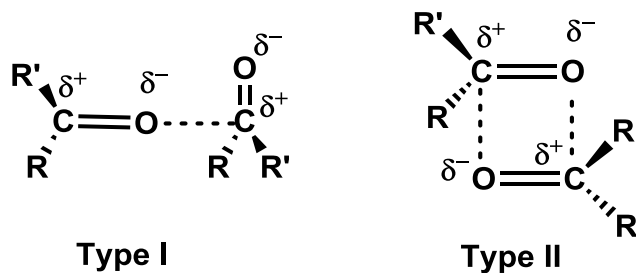


Figure 1.09 Dipole-dipole interactions between two carbonyl groups.

1.2.4 van der Waals Interactions

In 1873 it was discovered that gases show less pressure than expected, due to the induced dipole and instantaneous dipole interaction between molecules which, today are known as van der Waals forces.¹³ These forces are weak non-covalent interactions having bond energies which range from 0-5 kJ mol⁻¹. This type of interaction arises not only from permanent dipoles but also from the polarization of the electron cloud of the molecules. van der Waals forces can be classified into three different types: (a) induced dipole; (b) instantaneous dipole; and (c) permanent dipole interactions. An example of a van der Waals inclusion complex is shown by the supramolecular inclusion of toluene in the molecular cavity of *p*-*tert*-butylcalix[4]arene¹⁸ (Figure 1.10). This complex shows methyl C-H... π interactions between the toluene and the *t*-butyl calix[4]arene.

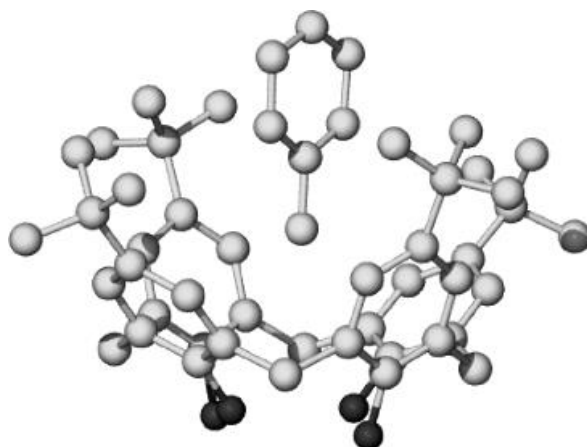


Figure 1.10 The crystal structure of a van der Waals inclusion complex, *p-tert-butylcalix[4]arene-toluene*.¹⁸

1.2.5 Hydrophobic effect

The hydrophobic effect can be defined as the aggregation of non-polar substances in aqueous solutions. These effects are important in supramolecular chemistry and also in biology. The hydrophobic effect can be observed in the binding of a host molecule like cyclodextrin with guest molecules in aqueous solutions.¹⁹

1.3 Host-guest complexation studies

The determination of host-guest complexation may involve several analytical techniques such as nuclear magnetic resonance spectroscopy (NMR), fluorescence spectroscopy, mass spectrometry, UV-vis, scanning probe microscopy (SPM), single crystal X-ray diffraction, atomic force microscopy (AFM) and electrochemical techniques. The most commonly used techniques are NMR, UV-vis and fluorescence spectroscopy. These techniques can provide information about the stoichiometry of the

host-guest complexation, the host-guest binding location and are also used to determine the binding or association constants. Some of these techniques are described below.

1.3.1 Nuclear magnetic resonance (NMR) spectroscopy

NMR spectroscopy is one of the most useful techniques for detecting and measuring supramolecular host-guest complexation. This method is used to detect the chemical shift changes ($\Delta\delta$ ppm) which occur due to the changes in the respective protons' environment that shield or deshield the host and the guest. This provides useful information about the location of the interaction between a host and its guest. The observed chemical shift changes potentially can permit the binding constants between the host and guest to be determined. The variation of chemical shift changes of the host and guest protons are affected by the rapid exchange occurring between host and guest with respect to the NMR time-scale ($\delta\nu$). The NMR time scale is dependent on the spectrometer frequency and also on the nucleus being considered (^1H , ^{13}C and so on). This technique however has some limitations, such as low sensitivity, as compared to fluorescence spectroscopy; also, it requires relatively high concentrations of the host molecules and is also limited by the solubility of the host and guest molecules in the NMR solvents.²⁰

1.3.2 UV-visible spectroscopy

The sensitivity of UV-vis spectroscopy is higher than that of NMR for the detection of supramolecular host-guest complexation. This technique can be used to measure the binding constants with low concentrations of the host molecules (10^{-5} to 10^{-6} M). The

limitation of UV-vis spectroscopy however, is that it does not provide much information about the binding location of the host molecules.²⁰

1.3.3 Fluorescence spectroscopy

Fluorescence spectroscopy is one of the most widely used techniques for the detection of host-guest complexation, and can be used with concentrations of host molecules in the 10^{-5} to 10^{-6} M range.²¹ A fluorescent chemosensor for ions generally includes two components such as an ion recognition unit (ionophore) and a fluorogenic unit (fluorophore). These units can be independent species or can be covalently linked by a suitable spacer in a molecule. When the analytes bind to the ion recognition unit, changes occur in the optical properties of the chemosensor. Fluorophores are optically active molecules and have applications in self-assembled chemosensors,^{22a} in supramolecular chemistry,^{22b} and in fluorescent and photochromic chemosensors.^{22c} The response of a fluorophore to substrate binding is controlled by the following mechanisms:

a. Photoinduced electron transfer (PET):

Photoinduced electron transfer (PET) is the most accepted mechanism for the behavior of a class of “turn-on” fluorescent chemosensors.²³ Host molecules have both fluorophore and ionophore (receptor) units, which are connected by spacer. In the absence of analyte (‘off’ state), the HOMO of the receptor lies higher in energy than that of the fluorophore HOMO and can transfer an electron to the fluorophore and thus quench fluorescence. Binding of the sensors to a particular type of analyte lowers the receptor’s HOMO to below that of the fluorophore HOMO in the ‘on’ state (Figure 1.11),

which prevents the electron transfer and fluorescence is revived.^{24a} The molecular orbital energy diagram which illustrates PET between the fluorophore and receptor is shown in Figure 1.11. The direction of electron transfer in the excited state is determined by the reduction and oxidation potential of the excited and ground states. A wide variety of PET sensors have been reported with desirable properties such as selectivity for an analyte, and with functional groups added to the sensor which can affect the intensity of the fluorescence.^{24b}

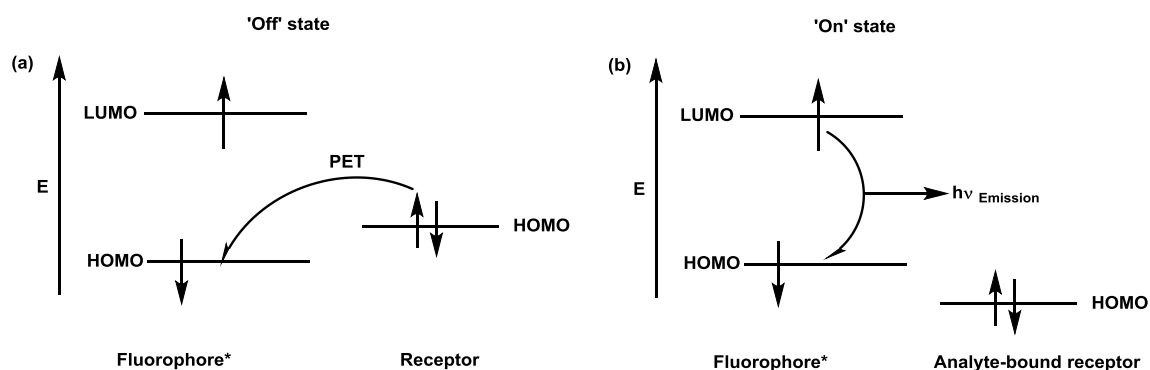


Figure 1.11 Molecular orbital energy diagrams of the relative energy dispositions of the frontier orbitals of fluorophore and receptor in (a) the analyte-free state, and (b) the analyte-bound state.^{24a}

b. Photoinduced charge transfer (PCT):

Photoinduced charge transfer (PCT) is also called “intramolecular charge transfer” (ICT), and plays an important role in the photophysics of donor-acceptor π -conjugated (D- π -A) compounds. The PCT may occur over long distances and is associated with major dipole moment changes in fluorophores which contain both electron-withdrawing and electron-donating groups. The photophysical properties of the fluorophore can be

affected by the nature of the substituents on the receptors, which cause changes in the fluorescence emission.²⁵

c. Excimer formation:

When aromatic rings are involved in weak interactions such as π - π stacking, the electronic excitation of one of the aromatic rings may result in an interaction with a neighboring aromatic ring.²¹ This forms what is termed as an excited dimer, or “excimer”. The IUPAC Gold Book defines an excimer as “an electronically excited dimer”, and is non-bonding in the ground state.^{26a} In general, an excimer is a complex formed by the interaction of an excited fluorophore with another fluorophore that is in its ground state. Pyrenes (Py) are one of the most important fluorogenic units due to their efficient excimer formation and emission.^{26b}

1.3.4 Mass spectrometry

Mass spectrometry is a reliable technique for the analysis of non-covalent complexes. This technique gives information about the mass of host-guest complexes, whose components are held together by weak intermolecular forces. Soft ionization mass spectrometry has been used for studying non-covalent complexes for many years.²⁷ The methods include electrospray ionization (ESI) and matrix-assisted laser desorption ionization (MALDI). These methods have been applied with great success in the areas of DNA sequencing, protein and peptide detection, protein folding, *in vitro* drug analysis and drug discovery.²⁷

1.3.5 Single-crystal X-ray diffraction

Single-crystal X-ray diffraction is an important technique for determining the solid-state structure of host-guest complexes. This technique gives important information about host-guest complexation, namely, which atoms are involved, how the atoms or molecules are positioned with respect to each other, and also gives information about individual bond angles and bond lengths in the complex. X-ray diffraction only gives the solid-state information and cannot be used to determine the binding constant.²⁰ An example of the X-ray structure of a ditopic salt receptor **8**, which is complexed with both K^+ and Cl^- is shown in Figure 1.12.²⁸

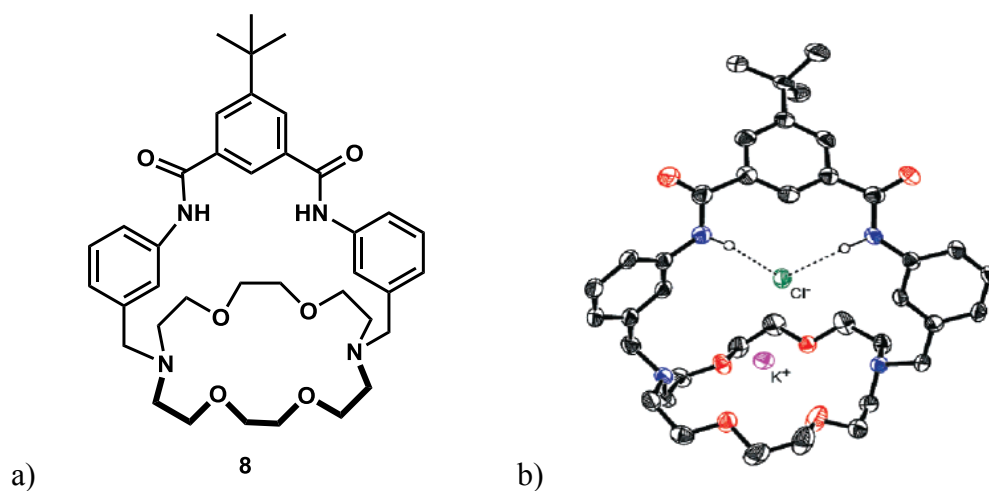


Figure 1.12 (a) Macrocycle **8** (b) X-ray structure of complex **8:KCl**, reprinted with permission from ref 28.

1.3.6 Scanning probe microscopy (SPM)

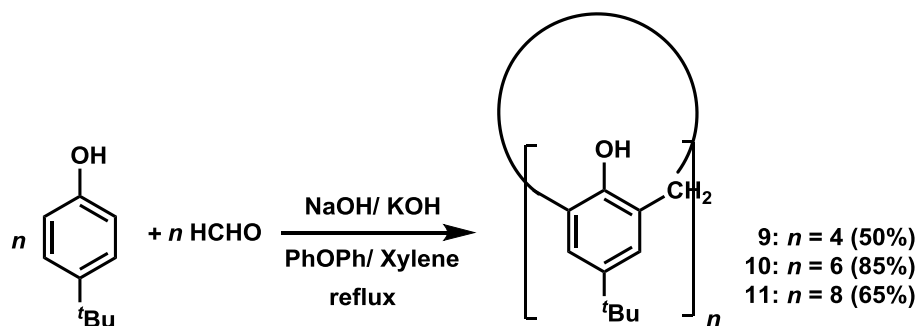
Scanning probe microscopy (SPM) is a branch of microscopy which is used to make images of nanoscale surfaces and also the structure of the molecules. SPMs are a

powerful family of microscopes with nanometer scale resolution. There are different types of SPMs such as scanning tunneling microscopy (STM), atomic force microscopy (AFM) and magnetic force microscopy (MFM), *etc.* These techniques can be employed in the characterization of host-guest complexes self-assembled onto a solid surface.²⁹

1.4 Calixarenes

In 1872, Adolph von Baeyer³⁰ observed a resinous tar formed in the reaction of *p*-*tert*-butylphenol and formaldehyde under basic conditions. Seventy years later, Zinke and Ziegler³¹ noticed the formation of a “resinous tar” which was decomposed above 300 °C. They proposed that the structure of the products formed from the reaction were “cyclic oligomers”, and proposed a tetrameric structure. In the early 1950s, Cornforth *et al.*³² reinvestigated the condensation reaction and they found that the “resinous tar” was a mixture of cyclic oligomers.

In the early 1970s as part of their enzyme catalysts studies, Gutsche *et al.*³³ characterized the cyclic oligomers which were formed from the condensation reaction of *p*-*tert*-butylphenol and paraformaldehyde in the presence of base as a cyclic tetramer, a cyclic hexamer and a cyclic octamer (Scheme 1.01). Gutsche’s group then developed efficient methods for the syntheses of these individual tetrameric, hexameric and octameric compounds, and as a result, these have found widespread and diverse applications.



Scheme 1.01 Gutsche's synthesis of **9-11**.

1.4.1 Nomenclature of calixarenes

According to the Cram and Steinberg nomenclature system, the macrocyclic oligomers **9-11** are classified as " $\text{--[}1_n\text{]metacyclophanes}$ ".³⁴ Based on the Chemical Abstracts system, the basic ring structure of the cyclic tetramer **9** is: " $\text{--[}19.3.1.1\text{]}^{3,7}19,13115,19\text{]octacos-1(25),3,5,7(28),9,11,13(27),15,17,19(26)21,23-dodecaene}$ ".³⁵ The resulting systematic names are very long and are not suitable for writing and communication purposes. Another shorter nomenclature was necessary for these cyclic compounds.

In 1975, Gutsche noticed that the 3-D shape of the tetramer **9** adopted a basket- or bowl-like shape, similar to a type of Greek vase (Figure 1.13) known as a " --calix krater ".³⁶ So he coined the name " --calixarenes " for these compounds. In 1978 the word " --calixarene " first appeared in the literature.^{33a}

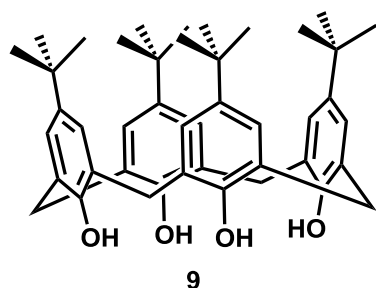


Figure 1.13 Cone conformer of **9** (left) and a calix krater (right).³⁶

The hydrogen bonding between hydroxyl groups in compound **9** forms the narrow rim (also referred to as the “lower rim”) of the bowl. In contrast, the opposite end having aromatic units and their alkyl substituent groups forms the wider rim (also referred to as the “upper rim”) of the bowl and is the hydrophobic binding pocket (Figure 1.14) of the structure.

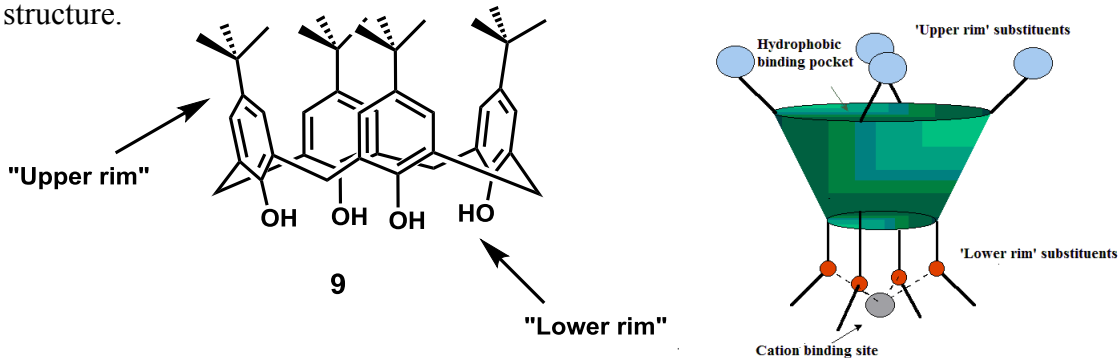


Figure 1.14 Rims defined in calix[4]arene.

Each of these rims can be selectively functionalized. In calix[4]arene the adjacent pairs of phenolic groups are referred to as the “proximal” (1,2) positions while the opposite pair of phenolic groups are referred to as the “distal” or diametrical (1,3) positions.

The different calixarenes can be distinguished by the value of “[*n*]”, and are represented as “calix[*n*]arenes”. The number of aromatic units in the calixarene is

possible rotational mode is known as “*para*-substituent-through-the annulus rotation” and the second possibility is “oxygen-through-the annulus rotation”.³⁸ The four distinct conformers of calix[4]arene were first recognized and defined by Cornforth. The aryl groups orient upward (“*u*”) or downward (“*d*”) relative to an average plane defined by the methylene bridges. Gutsche³⁶ proposed new names for these conformers as follows: *cone* or *crown*; *partial-cone*, *partial-crown* or “*paco*”; *1,2-alternate*, and *1,3-alternate* for the (u,u,u,u); (u,u,u,d); (u,u,d,d); and (u,d,u,d) Cornforth conformers, respectively (Figure 1.16).³²

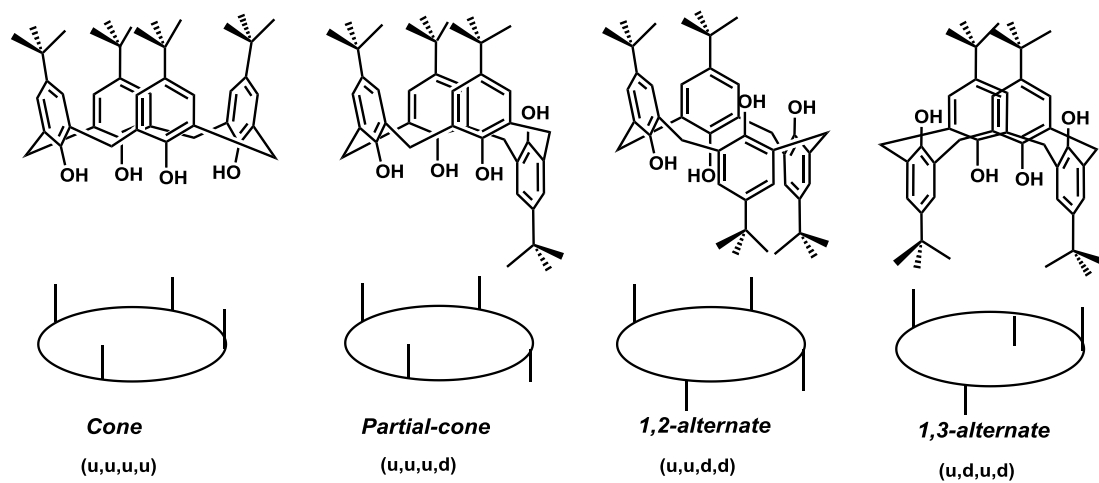


Figure 1.16 Four possible conformers of calix[4]arene.

The cone conformer of *p-tert*-butylcalix[4]arene (**9**) is the thermodynamically most stable one of the possible conformers. The stability of the *cone* conformer can be explained by the intramolecular hydrogen bonding between the hydroxyl groups in the narrow rim of the calixarenes.

These four conformers can be distinguished by the “*de* Mendoza rules” for correlation of both the ¹H- and ¹³C-NMR spectra of the methylene bridges of the

calix[4]arenes.³⁹ Based on these rules, the ¹H-NMR spectrum for the methylene bridges for the *cone* conformer shows an AB system, and the *1,3-alternate* conformer shows a singlet (Figure 1.17). In the case of the *1,2-alternate* and *partial-cone* conformers, a singlet and a pair of doublets can be seen (Figure 1.17). The ¹³C-NMR signals for the methylene bridge carbons appear as one signal at $\delta \approx 30$ ppm when the two aryl groups are *syn* to each other. If the signal appears at $\delta \approx 38$ ppm, this indicates that two adjacent aryl groups are *anti* to each other. Based on these rules, the *cone* and *1,3-alternate* conformers each show only one signal at $\delta \approx 30$ and 38 ppm, respectively. In the case of *partial cone* and *1,2-alternate* conformers, each shows a pair of signals at $\delta \approx 30$ and 38 ppm for their *syn* and *anti* aryl groups respectively (Figure 1.17).^{38,39} The “de Mendoza rule” has been extended to identifying the solution conformations of the calix[5]arenes and calix[6]arenes.

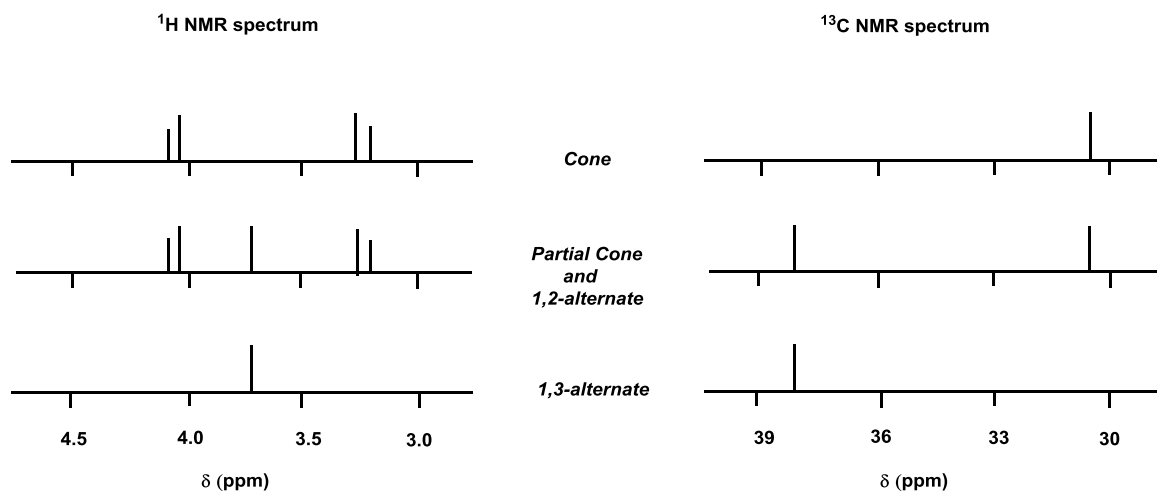


Figure 1.17 ¹H- and ¹³C-NMR spectral patterns of the methylene groups in the calix[4]arene conformers.^{38, 39}

The four conformers of calix[4]arene are interconvertible at ambient temperature. The rate of the interconversion among the four conformers is dependent upon the nature of the solvent. Gutsche⁴⁰ reported that the energy barrier for interconversion is higher in nonpolar solvents such as chloroform, toluene and carbon disulphide than in polar solvents. The inversion barrier of *p-tert*-butylcalix[4]arene is 14.7 kcal/mol in chloroform, while it is 11.8 kcal/mol in pyridine. Pochini⁴¹ found that calix[4]arenes stays in the *cone* conformation at room temperature in chloroform but is conformationally flexible in methanol-*d*₄. The solvent-dependence of the energy barriers is attributed to the disruption of the intramolecular hydrogen bonding between the hydroxyl groups.

A convenient way to control the conformational interconversion is to convert the calix[4]arene to a ether or ester derivatives. McKervey⁴² reported that ether derivatives of *p-tert*-butylcalix[4]arene are stable in the *cone* conformations. In the *tetra-O*-alkylation reaction of *p-tert*-butylcalix[4]arene by ethyl bromoacetate, Shinkai⁴³ found that the metal cation in the basic conditions strongly affects the conformational distribution of the products. When the base contains metal cations like Li⁺, Na⁺, and K⁺, the *cone* conformer products predominates. When the base contains non-templating metal cations such as Cs⁺, the *partial cone* and *1,3-alternate* conformers predominate.

1.4.3 Examples of *lower* and *upper* rim-modified calixarenes

Calix[*n*]arenes have a wide range of applications in supramolecular chemistry (host-guest chemistry). Since calixarenes and their derivatives are macrocyclic compounds possessing a rigid molecular framework and hydrophobic cavity, they can bind with various organic, inorganic or biological molecules such as amino acids. The general strategy used to exploit the important applications of these macrocycles, which include sensing, separation of metal ions and organic molecules, is dependent on the modification of either, or both, the upper- and lower- rims of the parent calixarenes.^{44,45} These types of modifications are reviewed below.

1.4.3.1 *Lower* rim functionalized calixarenes

Since the lower rim of calixarenes have hydroxyl groups, it is possible to introduce a different functionality to these groups. The synthetic method generally involves the introduction of bulky groups by Williamson-type modifications to give corresponding tetraesters, amides, thioamides and ketones. The bases used in these reactions include for example Na₂CO₃, K₂CO₃, NaH and Cs₂CO₃. A convenient method for introducing alkyl groups is treatment of the calixarene with alkyl halides in the presence of sodium hydride in THF-DMF solution. Allyl, methyl, ethyl, and benzyl ethers have been synthesized and reported in high yields.³⁸ By using potassium *tert*-butoxide a series of polyoxyethylene ethers has been reported.⁴⁶ Recent examples of lower rim-functionalized calixarenes are described below:

Rao and co-workers⁴⁷ reported the triazole-linked quinolone-appended calix[4]arene conjugate **14** (Figure 1.18), which shows a larger fluorescence turn-on response with Fe³⁺ ions among seventeen different metal ions which were tested. They also demonstrated the discrimination of Fe³⁺ from Fe²⁺ by using suitable conditions for the oxidation and reduction of the iron, and followed this process by measuring the fluorescence response of **14**. Calix[4]arene **14** can therefore be used as a sensitive and selective turn-on fluorescence sensor for Fe³⁺.

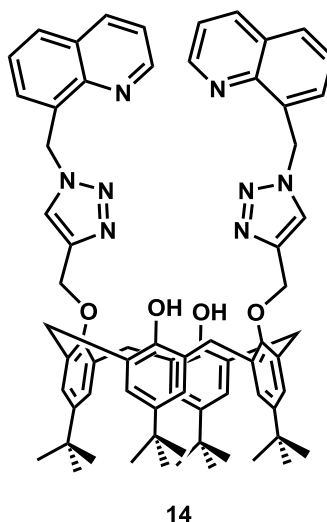
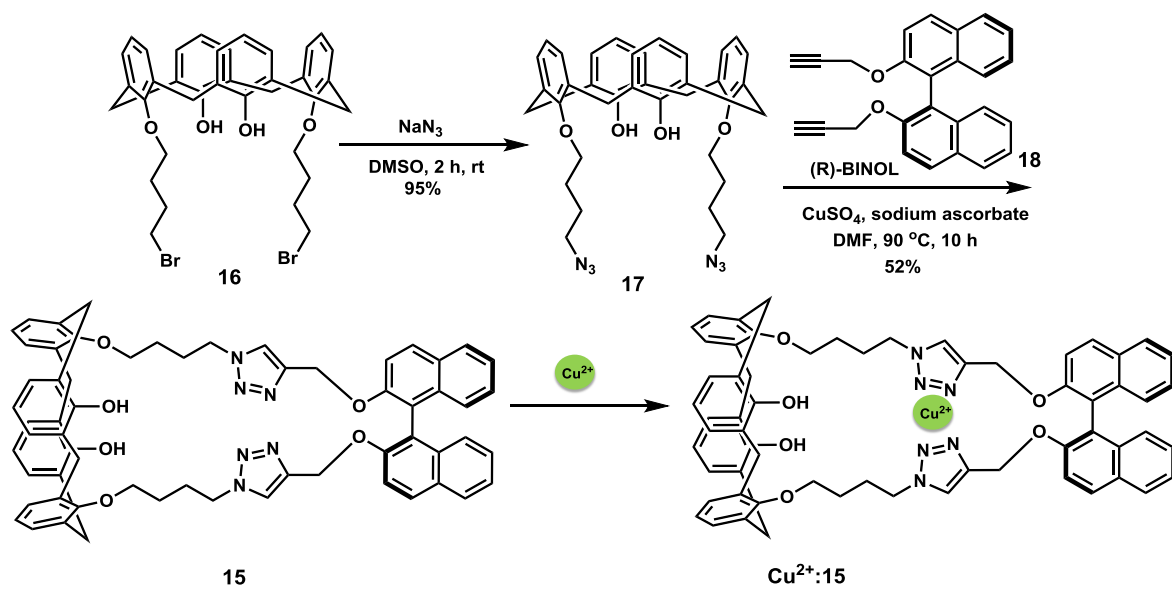


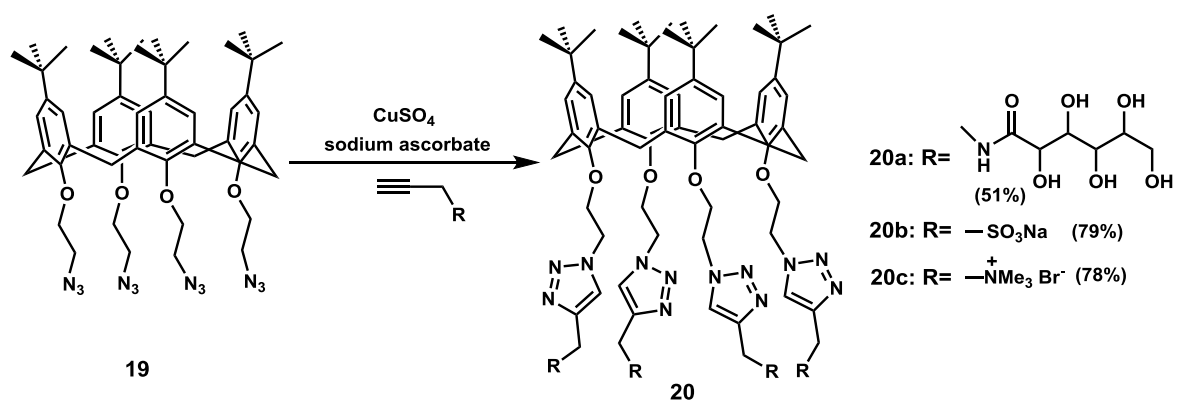
Figure 1.18 Triazole-linked quinoline appended calix[4]arene **14**.

Li's group⁴⁸ synthesized a chiral 1,1'-bi-2-naphthol-linked calix[4]arene **15** via a "click" reaction. Based on fluorescence and dynamic light-scattering studies, Cu²⁺:**15** complexes were generated *in situ* and exhibited excellent enantioselectivity toward mandelic acid. Also, Li reported that the detection sensitivity was improved **100** folds (limit of 2.0 X 10⁻⁷ M) by using a dynamic light-scattering technique (DLS). The synthesis of calix[4]arene **15** is shown in Scheme 1.02.



Scheme 1.02 Synthetic route to **15** and complexation with Cu^{2+} ion.

Several water soluble calix[4]arenes were reported by Ryu and Zhao via the “click” reaction between azides and alkynes (Scheme 1.03).⁴⁹ By using the azidocalixarene intermediate the cationic, anionic and nonionic calixarenes **20a-c** were reported. The aggregation behavior of these water-soluble calixarenes was determined using $^1\text{H-NMR}$ spectroscopy. The coupling reactions between nonpolar azides and water-soluble alkynes gave better results than reactions between non-polar alkynes and water-soluble azides.



Scheme 1.03 Click functionalization of a water-soluble calix[4]arenes.

There is much research being undertaken for developing materials and methods that can treat oil spills in an efficient way. Selective gelation of oil from an oil/water mixture is an important method for oil spill recovery problem. Work reported by the Bhattacharya group⁵⁰ in 2001 showed that an amino acid amphiphile can form phase-selective gelation (PSG) of the oil from oil/water mixtures. PSG is one of the easiest methods for separation of the oil from an oil/water mixture.

Chung's group⁵¹ reported the first example of a bis-calix[4]arene derivative **21** (Figure 1.19) which can form an efficient PSG for a simulated oil spill recovery. The bis-calixarene gelator **21** was synthesized in three steps from commercially-available calix[4]arene. Chung reported that bis-calixarene gelator **21** was not only useful for oil spill recovery but also for metal ion sensing.

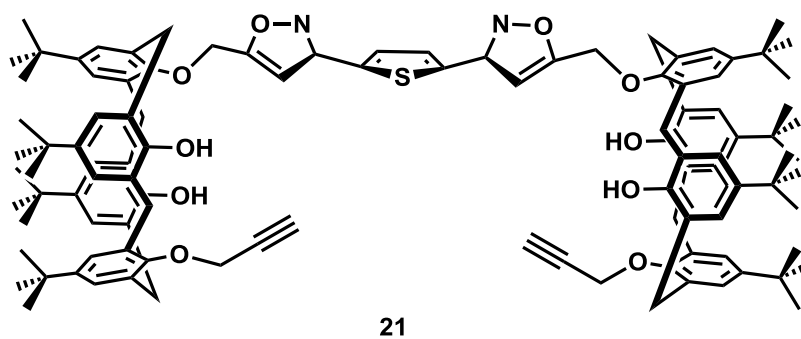


Figure 1.19 Biscalix[4]arene derivative **21**.

1.4.3.2 Upper rim functionalized calixarenes

A variety of functional groups can be introduced to the *para*-position of calix[4]arenes. This can be most conveniently accomplished by first removing the *tert*-butyl groups by using a Lewis acid catalyst such as AlCl_3 . The procedures for introducing new functionality to the de-*tert*-butylated calix[4]arene include electrophilic substitution (acylation, bromination, chlorosulfonation, diazo coupling, iodination, nitration, sulfonation),⁵² Claisen rearrangement of *O*-allyl to *p*-allyl,⁵³ and the Mannich reaction.⁵⁴ Bew and co-workers⁵⁵ reported the synthesis of hybrid calix[4]arenes **22-25** appended on the upper rim, with carbohydrates and *N,C*-protected α -amino acids, via the application of “click” chemistry. The chemoselective cleavage of either the *N*- or *C*-protected α -amino acids efficiently transformed them into the corresponding free multiple amino acids. They also reported the first example of a chemo-enzymatic synthesis of an upper rim-appended sialylated lactose calix[4]arene **25** (Figure 1.20).

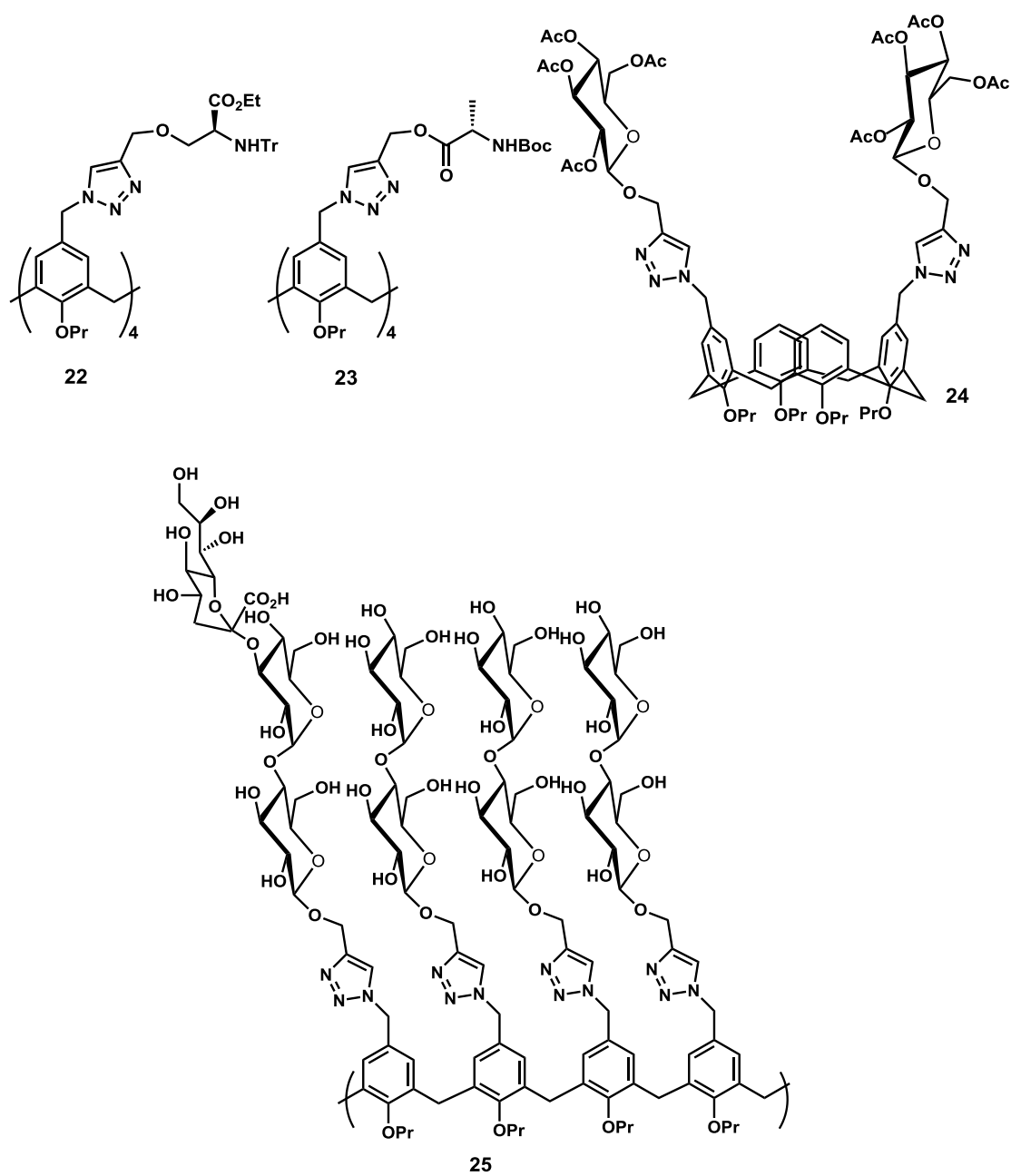


Figure 1.20 Bew and co-workers' hybrid calix[4]arenes.

p-Sulfonatocalix[4]arenes have received much attention due to their ability to bind with biologically-active guests in aqueous solution. Hof and co-workers⁵⁶ recently

reported a new family of desymmetrized trisulfonated calix[4]arenes **26-32** (Figure 1.21). They synthesized sulfonamide and biphenyl-functionalized hosts, each having additional binding elements which could be fine-tuned towards the guest affinities and selectivities. NMR titrations in phosphate-buffered aqueous solutions showed that the biphenyl-functionalized host **28** binds with the highest affinity to trimethyllysine. Trimethyllysine is an important signaling site in proteins that triggers protein-protein interactions.

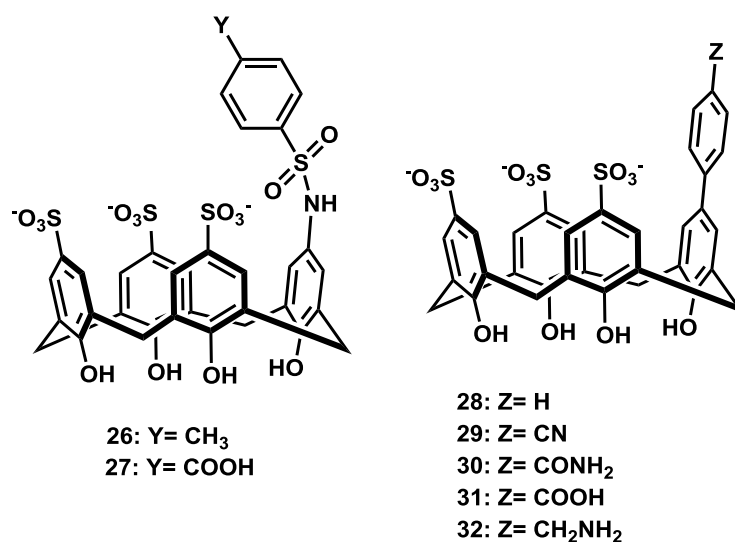


Figure 1.21 Hof and co-workers' trisulfonated calix[4]arene derivatives.

Salvio and co-workers⁵⁷ reported calix[4]arene derivatives functionalized with two- to-four guanidinium units in the upper rim. The guanidinium group has great importance as an anchoring and activating group in hydrolytic reactions and also plays an important role in nature as it is present in many proteins. In the past few years the guanidinium unit has been used in molecular receptors. Guanidinocalixarenes were synthesized for the purpose of binding to negatively-charged substrates through electrostatic interactions. Salvio's group reported the synthesis and catalytic activity of guanidinocalix[4]arenes **33-**

36 in the transesterification of the RNA model compound 2-hydroxypropyl *p*-nitrophenyl phosphate (HPNP) (Figure 1.22). The established mechanism for acid-base catalysis in the cleavage of 2-hydroxypropyl *p*-nitrophenyl phosphate (HPNP), involves the action of neutral and protonated forms of guanidine as shown in Figure 1.23.

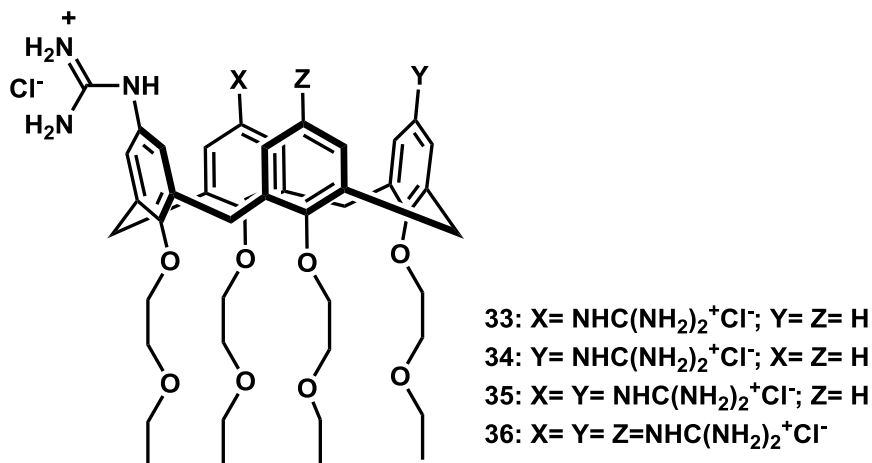


Figure 1.22 Guanidinocalix[4]arene derivatives **33-36**

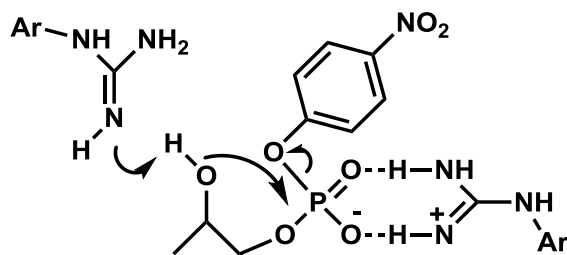


Figure 1.23 General-acid/base catalytic mechanism of HPNP transesterification in *N*-(4-methoxyphenyl) guanidine.

1.5 Calix[4]naphthalenes

In 1993 Georghiou and Li⁵⁸ reported a new class of calixarenes which they named as “calix[4]naphthalenes.” In these types of calixarenes the phenol units were replaced by naphthol units. The calix[4]naphthalenes are a new class of supramolecular hosts having deeper, wider and electron-rich cavities as compared to calix[4]arenes. The three isomeric *exo*-calix[4]naphthalenes **37-39** (Figure 1.24) were synthesized as a mixture in a “one-pot” procedure via the base-mediated condensation of 1-naphthol with formaldehyde.⁵⁸

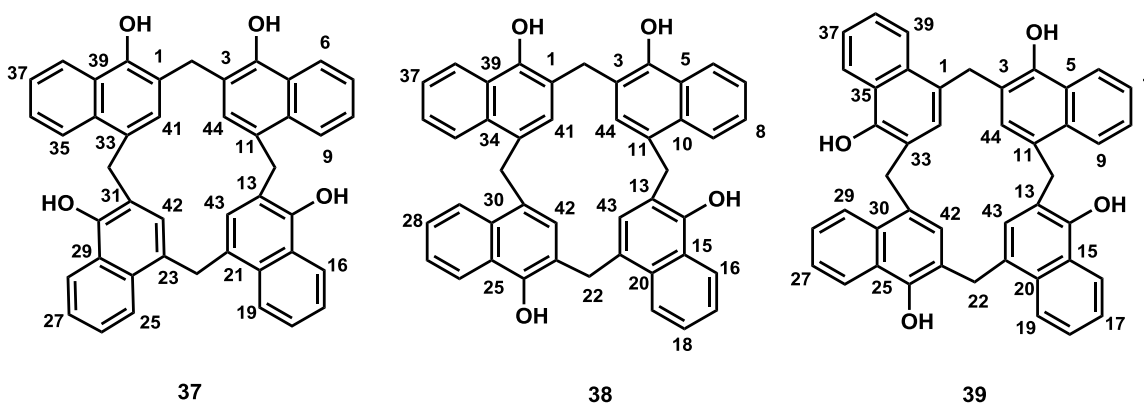
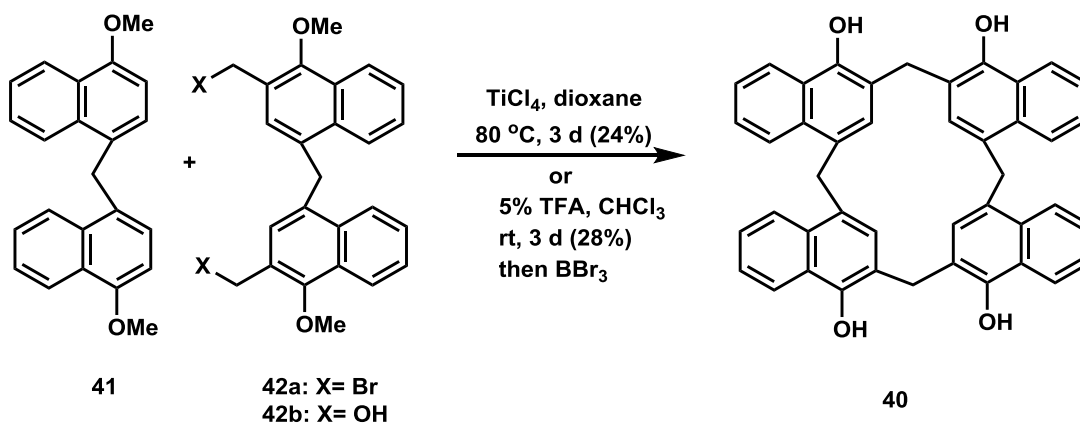


Figure 1.24 Regioisomeric calix[4]naphthalene derivatives **37-39**.

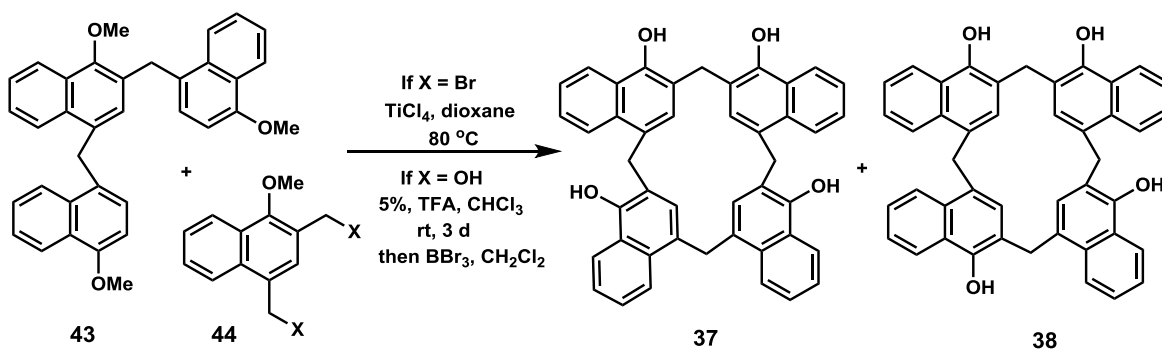
Georghiou and Ashram⁵⁹ later reported the convergent synthesis for all four regioisomeric *exo*-calix[4]naphthalenes by using [2+2] and [3+1] condensation approaches as shown in Schemes 1.04 and 1.05. The [2+2] approach involved the condensation of **41** with bis(bromomethyl)calix[4]naphthalene **42a** or bis(hydroxymethyl)calix[4]naphthalene **42b** using TiCl₄ or 5% TFA in chloroform respectively, to produce

the C_{2v} symmetrical compound **40** (Scheme 1.04).



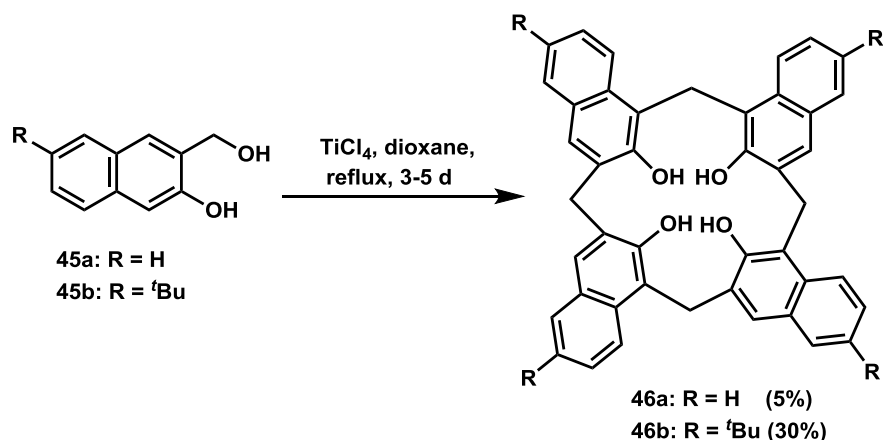
Scheme 1.04 Synthesis of calix[4]naphthalene **40** using a [2+2] condensation approach.

In the case of the [3+1] condensation approach involving the reaction of compound **44** with trimer **43** using TiCl_4 or 5% TFA in chloroform gave a mixture of calix[4]naphthalenes **37** and **38** as shown in Scheme 1.05.



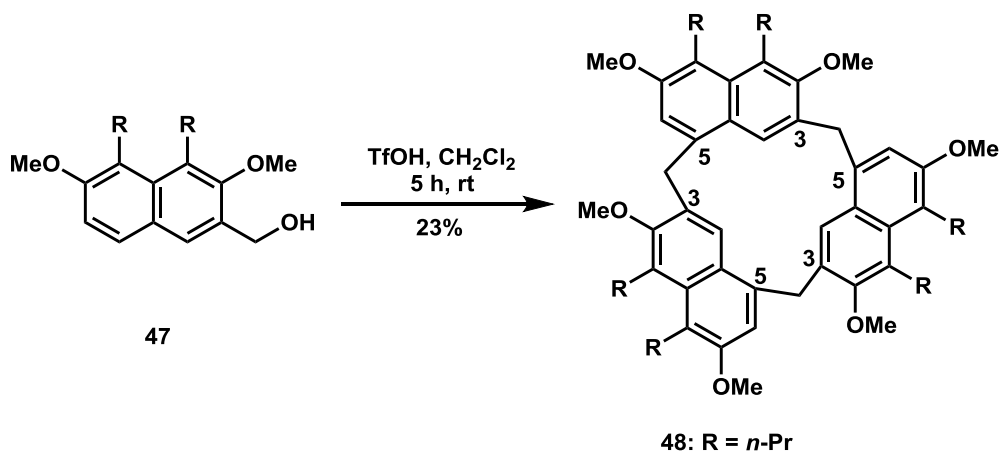
Scheme 1.05 Synthesis of calix[4]naphthalene **37** and **38** using a [3+1] condensation approach.

Endo-calixnaphthalenes are those in which the hydroxyl groups are situated *inside* the cavity in direct analogy with the calix[*n*]arenes described earlier. In 1993, Bohmer and co-workers⁶⁰ reported the synthesis of calix[4]naphthalene **46a** (Scheme 1.06) from 3-hydroxymethyl-2-naphthol **45a** via TiCl₄-mediated self-condensation in 1,4-dioxane. Using similar conditions, Georghiou and co-workers⁶¹ reported the *tert*-butylated *endo*-calix[4]naphthalene **46b** in yields of 30% (Scheme 1.06) from 6-*tert*-butyl-3-hydroxymethyl-2-naphthol **45b**.

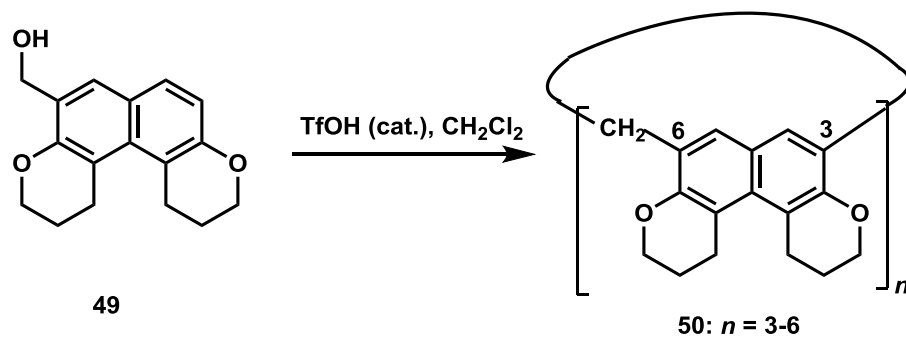


Scheme 1.06 Synthesis of calix[4]naphthalene **45a** and **45b** self-condensation approach.

Glass *et al.* reported⁶² the synthesis of “-3,5-linked” calix[3]naphthalene **48** derived from **47** (Scheme 1.07) and the “-3,6-linked” calix[*n*]naphthalenes (*n* = 3-6) oligomers **50** which were obtained via the triflic acid self-cyclocondensation reaction of hydroxymethyl compound **49** (Scheme 1.08).

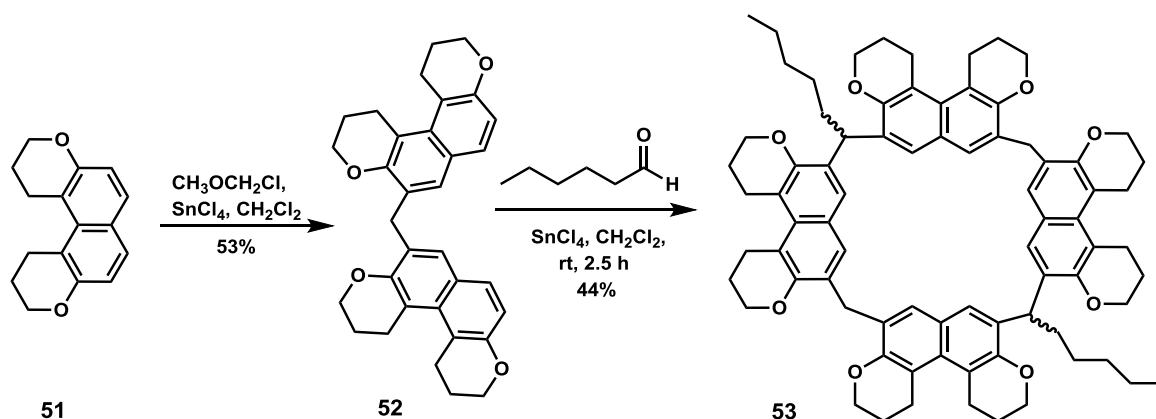


Scheme 1.07 Synthesis of “3,5-linked” calix[4]naphthalene **48**.



Scheme 1.08 Synthesis of “3,6-linked” calix[4]naphthalene **50**.

Glass *et al.* also reported a mixture of *cis/trans* isomers (1:1.2) of the 3,6-linked-calix[4]naphthalene **53**, which involves a [2+2] SnCl₄-catalyzed cyclocondensation-cyclodimerization of **52** with hexanal in dichloromethane (Scheme 1.09).



Scheme 1.09 Synthesis of “3,6-linked” calix[4]naphthalene **53**.

1.5.1 Homocalixarenes

Homocalixarenes are a class of calixarenes in which the methylene bridges are replaced by ethylene or a larger bridging group e.g. **54**.^{36,63} The modification of these calixarenes increases the size of the annulus and many complexation studies have been reported with several guest cations like transition metal ions, uranyl ion, alkali and alkaline earth metal ions.^{36,63,64} The Georghiou group⁶⁵ reported the new di-homocalix[4]naphthalene e.g. **55** in which one or more of the methylene bridges are replaced by ethylene bridges, as shown in Figure 1.25.

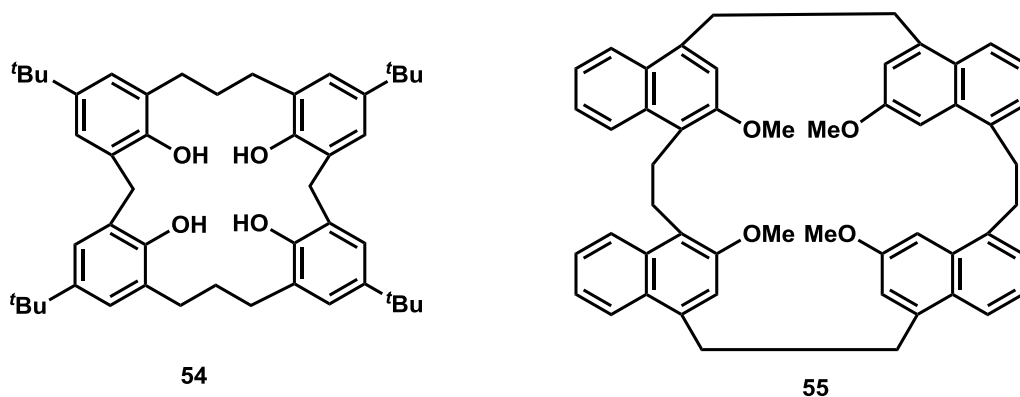


Figure 1.25 Some examples of homocalix[4]arene and calix[4]naphthalenes.

1.5.2 Homooxacalixnaphthalenes

Georghiou and Al-Hujran later reported⁶⁶ a new class of homooxacalixarenes which are derivatives of acenaphthene. Acenaphthene **56** is a polycyclic aromatic hydrocarbon which is a known constituent of coal tar and it consists of a naphthalene ring with the C-1 and C-10 *peri*-positions connected by an ethylene bridge. The synthesis of 5,6-dialkoxyethers (**56a-b**) of acenaphthene **56** has been reported for the first time under modified Ullmann reaction conditions. Subsequent conversions of **56a** formed **57** and **57a** which, via Williamson ether [2+2] coupling reaction formed macrocyclic homooxacalix[4]naphthalene **58**. The macrocycle **58** forms a 1:1 complex with C₆₀ fullerene in toluene-*d*₈ (Figure 1.26).

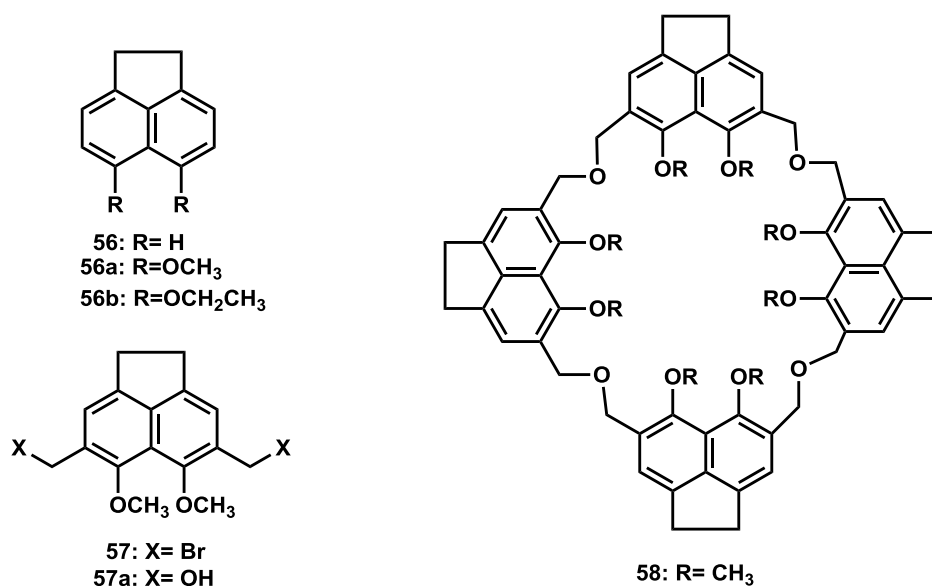


Figure 1.26 Homooxacalix[4]naphthalene **58**.

The Georghiou group has also reported^{59,61,65,66,67} different types of calix[4]naphthalenes from various subunits such as 1-naphthol, 2-naphthol, 1,8-naphthalene sultone, 3-hydroxy-2-naphthoic acid and 2,3-dihydroxynaphthalene.

1.6 Outline of the thesis

This Ph.D thesis focuses on four major projects which involve the synthesis and characterization of bimodal calix[4]arene and calix[4]naphthalene derivatives and their applications. Details of individual chapters are summarized below.

Chapter 2 focuses on the synthesis of some selected upper- and lower-rim functionalized calix[4]arene derivatives. The lower rim of the calixarene derivatives are modified with methyl and ethyl ester moieties which selectively bind to Group 2 ions. The upper rim of the calix[4]arene derivatives were further functionalized with thioacetate groups which allowed the calixarene to bind to gold (Au)-coated

microcantilevers. The gold-coated microcantilever sensor and scanning tunneling microscopy (STM) work is currently ongoing in collaboration with L.Y. Beaulieu's group in the Department of Physics and Physical Oceanography at Memorial University. Chapter 2 also includes a report of a new bimodal calix[4]arene-crown-5 derivative. The lower rim of the calixarene is functionalized with two different groups, one of which is a 1,3 bridged crown-5, and the other two positions have thioacetate groups. The thioacetate group enables the calixarene to form a stable self-assembled monolayer (SAM) onto the Au surface of a microcantilever, and the resulting SAM has been characterized by STM. The crown-5 group selectively binds to Group 1 (alkali metal) ions. Complexation studies of these new calixarene receptors with different metal ions were investigated by ^1H -NMR spectroscopy, and the binding constants for the complexes were determined. The ^1H -NMR experiments reveals which protons were most affected in the complex formation.

Chapter 3 focuses on the synthesis and applications of a new triazole-bridged anthracene-appended calix[4]arene derivative. The upper rim of the calix[4]arene was functionalized with a thioacetate functional group and the lower rim was functionalized with a triazole (as ionophore)-bridged anthracene fluorophore. A fluorescent chemosensor generally includes two components, one being an ion recognition unit (ionophore) and other being a fluorogenic unit (fluorophore). The synthetic strategy involved a "click" reaction as the key step. The complexation studies and association/binding constants of this new receptor with different metal ions were investigated by UV-vis, fluorescence and ^1H -NMR spectroscopic techniques. Chapter 3 also includes the synthesis and applications of another fluorescent chemosensor, a

triazole-bridged pyrene-appended calix[4]arene in a collaborative project with G. J. Bodwell's group at Memorial University. Using this receptor complexation studies were undertaken with various metal ions including the association/binding constants for the complexes. Metal ion competitive experiments were also investigated. Complexations of these two receptors with different metal ions were studied using ¹H-NMR and fluorescence techniques. The results of this project highlights the fact that these new triazole-bridged anthracene/pyrene appended calix[4]arene derivatives are effective fluorescent chemosensors.

Chapter 4 mainly focuses on the synthesis and applications toward selective metal ion recognition by new calix[4]arene-NHC derivatives. The lower rim of the calix[4]arene was functionalized with two different groups, one of which consists of a 1,3 bridged crown-5 and the other 1,3 positions with imidazole group. The generation of the carbenes from the corresponding imidazoles was conducted using Crudden's⁶⁸ methodology, and the resulting NHC enables the calix[4]arene to form a stable SAM onto the Au surface of microcantilever. In addition to the solid Au surface study of this modified calix[4]arene, studies were undertaken to form AuNPs.

Chapter 5 focuses on the synthesis and applications of some sulfonated calix[4]naphthalene derivatives. The three calix[4]naphthalenes that were synthesized and studied were *peri*-sulfonatocalix[4]naphthalene, oxacalix[4]naphthalenesultone and cyclotetrachromotropyrene. In another collaborative project with A. Coleman's group at the University of Lyon, these naphthalene derivatives were shown to be capable of capping and stabilizing silver nanoparticles and also to possess molecular recognition

properties with nucleobases and certain amino acids. Along with these properties, cyclotetrachromotropyene (–CTCT”) which was first reported by Poh and co-workers⁶⁹ was characterized and shown to be capable of selectively dispersing SWNTs into water. The resulting supramolecular complexes in a collaborative project with Y. Zhao’s group at Memorial University and A. Adronov’s group at McMaster University were characterized by UV-Vis-NIR analysis. The dried aggregates were examined by Raman spectroscopy and Atomic Force Microscopy (AFM). The results of this project highlighted the diverse properties of these calix[4]naphthalenes.

1.7 References

1. (a) Lehn, J.-M. (Nobel Lecture) *Angew. Chem., Int. Ed. Engl.* **1988**, *27*, 89-112.
(b) Atwood, J. L.; Davies, J. E. D.; MacNicol, D. D.; Vögtle, F.; Lehn, J.-M., *Comprehensive Supramolecular Chemistry*, Pergamon Press, Oxford, UK, 1996.
2. Lehn, J.-M. *Science* **1993**, *260*, 1762-1763.
3. Lehn, J.-M. *Supramolecular Chemistry*, 1st ed.; VCH, Weinheim, 1995.
4. Villiers A. *Compt. Rend. Fr. Acad. Sci.* **1891**, 435-438.
5. Werner, A. *Anorg. Chem.* **1893**, *3*, 267-330.
6. (a) Fischer, E. *Ber. Dtsch. Chem. Ges.* **1894**, *27*, 2985-2993. (b) Koshland, D. E. *Angew. Chem., Int. Ed. Engl.* **1994**, *33*, 2375-2378.
7. (a) Ehrlich, P. *Lancet* **1913**, *2*, 445–451. (b) Klotz, I. M. *Ligand-Receptor Energetics*, John Wiley and Sons, Inc., New York, 1997.

8. Wolf, K. L.; Frahm, H.; Harms, H. *Z. Phys. Chem., Abt. B.* **1937**, *36*, 237–287.
9. (a) Pedersen, C. J. *J. Am. Chem. Soc.* **1967**, *89*, 7017-7036. (b) Pedersen, C. J. (Nobel Lecture) *Angew. Chem., Int. Ed. Engl.* **1988**, *27*, 1021-1027.
10. Lehn, J.-M. *Angew. Chem., Int. Ed. Engl.* **1990**, *29*, 1304-1319.
11. Cram, D. J. (Nobel Lecture) *Angew. Chem., Int. Ed. Engl.* **1988**, *27*, 1009-1020.
12. Raymo, F. M.; Stoddart, J. F. *Chem. Rev.* **1999**, *99*, 1643-1663.
13. (a) Steed, J. W.; Atwood, J. L. *Supramolecular Chemistry*, Wiley VCH: Weinheim, Germany, 2009. (b) Jeffery, G. A. *An Introduction to Hydrogen Bonding*, Oxford University Press, Oxford, UK, 1997. (c) Supramolecular hosts for pristine fullerenes- Georghiou, P. E. In *"Handbook of Carbon Nano Materials Volume 1. Syntheses and Supramolecular Systems"* D'Souza, F.; Kadish, K. M. Eds., World Scientific Publishers, Singapore, **2011**.
14. (a) Ma, J. C.; Dougherty, D. *Chem. Rev.* **1997**, *97*, 1303-1324. (b) Muller-Dethlefs, K.; Hobza, P. *Chem. Rev.* **2002**, *100*, 143-167.
15. (a) Berryman, O. B.; Bryantsev, V. S.; Stay, D. P.; Johnson, D. W.; Hay, B. P. *J. Am. Chem. Soc.* **2007**, *129*, 48-58. (b) Rosokha, Y. S.; Lindeman, S. V.; Rosokha, S. V.; Kochi, J. K. *Angew. Chem., Int. Ed.* **2004**, *43*, 4650-4652. (c) Schottel, B. L.; Chifotides, H. T.; Shatruk, M. *J. Am. Chem. Soc.* **2006**, *128*, 5895-5912.
16. Sinnokrot, M. O.; Valeev, E. F.; Sherril, C. D. *J. Am. Chem. Soc.* **2002**, *124*, 10887-10893.

17. Garratt, P. J.; Ibbett, A. J.; Ledbury, J. E.; Brien, R.; Hursthouse, M. B.; Malik, K. M. A. *Tetrahedron* **1998**, *54*, 949-968.
18. Enright, G. D.; Brouwer, E. B.; Udachin, K. A.; Ratcliffe, C. I.; Ripmeester, J. A. *Acta. Cryst.* **2002**, B58, 1032-1035.
19. Steed, J. W.; Turner, D. R.; Wallace, K. J. *Core Concepts in Supramolecular Chemistry and Nanochemistry*, John Wiley & Sons Ltd, Oxford, England, 2007.
20. Schneider, H. J.; Yatsimirsky, A. K. *Principles and Methods in Supramolecular Chemistry*, John Wiley & Sons Ltd, Chichester, 2000.
21. Lakowics, J. R. *Principles of Fluorescence Spectroscopy*, Springer, Maryland, USA, 2006.
22. (a) Yang, X.-F.; Guo, X.-Q.; Zhao, Y.-B. *Talanta* **2002**, *57*, 883-890. (b) Anslyn, E. V. *J. Org. Chem.* **2007**, *72*, 687-699. (c) Bell, T. W.; Hext, N. M. *Chem. Soc. Rev.* **2004**, *33*, 589-598.
23. Davidson, R. S. *Adv. Phys. Org. Chem.* **1983**, *19*, 1-130.
24. (a) de Silva, A. P.; Moody, T. S.; Wright, G. D. *Analyst* **2009**, *134*, 2385-2393. (b) de Silva, A. P.; Gunaratne, H. Q.; Gunnlaugsson, T.; Huxley, A. J.; McCoy, C. P.; Rademacher, J. T.; Rice, T. E. *Chem. Rev.* **1997**, *97*, 1515-1566.
25. Zhao, G.-J.; Chen, R.-K.; Sun, M.-T.; Liu, J.-Y.; Li, G.-Y.; Gao, Y.-L.; Han, K.-L.; Yang, X.-C.; Sun, L. *Chem. Eur. J.* **2008**, *14*, 6935-6947.

26. (a) Nic, M.; Jirat, J.; Kosata, B. *IUPAC Gold Book*, International Union of Pure and Applied Chemistry, Prague, 2005. (b) Briks, J. B. *Photophysics of Aromatic Molecules*; John Wiley: New York, 1970.
27. Daniel, J. M.; Friess, S. D.; Rajagopalan, S.; Wendt, S.; Zenobi, R. *Int. J. Mass Spectrom.* **2002**, *216*, 1-27.
28. Mahoney, J. M.; Beatty, A. M.; Smith, B. D. *J. Am. Chem. Soc.* **2001**, *123*, 5847-5848.
29. Pan, G.; Bu, J.; Wang, D.; Liu, J.; Wan, L.; Zheng, Q.; Bai, C. *J. Phys. Chem. B.* **2003**, *107*, 13111-13116.
30. Baeyer, A. V. *Ber. Dtsch. Chem. Ges.* **1872**, *5*, 1094-1100.
31. (a) Zinke, A.; Ziegler, E. *Ber. Dtsch. Chem. Ges.* **1944**, *77*, 264-272. (b) Zinke, A.; Ziegler, E. *Ber. Dtsch. Chem. Ges.* **1941**, *74*, 1729-1736.
32. Cornforth, J. W.; D'Arcy Hart, P.; Nicholls, G. A.; Rees, R. J. W.; Stock, J. A. *J. Pharmacol.* **1955**, *10*, 73-86.
33. (a) Gutsche, C. D.; Muthukrishnan, R. *J. Org. Chem.* **1978**, *43*, 4905-4906. (b) Muthukrishnan, R.; Gutsche, C. D. *J. Org. Chem.* **1979**, *44*, 3962-3964 (c) Gutsche, C. D.; Dhawan, B.; No, K. H.; Muthukrishnan, R. *J. Am. Chem. Soc.* **1981**, *103*, 3782-3792. (d) Gutsche, C. D.; Iqbal, M.; Stewart, D. *J. Org. Chem.* **1986**, *51*, 742-745.
34. Cram, D. J.; Steinberg, H. *J. Am. Chem. Soc.* **1951**, *73*, 5691-5704.

35. Patterson, A. M.; Capell, L. T.; Walker, D. F. *The Ring Index*, 2nd ed.; American Chemical Society, Washington D. C., **1960**, Ring index No. 6485.
36. Gutsche, C. D. *Calixarenes, Monographs in Supramolecular Chemistry*; Stoddart, J. F., Ed.; The Royal Society of Chemistry, Cambridge, 1989.
37. Dodziuk, H. *Introduction to Supramolecular Chemistry*. Kluver Academic Publishers, Hingham, MA, USA, 2001, p. 102.
38. Gutsche, C. D.; Dhawan, B.; Levine, J. A.; No, K. H.; Bauer, L. J. *Tetrahedron* **1983**, *39*, 409-426.
39. Jaime, C.; de Mendoza, J.; Prados, P. D.; Sanchez, C. *J. Org. Chem.* **1991**, *56*, 3372-3376.
40. Gutsche, C. D.; Bauer, L. J. *J. Am. Chem. Soc.* **1985**, *107*, 6052-6059.
41. Arduini, A.; Fabbi, M.; Mantovani, M.; Mirone, L.; Pochini, A.; Secchi, A.; Ungaro, R. *J. Org. Chem.* **1995**, *60*, 1454-1457.
42. McKerverey, M. A.; Seward, E. M.; Ferguson, G.; Ruhl, B. L. *J. Org. Chem.* **1986**, *51*, 3581-3584.
43. Iwamoto, K.; Shinkai, S. *J. Org. Chem.* **1992**, *57*, 7066-7073.
44. (a) Ji, H.-F.; Finot, E.; Dabestani, R.; Thundat, T.; Brown, G. M.; Britt, P. F. *Chem. Commun.* **2000**, 457-458. (b) Zhang, S.; Song, F.; Echegoyan, L. *Eur. J. Org. Chem.* **2004**, 2936-2943.

45. (a) Evans, C. J.; Nicholson, G. P. *Sens. Actuators B* **2005**, *105*, 204-207. (b) Joseph, R.; Rao, C. P. *Chem. Rev.* **2011**, *111*, 4658-4702.
46. Cornforth, J. W.; Morgan, E. D.; Potts, K. T.; Ress, R. J. W. *Tetrahedron* **1973**, *29*, 1659-1662.
47. Pathak, R. K.; Dessingou, J.; Hinge, V. K.; Thawari, A. G.; Basu, S. K.; Rao, C. P. *Anal. Chem.* **2013**, *85*, 3707-3714.
48. Miao, F.; Zhou, J.; Tian, D.; Li, H. *Org. Lett.* **2012**, *14*, 3572-3575.
49. Ryu, E.-H.; Zhao, Y. *Org. Lett.* **2005**, *7*, 1035-1037.
50. Bhattacharya, S.; Krishnan-Ghosh, Y. *Chem. Commun.* **2001**, 185-186.
51. Tsai, C.-C.; Cheng, Y.-T.; Shen, L.-C.; Chang, K.-C.; Ho, I.-T.; Chu, J.-H.; Chung, W.-S. *Org. Lett.* **2013**, *15*, 5830-5833.
52. (a) Gutsche, C. D.; Pagoria, P. F. *J. Org. Chem.* **1985**, *50*, 5795-5802. (b) Arduini, A.; Pochini, A.; Sicuri, A. R.; Secchi, A.; Ungaro, R. *Tetrahedron*. **1990**, *31*, 4653-4670. (c) Shinkai, S.; Tsubaki, T.; Sone, T.; Manabe, O. *Tetrahedron Lett.* **1985**, *26*, 3343-3346. (d) Morzherin, Y.; Rudkevich, D. M.; Veboom, W.; Reinhoudt, D. N. *J. Org. Chem.* **1993**, *58*, 7602-7605. (e) Gutsche, C. D.; Lin, L. G. *Tetrahedron* **1986**, *41*, 1633-1640.
53. Gutsche, C. D.; Levine, A.; Sujeeth, P. J. *J. Org. Chem.* **1985**, *50*, 5802-5806.
54. Gutsche, C. D.; Nam, K. C. *J. Am. Chem. Soc.* **1988**, *110*, 6153-6162.

55. Bew, S. P.; Brimage, R. A.; Hermite, N. L.; Sharma, S. V. *Org. Lett.* **2007**, *9*, 3713-3716.
56. Daze, K. D.; Ma, M. C. F.; Pineux, F.; Hof, F. *Org. Lett.* **2012**, *14*, 1512-1515.
57. Baldini, L.; Cacciapaglia, R.; Casnati, A.; Mandolini, L.; Salvio, R.; Sansone, F.; Ungaro, R. *J. Org. Chem.* **2012**, *77*, 3381-3389.
58. (a) Georghiou, P. E.; Li, Z. *Tetrahedron Lett.* **1993**, *34*, 2887-2889. (b) Georghiou, P. E.; Li, Z. *J. Incl. Phenom. Mol. Recognit. Chem.* **1994**, *19*, 55-66.
59. Georghiou, P. E.; Ashram, M.; Li, Z.; Chaulk, S. G. *J. Org. Chem.* **1995**, *60*, 7284-7289.
60. Andretti, G. D.; Bohmer, V.; Jordon, J. G.; Tabatabai, M.; Ugozzoli, F.; Vogt, W.; Wolff, W. *J. Org. Chem.* **1993**, *58*, 4023-4032.
61. Georghiou, P. E.; Ashram, M.; Clase, H. J.; Bridson, J. N. *J. Org. Chem.* **1998**, *63*, 1819-1826.
62. (a) Shorthill, B. J.; Granucci, R. G.; Powell, D. R.; Glass, T. E. *J. Org. Chem.* **2002**, *67*, 904-909. (b) Shorthill, B. J.; Glass, T. E. *Org. Lett.* **2001**, *3*, 577-579.
63. (a) Brodesser, G.; Vögtle, F. *J. Incl. Phenom. Mol. Recognit. Chem.* **1994**, *19*, 111-135. (b) Schmitz, J.; Vögtle, F.; Nieger, M.; Gloe, K.; Stephen, H.; Heitzsch, O.; Buschmann, H.-J.; Hass, W.; Cammann, K. *Chem. Ber.* **1993**, *126*, 2483-2491. (c) Ibach, S.; Prautzsch, V.; Vögtle, F.; Chartroux, C.; Gloe, K. *Acc. Chem. Res.* **1999**, *32*, 729-740.

64. (a) Yamato, T. *J. Incl. Phenom. Mol. Recognit. Chem.* **1998**, *32*, 195-207. (b) Yamato, T.; Iwasa, T.; Zhang, F. *J. Incl. Phenom. Macro. Chem.* **2001**, *39*, 285-294. (c) Yamato, T.; Saruwatari, Y.; Yasumatsu, M.; Tsuzuki, H. *New. J. Chem.* **1998**, 1351-1358.
65. (a) Ashram, M. , PhD Dissertation. Memorial University of Newfoundland, 1997. (b) Georghiou, P. E.; Ashram, M.; Miller, D. O. *J. Org. Chem.* **1996**, *61*, 3865-3869.
66. Al-Hujran, T. A.; Dawe, L. N.; Georghiou, P. E. *Org. Lett.* **2012**, *14*, 3530-3533.
67. (a) Chowdhury, S. PhD Dissertation., Memorial University of Newfoundland, 2001. (b) Georghiou, P. E.; Li, Z.; Ashram, M.; Miller, D. O. *J. Org. Chem.* **1996**, *61*, 3865-3869.
68. Crudden, M. C.; Horton, H. J.; Ebralidze, I.; Zenkina, O. V.; McLean, A. B.; Drevniok, B.; She. Z.; Kraatz, H-B.; Mosey, N. J. Seki, T.; Keske, E. C.; Leake, J. D.; Rousina-Webb, A.; Wu, G. *Nat. Chem.* **2014**, *6*, 409-414.
69. Poh, B.-L.; Lim, C. S.; Khoo, K. S.; *Tetrahedron Lett.* **1989**, *30*, 1005-1008.

Chapter 2

Synthesis and applications of new bimodal

upper and lower rim-functionalized calix[4]arenes

2.1 Introduction

Along with other macrocyclic compounds such as cyclotrimeratrylenes, cyclodextrins and resorcinarenes, calix[n]arenes are widely studied chemical entities in supramolecular chemistry.¹ Calixarenes have served as building blocks in supramolecular structures and have also been involved in the design of enzyme models, catalysts and sensors, *etc.*² Efficient syntheses of the classical calix[n]arenes ($n = 4, 6$ or 8), having 4, 6 or 8 phenolic rings bridged by the same number of methylene units have been developed largely by the pioneering work of Gutsche and co-workers.³ The lower and upper rims of calixarenes can be modified to produce a vast number of derivatives, many of which have been used in molecular recognition studies with a variety of guest molecules such as cationic, anionic and neutral species.²

Calix[n]arenes have been used in complexation studies with different metal ions as well as in the extraction and detection of toxic metals from waste water, an application of great importance for environmental monitoring and protection. The binding of cesium ions with calixarene-crown derivatives is especially important for the removal of radioactive cesium from nuclear waste.⁴ Calix[n]arene derivatives can non-covalently bond with metal ions, fullerenes and drugs, and covalently with carbohydrates,

porphyrins and nucleobases.^{2,5} Recently, a great deal of attention has been directed towards host-guest sensing using calix[*n*]arenes on solid surfaces.⁶ Modification of either or both rims allows calixarenes to be anchored to various substrates and form highly-ordered self-assembled monolayers (SAMs) on solid surfaces.

Several review articles have focused on the supramolecular chemistry of calix[*n*]arenes, along with their ability involved in self-assembly processes. Self-assembled monolayers of thiols (and other sulfur-based head group-containing compounds like thioacetates, dithiols and disulfides) on gold (Au) surfaces are popular due to their wide range of applications in nanotechnology.

2.2 Self-assembled monolayers of thiols on gold surfaces

SAMs, in which intermolecular forces play an important role, are molecular assemblies formed spontaneously on solid surfaces or interfaces by adsorption.⁷ In the process of self-assembly in general, subunits such as atoms, molecules and biological structures. Combine in a way that secondary or more complex structures with lower degrees of freedom are formed.⁷ Each molecule in a SAM can be divided into three different parts: the head group (linker group), the backbone (main chain), and the specific terminal group (active group) (Figure 2.01). SAMs can be formed not only on planar surfaces but also on curved surfaces.

SAMs have been studied by different surface analysis techniques including: surface probe microscopies (mainly atomic force microscopy (AFM) and scanning tunneling microscopy (STM)), diffraction techniques like X-ray diffraction (XRD), grazing

incidence X-ray diffraction (GIXD), X-ray photoelectron diffraction (XPD), vibrational spectroscopies such as infrared (IR) spectroscopy, sum frequency generation (SFG), Fourier transform infrared (FTIR) spectroscopy, infrared reflection/absorption spectroscopy (IRRAS), Raman spectroscopy, electron-based spectroscopies such as X-ray photoelectron spectroscopy (XPS), auger electron spectroscopy (AES), Ultraviolet photoelectron spectroscopy (UPS), extended X-ray absorption fine structure (EXAFS), X-ray absorption of near-edge structure (XANES), ion-based spectroscopies such as ion scattering spectroscopy (ISS) and time-of-flight direct recoil spectroscopy (TOF-DRS). Other techniques include ellipsometry, temperature programmed desorption (TPD) and also electrochemical techniques *etc.*^{7,8} Using these techniques a wide variety of SAMs on different surfaces have been studied and reported in the literature. SAMs have been formed from a variety of compounds, including fatty acids, trialkoxysilanes and trichlorosilanes on silicon and glass, and alkyl phosphates and carboxylic acids on metal oxides.⁷

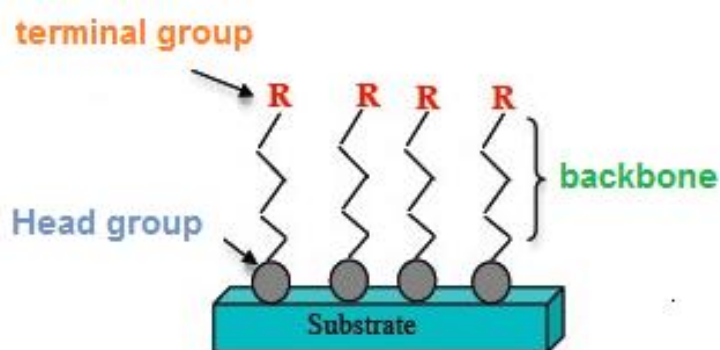


Figure 2.01 Representation of a self-assembled monolayer (SAM) structure.

SAMs of thiols on Au surfaces are particularly attractive due to their relative ease of preparation from solution or gas phase, and also the strength of the S-Au bond. These monolayers are stable under ambient conditions and also exhibit molecular order.⁷ In 1983 Nuzzo and Allara reported the first sulfur-based SAMs on gold surfaces.⁹ Thiol SAMs on gold have been studied extensively with all existing surface techniques. Many reviews and papers have been published focusing on different aspects of thiol SAMs, which describe their adsorption/desorption kinetics, electronic properties, charge-transfer and also other applications.^{7,10} Some applications of thiol SAMs on gold surfaces include their use in device fabrication, as inks or resists in lithography, and in molecular machines, in sensors and biosensors *etc.*⁷ Also, thiol SAMs can be used in the synthesis of gold nanoparticles for stabilizing nanostructures against aggregation, and by tuning the hydrocarbon chain length (back bone), it is possible to control the cluster size.¹¹ Thiol molecules can also self-assemble on different metallic surfaces like silver (Ag), palladium (Pd), copper (Cu), nickel (Ni), platinum (Pt) and iron (Fe).^{7,10} SAMs on gold surfaces with of thiol and disulfide functionalized calix[*n*]arenes have been reported (Figures 2.02-2.08).

2.2.1 Cation sensors

The use of supramolecular chemistry as a tool for cation recognition was first reported by C. J. Pedersen in 1967.¹² Since then there has been a rapid progress in supramolecular cation recognition using a broad range of cyclic and acyclic multidentate receptors. An example of a gold-supported calixarene cationic sensor is that of Koh's group¹³ who reported the SAM of a calix[4]crown-5 derivative on a gold surface (Figure

2.02). The SAM of this derivative exhibited more selective and sensitive sensing of K^+ ions as compared to the other Group 1 (alkali metal) and Group 2 (alkaline-earth metal) ions. The formation of the SAM on the gold surface was confirmed by surface plasmon resonance (SPR), cyclic voltammetry (CV) and AFM. Based on the SPR experiments, the angle shift of calix[4]crown-5 derivative was 0.38° at the highest concentration of K^+ ion (0.01 M). This value is four times greater than that of other metal ions.

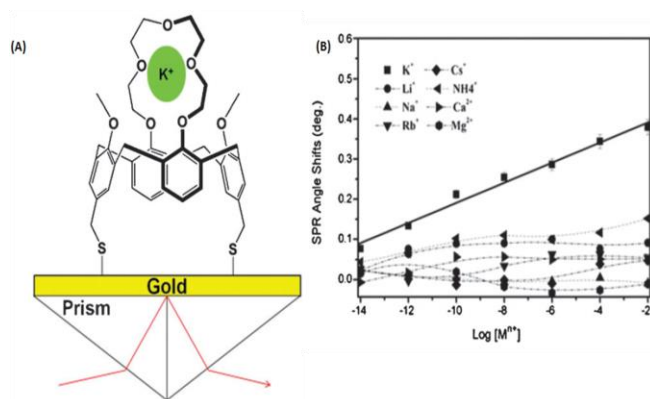


Figure 2.02 (A) A sensor chip configuration. (B) SPR angle shifts with respect to various concentrations of several metal ions. Solid line is the linear fit ($r^2 = 0.9928$), reprinted with permission from ref 13.

Calix[4]-crown compounds show high affinity for complexation of alkali and alkaline-earth metal ions.^{1,14a} In particular, the *1,3-alternate* conformation of calix[4]crown-6 ethers exhibit high selectivity towards Cs^+ ion and they exhibit efficiency in extracting cesium ion from nuclear waste.^{4,14b-c} Another example of a cationic sensor is that designed by Echegoyen and Zhang¹⁵ who reported the SAMs of different conformers of *p-tert-butylcalix[4]crown-6* derivatives and their recognition properties. Two conformational isomers of bis-thioctic ester calix[4]crown-6 derivatives

59 and **60** (Figure 2.03) form stable SAMs on gold. CV experiments indicated that modified calix[4]arene derivative **59** on the gold electrode showed significant changes upon addition of CsCl to the electrolyte, but in the case of **60**, such changes were not observed. Therefore it was concluded that calix[4]crown-6 derivative **59** could detect Cs⁺ ion very efficiently, but derivative **60** could not. The selectivity of **59** is determined by two factors: one is the cation- π interaction between the Cs⁺ ion and the aromatic rings and the other is the optimal cavity of the crown ether for binding Cs⁺ ions.

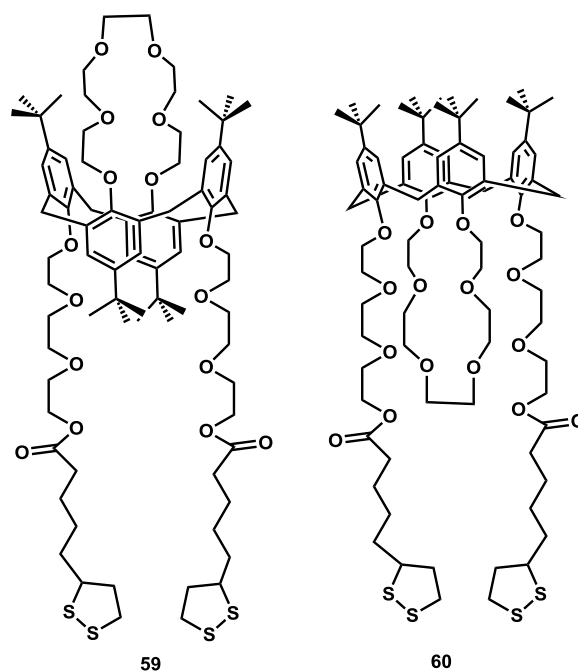


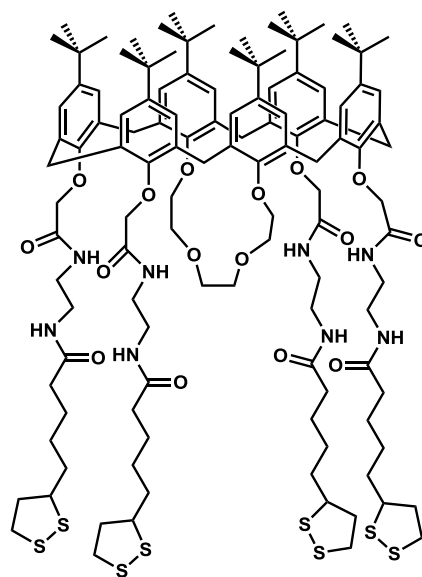
Figure 2.03 Calix[4]crown-6 derivatives **59** and **60**.

2.2.2 Anion sensors

In contrast to cation recognition, progress in the recognition of anions has been much slower due to their larger ionic radii, variety of topologies, solvation energy and pH sensitivity.^{16a} However, over the past decade, the design of anion receptors and their

sensing applications has gained significant attention in supramolecular chemistry. Many structurally-modified hosts have been developed, some of which exhibit excellent anion selectivity, and hydrogen bonding plays an important role in anion recognition.^{16b-d} Most of the anion receptors rely on hydrogen bond donors, such as amides or ureas. Anion sensors are involved in a variety of applications such as biological processes, medicine, food chemistry and environmental chemistry.¹⁷ Examples of anionic sensors are shown below.

Echegoyen and coworkers¹⁸ synthesized and characterized an anion receptor based on the tetra-amido calix[6]crown-4 derivative **61** with thioctic ester groups as shown in Figure 2.04. In their study, they demonstrated that the receptor calix[6]crown-4 derivative shows the highest binding affinity for fluoride ion over other anions tested, including Cl^- , NO_3^- , H_2PO_4^- , HSO_4^- , Br^- and AcO^- . SAMs of compound **61** formed on gold-surfaces were characterized by reductive desorption, CV and electrochemical impedance spectroscopy.



61

Figure 2.04 Calix[6]crown-4 derivative **61**.

Beer *et al.*¹⁹ reported the disulfide-functionalized bis-ferrocene urea receptor and ferrocene-calix[4]arene receptors designed for the fabrication of SAM-electrochemical anion sensors. Electrochemistry is an important approach for anion sensing and many examples of redox-active anion sensors have been reported.²⁰ The ferrocene-functionalized receptors have been shown to exhibit significantly larger magnitudes of cathodic response upon anion addition (Figure 2.05A and 2.05B). Also, SAMs of the calixarene-ferrocene receptor shown in Figure 2.05B are capable of sensing the perrhenate anion in aqueous solution.

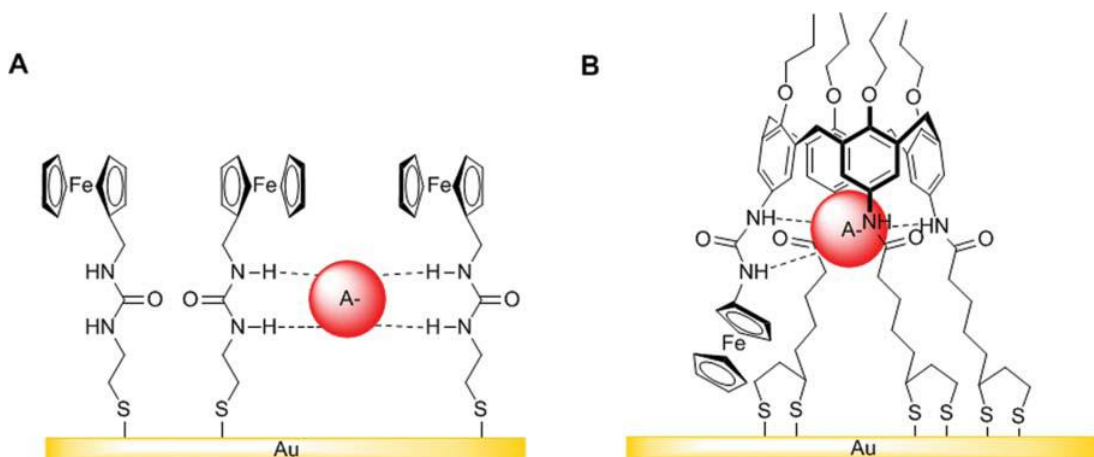
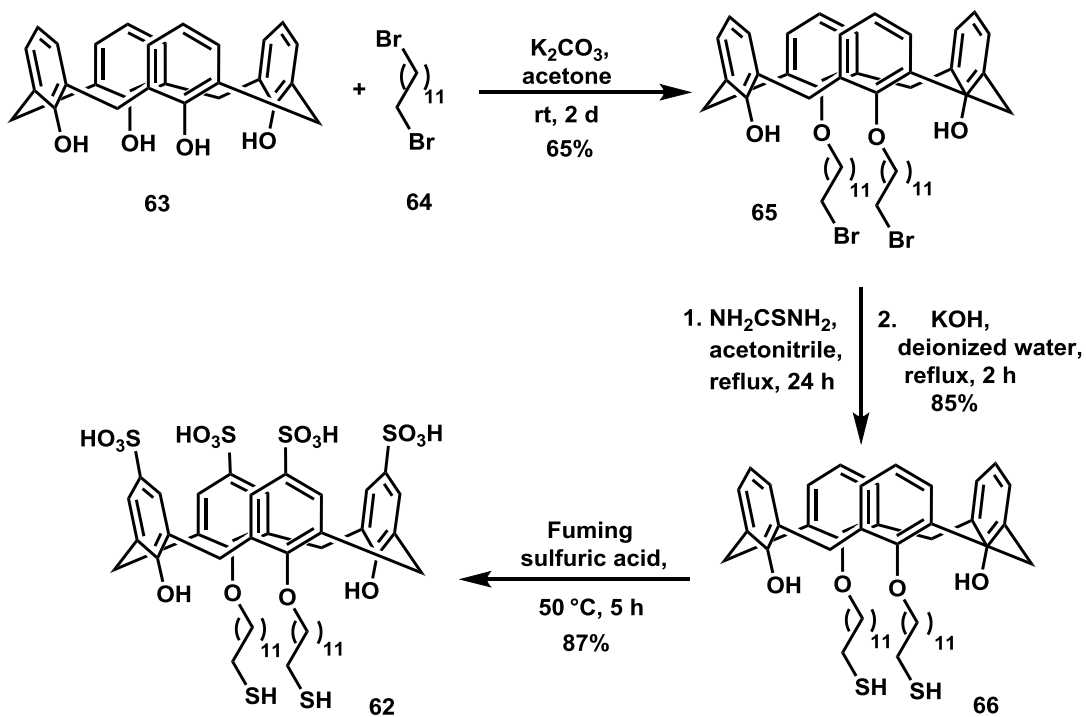


Figure 2.05 A) Scheme of a receptor adsorbed at a gold electrode binding anions cooperatively. B) Scheme of the preorganization of receptor at a gold electrode, reprinted with permission from ref 19.

2.2.3 Biomolecule sensors

Menon and Patel^{21a} reported *p*-sulfonatocalix[4]arene thiol-functionalized gold nanoparticles as a colorimetric sensor in aqueous solution. *p*-Sulfonatocalix[4]arenes are macrocyclic host molecules that have a wide range of applications due to their ability to bind with biologically-active guest molecules in aqueous solution. Menon and Patel reported the recognition of different amino acids by **62** (Scheme 2.01) attached to gold nanoparticles, in which recognition of a given amino acid triggers particle aggregation via host-guest interactions, and also a color change of the resulting solution. The synthetic approach for the water-soluble 25,27-bis(12-thio-1-oxydodecan)-26,28-dihydroxysulfonato calix[4]arene ligand **62** is shown in Scheme 2.01. In this approach, the bromo compound **65** was synthesized from de-*tert*-butylated calix[4]arene **63**. Compound **65** was treated with thiourea followed by base hydrolysis of the corresponding intermediate to form a thiol compound **66**. For the conversion of **66** to *p*-

sulfonatocalix[4]arene thiol ligand **62**, Shinkai's method^{21b} was employed (Scheme 2.01). The *p*-sulfonatocalix[4]arene thiol ligand **62** anchored onto the gold nanoparticles gave a red color in solution. Eleven different amino acids were tested in their molecular recognition studies. After the addition of the amino acids to the calix[4]arene functionalized gold nanoparticles (calix-AuNP), solutions containing lysine (lys), arginine (arg) and histidine (his) changed color from red to purple (Figure 2.06). The other amino acids had no effect on the color or absorption spectra of the functionalized AuNPs. Upon addition of these three amino acids, red shifts could be seen in the wavelength (524 nm to 550 nm), and broadening of the surface plasmon band occurred which is accompanied by aggregation of nanoparticles. The stability of the calix-AuNP assembly in different ranges of pH was determined and it was found that the assemblies are less stable in low pH solutions, ranging from pH 2 to 4. However, the calix-AuNP assemblies were very stable in solutions of pH ranging from 6 to 10, and at elevated temperatures which were not reported, for weeks to months with no sign of aggregation.



Scheme 2.01 Synthesis of *p*-sulfonatocalix [4] arene thiol ligand **62**.

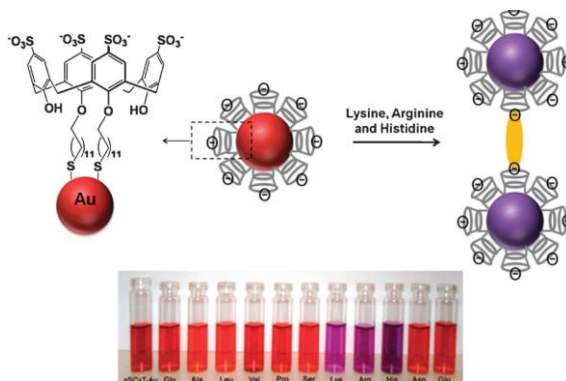


Figure 2.06 A schematic representation of the amino acid-induced aggregation of *p*-sulfonatocalix[4]arene thiol **62**-capped gold nanoparticles, reprinted with permission from ref 21a.

Another example of a SAM of a calixarene derivative on a gold surface (Figure 2.07) was reported by Echegoyen *et al.*²² Echegoyen's calix[6]crown-4 derivative **67** has a

rigid cavity immobilized on the gold surface via self-assembly and can act as an efficient and selective sensor for aniline over alkylamines. The ability to recognize ammonium cations were detected using CV and impedance spectroscopic. The efficient recognition of anilinium chloride by SAMs of **67** is due to the good fit between the sizes of the cavity of calix[6]crown **67** and the aniline. Cation- π , hydrophobic interactions, CH_3 - π and π - π stacking between the anilinium ion and the host molecule **67** may also contribute to the molecular recognition. Echegoyen's group also studied the binding affinity of **67** with biogenic aromatic amine such as dopamine.

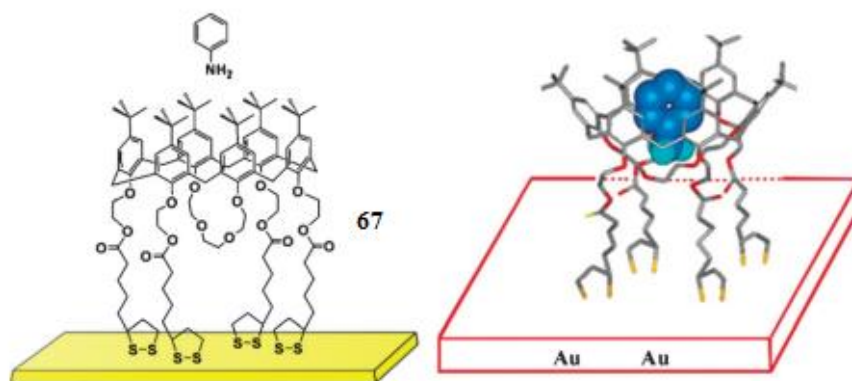


Figure 2.07 Self-assembled monolayer of a calix[6]arene **67** on gold surface with an aniline guest, reprinted with permission from ref 22.

2.2.4 Other sensors

Since the first reported inclusion complex of C_{60} and γ -cyclodextrin, many papers have been published using C_{60} and C_{70} fullerenes in supramolecular architectures.²³ A wide variety of host molecules form stable complexes with fullerenes, including cyclodextrins, cyclotrimeratrylenes (CTV), cyclo[6]paraphenyleneacetylene ([6]CPPA),

azacrown ethers, porhyrazine, and corannulenes, *etc.*²⁴ Among the various host molecules for fullerenes, calix[*n*]arenes have received considerable attention. The pioneering work was reported by Atwood *et al.*^{25a} and Shinkai *et al.*^{25b} to purify C₆₀ from carbon soot by the selective and reversible complexation with *p*-*tert*-butylcalix[8]arene. Bai and co-workers²⁶ reported the well-ordered arrays of complexes of C₆₀ with a *p*-*tert*-butylcalix[8]arene derivative anchored on a Au (111) surface, and the configuration has been observed by using scanning tunneling microscopy (STM). Haino *et al.*^{5a} reported that the complexation of a calix[5]arene dimer with C₆₀ gave a large binding constant in organic solvents.

Echegoyen and Zhang²⁷ reported a comparative study of noncovalent interactions between calixarene derivatives and C₆₀ to immobilize on gold surfaces. One calix[4]-, three calix[6]-, and one calix[8]arene thioctic acid derivatives were synthesized and characterized by ¹H and ¹³C NMR spectroscopies, and these derivatives formed SAMs on gold surfaces. It was found that calix[8]arene derivative **68** was a better fit for complexation with C₆₀, as compared to the other calixarene derivatives. A schematic representation of the gold-supported SAM of calix[8]arene **68** as shown in Figure 2.08.

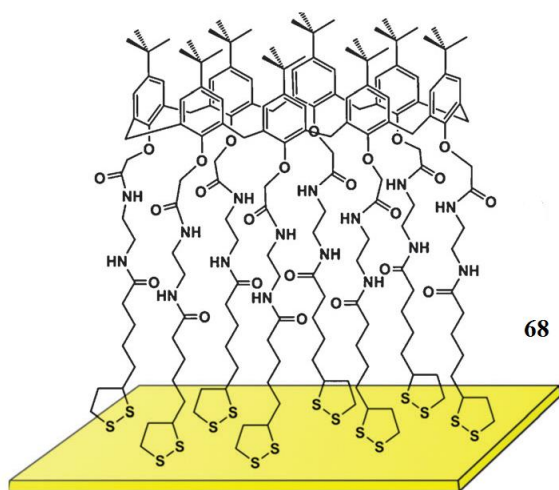


Figure 2.08 Gold-supported calix[8]arene **68**, reprinted with permission from ref 27.

2.3 Gold-coated microcantilever sensors

Microcantilevers are micromechanical beams that are fixed at one end and are free at the other end (Figure 2.09). These are readily fabricated on silicon wafers and other materials.²⁸ The typical dimensions of cantilevers are approximately 100- μm long, 20- μm wide and 1- μm thick. These sensors are physical sensors that respond to surface changes due to biological or chemical processes. Due to the nanometer deflections which occur on their surfaces, these sensors are also called “nanomechanical sensors”.²⁸ Microcantilevers are formed into two different shapes, V- and rectangular. Molecules adsorbed on the surface of microcantilevers are functionalized with receptor molecules bound to analytes, which results in the bending of the microcantilever due to surface stress (Figure 2.09). The adsorption of molecules on microcantilevers also causes vibrational frequency changes. Microcantilever sensors can be operated in different environments such as vacuum, air or liquids, all of which have been employed for biological, chemical and

physical sensing. These sensors have a wide range of applications in the field of medicine, especially for the screening of diseases, blood glucose monitoring, the detection of biological and chemical warfare agents and most notably for the diagnosis of prostate cancer and HIV.²⁹ As well, these sensors have applications in simpler host-guest complexation studies.²⁹

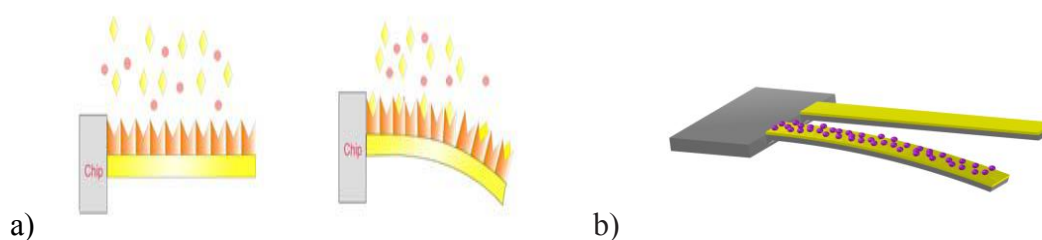


Figure 2.09 Schematic representation of cantilever changes before and after the interaction between probe and target molecules shown in a) and b) The bending occurs due to the surface stress. Reprinted with permission from ref 28.

Microcantilever-based sensors have several advantages over some other analytical techniques, such as their high sensitivity, cost-efficiency, reliability, reproducibility, non-hazardous operation and quick response times. In the past few years, new technologies have been developed especially for fabrication and sensing applications of nanocantilevers, with the result that increases in their sensitivity are now at a level making it possible to detect single molecules.²⁹

Research in the area of sensor development for the detection of metal ions in chemical and biological applications has received much attention in recent years. In particular, developments in sensors have been useful for host-guest complexation studies.

Dabestani and coworkers³⁰ reported the use of a 25,27-bis(11-mercapto-1-undecanoxy)-26,28-calix[4]benzocrown-6 **69** coated as a SAM onto the gold surface of a microcantilever sensor. They showed that this sensor acted as a selective and sensitive detector for cesium ions. Their calix[4]arene **69** was in a *1,3-alternate* conformation, which was functionalized only at the lower rim with a benzocrown-6 ether linkage at a pair of distal phenolic groups. The other distal pair of phenolic groups were functionalized as their 11-mercapto-1-undecanoxy ethers (Figure 2.10 A). The thiol groups were used to “anchor” the functionalized calix[4]arene **69** to the gold-coated microcantilever as a SAM. The sensor can be used to detect cesium ions in the concentration range of 10^{-12} to 10^{-7} M. As shown in Figure 2.10 B the cantilever undergoes larger deflections with cesium ions as compared to potassium ions in the range of 10^{-7} to 10^{-11} M. The cantilever bending response of the calix[4]arene-SAM-coated microcantilever upon Cs^+ , K^+ and Na^+ complexation were compared at the same concentrations of each ion (10^{-5} M) which were tested separately at the same temperatures.

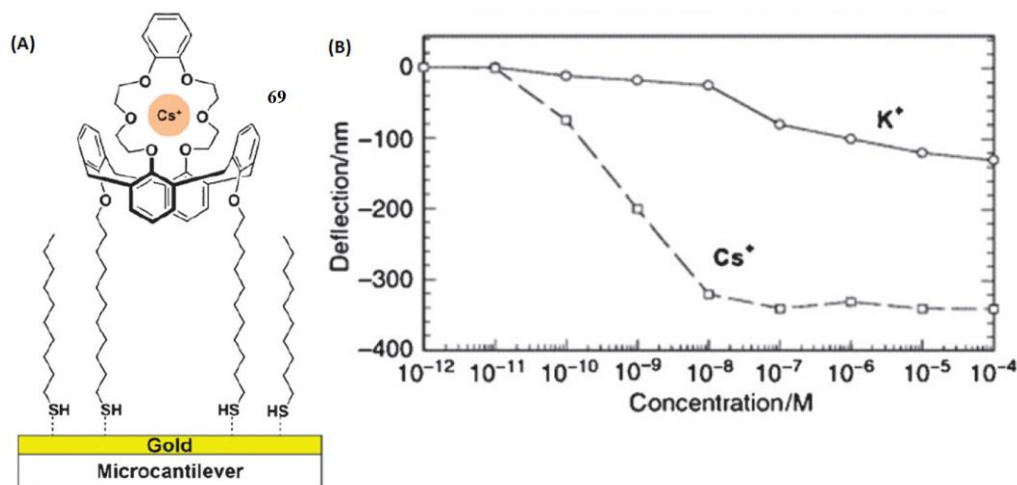


Figure 2.10 (A) Molecular structure of modified calix[4]arene **69** co-absorbed with decane-1-thiol on the gold surface of a microcantilever via the SAM technique. (B) Bending deflection response of the SAM-coated microcantilever as a function of the change in the concentration of Cs⁺ and K⁺ ions. Reprinted with permission from ref 30.

Apart from the patent literature³¹ and the work done by Dabestani's group, there are no other reports on calix[*n*]arene-modified microcantilever sensor applications. Thundat and co-workers³² reported an ultrasensitive chromate ion microcantilever sensor coated with a triethyl-12-mercaptododecylammonium bromide layer. Ji *et al.*³³ reported a novel selective beryllium ion detector using a microcantilever coated with a benzo-9-crown-3 doped chitosan-gelatin hydrogel. Most of the SAMs on gold surfaces which have been reported, especially those involving calixarenes, have thiol groups, or the disulfide group of thiotic acid to bind to the gold. The exact mechanism involved in such binding has not been fully understood.³⁴

2.4 Determination of the association constant (K_{assoc}) values

For the quantitative measurement of the relative strength of the complexations in host-guest solution chemistry, the most commonly used methods are NMR spectroscopy, fluorescence spectrophotometry and potentiometry.³⁵ In general, stronger host-guest interactions in solution are associated with higher binding, stability, or association constants.³⁵ In 1928 the method of determining the stoichiometry of host-guest binding was elucidated by Job.³⁶ In this method, the measurements are conducted on a series of samples with varying host: guest mole fractions. The guest's mole fraction can be plotted against the observed UV-vis absorbance changes at a specific wavelength. Alternatively, the mole fraction of the guest can be plotted using the NMR observed chemical shift changes of the host or guest protons ($\Delta\delta$). The stoichiometry of binding can be determined from the shape of the titration curves that result. In order to calculate the K_{assoc} value for free host, several factors are taken into consideration including the free guest and the host-guest complex. For a binding involving a 1:1 ratio, the equilibrium state can be represented as follows:



In the equilibrium equation, **H** and **G** represent the host and guest respectively while **H:G** represents the host-guest complex. The corresponding binding constant (K_{assoc}) of this kind of system can be calculated as shown below:

$$K_{assoc} = [\mathbf{H:G}] / ([\mathbf{H}] \cdot [\mathbf{G}]) \quad \text{Equation 2.2}$$

In the above equation 2.2, [**H**] and [**G**] represent the molar concentrations of the host

and guest respectively while $[\mathbf{H}:\mathbf{G}]$ represent the concentration of the host-guest complex at the equilibrium state. Where another host has the ability to bind the guest, the equilibrium can be represented as follows:



The corresponding K_{assoc} of such a system can be calculated as shown in the equation below:

$$K_{assoc} = [2\mathbf{H}:\mathbf{G}] / ([\mathbf{H}] \cdot [\mathbf{H}:\mathbf{G}]) \quad \text{Equation 2.4}$$

By using the $^1\text{HNMR}$ titration data, it can be possible to determine K_{assoc} value by plotting the concentration of the host $[\mathbf{H}]$ or guest $[\mathbf{G}]$ against the changes in the chemical shifts and using a non-linear curve 1:1 binding constant isotherm.³⁵ In the Benesi-Hildebrand method, the calculation involves plotting of $(1/[\mathbf{G}])$ or $(1/[\mathbf{H}])$ against $(1/\Delta\delta)$ to obtain a linear curve. The K_{assoc} of such a system can be calculated as shown in the equation below.^{37a}

$$K_{assoc} = \text{intercept} / \text{slope} \quad \text{Equation 2.5}$$

However, recently Prof. Pall Thordarson^{37b,c} has developed a non-linear fitting computer program and treatise for the use of a global-fit approach towards the calculation of K_{assoc} values. This approach avoids the linearization which the Benesi-Hildebrand or other non-linear methods of the past employ.

2.5 Objectives of the work reported in this Chapter

The objective of this work is to develop calix[4]arene derivatives for rapid and real-time detection of metal ions in freshwater samples by using microcantilever-based sensor(s). VALE's Hydromet plant at Long Harbour, NL using Voisey's Bay ore for processing nickel, cobalt and copper will generate a considerable amount of iron and sulphur residues (acid generating) as byproducts. These residues are pumped into Sandy Pond which is envisioned as a containment pond. The monitoring of selected trace heavy metals is required by the company for environmental considerations. A real-time method of monitoring the effluent going into Sandy Pond is therefore desirable.

Currently studies on the development of such a microcantilever-based real time device employing upper and lower rim modified calix[4]arene-derived sensing layers are on-going in collaborative work with L.Y. Beaulieu's group at the Department of Physics and Physical Oceanography at Memorial University.

In this Chapter the synthesis of upper- and lower-rim modified calix[4]arenes **70-72** (Schemes 2.06 and 2.08) is reported. These bimodal calix[4]arenes are functionalized with thioacetate groups which allowed the calixarene to bind to gold (Au)-coated microcantilevers and form stable SAMs on Au surfaces. The lower rims of these derivatives are functionalized with methyl, or ethyl esters, and 1,3-bridged ~~er~~ "crown[5]ether" moieties. The calix[4]arene derivatives can selectively bind to Group 1 and Group 2 ions. Solution-phase complexation studies of these bimodal calix[4]arene receptors with different metal ions were investigated by ¹H-NMR spectroscopy. Also presented are attempts toward the syntheses of calix[4]arene derivatives **73-76** (Schemes

2.05 and 2.07). The major results obtained from this work have been published in 2013 and 2014 in the *New Journal of Chemistry*.³⁸

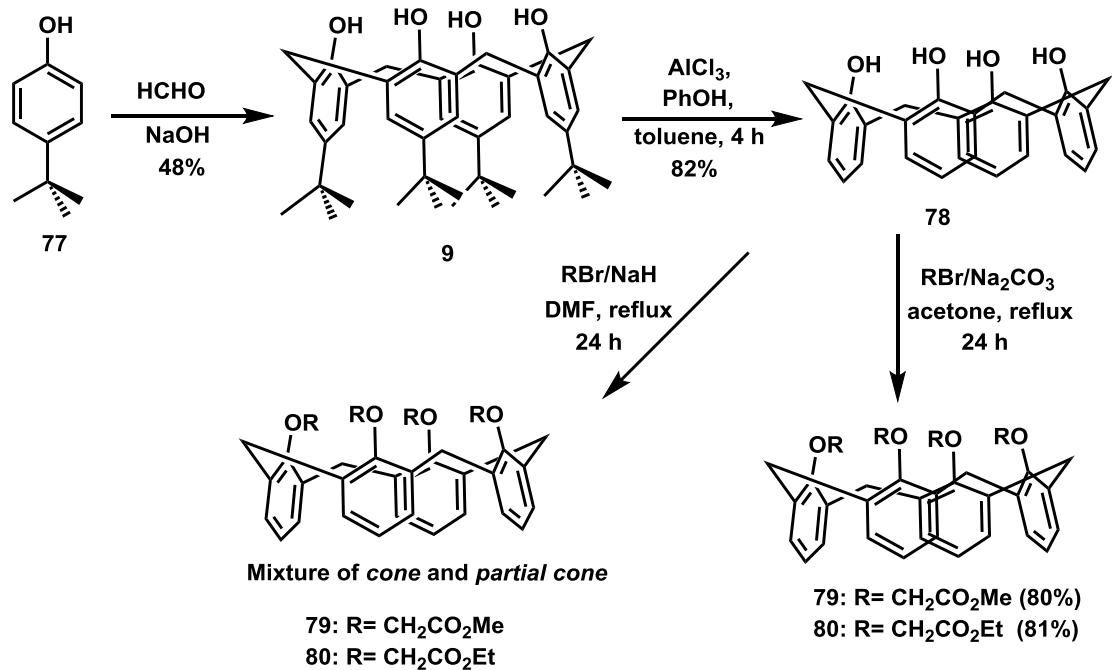
2.6 Results and discussions

2.6.1 Attempted at the synthesis of thioacetate-bearing calix[4]arenes **73** and **74**

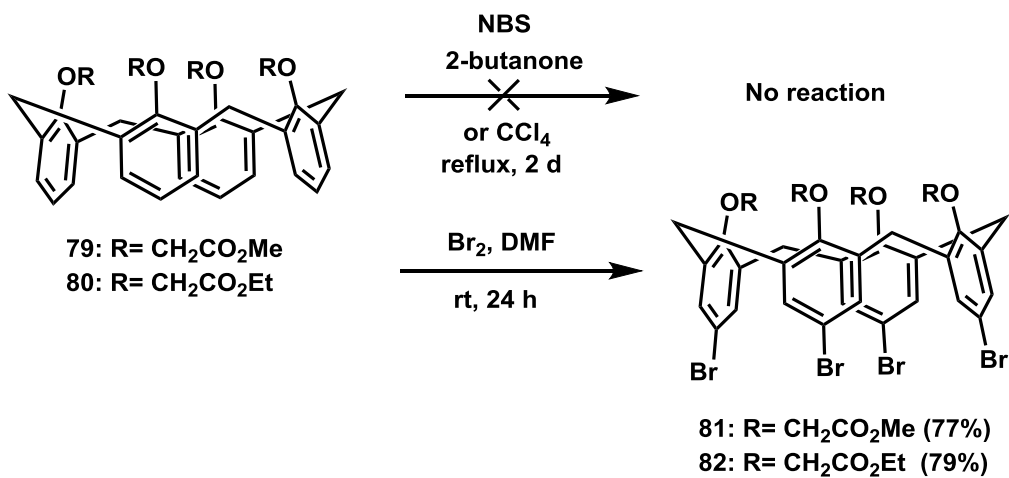
In this project the synthesis of upper- and lower-rim bimodal calix[4]arene derivatives were targeted for their use as sensing layers on gold-coated microcantilevers (MCLs). Initial attempt towards the synthesis of thioacetate-bearing calix[4]arene derivatives **73** and **74** are shown in Scheme 2.05. The synthesis of the corresponding *O*-(methoxy)- and *O*-(ethoxycarbonyl)-methoxy calix[4]arene intermediates **79** and **80** respectively, is outlined in Scheme 2.02. The synthetic strategy involved *p*-*tert*-butylcalix[4]arene **9** as the starting compound, which was synthesized from *p*-*tert*-butyl phenol **77** according to the procedure of Gutsche *et al.*² De-*tert*-butylation of **9** to form **78** was achieved using AlCl₃ and phenol in toluene as reported by Chawla *et al.*³⁹ Alkylation of **78** with methyl and ethyl bromoacetates under reflux in dry acetone, using Na₂CO₃ as base according to the well-known procedure reported by Lhotak and co-workers⁴⁰ afforded **79** and **80** which were found to be in the *cone* conformation. Mixture of *cone* and *partial cone* **79** and **80** were obtained when NaH was used as the base, and DMF as the solvent.⁴¹

The synthesis of tetra-bromo calix[4]arene derivatives **81** and **82** is outlined in Schemes 2.03 and 2.04. Treatment of **79** and **80** with NBS (*N*-bromosuccinimide) in 2-butanone or in CCl₄⁴² failed to produce the desired brominated products. The treatment of

79 and **80**, however, with bromine in DMF did form the corresponding tetrabromo calix[4]arene derivatives **81** and **82** in 77% and 79% yields, respectively (Scheme 2.03).⁴³

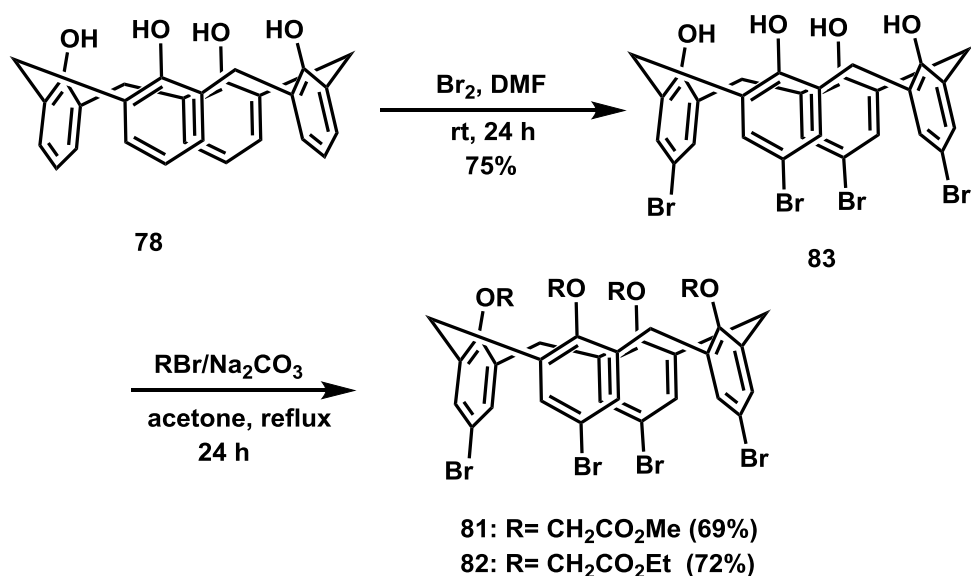


Scheme 2.02 Synthesis of calix[4]arenes **79** and **80**.



Scheme 2.03 Synthesis of tetrabromocalix[4]arenes **81** and **82**.

In an alternative approach, the de-*tert*-butylated compound **78** was treated with bromine to afford the tetraphenolic intermediate **83**.⁴³ Etherification of the lower rim hydroxyl groups of **83** with methyl- and ethyl- bromoacetates in dry acetone under reflux, using Na₂CO₃ as base afforded the respective tetrabromocalix[4]arenes **81** and **82** in 69% and 72% yields, respectively.⁴⁰ Based on the overall yields the synthetic approach to tetrabromides **81** (61%) and **82** (64%) outlined in Scheme 2.03 is more efficient.

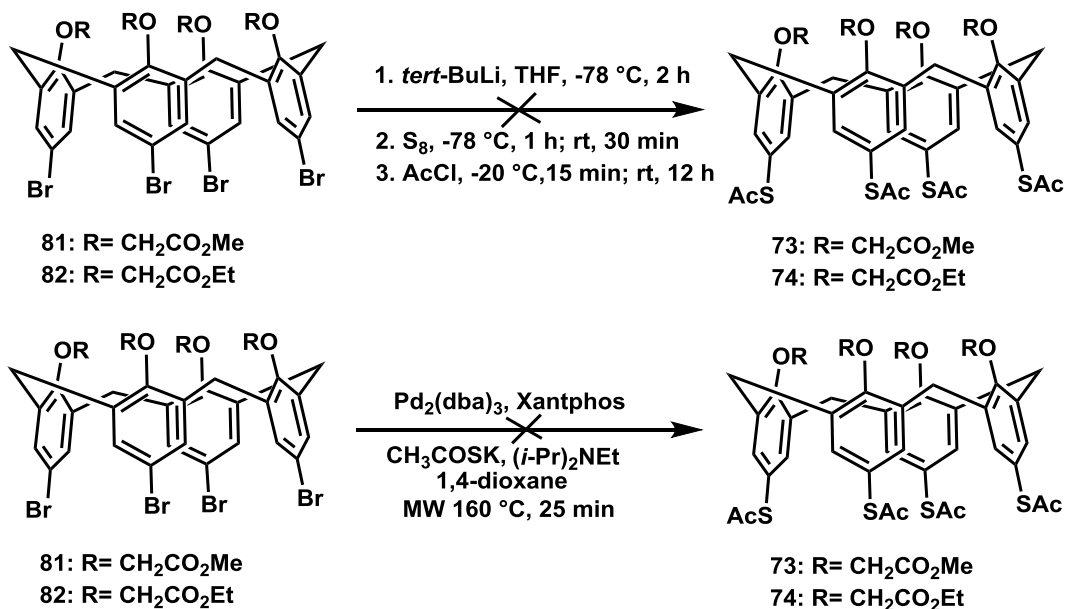


Scheme 2.04 Alternative approach to tetrabromocalix[4]arenes **81** and **82**.

Conversion of tetrabromides **81** and **82** into the corresponding tetrakis(thioacetate)s **73** and **74** was attempted by reaction with *tert*-BuLi, sulfur S₈ at -78 °C and then quenching with AcCl at -20 °C.⁴² Unfortunately, the desired thioacetate were not formed under these conditions. Alternatively, a method based on Lai's⁴⁴ report, was used. In the reaction **81** and **82** were reacted with Pd₂(dba)₃/Xantphos, (*i*-Pr)₂NEt, potassium thioacetate and 1,4-dioxane under microwave heating conditions at 160 °C (Scheme 2.05)

for 25 min to 12 h. These reaction conditions were also not successful. Even under refluxing conditions with 1,4-dioxane as solvent at 100 °C for 24 h, no conversion took place. No further attempts were carried out for the conversion of tetra-bromides **81** and **82** to the corresponding tetrakis(thioacetate) derivatives using this approach.

Instead, the synthesis of the extended chain thioacetates **70** and **71** was targeted.

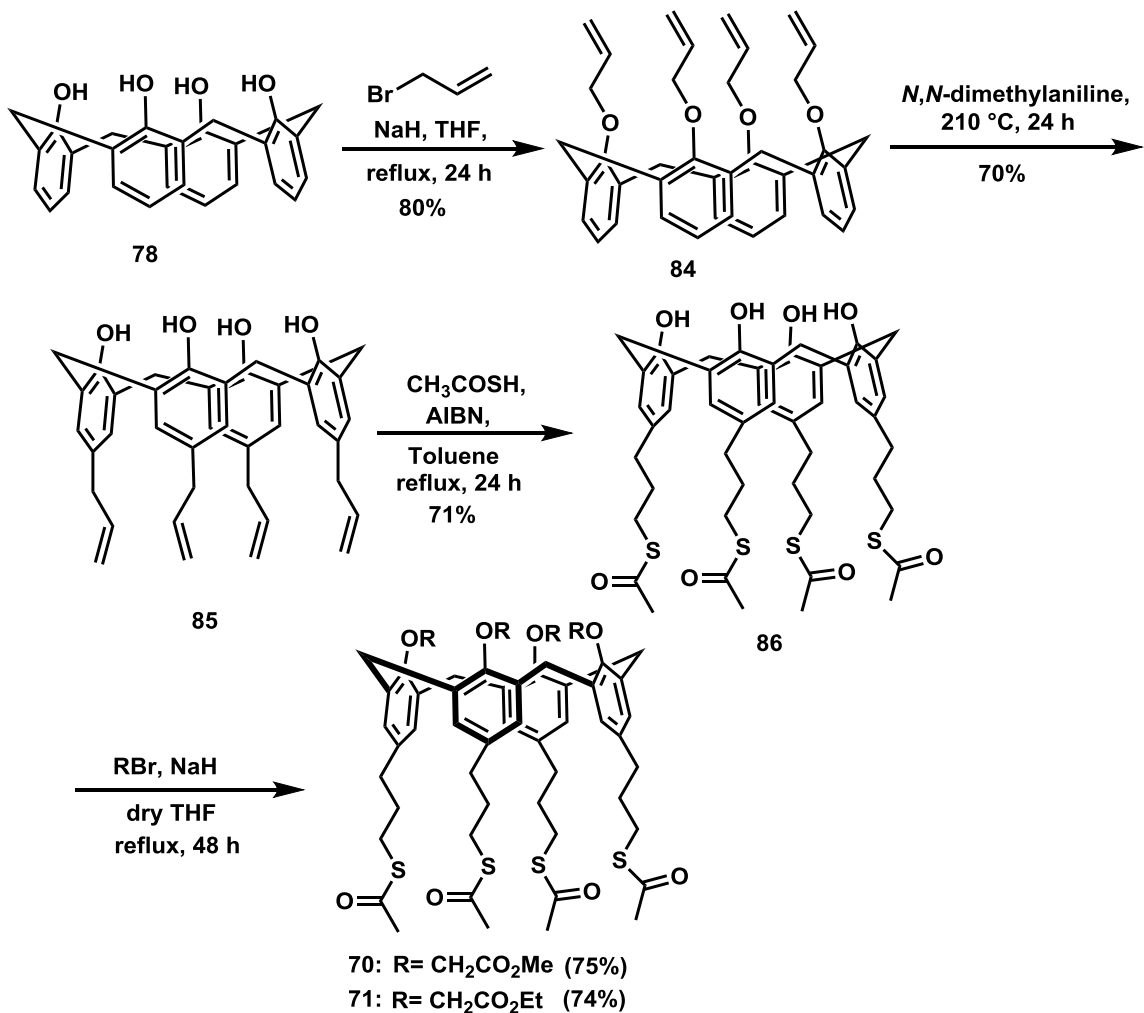


Scheme 2.05 Attempts to synthesize thioacetate-bearing calix[4]arenes **73** and **74**.

2.6.2 Synthesis of thioacetate-bearing calix[4]arenes **70** and **71**

The synthesis of **70** and **71** is outlined in Scheme 2.06. The starting material for the synthesis was once again the de-*tert*-butylated calix[4]arene **78**.³⁹ Reaction of **78** with allyl bromide in the presence of NaH in dry THF afforded the corresponding tetra-*O*-allylated product **84**.⁴⁵ Claisen rearrangement⁴⁶ of **84** in *N,N*-dimethylaniline led to the upper rim-functionalized intermediate **85**. The terminal alkenes of **85** were then

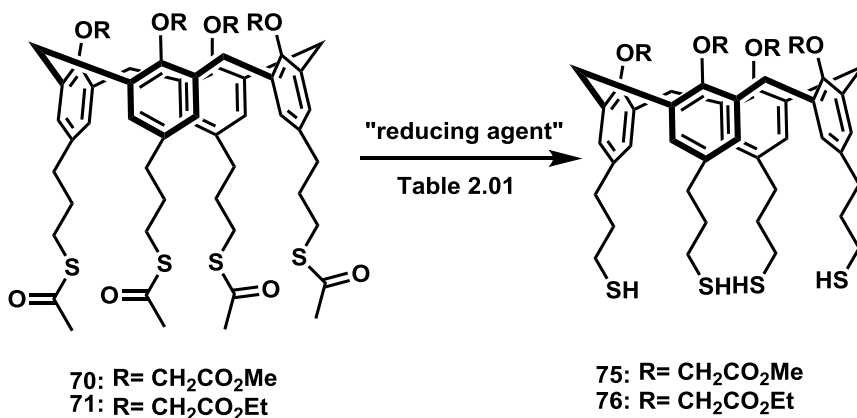
converted into thioacetyl groups by reacting with thioacetic acid, AIBN (azobisisobutyronitrile) in 1,4-dioxane to afford **86** in 60% yield.⁴⁷ The yield was improved by performing the reaction in toluene (71%).



Scheme 2.06 Synthesis of thioacetate-bearing calix[4]arenes **70** and **71**.

Conversion of **86** to tetrakis-[*O*-(methoxycarbonyl)methoxy]calix[4]arene **70** and tetrakis-[*O*-(ethoxycarbonyl)methoxy]calix[4]arene **71** respectively was achieved upon reaction with methyl- and ethyl bromoacetates in the presence of NaH in dry THF.⁴⁸

Attempted conversion of **70** and **71** to the corresponding thiols **75** and **76** (Scheme 2.07) is shown in Table 2.01. None of the desired products was obtained using NaCNBH₃ or NaBH₄.⁴⁹ No further attempts were therefore carried out for conversion of **70** and **71** to their corresponding thiol derivatives, so further experiments to form SAMs were conducted directly with **70** and **71**.



Scheme 2.07 Attempted synthesis of thiol-bearing calix[4]arenes **75** and **76**.

The formation and study of SAMs, and the properties of **70** and **71** on gold-coated microcantilevers and their solution-phase complexation studies are described below.

Table 2.01 Attempted conditions for conversion of thioacetate to thiol group.

Conditions	Result
1. NaCNBH ₃ , dry THF rt for 3 h and then reflux for 24 h.	No required product
2. NaCNBH ₃ , THF: MeOH, reflux for 12 h.	No required product
3. NaBH ₄ , THF:MeOH (1:1), -78 °C for 4 h.	No reaction (SM recovered)
4. NaBH ₄ , THF:MeOH (1:1), 0 °C to rt for 4 h.	No required product

2.6.3 X-ray crystallography of **70**

Slow evaporation of a solution of **70** in acetonitrile and methanol formed colourless crystals of **70**, which are in the monoclinic space group C2/c. Single-crystal X-ray analysis of **70** shows a *pinched-cone* conformation (Figure 2.11).

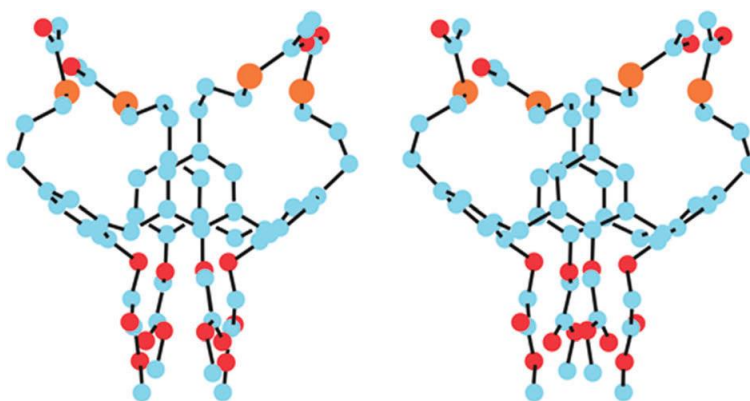


Figure 2.11 PLUTO stereoview of the single-crystal X-ray structure (hydrogen atoms and minor disorder components omitted for clarity) showing calixarene **70** in a *pinched cone*-conformation.^{38a}

2.6.4 Study of SAMs of **70** on a Au-coated microcantilever

The objective for the synthesis of **70** was to test its suitability as a selective metal ion sensing layer functioning on a Au-coated microcantilever. The Au-coated microcantilevers were incubated for 1 h in a solution of calix[4]arene **70**, during which process the calix[4]arene formed a SAM on the Au surface. Figure 2.12 shows the STM images of **70**.^{38a} The image on the left-hand side shows a 57×57 nm area indicating the presence of a highly-ordered SAM of the bimodal calix[4]arene **70** molecules. The image on the right-hand side shows a magnified portion of the STM image taken from the area indicated by the white square, 9×9 nm in size. Each bright spot corresponds to a single calix[4]arene **70** molecule.

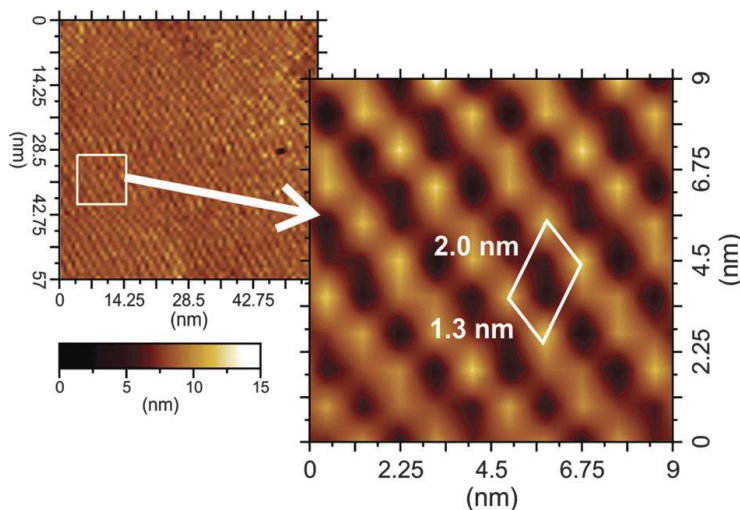


Figure 2.12 STM images of SAM of the bimodal calix[4]arene **70** on a gold surface.^{38a}

The lower rim of **70** has binding sites which are capable of binding to cations such as Ca^{2+} , K^{+} *etc.* The microcantilevers coated with **70** therefore have the potential of serving as chemical sensors to detect cations for real-time water quality monitoring. Once the cations bind with the sensing layer of the calix[4]arene such as **70**, a surface stress is developed, causing the cantilevers to bend downwards. Figure 2.13 shows the deflection of microcantilevers functionalized with calix[4]arene **70**, as a function of time for varying concentrations of CaCl_2 from 10^{-11} to 10^{-6} M. It is observed that the cantilevers undergo larger deflections for higher concentration CaCl_2 solutions. The reference microcantilever, represented by the red curve (Figure 2.13), was not coated with **70** but with only 1-decanethiol. It showed no deflection when exposed to the CaCl_2 solutions. It is clear that calix[4]arene **70**-coated cantilever sensors can readily detect Ca^{2+} cation at concentrations as low as 10^{-11} M.

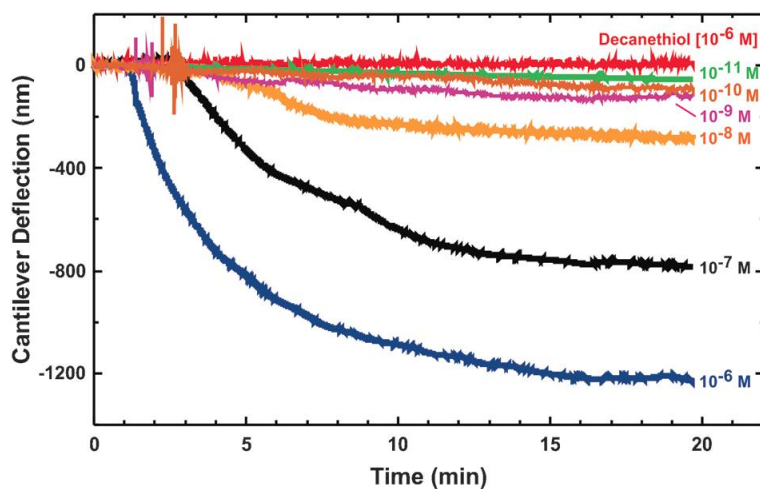


Figure 2.13 Response to different concentrations of CaCl_2 (in water) for microcantilevers functionalized with the bimodal calix[4]arene **70**.^{38a}

2.6.4.1 Detection of cations and their selectivity

The selectivity of calix[4]arene **70**-coated microcantilevers was studied in the presence of two different cations such as Mg^{2+} (from MgCl_2) and Sr^{2+} (from SrCl_2). These cations were selected because they are from the same group in the periodic table and have different ionic radii, with $\text{Mg}^{2+} < \text{Ca}^{2+} < \text{Sr}^{2+}$ ($0.064 < 0.094 < 0.110$). Figure 2.14a shows a comparison of the deflection signals of microcantilevers exposed to the same concentration (10^{-6} M) of CaCl_2 , SrCl_2 , and MgCl_2 solutions in water.⁵⁰

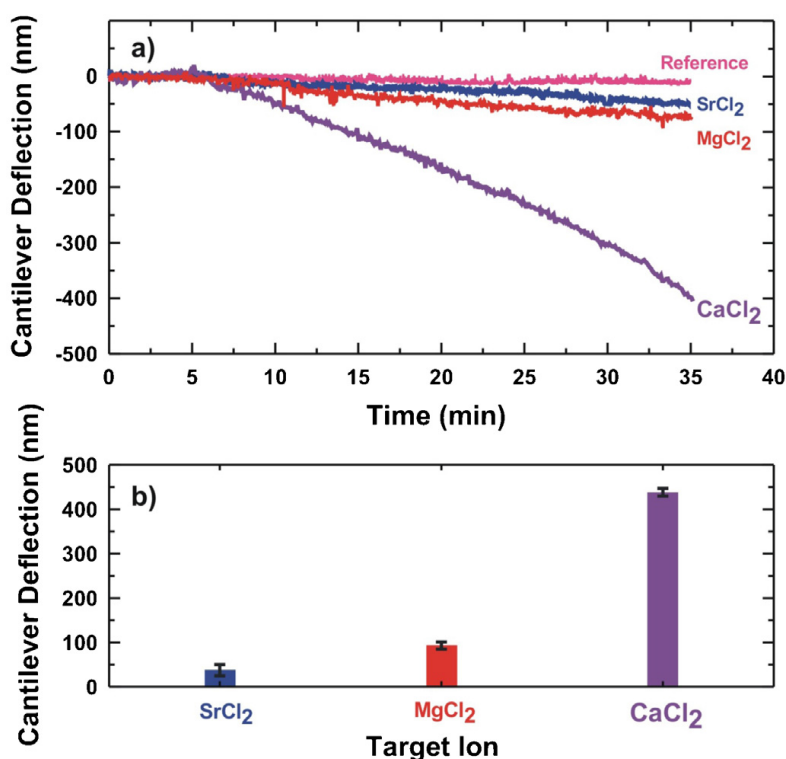


Figure 2.14 a) Microcantilever sensor response to aqueous solutions of CaCl_2 , MgCl_2 and SrCl_2 . b) The microcantilever deflection is plotted as a function of the different cations.⁵⁰

The calix[4]arene **70**-functionalized microcantilever shows a greater deflection with Ca^{2+} over either Mg^{2+} or Sr^{2+} ions. Since all three cations had the same chloride

counterion, it can be surmised that the observed microcantilever deflections originate from the size differences of the cations and their corresponding charge densities. Figure 2.14b shows the microcantilever deflections plotted as a function of different cations. Each data point corresponds to the average microcantilever deflection (after 35 min) obtained from three experiments.

2.6.4.2 Effect of anions

The anions associated with the calcium salts tested were also found to play an important role in the microcantilever response. Figure 2.15 shows a comparison between four different calcium salts, CaCl_2 , CaBr_2 , CaI_2 and $\text{Ca}(\text{NO}_3)_2$. These salts were chosen to understand the effect of their corresponding counterions on the responses of the calix[4]arene **70** functionalized microcantilevers.⁵⁰ The counterions of these salts were found to play a significant role in the binding or complexation dynamics of the calcium ion with the bimodal calix[4]arene **70** immobilized on the surface of the cantilever. Based on molecular modeling calculations, (B3LYP/6-31G(d), gas-phase the volumes (\AA^3) of three halide ions Cl^- , Br^- , I^- are determined to be 23.70, 28.08 and 34.78, respectively. The increase in the volumes of these halide ions is inversely related to the cantilever deflections of the corresponding calcium halides. The computed volume of the NO_3^- anion (44.14 \AA^3) is larger than that of the iodide ion, and it also shows a larger microcantilever deflection than I^- . However, this could be due to the trigonal planar shape of NO_3^- anion and hence it cannot be directly compared with other ions which are spherical. Hence it can be hypothesized that if the anions are larger than Cl^- , as would be the case for Br^- , I^- and NO_3^- , the “ion triplet” formed by the calcium ion and its

associated counterions (Br^- , Γ^- , and NO_3^-) would not be bound to the calix[4]arene receptor as strongly as with the Cl^- counterions and this creates lower stresses on the microcantilever.

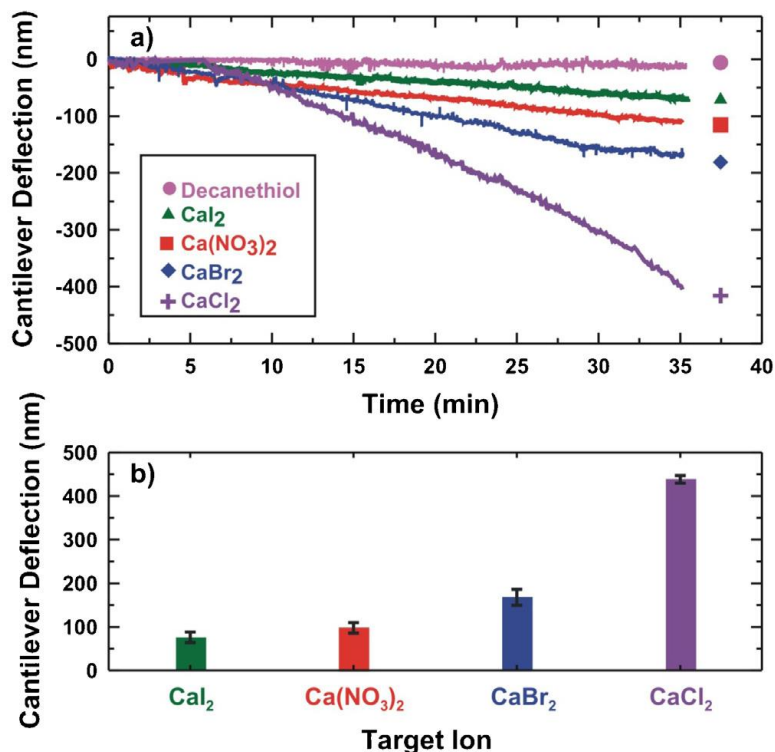


Figure 2.15 (a) Microcantilever sensor response to 10^{-6} M aqueous solutions of CaCl_2 , CaBr_2 , CaI_2 and $\text{Ca}(\text{NO}_3)_2$. (b) The response of the functionalized microcantilevers to the variation in the counterion.⁵⁰

Microcantilever sensitivity can be greatly affected by the thickness of the Au layer, and the incubation times. Details of these aspects have been documented in the literature.⁵⁰ Microcantilever studies of bimodal calix[4]arene **71** had not been finalized at the time of the writing of this thesis, and all of the microcantilever work was conducted by Abdullah. N. Alodhayb and S. M. Saydur Rahman in L.Y. Beaulieu's group in the Department of Physics and Physical Oceanography at Memorial University.

2.6.5 Solution-phase complexation studies of **70** and **71**

The solution-phase complexation studies of calix[4]arene **70** and **71** with different metal salts e.g. CaCl₂, CaBr₂, CaI₂, Ca(ClO₄)₂, Ca(NO₃)₂, Ca(OCOCF₃)₂, LiI, NaI, KI Ag(TFA)₂, MgCl₂, SrCl₂, Mg(ClO₄)₂ and Sr(ClO₄)₂ were carried out by using ¹HNMR spectroscopy. Stock solutions ($\sim 5.0 \times 10^{-3}$ M) of **70** and **71** were prepared in a 4:1 CD₃OD:CDCl₃ solvent mixture. Stock solutions ($\sim 2.0 \times 10^{-1}$ M) of the respective metal salts were prepared in the same solvent system. Small aliquots (~ 5.0 μ L) of the metal salt solutions were added directly to 0.60 mL of respective calix[4]arene solution in an NMR tube. The ¹HNMR spectra were recorded after each addition and the temperature of the NMR probe was kept constant at 24 \pm 1 $^{\circ}$ C. The binding or association constants (K_{assoc}) values for all of the titration studies were initially determined using a 1:1 non-linear binding curve fitting program according to Connors³⁵ and using *OriginPro* 6.0 Program, and were based on the chemically-induced shifts in the ¹HNMR (300 MHz) spectrum of the host molecule from the titration experiments. Using the *OriginPro 6.0* program the molar concentrations of the guest ([Guest]) were plotted against the observed chemical shift changes ($\Delta\delta$) in Hz. Subsequently, association constants were determined using Thordarson's non-linear global analysis methodology.^{37b}

Calix[4]arene **70** and **71** showed different K_{assoc} values for both CaCl₂ and CaI₂ salts, in both cases **71** showing the higher association values. In the case of Ca(ClO₄)₂ and Ca(NO₃)₂ salts, no chemical shift changes were noticed with either calix[4]arene. Table 2.02 shows the average K_{assoc} values obtained with the different metal salts. CaCl₂ had higher values than CaI₂ both for calixarenes **70** and **71**. Based on these values, the mode

of complexation could involve the salt binding to the host calixarenes, as tight contact linear “ion triplets” in the solvent system used.⁵¹ The larger iodide ions from the CaI_2 would therefore not be easily accommodated. By way of contrast, NaI being a smaller linear contact “ion doublet” shows a stronger binding constant.

Table 2.02 Average K_{assoc} values for representative salts.

Salt	K_{assoc} of 70 (M^{-1})	K_{assoc} of 71 (M^{-1})
CaCl_2	78	179
CaI_2	18	34
NaI	294	611
KI	18	44
AgOCOCF_3	254	682

NaCl , KCl , KBr and KNO_3 salts were used for comparison purposes, which are not completely soluble in the solvent mixture used. AgOCOCF_3 shows the highest binding constants shown in Table 2.02, the ethoxy derivative **71** showing an almost 3-fold higher K_{assoc} than **70** which is the corresponding methoxy derivative. In order to determine the binding location, on the host calixarenes, $\text{Ca}(\text{OCOCF}_3)_2$ was used in the same solvent system, but no chemical shift changes were noticed. This suggests that the binding sites for the Ag^+ complexation could be the thioacetate group in the upper rim and not the lower rim ester groups. MgCl_2 , SrCl_2 , $\text{Mg}(\text{ClO}_4)_2$, and $\text{Sr}(\text{ClO}_4)_2$ were also used for comparison purposes but no chemical shift changes for these salts were noticed with either of the calix[4]arenes.

2.6.6 Possible mechanism for thioacetate binding to gold surfaces

The exact mode by which a thioacetate (or thiols) bind to gold surfaces is a subject of ongoing investigation. Fischer *et al.*⁵² recently reported the adsorption of thioacetic acid (TAAH) on Au(111) from solution deposition (Figure 2.16). The authors suggest that the "acetyl" ($\text{CH}_3\text{C}=\text{O}$) fragment of thioacetic acid is cleaved off upon interaction with the Au surface. The result being that the sulfur binds directly to the gold. Fischer *et al.* proposed two possible mechanisms which are shown in Figure 2.17. In the first mechanism (Figure 2.17a), a chemisorption of the TAAH on the Au(111) surface takes place. Then a H-S homolytic bond cleavage occurs, resulting the chemisorbed TAA radical binds to the Au(111) surface. In the second mechanism (Figure 2.17b), physisorption of the TAAH to the Au(111) surface takes place. In this reaction mechanism the H atom does a [1,2] shift to the carbonyl carbon atom, producing a transient quasi-tetrahedral intermediate that leads to the final products. The authors supported their hypotheses with detailed computational arguments.

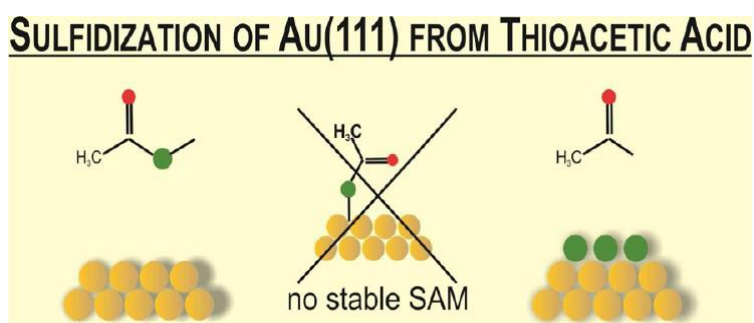


Figure 2.16 Sulfidization of Au(111) from thioacetic acid.⁵² Reprinted with permission from ref 52.

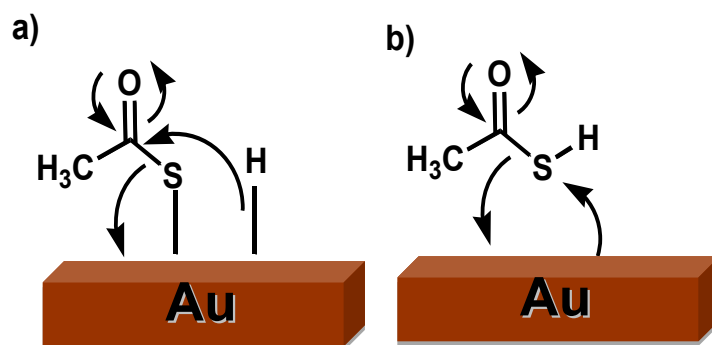


Figure 2.17 Scheme for two possible mechanisms (a and b) proposed to explain the S adlayer formation.

In the case of thioacetate it is conceivable that a similar phenomenon occurs, with the difference being that sulfur atoms on the thioacetate groups are attached to the three-carbon chains which are attached to the upper-rim of the calixarene. A possible mechanism for thioacetate binding to gold surfaces is shown in Figure 2.18.

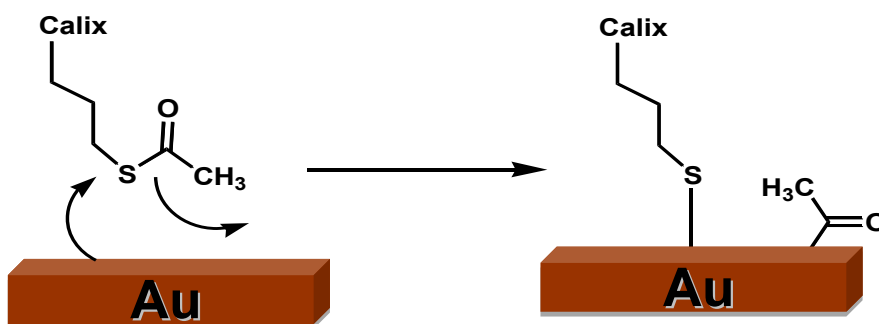


Figure 2.18 Possible mechanism to explain how the thioacetate binds to gold surfaces.

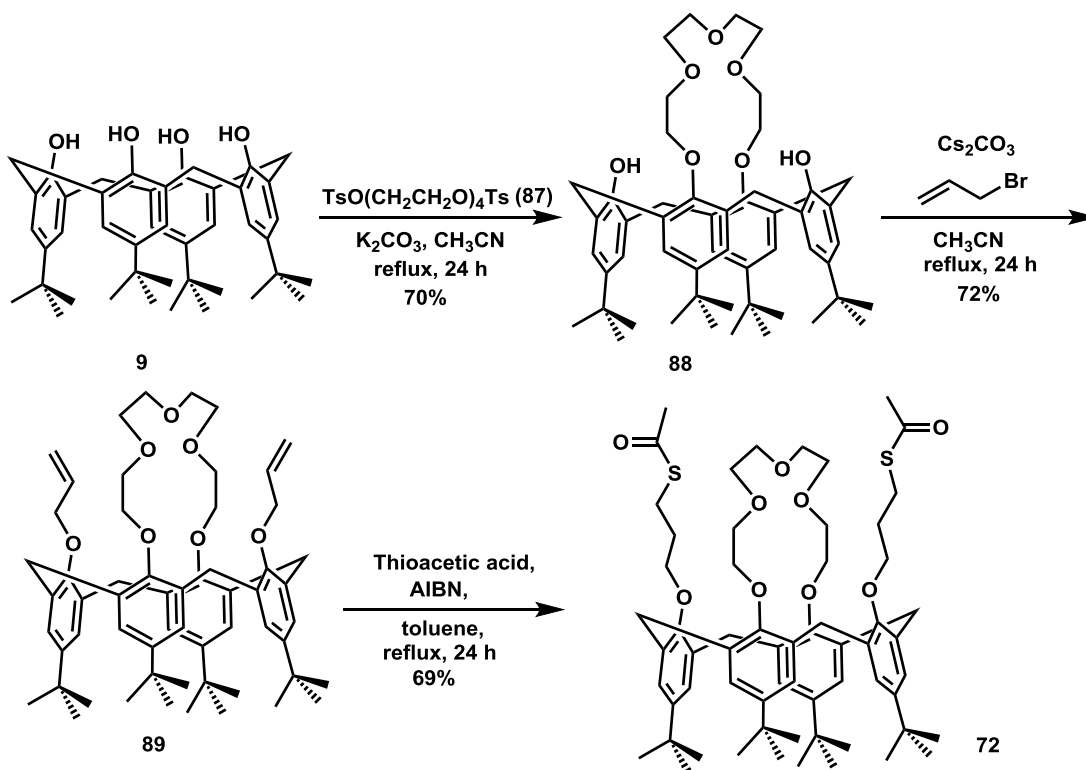
2.7 Synthesis of a *cone*-conformer bimodal calix[4]arene-crown-5 derivative 72

In order to test selectivity for different metal ions with the sensing layers needed for the different MCLs envisioned in the MCL instrument, the next designed calix[4]arenes

incorporate a “crown-ether” moiety. Crown ethers are among the first reported cation-complexing compounds in the literature. A new 1,3-bridged-crown-5” thioacetate-bearing calix[4]arene **72** which also forms a SAM on a Au-coated MCL and which binds selectively to Cs⁺ was targeted for synthesis. The synthetic procedure for receptor **72** is shown in Scheme 2.08. The calix[4]-crown-5 **88** was synthesized from *p*-tert-butylcalix[4]arene **9** according to the procedure of Chailap and Tuntulani.⁵² The reaction of calix[4]arene **88** with allyl bromide in the presence of Cs₂CO₃ in acetonitrile afforded **89** in 72% yield. The thioacetylation of terminal alkenes of calix[4]arene **89** with thioacetic acid, AIBN in toluene afforded the *cone*-conformer of calix[4]arene-crown-5 derivative **72** in 69% yield.^{38b} From the published literature on transformations of calix[4]arenes similar to **89**, it was anticipated that formation of *1,3-alternate* conformer **89** would result, and hence subsequently lead to the formation of the corresponding *1,3-alternate* conformer of **72**. However, the major products obtained from these transformations were found to be the corresponding *cone*-conformers of **89** and **72**.

The ¹HNMR spectrum of **89** suggested that the calix[4]arene unit is in a *cone* conformation since the proton chemical shifts of the bridging -CH₂- groups appeared as a pair of AB doublets at δ 4.37 and 3.14 ppm (*J* = 15.1 Hz) and the corresponding ¹³C chemical shifts was observed at δ 34.0 ppm. The *tert*-butyl groups (18-proton) appear as two singlets at δ 1.26 and 0.88 ppm. In the ¹HNMR spectrum of **72**, the chemical shifts of the bridging -CH₂- groups appeared as a pair of AB doublets each of which is centred at δ 4.30 and 3.15 ppm (*J* = 14.0 Hz) respectively, and in the corresponding ¹³CNMR

spectrum at δ 34.1 ppm positions, as noted for **89**, which are typical of a calix[4]arene in a *cone* conformation.



Scheme 2.08 Synthesis of calix[4]arene-crown-5 derivative **72**.

The 2D NOESY spectrum of **72** is shown in Figure 2.19. The NOESY is a homonuclear, shift correlated experiment, in which cross-peaks (blue) result from *dipolar* interactions between spins. These are due to correlations between protons separated by less than 5 Å no matter how many bonds are in between. The NOESY spectrum of **72** showed that exchange cross peaks (blue) exist between aromatic protons and the bridging -CH₂- groups.

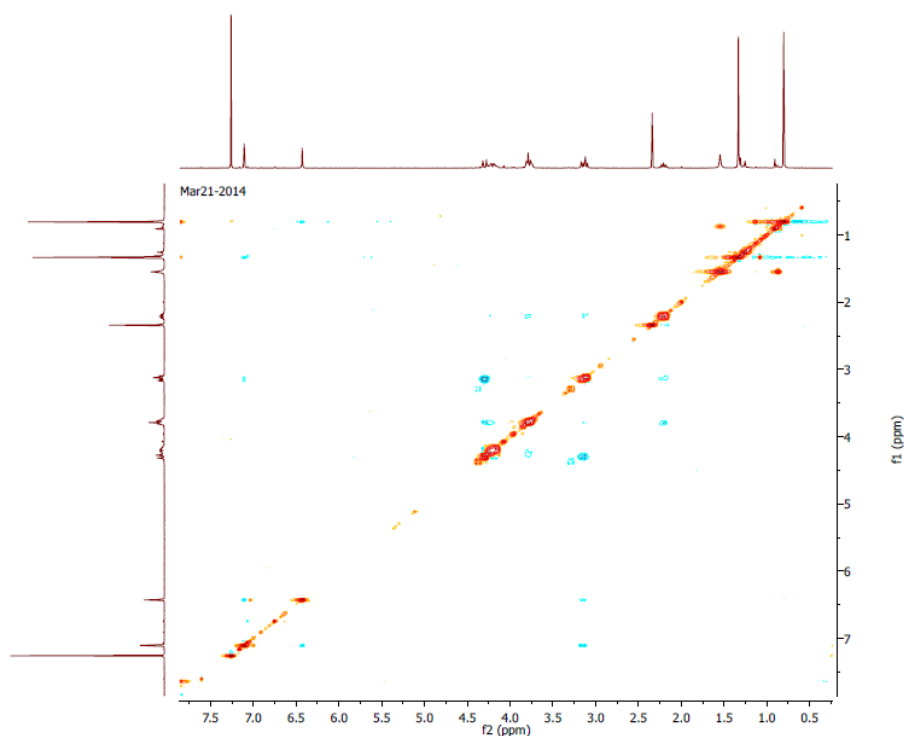


Figure 2.19 2D NOESY spectrum for calix[4]arene **72**.

The NOESY spectra of both **89** (see in Appendix Figure 2.34) and **72** however were not unambiguous. The single-crystal X-ray analysis of **72** however, unequivocally showed it to be in a *cone* conformation (Figure 2.20) which is consistent with the postulated NMR interpretations of the solution state conformation.

Synthesis under other conditions, which usually results in products with different conformations. For example, NaH in THF, or Na₂CO₃ in acetone, under reflux conditions nevertheless produced the same *cone* conformer of **89**. Presumably, the relatively smaller steric bulkiness of the allyl groups did not lead to the preferential formation of the *1,3-alternate* conformers.

2.7.1 X-ray crystallography of **72**

Slow evaporation of a solution of **72** in acetonitrile and ethanol (1:1) formed crystals of **72** which crystallized in the monoclinic space group $P2_1/n$, with three chemically identical molecules in the asymmetric unit. Each molecule adopts a *cone*-like configuration (Figure 2.20). The molecules are packed in discrete chains perpendicular to the *c*-axis, and no significant intermolecular interactions are present. Several attempts to collect suitable X-ray diffraction data using a Mo source afforded only weakly diffracted data which could not be solved. Only a set of data obtained using a Cu source at Boston College afforded data sufficient to enable Dr. Louise Dawe at Wilfrid Laurier University to solve the structure with sufficient refinement.

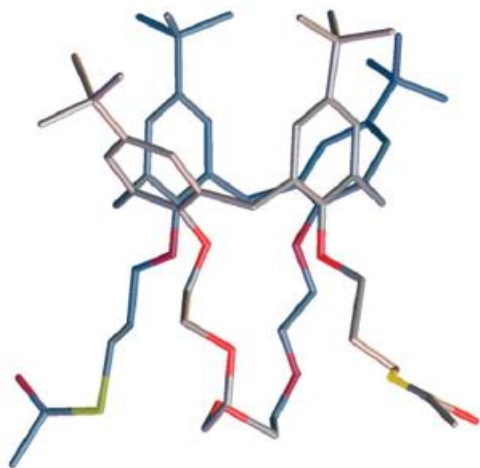


Figure 2.20 A single molecule of **72**, represented as capped sticks, showing the *cone* conformation. H-atoms and minor disorder components were omitted for clarity.^{38b}

2.7.2 Study of a SAMs of **72** on a Au-coated microcantilever

The objective for the synthesis of **72** was to test its suitability as a selective metal ion sensing layer within the crown ether moiety of **72** on a Au-coated microcantilever

application. STM imaging was performed to assure that new calixarene **72** was capable of adhering to a Au surface. Figure 2.21a shows a 26 nm x 26 nm-sized image of molecules of **72** on the gold surface, clearly indicating the presence of a highly-ordered SAM of the calixarene **72** molecules. Figure 2.21b shows the magnified portion of the STM image shown in Figure 2.21a, taken from the area indicated by the white square 9.5 nm x 10.5 nm in size. The image more clearly reveals the high ordering of calix[4]arene **72** molecules on the Au surface. Each bright spot corresponds to a single calix[4]arene **72** molecule. Thus, this sensing layer should be very stable on the Au surface of a MCL due to the strong bonding between the sulphur atoms and the gold surface.

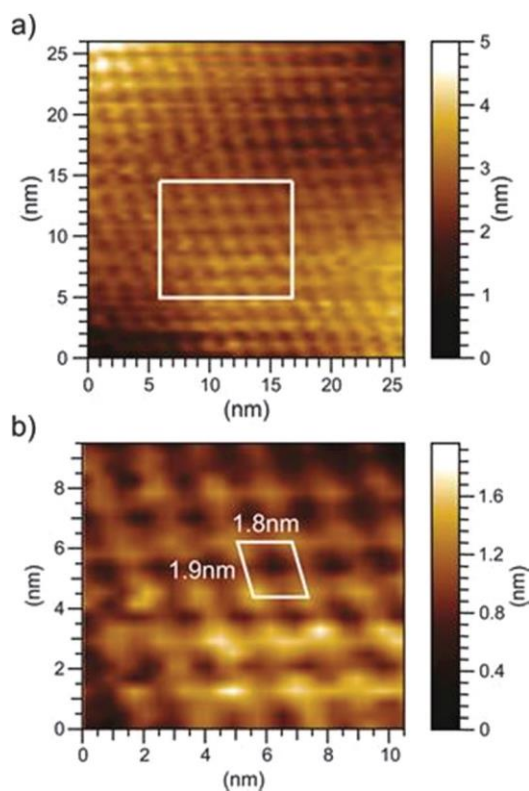


Figure 2.21 STM images of calix[4]arene-5'' compound **72** which forms a self-assembled monolayer on the gold surface.^{38b}

Figure 2.22a shows the deflections of calix[4]arene **72**-coated MCLs to four different metal chloride aqueous solutions, CaCl₂, KCl, RbCl and CsCl. The largest deflections seen were for Cs⁺ which was significantly greater than the deflection seen for K⁺, similar to results reported by Ji *et al* with their system.³⁰ In their case, the receptor was a benzo-crown-6-moiety. The deflection seen for Rb⁺ was smaller than for Cs⁺ but greater than for K⁺. Crown-ethers are highly selective towards particular metal cations. Only a very weak response was seen for Ca²⁺. In order to demonstrate that the reproducibility of results obtained for different target ions, the average microcantilever deflections for three experiments was calculated and shown in Figure 2.22b.

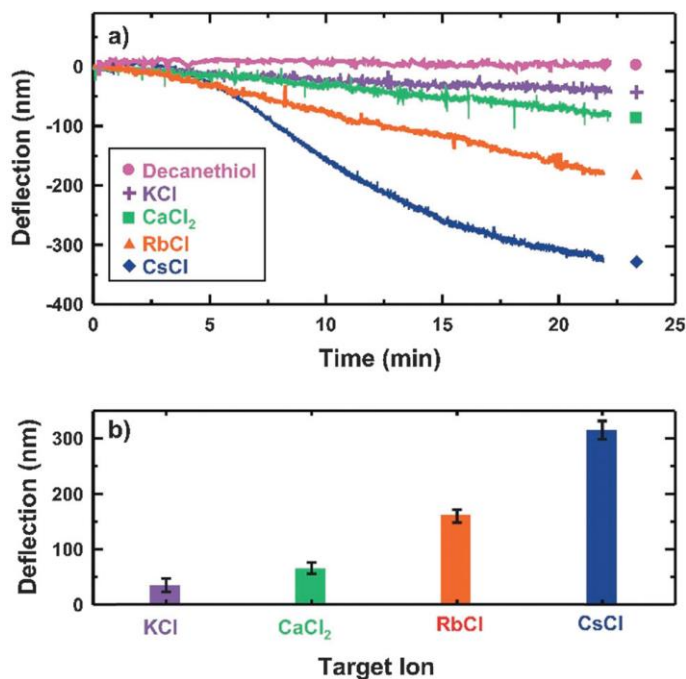


Figure 2.22 a) Response to the different metal ions of a microcantilever sensor functionalized with calixarene-crown-5⁺ compound **72**. b) Microcantilever deflection plotted as a function of different metal ions.^{38b}

Zhang and Echegoyen¹⁵ reported the synthesis and cation recognition properties of the SAMs of their *cone* and *1,3-alternate* bis-thioctic ester derivatives of *p-tert-butylcalix[4]arene-crown-6* **59** and **60** (Figure 2.03) on gold-coated electrodes. In contrast with **72** these authors showed that their *cone* conformer **60** did not show any binding with Cs⁺ and that only the corresponding *1,3-alternate* **59** could bind Cs⁺. It should be noted that besides having a “18-crown[6]” functionality, their thioctic acid ester groups are linked *via* triethyleneglycol tethers which are much longer than the thioacetate tether in **72**. According to the STM image of **72** on the Au surface there are at least two possibilities: (a) that only one sulfur in each molecule of **72** is directly attached to the Au surface; or (b) that despite the evidence that **72** is in a *cone* conformation, it cannot be ruled out that a conversion to the *1,3-alternate* atropisomer occurs upon formation of the SAM on the Au surface. In either case, Cs⁺ as well as Rb⁺ binding could be accommodated within the “crown” but with the *1,3-alternate* conformer being the more favourable for the binding as was seen by Zhang and Echegoyen¹⁵ in their case. However, should the crown be in a “puckered” type conformation as in the case of (a), it could “trap” Rb⁺ or Cs⁺ from one side of the coordination sphere. Alternatively, these large cations could be more favorably accommodated within the cavity formed by the calixarene phenyl groups instead of within the “crown-5”, as a result of favourable cation- π interactions. A detailed DFT computational study is currently on-going.

2.7.3 Solution-phase complexation studies of **72**

The solution-phase titration experiments of the host compound calix[4]arene-crown **72** with different metal salts e.g. LiI, NaI, KI, RbI and CsI were carried out by using ¹H-

NMR spectroscopy. A stock solution of the host compound **72** ($\sim 1.5 \times 10^{-3}$ M) was prepared in CD₃OD:CDCl₃ (4:1) solvent mixture. Stock solutions ($\sim 2.0 \times 10^{-2}$ M) of the respective metal salts were prepared in the same solvent system. Small aliquots (~ 2.5 μ L) of the metal salt solution were added to 0.60 mL of the host calix[4]arene-crown **72** solution in an NMR tube. The ¹H NMR spectra were recorded after each addition with the temperature of the NMR probe kept constant at 24 \pm 1 °C. The binding or association constants (K_{assoc}) values for all of the titration studies were initially determined using a 1:1 non-linear binding curve fitting program according to Connors³⁵ implemented in *OriginPro* 6.0 Program, and subsequently using Thordarson's non-linear global analysis methodology.^{37b}

No chemical shift changes were noticed with the LiI or CsI.

2.7.3.1 ¹H-NMR titration experiments of **72** with NaI

Figures 2.23a-d show the ¹H NMR titration spectra of **72** with successive additions of anhydrous NaI salt in a 4:1 CD₃OD:CDCl₃ solvent mixture. It can be seen that by increasing the amounts of added NaI to the solution of **72** downfield chemical shift changes for the SCOCH₃ protons occur from δ 2.35 to 2.37 ppm; for the aromatic singlet signals (Ar-H) from δ 7.15 to 7.24 ppm and for the Ar-CH₂- doublet signals from δ 4.32 to 4.43. However, one of the *t*-butyl proton signals is shifted upfield from δ 1.34 to 1.20 ppm (Table 2.03).

The association constants (K_{assoc}), were determined using the non-linear 1:1 binding isotherms with the assistance of *OriginPro* 6.0 program, and were based on the

chemically-induced shifts in the 300 MHz $^1\text{H-NMR}$ spectrum of the host molecule **72** from the titration experiments. Using the *OriginPro* 6.0 program the molar concentrations of the guest ($[\text{Guest}]$) were plotted against the observed chemical shift changes ($\Delta\delta$) in Hz. The resulting K_{assoc} values were determined to be 278 ± 12 , 252 ± 18 , 252 ± 21 and $317 \pm 93 \text{ M}^{-1}$ respectively, based on the *t*-butyl, Ar-*H*, Ar- CH_2 , and - SCOCH_3 proton chemical shift changes (Figure 2.24).

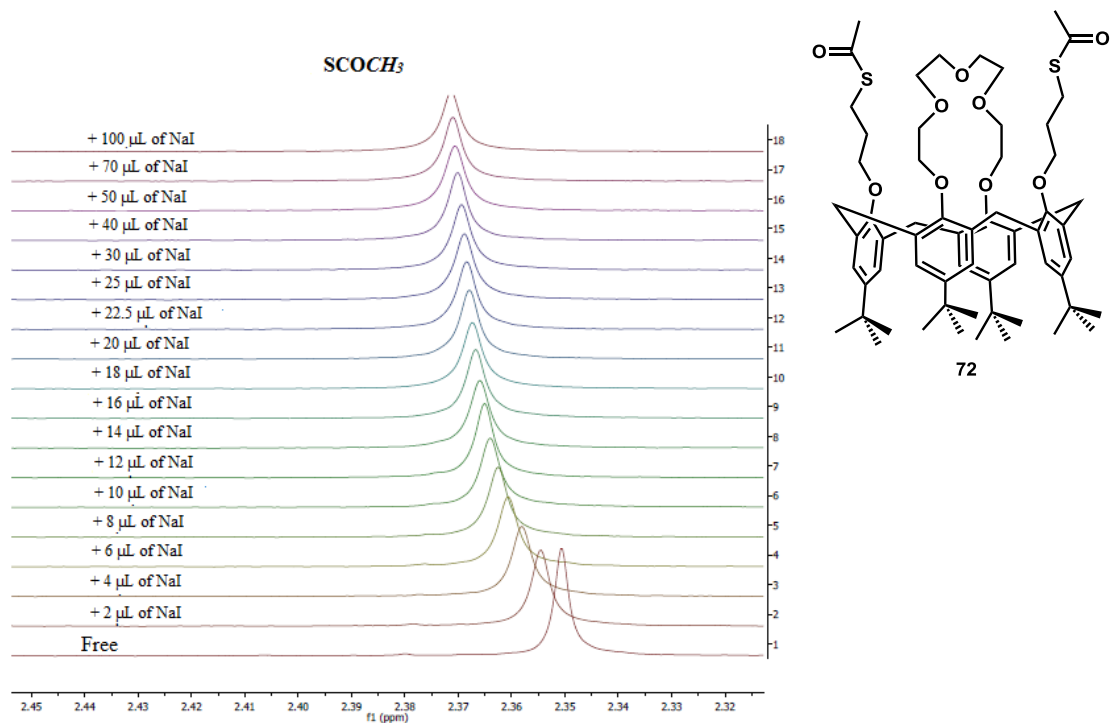


Figure 2.23a $^1\text{H-NMR}$ (300 MHz) titration spectra for SCOCH_3 of **72** ($1.5 \times 10^{-3} \text{ M}$) with NaI ($2.0 \times 10^{-2} \text{ M}$) solution.

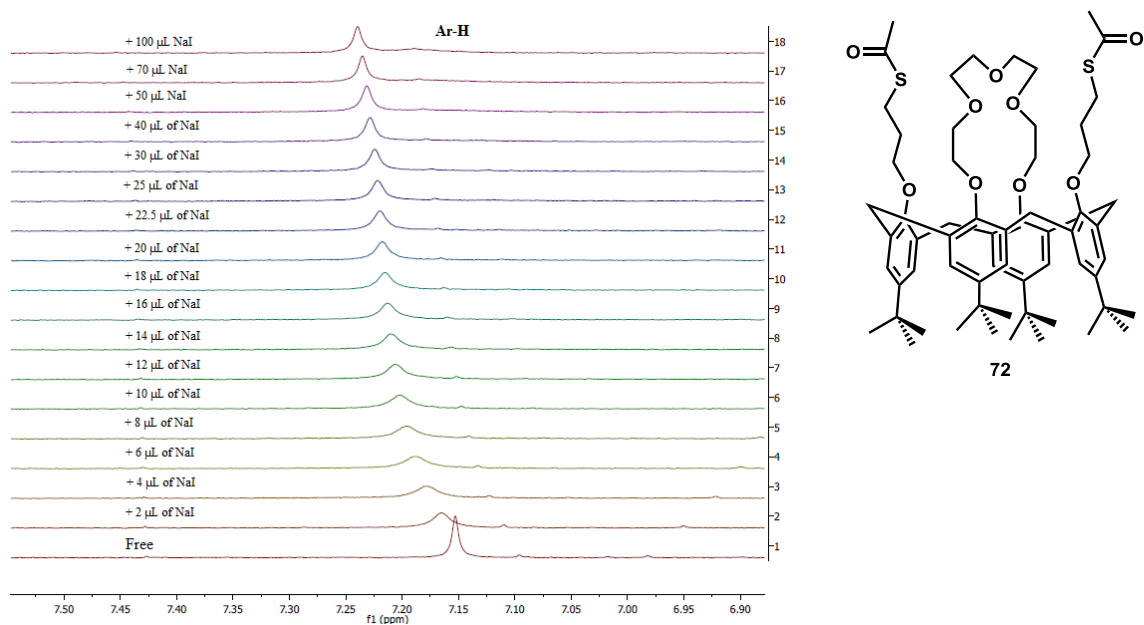


Figure 2.23b $^1\text{H-NMR}$ (300 MHz) titration spectra for Ar-*H* of **72** (1.5×10^{-3} M) with NaI (2.0×10^{-2} M) solution.

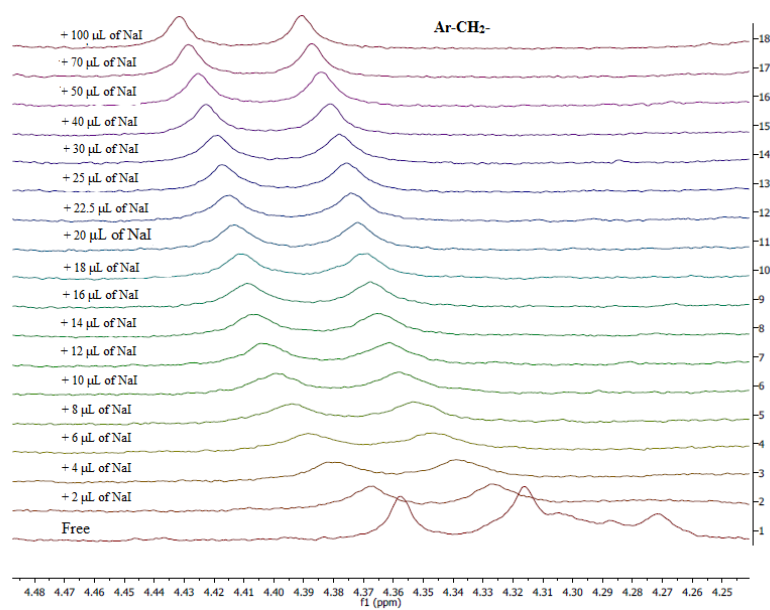


Figure 2.23c $^1\text{H-NMR}$ (300 MHz) titration spectra for Ar- CH_2 of **72** (1.5×10^{-3} M) with NaI (2.0×10^{-2} M) solution.

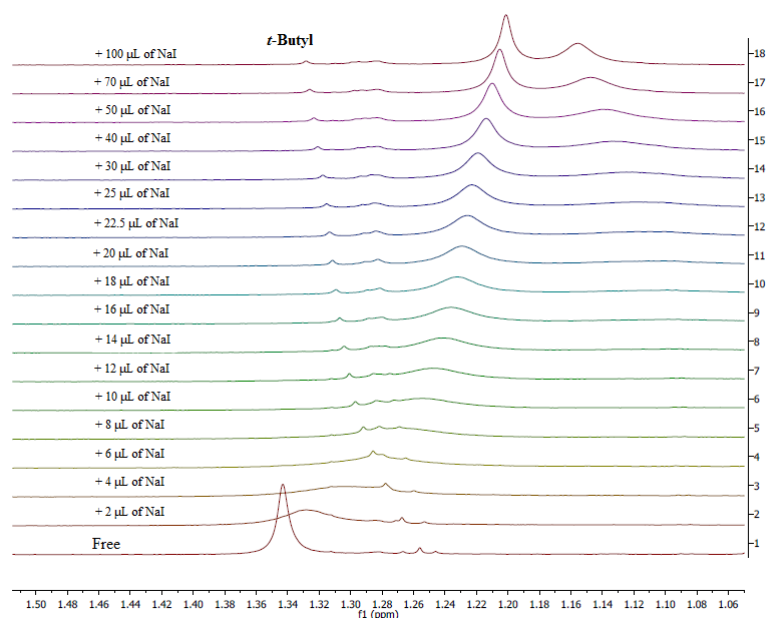


Figure 2.23d ^1H NMR (300 MHz) titration spectra for *t*-butyl of **72** (1.5×10^{-3} M) with NaI (2.0×10^{-2} M) solution.

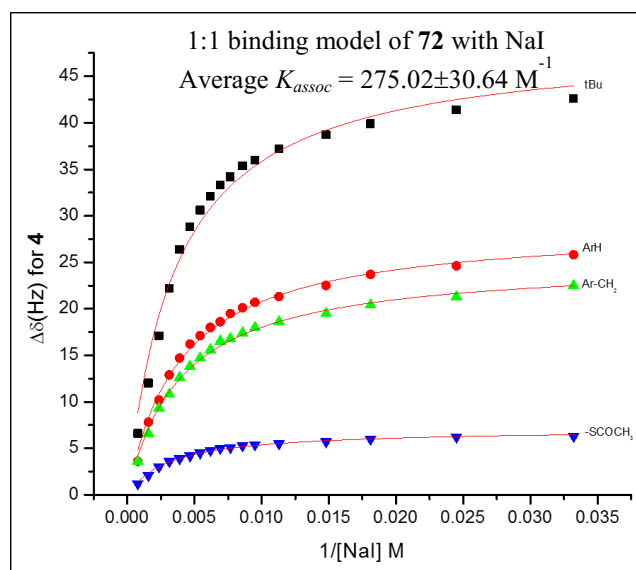
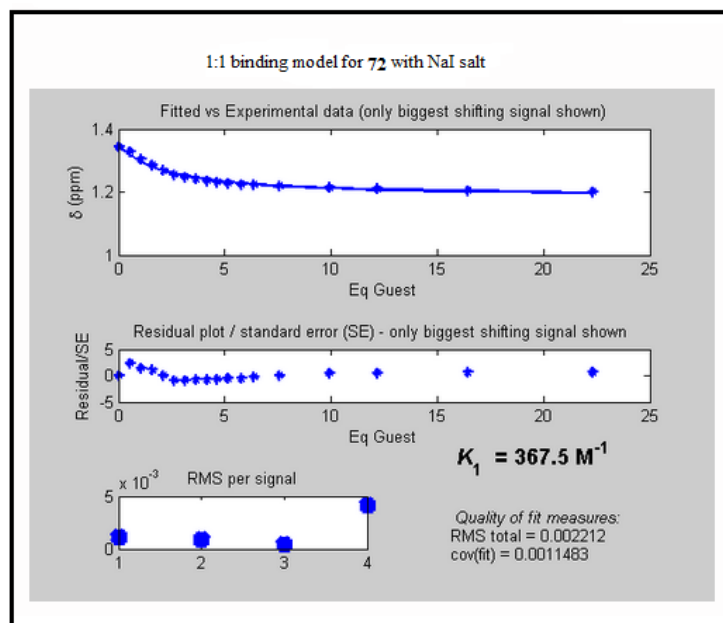


Figure 2.24 Binding constant (K_{assoc}) were determined by ^1H NMR titration experiments using the *OriginPro 6.0* program.

Table 2.03 ^1H NMR (300 MHz) titration chemical shift data for Ar-*H*, Ar-*CH*₂, *SCOCH*₃ and *t*-Bu of **72** (1.5×10^{-3} M) upon the addition of NaI (0.53-22.31 eq) solution.

Sample	Host [87]	Guest [NaI]	G/H	Ar- <i>H</i> δ (ppm)	Ar- <i>CH</i> ₂ δ (ppm)	<i>SCOCH</i> ₃ δ (ppm)	<i>t</i> -Bu δ (ppm)
1	1.49E-03	0		7.153	4.337	2.351	1.343
2	1.49E-03	7.95E-04	0.53	7.165	4.349	2.355	1.321
3	1.49E-03	1.58E-03	1.06	7.179	4.359	2.358	1.303
4	1.49E-03	2.37E-03	1.59	7.187	4.368	2.361	1.286
5	1.49E-03	3.14E-03	2.11	7.200	4.373	2.363	1.269
6	1.49E-03	3.91E-03	2.63	7.202	4.379	2.364	1.255
7	1.49E-03	4.68E-03	3.14	7.207	4.383	2.365	1.247
8	1.49E-03	5.43E-03	3.65	7.210	4.386	2.366	1.241
9	1.49E-03	6.19E-03	4.15	7.213	4.389	2.367	1.236
10	1.49E-03	6.93E-03	4.65	7.215	4.392	2.3675	1.232
11	1.49E-03	7.67E-03	5.15	7.218	4.393	2.368	1.229
12	1.49E-03	8.59E-03	5.77	7.220	4.395	2.3685	1.225
13	1.49E-03	9.50E-03	6.38	7.222	4.397	2.369	1.223
14	1.49E-03	1.13E-02	7.58	7.224	4.399	2.3695	1.219
15	1.49E-03	1.48E-02	9.92	7.228	4.402	2.370	1.214
16	1.49E-03	1.81E-02	12.17	7.232	4.405	2.371	1.210
17	1.49E-03	2.45E-02	16.44	7.235	4.408	2.3715	1.205

The binding constants (K_{assoc}) were also determined using a global analysis program developed by Prof. Pall Thordarson, UNSW, Australia (www.supramol.com).^{37b} The resulting global K_{assoc} was determined to be $3.7 \times 10^2 \text{ M}^{-1}$ (Figure 2.25) based on the Ar-*H*, Ar-*CH*₂, -*SCOCH*₃ and *t*-Bu proton chemical shift changes (Table 2.03) which to two significant figures is in reasonable agreement with the average value determined using the previous method.



$$K = 3.7 \times 10^2 \text{ M}^{-1}$$

Figure 2.25 The output from the calculation from the 1:1 ^1H NMR global analysis binding isotherm.^{37b}

2.7.3.2 ^1H NMR titration experiments of **72** with KI

Figures 2.26a-d show the ^1H -NMR titration spectra of **72** with successive additions of anhydrous KI salt ($2.0 \times 10^{-2} \text{ M}$) in the 4:1 $\text{CD}_3\text{OD}:\text{CDCl}_3$ solvent mixture. It can be seen that the increasing amounts of KI added to the solution of **72** results in downfield chemical shift changes for one of the Ar-*H* proton from δ 6.47 to 7.26 ppm. Upon addition of 0.12 eq of KI to **72**, the intensity of the Ar-*H* proton signal at δ 6.47 decreases gradually, and that of the signal at δ 7.26 gradually increases. Addition of 0.36 eq of KI (15 μL) to **72** causes the Ar-*H* peak at δ 6.47 to completely disappear. The other aromatic singlet shows downfield chemical shift changes from δ 7.15 to 7.17 ppm. The SCOCH_3 proton signals are shifted downfield from δ 2.35 to 2.39 ppm and the Ar- CH_2 - proton

signals are shifted from δ 4.31 to 4.42 ppm. However, of the two *t*-Bu signals at δ 1.35 and 0.83, one is shifted upfield and the other downfield, (Figure 2.26d). All of the observed chemical shift changes clearly indicate that complexation occurred between **72** and KI. The spectra shown in Figure 2.26d in particular for the chemical shift changes for the *t*-butyl groups are suggestive of a significant conformational change. Upon saturation of the host by the addition of up to at least 50 μ L of the KI solution the two *t*-butyl signals appear as singlets at δ 1.22 and 1.12 ppm. Thus, it appears that the δ 1.35 ppm signal has shifted upfield to δ 1.22 ppm and that the δ 0.80 ppm signal has shifted downfield to δ 1.12 ppm. It is hypothesized that **72** changes its conformation from a *pinched-cone* to a *cone* conformer. In the former, the two *t*-butyl groups which are attached to the phenyl groups that are linked by the crown-5 and are closer to each other, are the relatively shielded protons (see Figure 2.20). Thus, upon K^+ complexation **72** is now in a *cone* conformer as a result of which the two *t*-butyls move outward and the other two *t*-butyl groups which are on the thio-acetate containing phenol groups move inwards thus becoming more shielded. A similar phenomenon is observed with **72** upon complexation with RbI (Figure 2.27d).

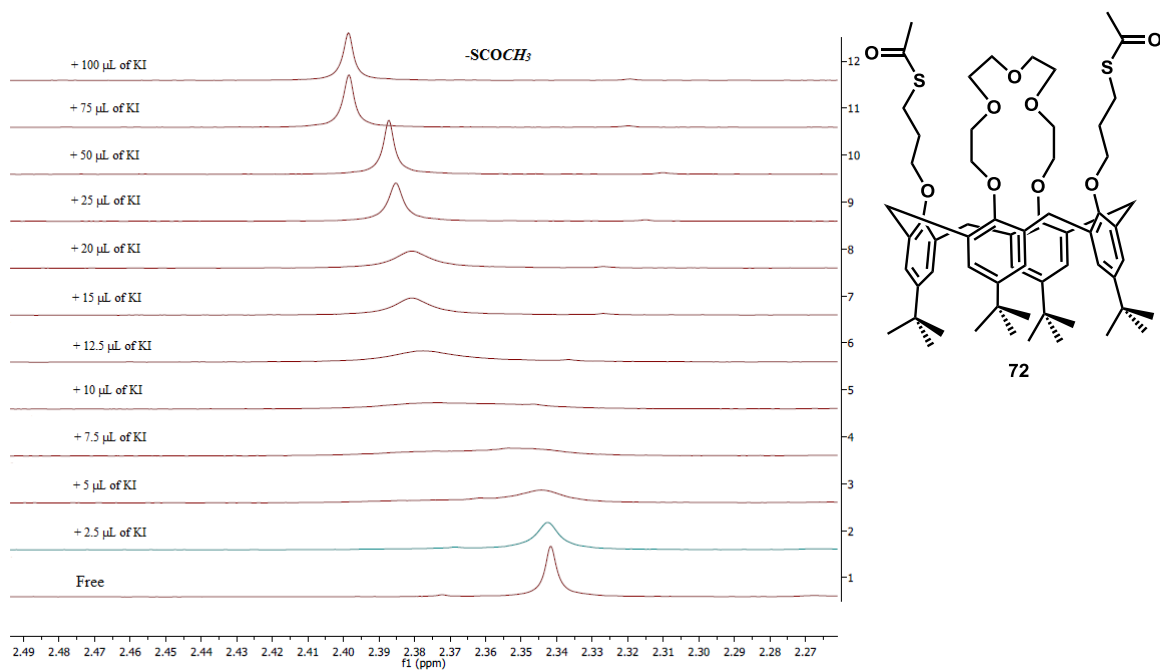


Figure 2.26c ^1H NMR (300 MHz) titration spectra for $-\text{SCOCH}_3$ of **72** (1.5×10^{-3} M) with KI (2.0×10^{-2} M) solution.

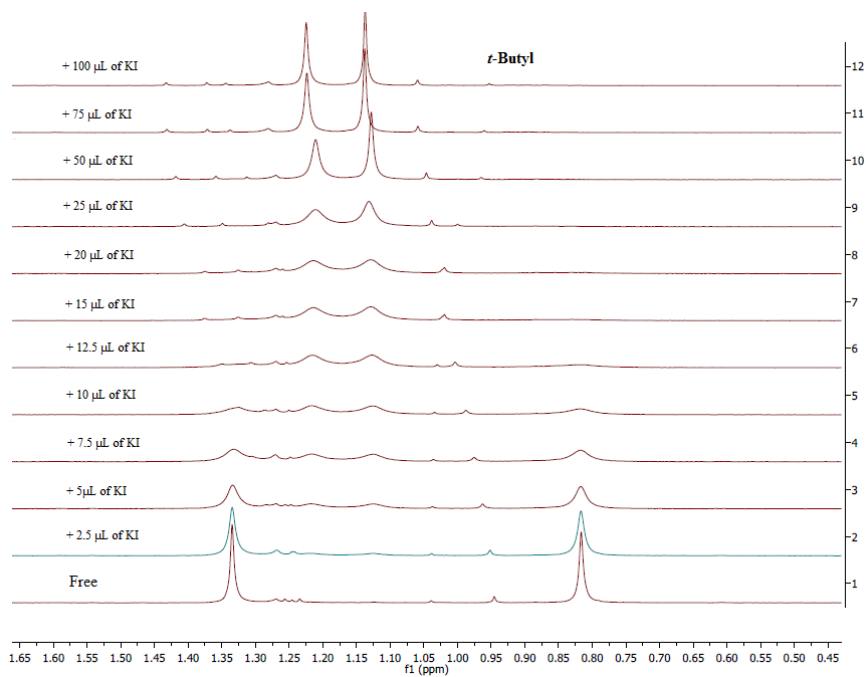


Figure 2.26d ^1H NMR (300 MHz) titration spectra for *t*-butyl of **72** (1.5×10^{-3} M) with KI (2.0×10^{-2} M) solution.

2.7.3.3 ^1H -NMR titration experiments of **72** with RbI

Figure 2.27a-d shows the ^1H -NMR titration spectra of **72** with successive additions of anhydrous RbI in a 4:1 $\text{CD}_3\text{OD}:\text{CDCl}_3$ solvent mixture. It can be seen that by increasing the additions of RbI to the solution of **72** results in downfield chemical shift changes for the aromatic singlet signals (Ar-H) from δ 7.15 to 7.21 ppm, while the aromatic singlet signal (Ar-H) at δ 6.48 ppm completely disappeared. The SCOCH_3 proton signal shifted downfield from δ 2.35 to 2.38 ppm, and the Ar- CH_2 - doublet signal changes from δ 4.31 to 4.48 ppm. However, one of the *t*-butyl proton signals is shifted upfield from δ 1.34 to 1.23 ppm (Table 2.04), the other *t*-butyl proton signal disappeared and shows only one peak after complexation. This indicates that large *cone* angle changes occur in the *cone* conformation of **72** upon binding with RbI.

The association constants (K_{assoc}), were determined using the non-linear 1:1 binding isotherms according to the *OriginPro* 6.0 program. The resulting average K_{assoc} value is $921.5 \pm 29.4 \text{ M}^{-1}$ respectively, based on the *t*-butyl, Ar-H, Ar- CH_2 , and - SCOCH_3 proton chemical shift changes (Figure 2.28).

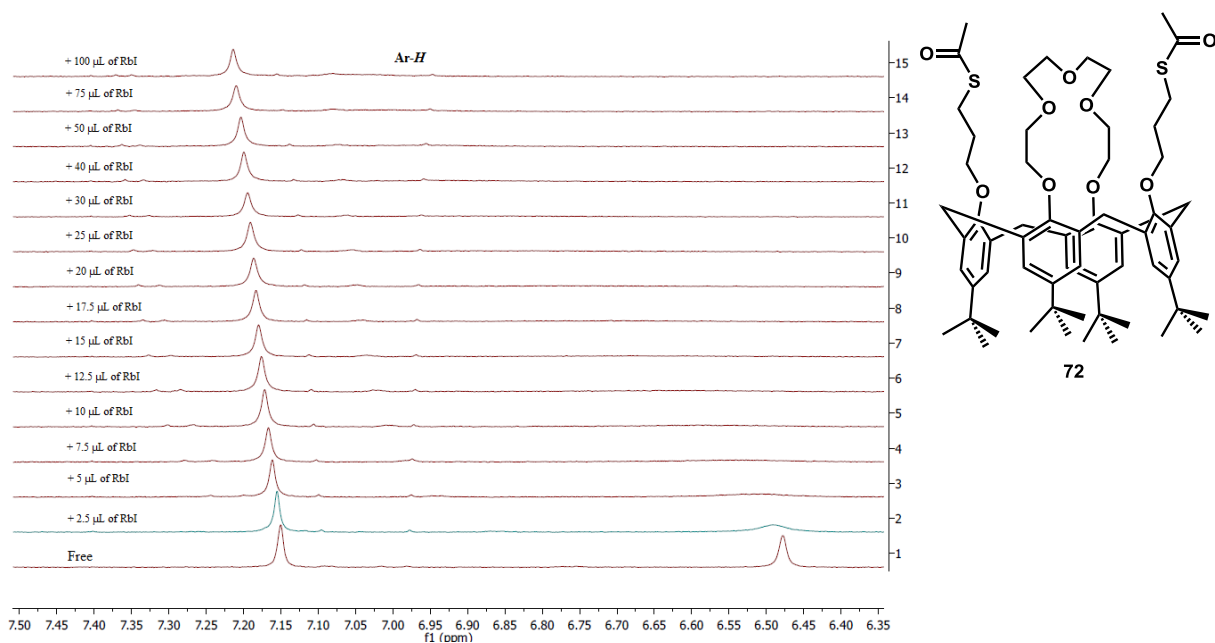


Figure 2.27a ^1H NMR (300 MHz) titration spectra for Ar-H of **72** (1.5×10^{-3} M) with RbI (2.0×10^{-2} M) solution.

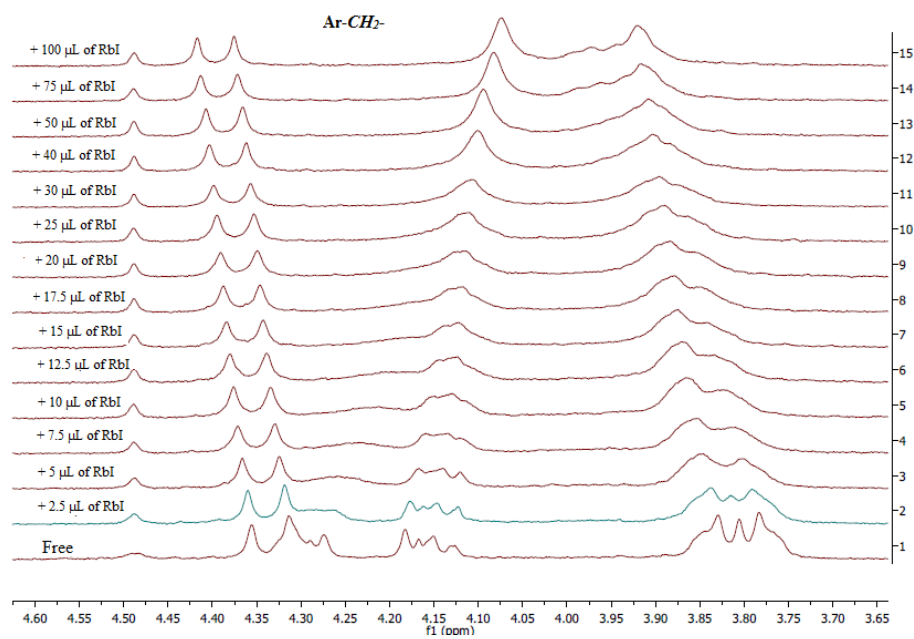


Figure 2.27b ^1H NMR (300 MHz) titration spectra for Ar-CH₂ of **72** (1.5×10^{-3} M) with RbI (2×10^{-2} M) solution.

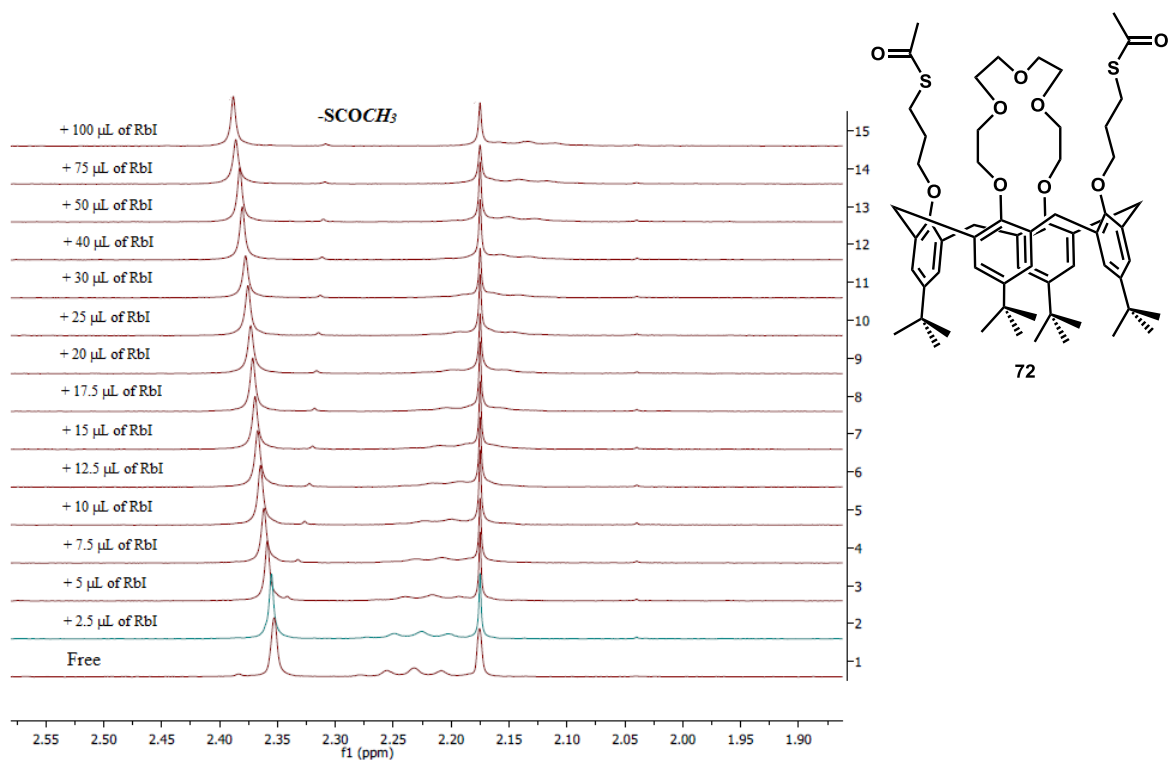


Figure 2.27c ^1H NMR (300 MHz) titration spectra for $-\text{SCOCH}_3$ of **72** (1.5×10^{-3} M) with RbI (2.0×10^{-2} M) solution.

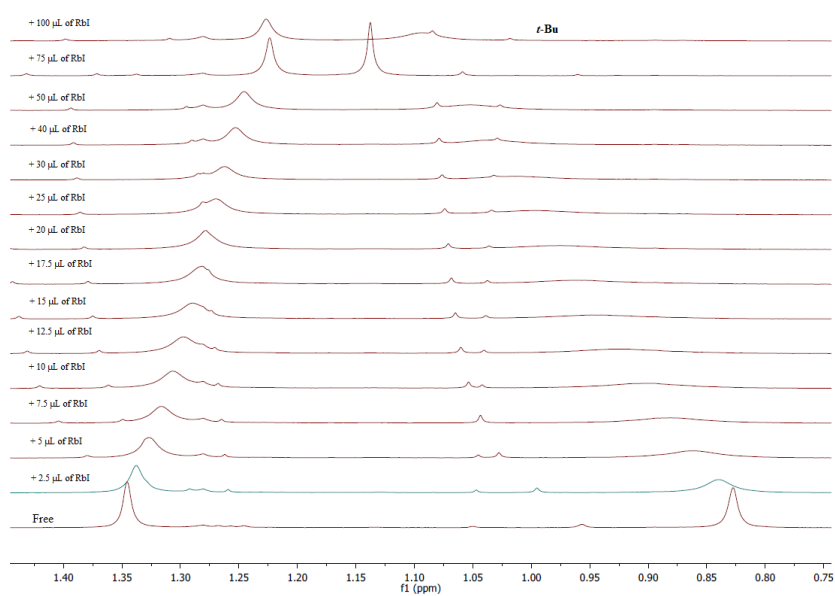


Figure 2.27d ^1H NMR (300 MHz) titration spectra for *t*-butyl of **72** (1.5×10^{-3} M) with RbI (2.0×10^{-2} M) solution.

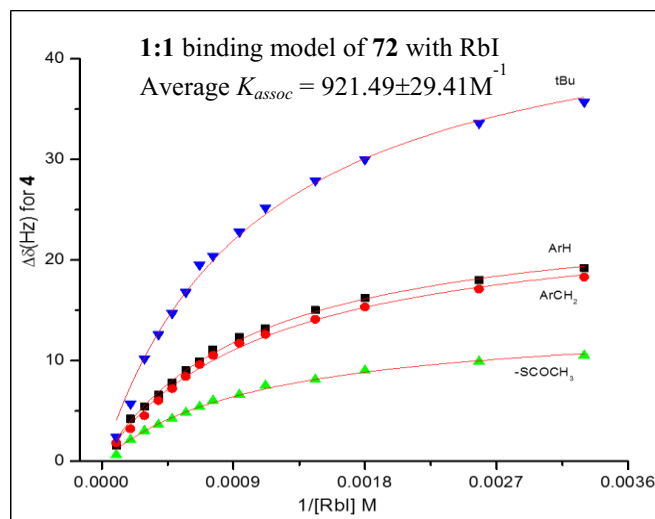
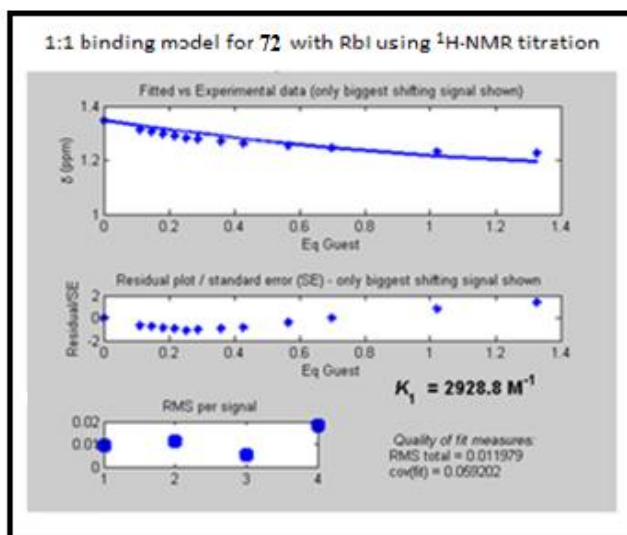


Figure 2.28 $^1\text{H-NMR}$ (300 MHz) titration curves for Ar-*H*, Ar-*CH*₂, *SCOCH*₃ and *t*-butyl, respectively of **72** (1.5×10^{-3} M) with RbI (2.0×10^{-2} M) solution.

The binding constants (K_{assoc}) were also determined using the global analysis program developed by Prof. Pall Thordarson.^{37b} The resulting global K_{assoc} was determined to be $3.0 \times 10^3 \text{ M}^{-1}$ (Figure 2.29) based on the Ar-*H*, Ar-*CH*₂, -*SCOCH*₃ and *t*-Bu proton chemical shift changes (Table 2.04).



$$K = 3.0 \times 10^3 \text{ M}^{-1}$$

Figure 2.29 The output from the calculation from the 1:1 $^1\text{H-NMR}$ global analysis binding isotherm.^{37b}

Table 2.04 $^1\text{H-NMR}$ (300 MHz) titration chemical shift data for Ar-*H*, Ar-*CH*₂, *SCOCH*₃ and *t*-Bu of **72** (1.5×10^{-3} M) upon the addition of RbI (0.07-2.21 eq) solution.

Sample	Host [87]	Guest [RbI]	G/H	Ar- <i>H</i> δ (ppm)	Ar- <i>CH</i> ₂ δ (ppm)	<i>SCOCH</i> ₃ δ (ppm)	<i>t</i> -Bu δ (ppm)
1	1.49E-03	0		7.150	4.335	2.353	1.346
2	1.49E-03	9.84E-05	0.07	7.155	4.341	2.355	1.338
3	1.49E-03	1.96E-04	0.13	7.164	4.346	2.360	1.327
4	1.49E-03	2.92E-04	0.20	7.168	4.350	2.363	1.312
5	1.49E-03	3.88E-04	0.26	7.170	4.355	2.365	1.304
6	1.49E-03	4.82E-04	0.32	7.176	4.359	2.367	1.297
7	1.49E-03	5.76E-04	0.39	7.180	4.363	2.369	1.290
8	1.49E-03	6.69E-04	0.45	7.183	4.367	2.371	1.281
9	1.49E-03	7.61E-04	0.51	7.187	4.370	2.373	1.278
10	1.49E-03	9.42E-04	0.63	7.191	4.374	2.375	1.270
11	1.49E-03	1.12E-03	0.75	7.194	4.377	2.378	1.262
12	1.49E-03	1.46E-03	0.98	7.200	4.382	2.380	1.253
13	1.49E-03	1.80E-03	1.21	7.204	4.386	2.383	1.246
14	1.49E-03	2.58E-03	1.73	7.210	4.392	2.386	1.234
15	1.49E-03	3.30E-03	2.21	7.214	4.396	2.388	1.227

2.8 Computational studies:

To better understand the binding properties of receptor **72** with the cations tested. A computational study was carried out. The individual structures for all studies in the gas-phase were fully geometry-optimized using Gaussian 09⁵⁴ with the B3LYP level of DFT and the Def2SVP basis set.

Binding energy:

The calculated binding energies (ΔE) of the complexes M^+/L formed between the cations: Li^+ , Na^+ , K^+ , Rb^+ and Cs^+ and the free calix[4]arene-crown **72** (**L**) in gas phase at 298 K, at the B3LYP/Def2SVP basis set -based on Equation 2.6 are summarized in Table

2.05. Geometry-optimized structures of the complexes formed between the cations and calix[4]arene-crown **72** are shown in Figure 2.30, 2.31 and 2.32.

For this system, the binding energy ΔE can be calculated as follows:

$$\Delta E = E_{L:\text{metal ion}(\text{complex})} - E_{L(\text{free})} - E_{\text{metal ion}(\text{free})} \quad (\text{Equation 2.6})$$

Table 2.05 Calculated binding energies for the receptor **72** with metal ions.

Parameter	72:Cs ⁺	72:Rb ⁺	72:K ⁺	72:Na ⁺	72:Li ⁺
Binding Energies (kJ mol ⁻¹) for metals in the crown	-200.56	-261.27	-309.22	-325.47	-417.78
Binding Energies (kJ mol ⁻¹) for metals in the cavity	-160.95	-192.54	-228.90	-324.95	-417.24

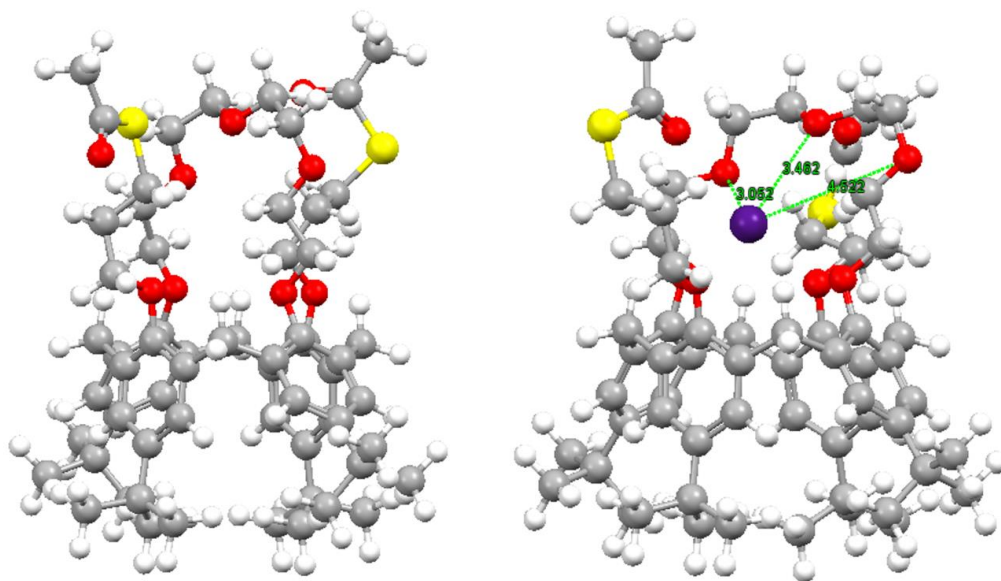


Figure 2.30 Geometry-optimized structures of: *Left*: Free calix-crown **72** and *Right*: **72:Cs⁺** complex. Colour code: Cs⁺ = **purple**, sulphur = yellow, hydrogen = white, carbon = dark grey, and oxygen atom = red.

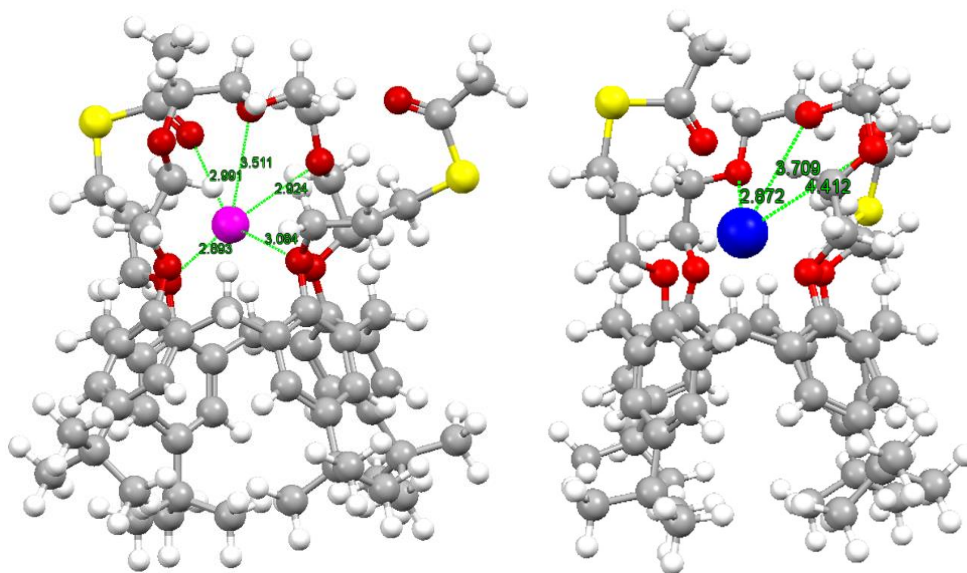


Figure 2.31 Geometry-optimized structures of: *Left*: $72:\text{Rb}^+$ complex and *Right*: $72:\text{K}^+$ complex. Colour code: Rb^+ = magenta, K^+ = blue, sulphur = yellow, hydrogen = white, carbon = dark grey, and oxygen atom = red.

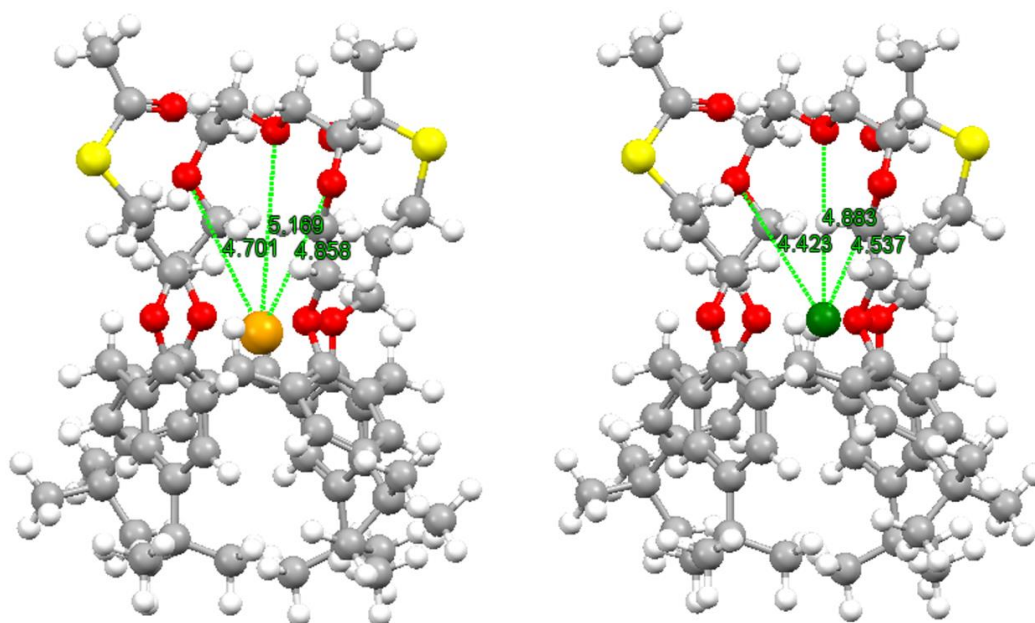


Figure 2.32 Geometry-optimized structures of: *Left*: $72:\text{Na}^+$ complex and *Right*: $72:\text{Li}^+$ complex. Colour code: Na^+ = orange, Li^+ = green, sulphur = yellow, hydrogen = white, carbon = dark grey, and oxygen atom = red.

Table 2.06 Selected interatomic distances between M^+ (Cs^+ , Rb^+ , K^+ , Na^+ and Li^+) and oxygen atoms of polyether fragments in the complexes **72**: M^+ optimized at B3LYP/Def2SVP Level (distances in Å).

Parameter	72:Cs ⁺ Distance (Å)	72:Rb ⁺ Distance (Å)	72:K ⁺ Distance (Å)	72:Na ⁺ Distance (Å)	72:Li ⁺ Distance (Å)
M^+-O_{22}	2.960	2.893	2.851	2.373	1.955
M^+-O_{53}	3.385	3.084	2.919	3.586	4.030
M^+-O_{79}	2.891	2.734	2.606	2.196	2.009
M^+-O_{84}	3.052	2.924	2.872	4.858	4.537
M^+-O_{87}	4.522	3.511	3.709	5.169	4.883
M^+-O_{90}	3.052	4.441	4.412	4.701	4.423
M^+-O_{93}	3.58	2.850	2.692	2.202	2.003

The data summarized in Table 2.05 suggest that for the larger cations Cs^+ , Rb^+ and K^+ the “crown-ether”, presumably in a “puckered” form,⁵⁵ is the preferred site for the metal binding. For Li^+ and Na^+ there is not much of a difference. The figures shown in Figure 2.32 indicate that Li^+ and Na^+ are closer to the phenolic oxygen atoms as compared with the positions of the larger cations which clearly are located within the “crown-5” moiety. A diagram of **72** with the oxygen atoms labelled is shown in Figure 2.33. A detailed DFT computational study of complexation of different metal salts with calix-crown **72** with solvent corrections is currently on going.

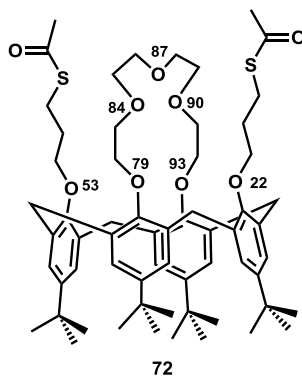
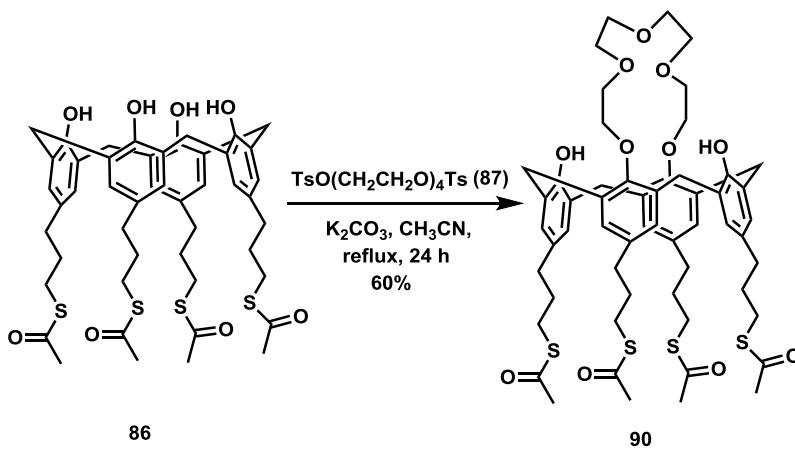


Figure 2.33 Structure of **72** with oxygen atoms labelled.

2.9 Synthesis of calix[4]arene-crown-5 derivative **90**.

As a further part of the ongoing studies of potential calixarene-based sensing layers for MCLs, the next designed 1,3-bridged-crown-5 receptor was **90** which has the free phenolic hydroxyl groups. The synthetic procedure for **90** is shown in Scheme 2.09. Substitution reaction of calix[4]arene derivative **86** with tetraethyleneglycol ditosylate **87** using K_2CO_3 as base in CH_3CN gave **90** in 60% yield.⁵³



Scheme 2.09 Synthesis of calix[4]arene-crown derivative **90**.

The microcantilever studies and solution phase complexation studies of **90** were still ongoing at the time of the writing of this thesis.

2.10 Conclusions

Two new bimodal upper- and lower-rim functionalized calix[4]arenes **70** and **71** have been synthesized. The upper rim of these calix[4]arenes were functionalized with thioacetate groups which allowed the calixarene to form a stable SAM onto a Au surface and which has been characterized by Scanning Tunneling Microscopy (STM). The lower rim of the **70** was modified with methyl ester group and the lower rim of the **71** was modified with ethyl ester group. Microcantilevers functionalized with the bimodal calix[4]arene **70** were capable of detecting calcium ion concentrations as low as 10^{-11} M in aqueous solutions. Also based on $^1\text{H-NMR}$ titration experiments of **70** and **71** with various Group 2 ions, the ester groups of calix[4]arenes **70** and **71** selectively bind to Ca^{2+} ions. The modified calix[4]arenes **70** and **71** are therefore shown to be sensitive calcium ion sensors on MCLs.

A bimodal or upper- and lower-rim functionalized calix[4]arene **72** has also been synthesized. The lower rim of the calixarene is functionalized with two different groups, one of which is a 1,3 bridged crown-5, and the other two positions have thioacetate groups. The thioacetate group enables the calixarene to form a stable SAM onto a Au surface, and the resulting SAM has been characterized by STM. The crown-5 group selectively binds to Group 1 (alkali metal) ions and forms a sensitive cesium ion MCL sensor. Calix[4]arene **72** was unexpectedly formed preferentially in a *cone* conformation.

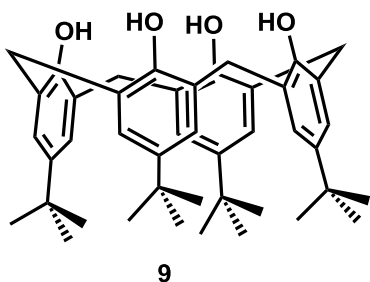
This was confirmed both by NMR spectroscopy and by single-crystal X-ray crystallography.

2.11 Experimental section

All reagents used for the synthesis of functionalized upper- and lower-rim calix[4]arenes and reagents used in the complexation studies were purchased from Sigma-Aldrich or AlfaAesar. ^1H NMR spectra were recorded at either 300 or 500 MHz, as noted, and the ^{13}C NMR spectra at 75 MHz as noted. Mass spectra were measured on an APCI-LC/MSD Trap instrument.

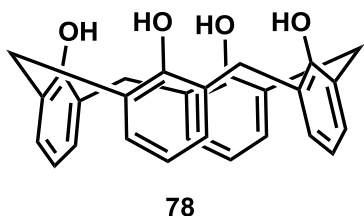
2.11.1 Experimental

5,11,17,23-Tetra-*tert*-butyl-25,26,27,28-tetrahydroxycalix[4]arene or *p*-*tert*-butyl calix[4]arene (9).



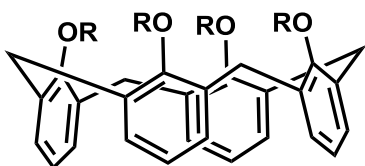
The *p*-*tert*-butylcalix[4]arene **9** was synthesized from *p*-*tert*-butylphenol **77** according to the procedure of Gutsche *et al.*³

25,26,27,28-Tetrahydroxycalix[4]arene (78).



The conversion of *p*-*tert*-butylcalix[4]arene **9** to de-*tert*-butylated **78** via a retro-Friedel-Crafts alkylation reaction was conducted as described by Chawla *et al.*³⁹

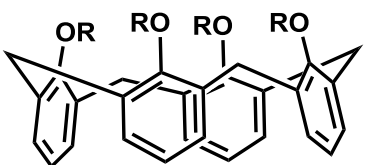
25,26,27,28-Tetrakis[(*O*-methoxycarbonyl)methyl]calix[4]arene (79).



79: R = CH₂CO₂Me

To a mixture of **78** (1.02 g, 2.35 mmol) and sodium carbonate (3.01 g, 28.3 mmol) in dry acetone (50 mL) was added methyl bromoacetate (2.68 mL, 28.3 mmol), which was then heated at reflux for 24 h. After cooling to room temperature, the reaction mixture was neutralized with aqueous 1.0 M HCl and then extracted with ethyl acetate (3 × 50 mL) and washed with water (2 × 50 mL). The separated organic layer was dried over anhydrous MgSO₄ and the solvent was removed using a rotary evaporator. The residue was purified by column chromatography (silica gel, eluting with 80:20 hexanes: ethylacetate) to give **79** as a colourless solid (1.34 g, 80%) m.p. 118.8-120.2 °C. ¹HNMR (CDCl₃, 300 MHz): δ 6.66-6.62 (m, 12H, ArH), 4.84 (d, *J* = 13.5 Hz, 4H, ArCH₂), 4.75 (s, 8H, ArOCH₂), 3.76 (s, 12H, -CO₂CH₃), 3.24 (d, *J* = 13.5 Hz, 4H, ArCH₂). ¹³CNMR (CDCl₃, 75.4 MHz): δ 170.6, 155.8, 134.5, 128.6, 122.9, 71.2, 51.5, 31.3. APCI(+) MS (*m/z*): 713.2 [M+1]⁺.

25,26,27,28-Tetrakis-[(*O*-ethoxycarbonyl)methyl]calix[4]arene (80).

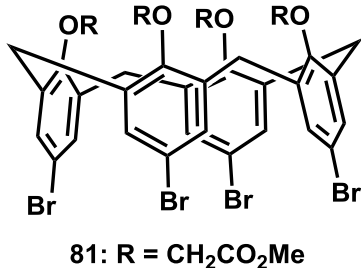


80: R = CH₂CO₂Et

To a mixture of **78** (1.02 g, 2.35 mmol) and sodium carbonate (3.01 g, 28.3 mmol) in dry acetone (50 mL) was added ethyl bromoacetate (3.13 mL, 28.3 mmol), which was then heated at reflux for 24 h. After cooling to room temperature, the reaction mixture was neutralized with aqueous 1.0 M HCl and then extracted with ethyl acetate (3 × 50 mL) and washed with water (2 × 50 mL). The

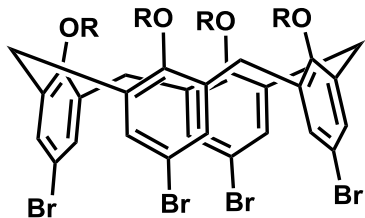
separated organic layer was dried over anhydrous MgSO_4 and the solvent was removed using a rotary evaporator. The residue was purified by column chromatography (silica gel, 80:20 hexanes: ethyl acetate) to give **80** as a yellow oil (1.46 g, 81%). ^1H NMR (CDCl_3 , 300 MHz): δ = 6.66-6.59 (m, 12H, ArH), 4.87 (d, J = 13.5 Hz, 4H, ArCH₂), 4.73 (s, 8H, ArOCH₂), 4.21 (q, J = 7.2 Hz, 8H, -CO₂CH₂CH₃), 3.24 (d, J = 13.5 Hz, 4H, ArCH₂), 1.29 (t, J = 7.2 Hz, 12H, -CO₂CH₂CH₃). ^{13}C -NMR (CDCl_3 , 75.4 MHz): δ 170.2, 155.9, 134.6, 128.6, 122.8, 71.3, 60.5, 31.5, 14.2. APCI(+) MS (m/z): 769.3 [M+1]⁺.

5,11,17,23-Tetrabromo-25,26,27,28-tetrakis-[(*O*-methoxycarbonyl)methyl] calix[4]arene (81**)**



Bromine (570 μL , 11 mmol) in DMF (10 mL) was added to dropwise with stirring to a solution of **79** (1.01 g, 1.41 mmol) in DMF (40 mL). The reaction mixture was stirred for 4 h with a precipitate forming after about 1 h. Methanol (40 mL) was added to the reaction mixture; the precipitate was filtered off and washed with methanol (3×5 mL) to yield **81** (1.12 g, 77%) m.p. 164.6-166.1 $^\circ\text{C}$ as a colourless solid. ^1H NMR (CDCl_3 , 300 MHz): δ 6.85 (s, 8H, ArH), 4.80 (d, J = 13.8 Hz, 4H, ArCH₂), 4.69 (s, 8H, ArOCH₂), 3.75 (s, 12H, -CO₂CH₃), 3.17 (d, J = 13.8 Hz, 4H, ArCH₂). ^{13}C NMR (CDCl_3 , 75.4 MHz): δ 170.1, 154.9, 135.9, 131.5, 116.3, 71.2, 51.7, 31.1. APCI(+) MS (m/z): 1028.9 [M+1]⁺.

5,11,17,23-Tetrabromo-25,26,27,28-tetrakis-[(*O*-ethoxycarbonyl)methyl]calix[4]arene (82)

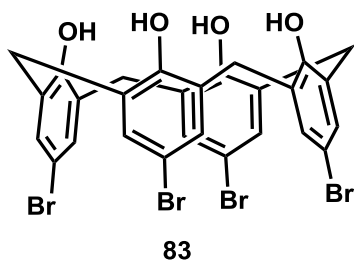


82: R = CH₂CO₂Et

Bromine (570 μ L, 11 mmol) in DMF (10 mL) was added to dropwise with stirring to a solution of **80** (1.08 g, 1.41 mmol) in DMF (40 mL). The reaction mixture was stirred for 4 h with a precipitate forming after about 1 h.

Methanol (40 mL) was added to the reaction mixture; the precipitate was filtered off and washed with methanol (3×5 mL) to yield **82** (1.20 g, 79%) m.p. 179.4-180.8 $^{\circ}$ C as a colourless solid. 1 H-NMR (CDCl₃, 300 MHz): δ 6.84 (s, 8H, ArH), 4.83 (d, $J = 13.8$ Hz, 4H, ArCH₂), 4.67 (s, 8H, ArOCH₂), 4.19 (q, $J = 7.2$ Hz, 8H, -CO₂CH₂CH₃), 3.16 (d, $J = 13.8$ Hz, 4H, ArCH₂), 1.28 (t, $J = 7.2$ Hz, 12H, -CO₂CH₂CH₃). 13 C-NMR (CDCl₃, 75.4 MHz): δ 169.6, 154.9, 136.0, 131.4, 116.2, 71.4, 60.7, 31.2, 14.2. APCI(+) MS (m/z): 769.3 [M+1]⁺.

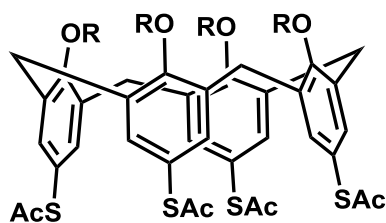
5,11,17,23-Tetrabromo-25,26,27,28-tetrahydroxycalix[4]arene (83).



83

5,11,17,23-Tetrabromo-25,26,27,28-tetrahydroxycalix[4]arene (**83**) was prepared as described by Raston *et al.*⁴³

Attempted synthesis of thioacetate-bearing calix[4]arenes **73** and **74**.



73: R = CH₂CO₂Me

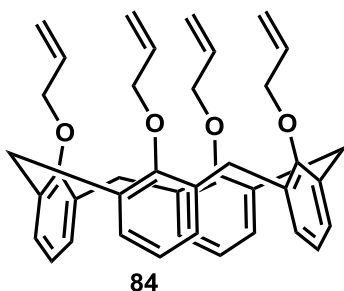
74: R = CH₂CO₂Et

A solution of tetrabromocalix[4]arenes **81** (0.20 g, 0.19 mmol) or **82** (0.21 g, 0.19 mmol) in THF (25 mL) was cooled to $-78\text{ }^{\circ}\text{C}$ and *tert*-BuLi (1.7 M in pentane) (0.861 mL, 1.55 mmol) was added. The reaction mixture was stirred for 2 h and sulfur (0.051 g, 1.55

mmol) was added at $-78\text{ }^{\circ}\text{C}$. The reaction was allowed to warm to room temperature and stirred for 30 min. The mixture was then cooled to $-20\text{ }^{\circ}\text{C}$, and AcCl (0.12 mL, 1.55 mmol) was added and the mixture was allowed to warm to room temperature and was stirred for 12 h. The reaction was not successful, with 95% of the starting material recovered. An alternative approach is as follows.

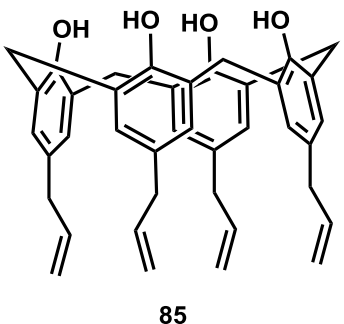
A mixture of bromocalix[4]arene **81** (0.25 g, 0.24 mmol) or **82** (0.26 g, 0.24 mmol), potassium thioacetate (0.22 g, 1.9 mmol), Pd₂(dba)₃ (5.20 mg, 0.061 mmol) and Xantphos (0.013 g, 0.024 mmol) were placed in a microwave tube capped with a rubber septum. The tube was evacuated under vacuum and refilled with nitrogen and then, (*i*-Pr)₂NEt (80 μL , 0.46 mmol) and degassed dry 1,4-dioxane (10 mL) were added to the tube. The reaction mixture was heated in a microwave reactor at $160\text{ }^{\circ}\text{C}$ for 25 min to 5 h; the reaction was not successful under these conditions, and starting material (98%) was recovered.

25,26,27,28-Tetra-*O*-allyl-calix[4]arene (**84**).



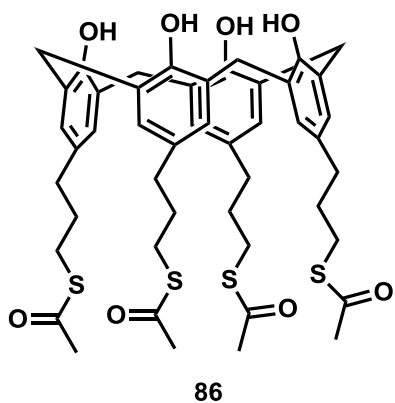
The tetra-*O*-allylated calix[4]arene **84** was synthesized from 25,26,27,28-tetrahydroxycalix[4]arene **78** according to the procedure of Kimura *et al.*⁴⁵

5,11,17,23-Tetrakis(allyl)-25,26,27,28-tetrahydroxycalix[4]arene (**85**).



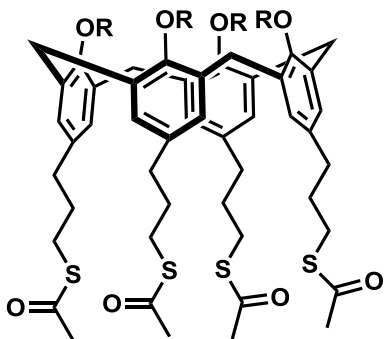
Tetra-*O*-allylcalix[4]arene **84** (1.01 g, 1.71 mmol) was dissolved in 20 mL of *N,N*-diethylaniline and stirred at 210 °C for 12 h under nitrogen. The reaction mixture was poured into water. After the addition of aqueous 2.0 M HCl, the aqueous phase was extracted with CH₂Cl₂ (2 × 50 mL). The combined organic layer was washed with water (2 × 25 mL) and then dried over MgSO₄ and filtered. The solvent was removed using a rotary evaporator and the residue was purified by the recrystallization from isopropyl alcohol to give **85** (0.710 g, 70%) m.p. 201.5-202.7 °C as a colourless solid. ¹HNMR (CDCl₃, 300 MHz): δ 10.15 (s, 4H, ArOH), 6.84 (s, 8H, ArH), 5.93-5.79 (4H, m, -CH=CH₂), 5.07-5.00 (m, 8H, -CH=CH₂), 4.19 (s, 4H, ArCH₂), 3.46 (s, 4H, ArCH₂), 3.18 (d, *J* = 6.6 Hz, 8H, -CH₂-CH=CH₂). ¹³CNMR (CDCl₃, 75.4 MHz): δ 147.1, 137.6, 133.5, 128.9, 128.2, 115.6, 39.3, 31.8. APCI(+) MS (*m/z*): 585 [M+1]⁺.

5,11,17,23-Tetrakis(3-propylthioacetate)calix[4]arene (86).



A solution of 5,11,17,23-tetrakis(-allyl)-25,26,27,28-tetrahydroxycalix[4]arene (**85**) (1.02 g, 1.71 mmol), thioacetic acid (1.46 mL, 20.5 mmol) and AIBN (0.0281 g, 0.171 mmol) in 1,4-dioxane (20 mL) was degassed and then stirred at 90 °C for 48 h under N₂. After cooling to room temperature, the solvent was removed using a rotavap. The residue was dissolved in ethylacetate (100 mL), and washed with water (50 mL) and brine (50 mL). The organic layer was separated and dried over MgSO₄ and filtered. The solvent was removed using a rotary evaporator and the residue was purified by column chromatography (silica gel, eluting with hexane: ethylacetate 70:30) to give a colourless solid (0.72 g, 60%) m.p. 117.4–118.4 °C. ¹H-NMR (CDCl₃, 500 MHz): δ 10.15 (s, 4H, ArOH), 6.83 (s, 8H, ArH), 4.19 (d, *J* = 12.0 Hz, 4H, ArCH₂), 3.42 (d, *J* = 12.0 Hz, 4H, ArCH₂), 2.83 (t, *J* = 7.5 Hz, 8H, CH₂S–), 2.47 (t, *J* = 7.5 Hz, 8H, ArCH₂CH₂–), 2.33 (s, 12H, –SCOCH₃), 1.82–1.76 (m, 8H, –CH₂CH₂CH₂S–). ¹³CNMR (CDCl₃, 75.4 MHz): δ = 195.8, 146.9, 134.6, 128.4, 128.1, 33.9, 31.8, 31.0, 30.7, 28.6. APCI(–) MS (*m/z*): 887.3 [M–1].

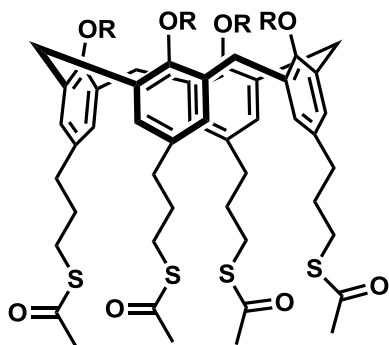
5,11,17,23-Tetrakis(3-propylthioacetate)-25,26,27,28-tetrakis-[(*O*-methoxycarbonyl)methyl]calix[4]arene (70).



70: R = CH₂CO₂Me

NaH (60% in mineral oil; 0.26 g, 11.0 mmol) was added slowly to a solution of **86** (0.60 mg, 0.67 mmol) in anhydrous THF (25 mL) and the reaction mixture was heated at reflux for 1 h. After cooling to room temperature, methyl bromoacetate (0.761 mL, 8.11 mmol) was added to the reaction mixture, which was then heated at reflux for an additional 48 h. After cooling to room temperature, the reaction mixture was neutralized with aqueous 1.0 M HCl, and then extracted with ethylacetate (3 × 50 mL). The combined organic layer was washed with water (2 × 25 mL) and then dried over anhydrous MgSO₄ and filtered. The solvent was removed using a rotary evaporator and the residue was purified by column chromatography (silica gel, eluting with 80:20 hexanes: ethyl acetate) to yield a colourless solid **70** (0.60 g, 75%) m.p. 107.5-108.4 °C. ¹HNMR (CDCl₃, 500 MHz): δ = 6.46 (s, 8H, ArH), 4.76 (d, *J* = 13.5 Hz, 4H, ArCH₂), 4.72 (s, 8H, ArOCH₂), 3.75 (s, 12H, -CO₂CH₃), 3.13 (d, *J* = 13.5 Hz, 4H, ArCH₂-), 2.76 (t, *J* = 7.5 Hz, 8H, CH₂S-), 2.35 (t, *J* = 7.5 Hz, 8H, ArCH₂CH₂CH₂S-), 2.33 (s, 12H, -SCOCH₃), 1.71-1.65 (m, 8H, -CH₂CH₂CH₂S-). ¹³CNMR (CDCl₃, 75.4 MHz): δ 195.8, 170.7, 153.9, 135.2, 134.2, 128.4, 71.1, 51.5, 34.0, 31.3, 31.1, 30.7, 28.4. APCI(+) MS (*m/z*): 1177.3 [M+1]⁺.

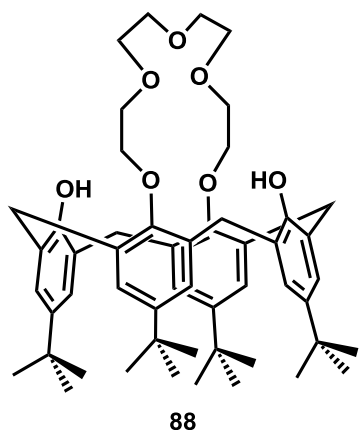
5,11,17,23-Tetrakis(3-propylthioacetate)-25,26,27,28-tetrakis-[(*O*-ethoxycarbonyl)methyl]calix[4]arene (71).



71: R = CH₂CO₂Et

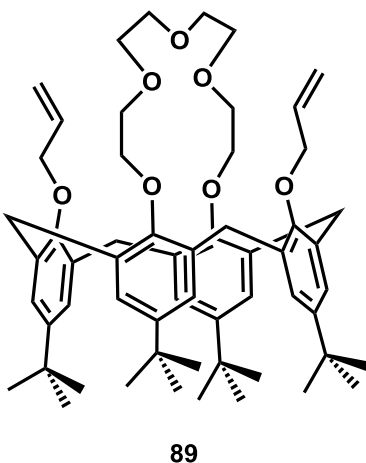
NaH (60% in mineral oil; 0.36 g, 9.1 mmol) was added slowly to a solution of **86** (0.50 g, 0.56 mmol) in anhydrous THF (25 mL) and the reaction mixture was heated at reflux for 1 h. After cooling to room temperature ethyl bromoacetate (0.66 mL, 6.8 mmol) was added to the reaction mixture, which was then heated at reflux for an additional 48 h. After cooling to room temperature, the reaction mixture was neutralized with aqueous 1.0 M HCl, then extracted with ethylacetate (3 × 50 mL). The combined organic layer was washed with water (2 × 25 mL) and then dried over anhydrous MgSO₄ and filtered. The solvent was removed using a rotary evaporator and the residue was purified by column chromatography (silica gel, eluting with 80:20 hexanes: ethyl acetate) to yield a pale yellow colour oil **71** (0.51 g, 74%). ¹H-NMR (CDCl₃, 300 MHz): δ 6.45 (s, 8H, ArH), 4.79 (d, *J* = 13.2 Hz, 4H, ArCH₂), 4.70 (s, 8H, ArOCH₂), 4.19 (q, *J* = 6.9 Hz, 8H, -CO₂CH₂CH₃), 3.13 (d, *J* = 13.2 Hz, 4H, ArCH₂), 2.76 (t, *J* = 7.2 Hz, 8H, -CH₂S-), 2.33 (s, 12H, SCOCH₃), 2.33-2.31 (m, 8H, ArCH₂CH₂CH₂S-), 1.70-1.66 (m, 8H, -CH₂CH₂CH₂S-), 1.27 (t, *J* = 7.2, 12H, -CO₂CH₂CH₃). ¹³CNMR (CDCl₃, 75.4 MHz): δ 195.8, 170.3, 154.0, 135.1, 128.4, 71.3, 60.4, 34.0, 31.5, 31.1, 30.7, 28.5, 14.2. APCI(+) MS (*m/z*): 1233.5 [M+1]⁺.

5,11,17,23-Tetra-*tert*-butyl-25,27-crown[5]ether-26,28-dihydroxycalix[4]arene (88).



The 1,3-Calix[4]-crown-5 (**88**) was synthesized from *p-tert*-butylcalix[4]arene (**9**) according to the procedure of Chailap and Tuntulani.⁵³

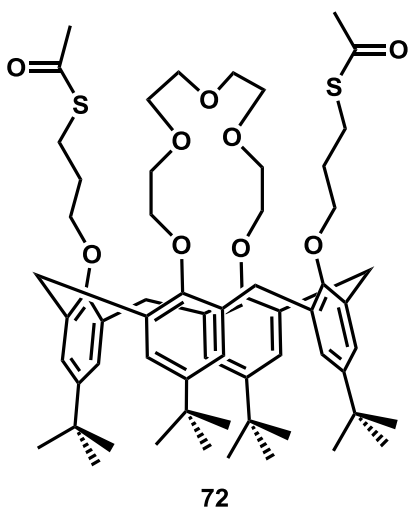
5,11,17,23-Tetra-*tert*-butyl-25,27-crown[5]ether-26,28-di-*O*-allyl-calix[4]arene (89).



To a solution of calix[4]arene **88** (1.02 g, 1.21 mmol), prepared from calix[4]arene **9**, in acetonitrile (50 mL) was added Cs₂CO₃ (1.61 g, 4.96 mmol) and the reaction mixture was heated at reflux for 30 min. Allyl bromide (0.42 mL, 5.1 mmol) was added to the reaction mixture and heated under reflux for 24 h. After cooling to room temperature, the reaction mixture was neutralized with aqueous 1.0 M HCl, and then extracted with ethylacetate (3 × 100 mL). The combined organic layer was washed with water (2 × 50 mL) and then dried over anhydrous MgSO₄ and filtered. The solvent was removed using a rotary evaporator and the residue was purified by column chromatography silica gel, eluted with 70:30 hexanes: ethyl acetate to yield **89** (0.79 g, 72%) m.p. 120.1-121.3 °C as a colourless solid. ¹HNMR (CDCl₃, 300 MHz): δ = 7.03 (s, 4H, ArH), 6.53 (s, 4H, ArH), 6.43-6.30 (m, 2H, CH=CH₂), 5.33 (d, J

= 18.1 Hz, 2H, CH=CH₂), 5.22 (d, *J* = 18.1 Hz, 2H, CH=CH₂), 4.41-4.34 (m, 8H, -OCH₂ and ArCH₂-), 4.20 (s, 8H, -OCH₂-), 3.81-3.76 (m, 8H, -OCH₂-), 3.13 (d, 4H, *J* = 15.1 Hz, ArCH₂-), 1.26 (s, 18H, *t*-Bu), 0.88 (s, 18H, *t*-Bu). ¹³CNMR (CDCl₃, 75.4 MHz): δ 154.7, 152.0, 144.9, 144.3, 135.7, 134.9, 132.5, 125.3, 124.5, 117.6, 72.6, 71.6, 71.4, 70.2, 34.0, 33.7, 31.6, 31.3, 31.2. APCI(+) MS (*m/z*): 887.5 [M+1]⁺.

5,11,17,23-Tetra-*tert*-butyl-25,27-crown[5]ether-26,28-di-*O*-(3-propylthioacetate)-calix[4]arene (72).



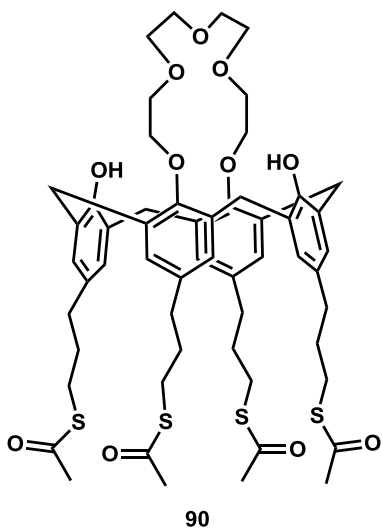
A solution of **89** (0.52 g, 0.61 mmol), thioacetic acid (0.261 mL, 3.41 mmol) and AIBN (0.0091 g, 0.061 mmol) in toluene (30 mL) was degassed and then stirred at reflux temperature for 24 h under N₂. After cooling to room temperature, the solvent was removed using a rotavap. The residue was dissolved in ethyl acetate (100 mL), and washed with water (50 mL).

The organic layer was separated and dried over

anhydrous MgSO₄ and filtered. The solvent was removed using a rotary evaporator and the residue was purified by column chromatography (silica gel hexane: ethyl acetate 60:40) to yield **72** (0.41 g, 69%) m.p. 194.5-195.3 °C as a colourless solid. ¹HNMR (CDCl₃, 300 MHz): δ 7.10 (s, 4H, ArH), 6.43 (s, 4H, ArH), 4.29 (d, *J* = 12.6 Hz, 4H, ArCH₂-), 4.22-4.19 (m, -OCH₂-), 3.81-3.74 (m, 12H, -OCH₂- and ArOCH₂-), 3.17-3.09 (m, 8H, ArCH₂-; -CH₂CH₂SCO-), 2.33 (s, 6H, -SCOCH₃), 2.20 (t, 4H, -CH₂CH₂SCO-), 1.33 (s, 18H, *t*-Bu), 0.80 (s, 18H, *t*-Bu). ¹³CNMR (CDCl₃, 75.4 MHz): δ 195.7, 154.7,

152.0, 145.1, 144.2, 135.2, 131.6, 125.6, 124.6, 74.2, 72.5, 71.2, 70.3, 34.1, 33.6, 31.7, 31.1, 31.0, 30.7, 26.3. APCI(+) MS (m/z): 1039.5 $[M+1]^+$.

5,11,17,23-Tetrakis(3-propylthioacetate)-25,27-crown[5]ether-26,28-dihydroxy calix[4]arene (90).



The mixture of 5,11,17,23-tetrakis(3-propylthioacetate)calix[4]arene (**86**) (0.51 g, 0.56 mmol) and K_2CO_3 (0.091 g, 0.68 mmol) in 25 mL of dried acetonitrile was heated at reflux under nitrogen atmosphere for 1 h. The solution of tetraethyleneglycol dithiolate, which was prepared from tetraethyleneglycol, (0.34 g, 0.68 mmol) in 10 mL of dried acetonitrile was added dropwise and the mixture was refluxed for 48 h.

Then, K_2CO_3 was removed by filtration. The residue was extracted with CH_2Cl_2 and water. The organic phase was separated and dried over anhydrous $MgSO_4$. The solvent was removed using a rotary evaporator and the residue was purified by column chromatography (silica gel, hexane: ethyl acetate 70:30) to yield **90** (0.35 g, 60%) as a pale yellow oil.

1H NMR ($CDCl_3$, 500 MHz): δ 7.66 (s, 2H, ArOH), 6.84 (s, 4H, ArH), 6.64 (s, 4H, ArH), 4.34 (d, $J = 12.9$ Hz, 4H, ArCH₂), 4.07 (s, 8H, OCH₂), 3.93 (t, $J = 5.4$ Hz, 4H, OCH₂), 3.83 (t, $J = 5.4$ Hz, 4H, OCH₂), 3.26 (d, $J = 12.9$ Hz, 4H, ArCH₂), 2.86 (t, $J = 7.2$ Hz, 8H, CH₂S-), 2.65 (t, $J = 7.2$ Hz, 4H, ArCH₂CH₂), 2.58 (t, $J = 7.2$ Hz, 4H, ArCH₂CH₂-), 2.33 (s, 6H, -SCOCH₃), 2.29 (s, 6H, -SCOCH₃), 1.91-1.81 (m, 4H, -CH₂CH₂CH₂S-), 1.69-

1.63 (m, 4H, -CH₂CH₂CH₂S-). ¹³CNMR (CDCl₃, 75.4 MHz): δ 195.9, 195.8, 151.5, 150.5, 137.4, 133.1, 131.1, 128.8, 128.4, 128.0, 71.2, 71.1, 70.2, 34.1, 34.0, 31.4, 31.3, 30.8, 30.7, 30.6, 28.6, 28.4. APCI(+) MS (*m/z*): 1047.4 [M+1]⁺.

2.12 References

1. Gutsche, C. D. *Calixarenes: An Introduction*, Royal Society of Chemistry, Cambridge, UK, 2nd edn, 2008. b) Rebily, J.-N.; Reinaud, O. *Supramol. Chem.* **2014**, *26*, 454-479. c) Vicens, J.; Harrowfield, J. *Calixarenes in the Nano World*, ed. Springer, Dordrecht, Holland, 2007.
2. a) Joseph, R.; Rao, C. P. *Chem. Rev.* **2011**, *111*, 4658-4702. b) Evans, C. J.; Nicholson, G. P. *Sens. Actuators B* **2005**, *105*, 204-207.
3. Gutsche, C. D.; Iqbal, M. *Org. Synth.* **1990**, *68*, 234-236.
4. a) Xu, C.; Yuan, L.; Shen, X.; Zhai, M. *Dalton Trans.* **2010**, *39*, 3897-3902. b) Harmon, B. W.; Ensor, D. D.; Delmau, L. H.; Moyer, B. A. *Solv. Extraction Ion Exchange* **2007**, *25*, 373-388. c) Sachleben, R. A.; Urvoas, A.; Bryan, J. C.; Haverlock, T. J.; Hay, B. P.; Moyer, B. A. *Chem. Commun.* **1999**, 1751-1752.
5. a) Haino, T.; Yanase, M.; Fukazawa, Y. *Angew. Chem., Int. Ed.* **1998**, *37*, 2747-2751. b) Antipin, I. S.; Stoikov, I. I.; Pinkhassik, E. M.; Fitseva, N. A.; Stibor, I.; Konovalov, A. I. *Tetrahedron Lett.* **1997**, *38*, 5865-5868.
6. Kim, H. J.; Lee, M. H.; Mutihac, L.; Vicens, J.; Kim, J. S. *Chem. Soc. Rev.* **2012**, *41*, 1173-1190.

7. a) Gates, B. D.; Xu, Q.; Stewart, M.; Ryan, D.; Willson, C. G.; Whitesides, G. M. *Chem. Rev.* **2005**, *105*, 1171-1196. b) Vericat, C.; Vela, M. E.; Benitez, G.; Carro, P. Salvarezza, R. C. *Chem. Rev.* **2010**, *110*, 1805-1834.
8. a) Fenter, P.; Eberhardt, A.; Eisenberger, P. *Science* **1994**, *266*, 1216-1218. b) Samant, M. G.; Brown, C. A.; Gordon II, J. G. *Langmuir* **1991**, *7*, 437-439. c) Lewis, P. A.; Donhauser, Z. J.; Mantooth, B. A.; Smith, R. K.; Bumm, L. A.; Kelly, K. F.; Weiss, P. S. *Nanotechnol.* **2001**, *12*, 231-237. d) Weisssharr, D. E.; Lamp, B. D.; Porter, M. D. *J. Am. Chem. Soc.* **1992**, *114*, 5860-5862. e) Finkela, H. O. *Encyclopedia of Analytical Chemistry: Applications Theory and Instrumentation*, John Wiley and Sons, Inc., New York, 2000.
9. Nuzzo, R. G.; Allara, D. L. *J. Am. Chem. Soc.* **1983**, *105*, 4481-4483.
10. a) Love, J. C.; Estroff, L. A.; Kriebel, J. K.; Nuzzo, R. G.; Whitesides, G. M. *Chem. Rev.* **2005**, *105*, 1103-1169. b) Ulman, A. *Chem. Rev.* **1996**, *96*, 1533-1554.
11. a) Brust, M.; Walker, M.; Bethell, D.; Schiffrin, D. J.; Whyman, R. *J. Chem. Soc. Chem. Commun.* **1994**, 801-802. b) Shimizu, T.; Teranishi, T.; Hasegawa, S.; Miyake, M. *J. Phys. Chem. B.* **2003**, *107*, 2719-2724.
12. Pedersen, C. J. *J. Am. Chem. Soc.* **1967**, *89*, 7017-7036.
13. Chen, H.; Gal, Y.-S.; Kim, S.-H.; Choi, H.-J.; Oh, M.-C.; Lee, J.; Koh, K. *Sens. Actuators B* **2008**, *133*, 577-581.

14. a) Asfieri, C.; dradi, E.; Pochina, A.; Ungaro, R.; Andreetti, G. D. *J. Chem. Soc., Chem. Commun.* **1983**, 1075-1077. b) Asfari, Z.; Bressot, C.; Rozol, J. F.; Rouquette, H.; Eymard, S.; Lamare, V.; Tourmois, B. *Anal. Chem.* **1995**, *66*, 3133-3139. c) Ji, H.-F.; Brown, G. M.; Dabestani, R. *Chem. Commun.* **1999**, 609-610.
15. Zhang, S.; Echegoyen, L. *Tetrahedron Lett.* **2003**, *44*, 9079-9082.
16. a) Beer, P. D.; Gale, P. A. *Angew. Chem., Int. Ed.* **2001**, *40*, 486-516. b) Gale, P. A. *Coord. Chem. Rev.* **2001**, *213*, 79-128. c) Best, M. D.; Tobey, S. L.; Anslyn, E. V. *Coord. Chem. Rev.* **2003**, *240*, 3-15. d) Kubik, S.; Reyheller, C.; Stuwe, S. *J. Incl. Phenom.* **2005**, *52*, 137-187.
17. a) Schemidtchen, F. P.; Berger, M. *Chem. Rev.* **1997**, *97*, 1609-1646. b) Bianchi, A.; Bowman-James, K.; Eds. Garcia-Espana, E. *Supramolecular Chemistry of Anions*; Wiley-VCH: New York, 1997.
18. Zhang, S.; Echegoyen, L. *Langmuir* **2006**, *22*, 10732-10738.
19. Cormode, D. P.; Evans, A. J.; Davis, J. J.; Beer, P. D. *Dalton Trans.* **2010**, *39*, 6532-6541.
20. Beer, P. D.; Hayes, E. J. *Coord. Chem. Rev.* **2003**, *240*, 167-189.
21. a) Patel, G.; Menon, S. *Chem. Commun.* **2009**, 3563-3565. b) Shinkai, S.; Mori, S.; Koreishi, H.; Tsubaki, T.; Manabe, O. *J. Am. Chem. Soc.* **1986**, *108*, 2409-2416.

22. Zhang, S.; Echegoyen, L. *Org. Lett.* **2004**, *6*, 791-794.
23. a) Anderson, T.; Nilsson, K.; Sundahl, M.; Westman, G.; Wennerstrom, O. *Chem. Commun.* **1992**, 604-606. b) Yoshida, Z.; Takekuma, H.; Takekuma, S.-I.; Matsubara, Y. *Angew. Chem., Int. Ed. Engl.* **1994**, *33*, 1597-1599.
24. a) Atwood, J. L.; Barnes, M. J.; Burkhalter, R. S.; Junk, P. C.; Steed, J. W.; Raston, C. L. *J. Am. Chem. Soc.* **1994**, *116*, 10346-10347. b) Diederich, F.; Effing, J.; Jonas, U.; Jullien, L.; Plesniviy, T.; Ringsdorf, H.; Thilgen, C.; Weinstein, D. *Angew. Chem., Int. Ed. Engl.* **1992**, *31*, 1599-1602. c) Eichhorn, D. M.; Yang, S.; Jarrell, W.; Baumann, T. F.; Beall, L. S.; White, A. J. P.; Williams, D. J.; Barrett, A. J.; Hoffman, B. M. *J. Chem. Soc., Chem. Commun.* **1995**, 1703-1704.
25. a) Atwood, J. L.; Koutsantonis, G. A.; Raston, C. L. *Nature* **1994**, *368*, 229-231. b) Suzuki, T.; Nakashima, K.; Shinkai, S. *Chem. Lett.* **1994**, 699-702.
26. Pan, G.-B.; Liu, J.-M.; Zhang, H.-M.; Wan, L.-J.; Zheng, Q.-Y.; Bai, C.-L. *Angew. Chem., Int. Ed.* **2003**, *42*, 2747-2751.
27. Zhang, S.; Echegoyen, L. *J. Org. Chem.* **2005**, *70*, 9874-9881.
28. a) Goeders, K. M.; Colton, J. S.; Bottomley, L. A. *Chem. Rev.* **2008**, *108*, 522-542. b) Raiteri, R.; Grattarola, M.; Butt, H.; Skladal, P. *Sens. Actuators B* **2001**, *79*, 115-126.
29. a) Fritz, J. *Analyst* **2008**, *133*, 855-863. b) Latin, Y.; Abu-Lail, N. I.; Alarn, M.; Zauscher, M. *Nanomedicine* **2009**, *2*, 222-229. c) Aldhayb, A.; Brown, N.;

- Rahman, S. M. S.; Harrigan, R.; Beaulieu, L. Y. *Appl. Phys. Lett.* **2013**, *102*, 173106.
30. Ji, H.-F.; Finot, E.; Dabestani, R.; Thundat, T.; Brown, G. M.; Britt, P. F. *Chem. Commun.* **2000**, 457-458.
31. Pinnaduwege, L. A.; Thundat, T. G.; Brown, G. M.; Bonnesen, P. V.; Boiadjiev, V.; Goretzki, G. *US Patent Application*, US2008/0206103 A1, August 28, 2008.
32. Ji, H.-F.; Dabestani, R.; Thundat, T.; Brown, G. M.; Britt, P. F.; Bonnesen, P. V. *Anal. Chem.* **2001**, *73*, 1572-1576.
33. Peng, R.-P.; Chen, B.; Ji, H.-F.; Wu, L.-Z.; Tung, C.-H. *Analyst* **2012**, *137*, 1220-1224.
34. Pensa, E.; Cortes, E.; Corthey, G.; Carro, P.; Vericat, C.; Fonticelli, M. H.; Benitez, G.; Rubert, A. A.; Salvarezza, R. C. *Acc. Chem. Res.* **2012**, *45*, 1183-1192.
35. Connors, K. A. *Binding Constants*, Wiley: New York, 1987.
36. Job, P. *Ann. Chim.* **1928**, *9*, 113-203.
37. a) Fielding, L. *Tetrahedron* **2000**, *56*, 6151-6170. b) Thordarson, P. *Chem. Soc. Rev.* **2011**, *40*, 1305-1323. c) <http://supramolecular.org/>
38. a) Georghiou, P. E.; Rahman, S.; Valluru, G. K.; Dawe, L. N.; Saydur Rahman, S. M.; Alodhayb, A. N.; Beaulieu, L. Y. *New J. Chem.* **2013**, *37*, 1298-1301. b)

- Valluru, G. K.; Rahman, S.; Georghiou, P. E.; Dawe, L. N.; Alodhayb, N. A.; Beaulieu, L. Y. *New J. Chem.* **2014**, *38*, 5868-5872.
39. Chawla, H. M.; Santra, A. *Synth. Commun.* **2001**, *31*, 2605-2611.
40. Lhotak, P.; Stastny, V.; Zlatuskova, P.; Stibor, I.; Michlova, V.; Tkadlecova, M.; Havlicek, J.; Sykora, J. *Collect. Czech. Chem. Commun.* **2000**, *65*, 757-771.
41. Iwamoto, K.; Shinkai, S. *J. Org. Chem.* **1992**, *57*, 7066-7073.
42. Genorio, B.; Subbaraman, R.; Strmcnik, D.; Tripkovic, D.; Stamenkovic, V. R.; Markovic, N. M. *Angew. Chem., Int. Ed.* **2011**, *50*, 5468-5472.
43. Clark, T. E.; Makha, M.; Sobolev, A. N.; Rohrs, H.; Atwood, J. L.; Raston, C. L.; *Chem. Eur. J.* **2008**, *14*, 3931-3938.
44. Lai, C.; Backes, B. J. *Tetrahedron Lett.* **2007**, *48*, 3033-3037.
45. Kimura, M.; Yokokawa, M.; Sato, S.; Fukawa, T.; Mihara, T. *Chem. Lett.* **2011**, *40*, 1402-1404.
46. Gutsche, C. D.; Levine, J. A.; Sujeeth, P. K. *J. Org. Chem.* **1985**, *50*, 5802-5806.
47. Buskas, T.; Soderberg, E.; Konradsson, P.; Fraser-Reid, B. *J. Org. Chem.* **2000**, *65*, 958-963.
48. Podyachev, S. N.; Burmakina, N. E.; Sudakova, S. N.; Syakaev, V. V.; Konovalov, A. I. *Supramol. Chem.* **2010**, *22*, 339-346.
49. a) Zheng, T.-C.; Burkart, M.; Richardson, D. E. *Tetrahedron Lett.* **1999**, *40*, 603-606. b) Pandya, A.; Sutariya, P. G.; Menon, S. K. *Analyst* **2013**, *138*, 2483-2490.

50. Alodhayb, N.; Rahman, S. M.; Rahman, S.; Valluru, G. K.; Georghiou, P. E.; Beaulieu, L. Y. *Sens. Actuators B.* **2014**, *203*, 766-773.
51. Sleem, H. F.; Dawe, L. N.; Georghiou, P. E. *New J. Chem.* **2012**, *36*, 2451-2455.
52. Fischer, J. A.; Zoldan, V. C.; Benitez, G.; Rubert, A. A.; Ramirez, E. A.; Carro, P.; Salvarezza, R. C.; Pasa, A. A.; Vela, M. E. *Langmuir* **2012**, *28*, 15278-15285.
53. Chailap, B.; Tuntulani, T. *Org. Biomol. Chem.* **2012**, *10*, 3617-3625.
54. Zheng, X.; Wang, X.; Yi, S.; Wang, N.; Peng, Y. *J. Comp. Chem.* **2009**, 1458-1468.
55. Gokel, G. W. in *Encyclopedia of Supramolecular Chemistry*, Ed. Atwood, J. L.; Steed, J. W.; Marcel Dekker Inc., NY, USA, 2004, Vol. 1.
56. *Handbook of Semiconductor Wafer Cleaning Technology*, ed. Kern, W. Noyes Publishing, Park Ridge, NJ, 1993, Ch.1

Chapter 3

Anthracene- and pyrene-appended triazole-based calix[4]arenes as fluorescent chemosensors

3.1 Introduction

The design and synthesis of fluorescent chemosensors with desirable properties is of current interest in supramolecular chemistry.¹ As a result, there have been extensive studies conducted on the use of calixarene-based devices as highly selective and sensitive chemosensors.¹ The lower and upper rims of calixarenes can be modified to produce a vast number of derivatives, many of which have been used in molecular recognition studies.² Calixarenes have served as the building blocks or templates for the development of fluorescent molecular receptors via the incorporation of appropriate sensor groups. Many fluorescent chemosensors based on calixarenes have been reported,^{1,3} and these show highly selective recognition properties towards alkali, alkali earth and transition metal ions. Most of the calixarene-based fluorescent sensors have been designed based on consideration of the photophysical changes that occur upon metal ion binding. The mechanisms of the photophysical changes include photoinduced charge transfer (PCT), photoinduced electron transfer (PET), formation of a monomer or excimers, energy transfer.^{1c,4}

A fluorescent chemosensor generally includes two components such as an ion recognition unit (ionophore) and a fluorogenic unit (fluorophore), which can be either an independent species or covalently linked in one molecule. When the analytes bind to the

ion recognition unit, changes occur in the optical properties (e.g. inhibition or enhancement of absorption or fluorescence) of the chemosensor.^{1c,5}

3.1.1 Metal ion receptors

The design and synthesis of new receptors for the detection of specific metal ions has become a growing field of research. This is because of the role that metal ions play in many fields, especially in biological, environmental and chemical process.^{1,6} Of different metal ions, iron is the most abundant essential trace element in the human body. It plays an indispensable role in many biological processes, since it is involved in oxygen metabolism and electron-transfer processes in DNA and RNA syntheses.⁷ Either a deficiency or an excess of Fe^{3+} can cause different diseases such as anemia, liver and kidney damage, diabetes and heart disease.^{7,8} The design of a fluorescent chemosensor capable of binding selectively to Fe^{3+} ions is still a challenge.

Besides the toxicity of iron and copper, mercury is considered as one of the most prevalent toxic metals. Mercury causes serious human health and environmental problems even at low concentrations due to its biological membrane permeability, bioaccumulation, and long retention time in the central nervous and endocrine systems.⁹ The development of highly sensitive and selective methods for the determination of Hg^{2+} is important for environmental and human health. In the past decades, numerous fluorometric and colorimetric Hg^{2+} probes based on conjugated polymers, proteins, organic chromophores, antibodies, biomolecules (DNA and proteins), synthetic polymers, quantum dots and metal nanoparticles have been developed.¹⁰ Although these methods have achieved high sensitivity toward the determination of Hg^{2+} , each of these

approaches has its own drawbacks. Therefore, it is desirable to design highly sensitive receptors that can bind selectively to Hg^{2+} .

Lead ions (Pb^{2+}) are among the most toxic heavy metal ions and are responsible for many environmental and health problems. A variety of symptoms has been attributed to lead poisoning such as anemia, memory loss, muscle paralysis, and mental retardation in children.¹¹ The selective signaling of Pb^{2+} is a very important for the detection and treatment of this metal ion in chemical and biological systems. Copper (Cu^{2+}) ions also play a significant role in biological systems as they can form complexes with proteins, generating vital energy and producing electron-transfer functions in the organism's cells.¹² However, an excess of copper ions in the organism's cells can cause diseases such as Wilson's and Alzheimer's.¹²

Cobalt ion (Co^{2+}) is one of the essential micronutrients and is present in a concentration of about 0.3 mg/L in the ocean. It also plays a significant role in the metabolism of iron and thereby in the synthesis of hemoglobin.¹³ Co^{2+} is an essential trace element found in the cobalamin coenzyme (vitamin B_{12}) and a deficiency of cobalt can cause anemia, retarded growth and loss of appetite, but in large doses, cobalt salts can be toxic.¹⁴

Cadmium ions (Cd^{2+}) have been used in pigments, Ni-Cd batteries, quantum dots and phosphate fertilizers.¹⁵ Cadmium causes serious human health problems even at low concentrations; chronic cadmium exposure causes calcium metabolism disorders, renal dysfunction and certain forms of cancers.¹⁶

In addition, after iron, zinc is the second most abundant transition metal in mammals;¹⁷ it plays an important role in various biological processes such as neurotransmission, gene expression and signal transduction.¹⁷ There is an increased interest in the design and synthesis of highly sensitive receptors that can bind selectively to transition metal ions for environmental and biological purposes.

3.1.2 Triazole bridge-based calixarene chemosensors

Fluorescent metal ion sensors have been designed using a variety of molecules such as crown ethers, porphyrins, and calixarenes *etc.*¹⁶ However, because of the unique robust framework of the calixarenes, the upper- and lower-rims can be selectively functionalized with suitable functional groups. Recently, calixarene-based chemosensors which incorporate 1,2,3-triazole units as fluorophores, have been reported.¹⁸ The 1,2,3-triazole units are stable functional groups which have been used as binding sites for cations and especially transition metal ions.¹⁸ The functionalization of calixarenes with triazole groups has been achieved through the use of what is referred to commonly as “click” chemistry (the term was introduced by K. B. Sharpless¹⁹ in 2001). Cu(I)-catalyzed azide-alkyne cycloaddition (or “CuAAC”) reaction conditions (a “click” reaction) are widely used for the triazole unit formation.

This method possesses several useful features, including the possible use of a variety of solvents and functional groups, the potential of high yields under mild reaction conditions and high reaction rates. The method has been adopted in a wide range of applications in the biological, materials, and medicinal chemistry areas.²⁰

In 2007, Chung's group²¹ reported a triazole-modified 1,3-*alternate* calix[4]crown-5 **91** (Figure 3.01) as a novel fluorescent "on-off" switchable chemosensor. Fluorescent receptor **91** has the ability to bind two different cationic guests which could attach to the two binding sites, namely the crown-5 unit on the lower rim and the triazole units on the upper rim. Using fluorescence and ¹H-NMR titration studies these authors reported that receptor **91** formed 1:1 complexes and exhibited selective binding to Hg²⁺, Cr³⁺, Cu²⁺ and Pb²⁺ ions, through the triazole units. The fluorescence intensity of chemosensor **91** was quenched due to the reverse PET and heavy metal effect from the anthracene unit to the triazole group.²¹ As a result of having a crown-5 in the lower rim as another binding site, the addition of K⁺ to a solution of **91** showed an enhancement in emission intensity due to the K⁺ ion becoming entrapped by the crown-5 moiety. The fluorescence of **91** is quenched by Pb²⁺ ion but can be revived by the addition of excess K⁺ into the solution of the **91**:Pb²⁺ complex. The metal ion exchange can therefore trigger the on-off switchable fluorescent chemosensor.

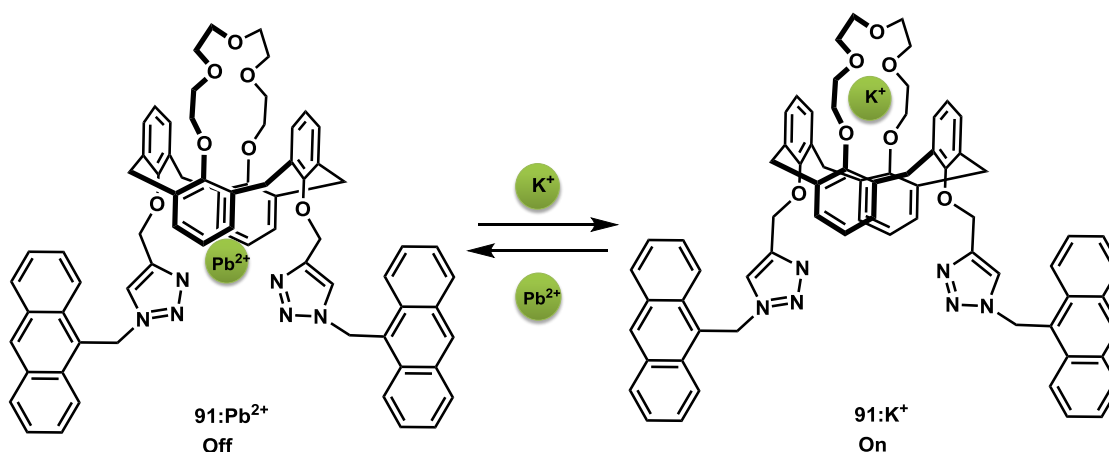


Figure 3.01 Triazole-modified calix[4]crown-5 as a novel fluorescent on-off switchable sensor.²¹

Yamato's group²² reported new types of chemosensors **92** and **93** (Figure 3.02) which are based on hexahomotrioxacalix[3]arene. The fluorescent sensors were highly selective for Pb^{2+} as determined by the enhancement of the monomer emission of pyrene. Hexahomotrioxacalix[3]arene which in its *cone* conformation has C_3 -symmetry and has been used to make receptors for ammonium cations, metal cations and fullerene derivatives.²³ The C_3 -symmetric structure of hexahomotrioxacalix[3]arene has potential application in the development of a new fluorescent sensor for heavy metal ions. The fluorescence intensity of the monomer emissions for receptors **92** and **93** change in the presence of various metal ions. The fluorescence sensing mechanism of receptors **92** and **93** is attributed to the presence of the pyrene moieties which form the fluorophore. Pyrenes are among the most important fluorogenic units due to their efficient excimer formation and emission properties. The characteristic decrease of the excimer emission intensity and increase of monomer emission intensities of **92** and **93** were noticed when the triazole rings selectively bind to cations. Among the metal ions tested, alkali metal ions showed no significant spectral changes. At the same concentration, a much weaker response was observed with Ag^+ , Co^{2+} , Ni^{2+} , Hg^{2+} , Cd^{2+} and Zn^{2+} when compared to Pb^{2+} ions. The fluorescence of the ionophore with two triazole moieties incorporated onto a calixarene scaffold is strongly quenched by Pb^{2+} . However, the fluorescence changes of receptors **92** and **93** depend on the C_3 symmetry of hexahomotrioxacalix[3]arene and the three nitrogen-rich triazole ligands co-ordinate with the Pb^{2+} , isolating it from the pyrene moieties and thereby maintain the fluorescence of the complex formed. Receptor **93** has a much higher affinity and selectivity toward Pb^{2+} than **92** due to the greater flexibility of

the triazole moieties on **93** which enables it to adopt the appropriate geometry. Yamato further investigated the selectivity for Pb^{2+} ions and interferences to the selective response of **93** to Pb^{2+} with co-existing ions evaluated; no significant interference to the detection of Pb^{2+} was noticed in the presence of other metal cations.

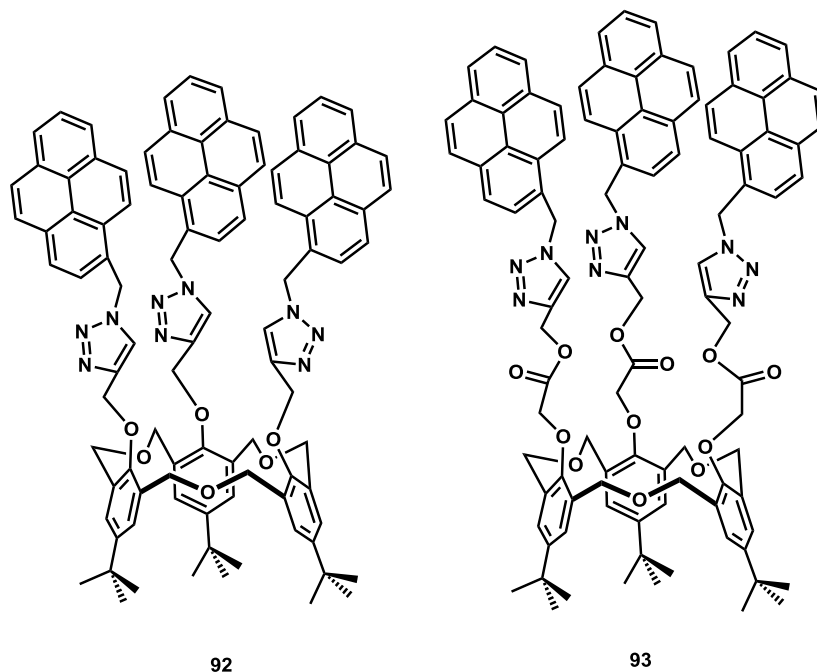
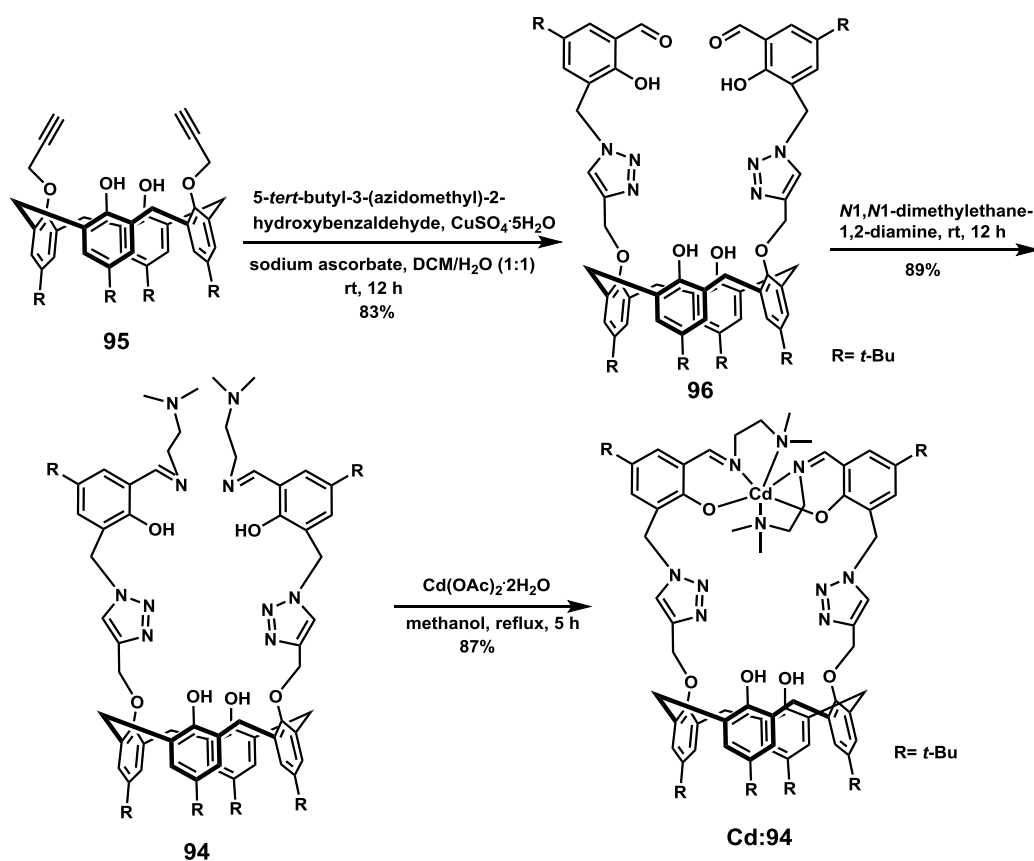


Figure 3.02 Pyrene-linked triazole-modified hexahomotrioxacalix[3]arenes **92** and **93**.²²

Amino acids play an important role in maintaining some biological functions due to their specific metal ion binding properties.²⁴ Among these, cysteine (Cys) plays a crucial role in biological systems by acting as a binding unit at the active site of some metalloproteins.²⁵ In proteins, Cd^{2+} exhibits specific binding with Cys due to its soft nature. Cd^{2+} is a nutrient for some deep sea species; the same Cd^{2+} however is toxic to living organisms present at the surface.²⁵ Rao's group²⁶ reported the Cd^{2+} complex of triazole-based calix[4]arene conjugate **94** as a selective fluorescent chemosensor for Cys

(Scheme 3.01). The synthesis of the *N,N*-dimethylamine ethylimino-based triazole-linked calix[4]arene conjugate **94** and its cadmium complex is shown in Scheme 3.01. The Cd²⁺ complex of **94** [**Cd:94**] has been isolated and characterized by different spectroscopic and analytical techniques. **Cd:94** recognized Cys selectively among the 20 naturally-occurring amino acids through the removal of Cd²⁺ from the complex by Cys and releasing the free **94**. Rao reported that [**Cd:94**] in methanol shows an intense fluorescent blue color under UV light. The visible blue color changes from fluorescent to nonfluorescent only in the presence of Cys. The color of [**Cd:94**] was unaltered in the presence of other amino acids. The sensing of Cys was demonstrated by using different techniques such as fluorescence, UV-vis, color change, ¹H-NMR, ESI MS and cell-imaging studies.

Recently, increasing attention has been focused on the heterocalixarenes in which phenol units of the calixarene are replaced by aromatic heterocycles. Cho *et al.*²⁷ reported a newly synthesized pyrenyl-appended calix[2]triazole[2]arene **97** (Figure 3.03) as a biomodal fluorescent ionophore toward Zn²⁺ (or Cd²⁺) and Fe²⁺ ions. Compound **97** shows conformational changes upon metal ion complexation to give excimeric emission changes of the two pyrenes. The fluorescence changes of **97** were examined by addition of perchlorate salts of various metal cations.



Scheme 3.01 Synthesis of triazole-linked calix[4]arene **94** and its cadmium complex.²⁶

Upon addition of Zn^{2+} (or Cd^{2+}), **97** selectively exhibits an enhanced monomeric emission and quenched excimer emission, compared to other metal ions tested. More interestingly, significant fluorescence changes were reported upon addition of Fe^{2+} to a solution of **97**, giving enhanced fluorescence as well as a blue shift of the excimer emission. This type of emission refers to a static pyrene excimer.²⁷ Compound **97** can be used to distinguish Fe^{2+} from Fe^{3+} with respect to the excimeric emission changes. The conformations of **97** were investigated by NMR and DFT (Density Functional Theory) calculations. DFT-calculations with the probe **97** and Fe^{2+} or Fe^{3+} , supported the experimental observations. The monomeric and excimeric emission has a large band

separation (378 nm and 476 nm). Calix[2]triazole[2]arene **97** can therefore distinctly identify Zn^{2+} (or Cd^{2+}) and Fe^{2+} with respect to its monomeric and excimeric changes in a quantitative and qualitative manner.

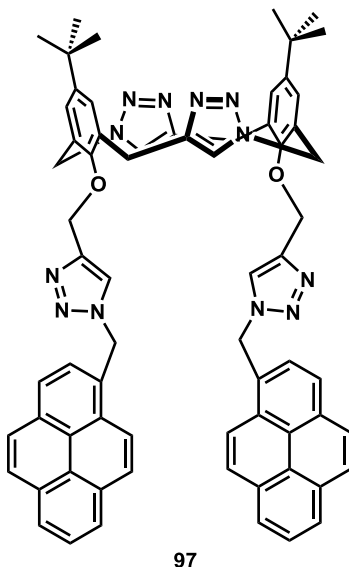


Figure 3.03 Structure of pyrenyl-appended calix[2]triazole[2]arene **97**.²⁷

3.2 Objectives of the research work conducted by the author and reported in this Chapter

In order to test for different metal ion selectivity with the sensing layers needed for the different microcantilevers (MCLs) envisioned in the multi-MCL instrument being designed by the Beaulieu group at Memorial University, a synthesis of calix[4]arene **98** which incorporates a “triazole” component was undertaken.

In this Chapter the focus will be on the synthesis and applications of this new triazole-bridged anthracene-appended calix[4]arene derivative **98**. The upper rim of the calix[4]arene **98** was functionalized with a thioacetate functional group and the lower rim

was functionalized with a triazole (as ionophore)-bridged anthracene fluorophore. The synthetic strategy involved a “click” reaction as the key step. The thioacetate group enables the calix[4]arene **98** to form a stable self-assembled monolayer (SAM) onto the Au surface of a microcantilever. Metal ion competitive experiments were also investigated. This Chapter also includes details of the synthesis and applications of another fluorescent chemosensor **99**, a triazole-bridged pyrene-appended calix[4]arene **99** in a collaborative project with the Bodwell group at Memorial University. Using this receptor **99** complexation studies were undertaken with various metal ions including the association/binding constants for the complexes. The complexation studies and association/binding constants of these two new receptors **98** and **99** with different metal ions were investigated by UV-vis, fluorescence and ¹H-NMR spectroscopic techniques. The results of this project indicate that these new triazole-bridged anthracene/pyrene appended calix[4]arene derivatives **98** and **99** are effective fluorescent chemosensors.

3.3 Results and discussion

The new bimodal calix[4]arenes **98** and **99** (see: Scheme 3.05 p 163) incorporate a triazole moiety. Since the observation by Sharpless^{28a} and Meldal^{28b} that the Huisgen 1,3-dipolar cycloaddition or “click” chemistry of alkynes and azides to give 1,2,3-triazoles can be catalyzed by Cu(I), this strategy has been exploited in a wide variety of areas including drug design, bioconjugation and material chemistry.^{29a-c} In addition to these properties, the multivalent derivatives can be exploited for the binding of cations. A property first identified and developed for the catalysis of the “click” reaction itself was the *in situ* formation of copper complex.^{29d}

As highlighted previously in this thesis, calixarenes have been used as an important framework of many fluorescent chemosensors. The copper-catalyzed “click” reaction conditions have been exploited for the functionalization of calixarene templates. Since the first report³⁰ in 2005 of the synthesis of water-soluble triazole-linked calix[4]arene derivatives, a wide variety of triazole-linked upper- and lower-rim modified calix[4]arene receptors has been reported.³¹ Rao’s group³² reported the triazole-linked anthracenyl-appended calix[4]arene conjugate as receptor for Co^{2+} . In the current project, the synthesis of the analogous upper- and lower-rim bimodal calix[4]arene derivative **98** (Figure 3.04) was targeted for its potential use as a sensing layer on gold-coated MCLs and also for selective binding of various metal ions.

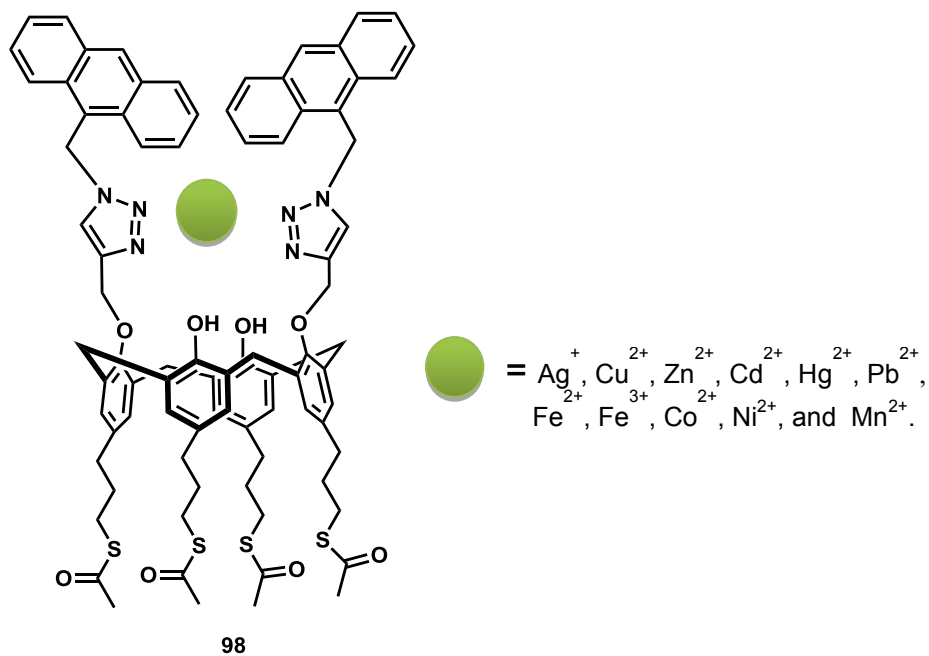
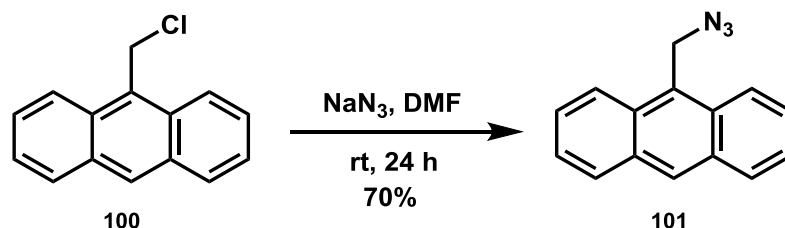


Figure 3.04 Structure of anthracene-appended triazole based calix[4]arene **98**.

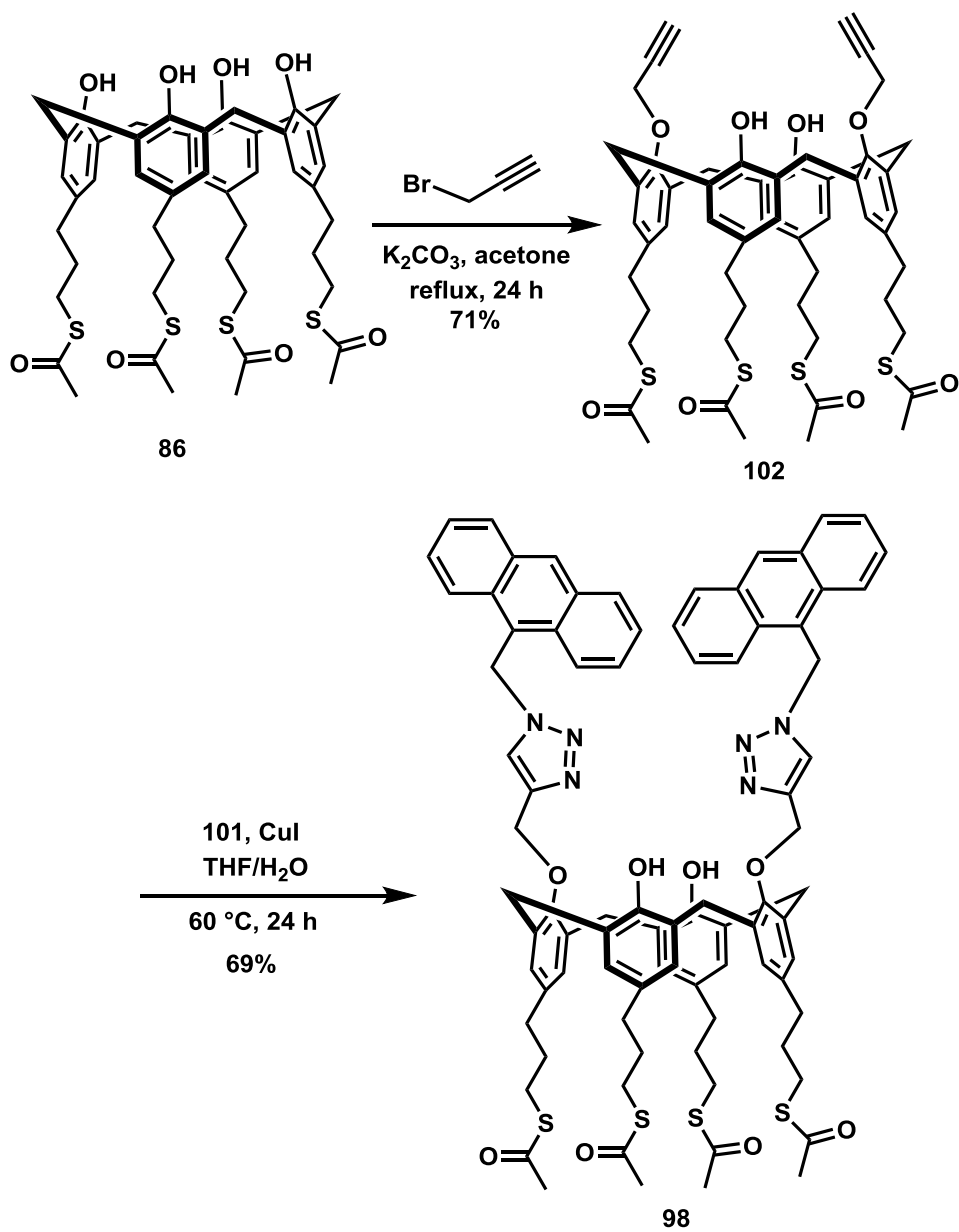
3.3.1 Synthesis of a new bimodal anthracene-appended triazole-based calix[4]arene derivative **98**

The synthesis of azidomethyl intermediate **101** is outlined in Scheme 3.02. Reaction of 9-chloromethylanthracene **100** with sodium azide in DMF afforded the 9-(azidomethyl) anthracene **101** in 70% yield.³² The synthesis of 5,11,17,23-tetrakis(3-propylthioacetate)calix[4]arene **86** has previously described in Chapter 2. The synthesis of **98** is outlined in Scheme 3.03. Alkylation of **86** employing the reported conditions³² with propargyl bromide in the presence of K_2CO_3 in dry acetone at room temperature, however, did not produce **102**. The reaction conditions were modified by using the same reagents but heating the reaction mixture under reflux conditions for 24 h to afford the dipropargyl intermediate **102** in 71% yield.



Scheme 3.02 Synthesis of azide intermediate **101**.

The CuAAC reaction between the dipropargyl intermediate **102** with the azide intermediate **101** was conducted with under CuI catalysis,³³ in a THF/H₂O mixed solvent system, with stirring at 60 °C for 24 h to afford a calix[4]arene **98** as a pale yellow solid in 69% yield.



Scheme 3.03 Synthesis of a new bimodal calix[4]arene **98**.

3.3.2 Characterization of bimodal calix[4]arene **98**

The newly-synthesized compound **98** was characterized by ^1H - and ^{13}C -NMR spectroscopy and mass spectrometry. The formation of the 1,2,3-triazole rings in **98** was apparent from the appearance of the triazole-*H* signal as a two-proton singlet at δ 7.23 ppm. A second four-proton singlet signal due to the anthracene- CH_2 -triazole methylene protons was affected by the triazole unit and was observed at δ 6.40 ppm; its corresponding C-13 chemical shift was present at δ 46.4 ppm. The signal at δ 4.75 ppm corresponding to the $-\text{OCH}_2$ -triazole linkers also appeared as a four-proton singlet and its corresponding C-13 chemical shift at δ 69.2 ppm. The ^1H -NMR spectrum of **98** suggested that the calix[4]arene unit is in a *cone* conformation since the proton chemical shifts of the bridging $-\text{CH}_2-$ groups appeared as a pair of four-proton AB doublets at δ 3.59 ppm and 2.77 ppm ($J = 13.1$ Hz). The corresponding ^{13}C chemical shift was observed at δ 34.0 ppm. The spectrum also shows eight aromatic protons (*Ar-H*) of **98**: four of each appear as singlets at δ 6.34 and 6.57 ppm. A two-proton singlet at δ 6.83 ppm is due to the hydroxyl groups of **98**.

Moreover, the ^1H -NMR spectrum of **98** shows a singlet at δ 8.39 ppm, two doublets at δ 8.18 ppm and 7.96 ppm and a multiplet at δ 7.45 ppm corresponding to the anthracene moiety. Four triplets were observed at δ 2.86, 2.60, 2.51 and 2.16 ppm and two multiplets were present at δ 1.84 and 1.50 ppm, corresponding to the propyl chains of **98**. The thioacetate groups of **98** appear as two six-proton singlets at δ 2.30 and 2.35 ppm, whose corresponding ^{13}C chemical shifts are observed at δ 195.8 and 195.9 ppm.

APCI-LC/MSD also confirmed the expected mass of **98** and clearly showed a m/z value at 1431.6 $[M+1]^+$.

3.4 Complexation studies

Complexation studies of the anthracene-linked triazole-based receptor **98** were conducted using UV-vis, fluorescence and ^1H NMR spectroscopic techniques. UV-vis spectra were recorded on an Agilent 8543 Diode Array spectrophotometer connected to an HP computer. Emission spectra were measured on a Photon Technology International (PTI) Quanta Master 6000 spectrofluorometer equipped with a continuous xenon arc lamp as the excitation source. The emitting light was collected at 90° to the excitation beam and was detected by a Hamamatsu R-928 photomultiplier tube (PMT) in the photon counting mode. All emission spectra were corrected for instrumental light loss using correction factors supplied by PTI. All of the metal ion salts as their perchlorates were purchased from Alfa Aesar in >99 % purity. High-purity spectral grade CHCl_3 and CH_3CN were purchased from Cambridge Isotope Laboratories. In a typical experiment, stock solutions of **98** (2.01×10^{-5} M) and metal salts (1.49×10^{-2} M) were prepared in a (9:1) $\text{CH}_3\text{CN}:\text{CHCl}_3$ mixed solvent system and various metal ions were used for complexation studies.

3.4.1 Complexation studies using fluorescence spectroscopy

3.4.1.1 Calculation of association constants

The association constants (K_{assoc}) determined for the complexation between host **98** and the metal ions (guests) examined were based on the fluorescence data and were calculated by using two different methods:

1. Modified Benesi-Hildebrand method.³⁴
2. Pall Thordarson's method.³⁵

The association constants were calculated employing a modified Benesi-Hildebrand method using the following equations (1) and (2):

$$\frac{1}{(F_o-F)} = \frac{1}{(F_o-F_{fc})} + \frac{1}{K(F_o-F_{fc})[M]} \quad (1)$$

$$\frac{1}{(F_o-F)} = \frac{1}{(F_o-F_{fc})} + \frac{1}{K(F_o-F_{fc})[M]^{1/2}} \quad (2)$$

In these equations, K is the association constant, F_o is the fluorescence intensity of the free host, F is the observed fluorescence intensity of the host-guest complex, and F_{fc} is the fluorescence intensity upon saturation. According to these equations, a plot of $1/(F_o-F)$ vs $1/[M]$ giving a straight line, indicates 1:1 stoichiometry between the host and guest. $[M]$ is the guest (metal ion) concentration in $\text{mol}\cdot\text{L}^{-1}$. A plot of $1/(F_o-F)$ vs $1/[M]^{1/2}$ giving a straight line, indicates 1:2 stoichiometry between the host and guest. In the present complexation studies, all of the plots showed clear linear relationships using equation (1), with correlation coefficients > 0.99 . The 1:1 binding constants were obtained from the equation (3):

$$K = (\text{y-intercept})/(\text{slope}) \quad (3)$$

Note: $[M]$ in the B-H approach assumes that it is $([M] + [M]_{\text{complex}})$.

However, recently Prof. Pall Thordarson, UNSW, Australia has developed an online computer-based non-linear fitting program³⁵ and a detailed treatise for the use of a global-fit approach towards the calculation of K_{assoc} values. This approach avoids the linearization which the Benesi-Hildebrand or other non-linear methods of the past employed. Furthermore, the entire spectra from either UV-vis absorption or fluorescence data can be analyzed instead of relying on selecting the changes of selected or specific wavelengths.

3.4.1.2 Fluorescence complexation studies of **98 with various metal ions.**

Since fluorescence spectroscopy is a sensitive technique, a solution of **98** (2.01×10^{-5} M) was used for all of the titrations. Solutions of the metals as their perchlorate salts (1.49×10^{-2} M) were prepared in the same 9:1 $\text{CH}_3\text{CN}:\text{CHCl}_3$ mixed solvent. The binding properties of **98** toward metal ions were investigated by the fluorescence changes upon addition of the perchlorate salt of the respective individual cations. Compound **98** displayed monomer emission in the 360-565 nm range at the 350 nm excitation wavelength. The fluorescence emissions were quenched upon adding the metal ions as a result of complexation occurring between the host **98** and the guest metal ions. The cationic guests investigated were Ag^+ , Co^{2+} , Cd^{2+} , Fe^{2+} , Fe^{3+} , Cu^{2+} , Hg^{2+} , Pb^{2+} , Zn^{2+} , Ni^{2+} and Mn^{2+} ions, all of which were used as their respective perchlorate salts. Fluorescence spectroscopic studies showed that the bimodal calix[4]arene **98** is highly selective for

Hg²⁺ and Fe³⁺ ions and these are highlighted in the following report. Association constants were calculated by using the Pall Thordarson's and Benesi-Hildebrand methods. The highest association constant values of **98** were obtained with Hg²⁺ and Fe³⁺ ions. Figure 3.05a/b shows the fluorescence titration experiments conducted for the **98** with Hg(ClO₄)₂. The fluorescence intensities of **98** gradually decreased as the concentration of Hg²⁺ ion increased from 0.18 to 6.8 eq. The average association constant calculated at three wavelengths for the **98**:Hg²⁺ complex by the Benesi-Hildebrand method was $6.66 \pm 0.0872 \times 10^4 \text{ M}^{-1}$ (Figure 3.05b). The fluorescence quenching of **98** may be explained by either a PET or a heavy-atom effect.³⁶ In the former case, when the Hg²⁺ ion is bound by the two triazole nitrogen atoms, the anthracene units may behave as PET donors whereas the triazole unit behave as electron acceptors.

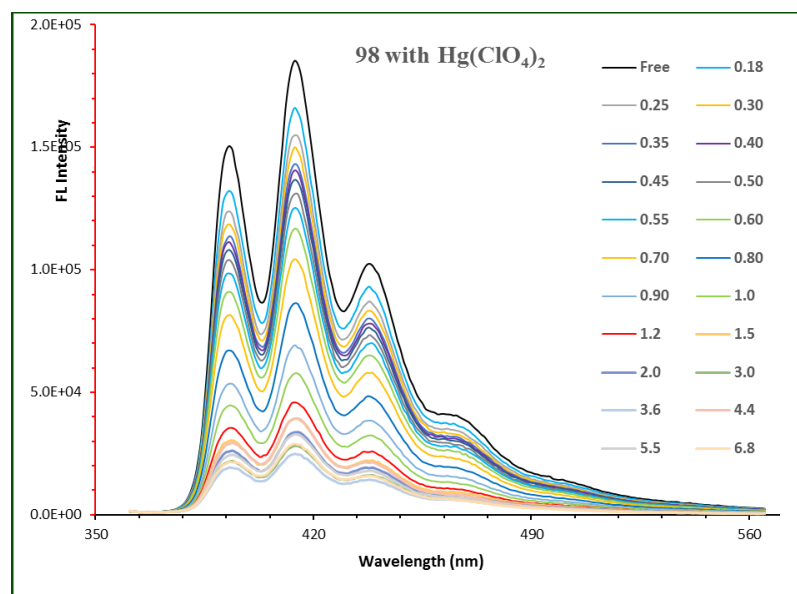


Figure 3.05a Fluorescence spectra of **98** upon addition of Hg²⁺ (0.18-6.8 eq) in acetonitrile/chloroform (v/v= 9:1) solutions. $\lambda_{exc} = 350 \text{ nm}$.

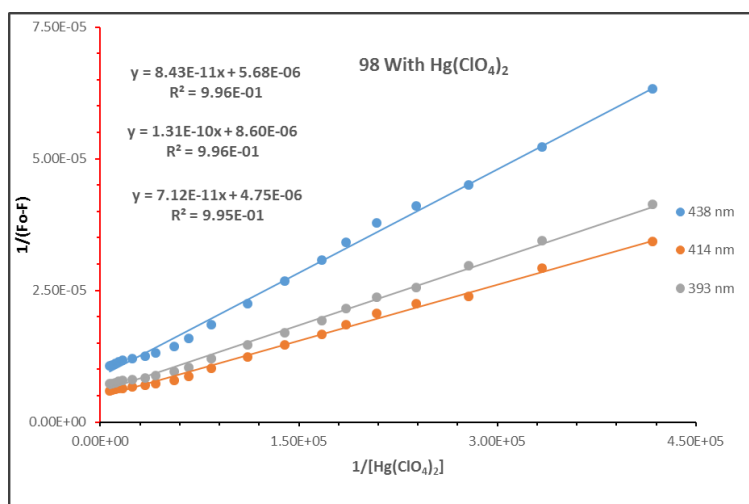


Figure 3.05b Benesi-Hildebrand plots of $1/(F_0-F)$ versus $1/[\text{Hg}(\text{ClO}_4)_2]$ for **98** upon titration with Hg^{2+} . The linear fits showed 1:1 complexation between **98** and Hg^{2+} . The association constants were calculated for the changes at the 393 nm, 414 nm and 438 nm wavelengths.

Figure 3.06 shows the corresponding **98**: Hg^{2+} binding constant (K_{assoc}) determined using Pall Thordarson's global analysis program. The resulting global K_{assoc} was determined to be $1.33 \times 10^5 \text{ M}^{-1}$. The covariance of the fit value is < 0.01 which is a reasonably good fit of the data to the model. The RMS value is also good as can be seen in the Residual/SE plot shown.

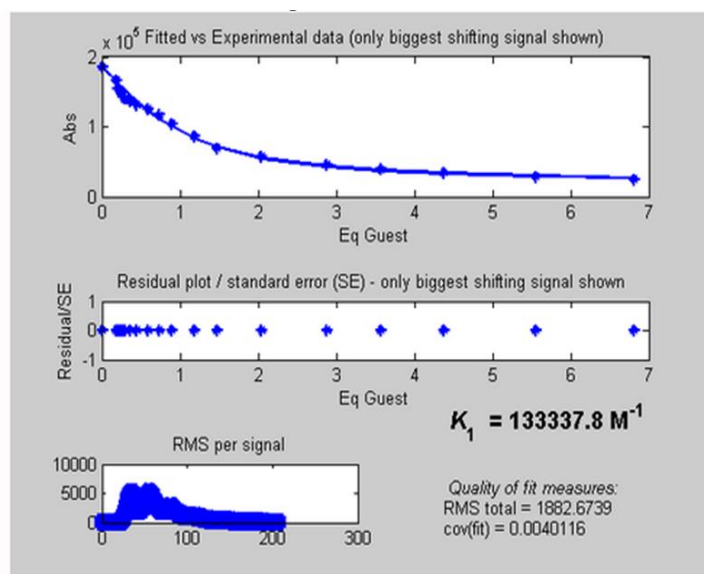


Figure 3.06 Screen-capture output showing 1:1 binding model for **98** with Hg^{2+} , ^{35b} using Thordarson's method.

Figure 3.07a/b shows the fluorescence titration experiments conducted for **98** with $\text{Fe}(\text{ClO}_4)_3$ in the same acetonitrile: chloroform solvent mixture. Figure 3.08 shows the binding constant (K_{assoc}) determined using Pall Thordarson's global analysis program. The resulting global K_{assoc} was determined to be $1.17 \times 10^5 \text{ M}^{-1}$. The corresponding association constant for the **98**: Fe^{3+} complex by the Benesi-Hildebrand method was calculated to be $4.38 \pm 0.108 \times 10^4 \text{ M}^{-1}$ (Figure 3.07b).

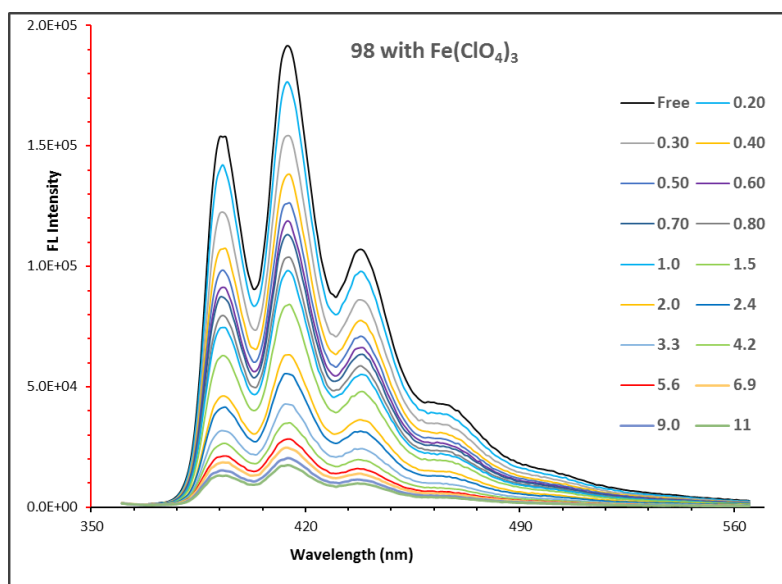


Figure 3.07a Fluorescence spectra of **98** upon addition of Fe^{3+} (0.20-11 eq) in acetonitrile/chloroform (v/v= 9:1) solutions. $\lambda_{exc} = 350$ nm.

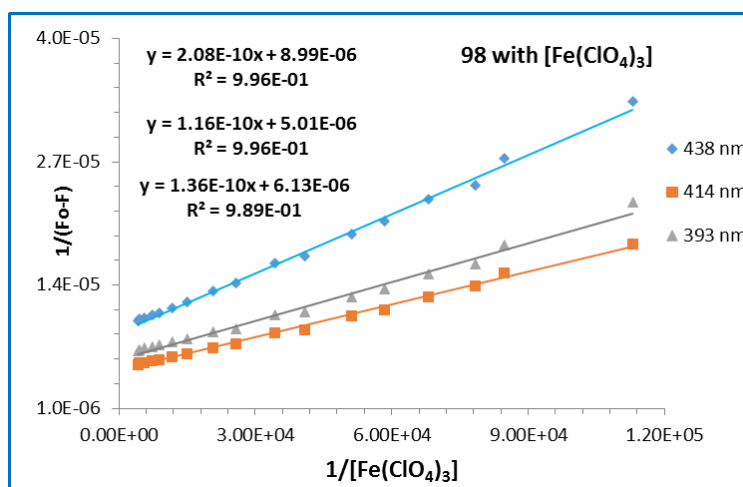


Figure 3.07b Benesi-Hildebrand plots of $1/(F_o-F)$ versus $1/[\text{Fe}(\text{ClO}_4)_3]$ for **98** upon titration with Fe^{3+} ion. The linear fits showed 1:1 complexation between **98** and Fe^{3+} . The association constants were calculated for the changes at the 393 nm, 414 nm and 438 nm wavelengths.

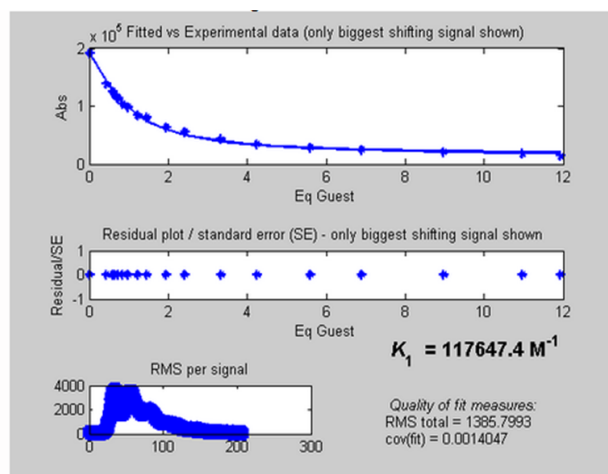


Figure 3.08 Screen-capture output showing 1:1 binding model for **98** with Fe^{3+} ,^{35b} using Thordarson's method.

3.4.1.3 Job plot analysis for **98** with Hg^{2+} and Fe^{3+} ions

The titration data which showed that 1:1 host-guest complexes were formed, were also confirmed by Job plot³⁷ analyses for **98** with Hg^{2+} and Fe^{3+} ions as shown in Figures 3.09 and 3.10. In both Job plots, maximum fluorescence changes were observed when the molar fractions of receptor **98** vs Hg^{2+} and of **98** vs Fe^{3+} were 0.5, indicative of 1:1 complex formation in both cases.

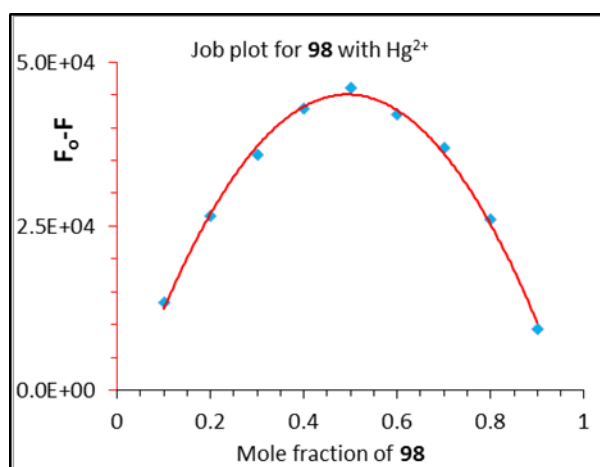


Figure 3.09 Job plot showing 1:1 complexation for **98** with $\text{Hg}(\text{ClO}_4)_2$.

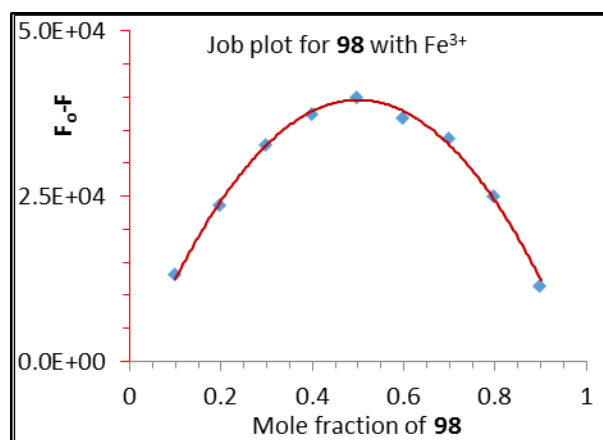


Figure 3.10 Job plot showing 1:1 complexation for **98** with Fe(ClO₄)₃.

3.4.1.4 Comparison of the association constants of receptor **98** with metal ions

Figure 3.11 shows the association constants determined for all of the complexes using the two different methods described previously^{34,35} and it is evident that the complexation between **98** and Hg²⁺ shows the largest K_{assoc} values of $\sim 1.33 \times 10^5 \text{ M}^{-1}$ based upon the changes in fluorescence intensity in the fluorescence titrations.

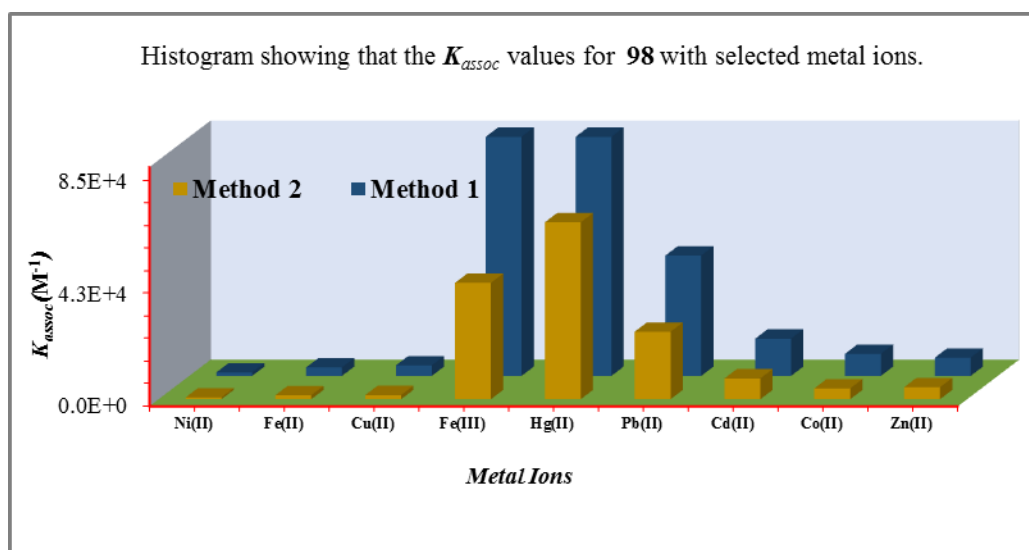


Figure 3.11 Histogram showing the association constants (K_{assoc}) values calculated by using two different methods for the fluorescence titrations of **98** with different metal ions.

Table 3.01 is a summary of the calculated binding constants for **98** with selected metal ions as their perchlorate salts, using the two computational methods. Based on these binding constant values it can be concluded that **98** is more selective for Hg^{2+} and Fe^{3+} among the ions examined. Note that in general, the Thordarson computational model afforded generally higher (34-63%) K_{assoc} values, and should be more reliable than the Benesi-Hildebrand calculated values since the entire spectra were analyzed in the former case and did not need an arbitrary selection of which data was analyzed by the Benesi-Hildebrand approach.

Table 3.01 Comparison of calculated binding constants for **98** with selected metal perchlorate salts in 9:1 $\text{CH}_3\text{CN}:\text{CHCl}_3$ using the Thordarson and Benesi-Hildebrand (B-H) methods.

Entry	M^{n+} mol eq.	M^{n+}	Thordarson (1) (M^{-1}) x 10^3 [cov(fit)]	Benesi-Hildebrand (2) (M^{-1}) x 10^3 [$r^2 > 0.99$]	* $\Delta_{1-2/1}$ (%)
1	0.20-6.8	Hg^{2+}	133 [0.0040]	66.6 ± 0.872	49.9
2	0.20-11	Fe^{3+}	117 [0.0014]	43.8 ± 1.08	62.6
3	0.30-16	Pb^{2+}	45.3 [0.0081]	25.4 ± 0.492	44.0
4	1.1-15	Cd^{2+}	14.0 [0.00097]	7.83 ± 0.985	44.0
5	1.7-8.2	Co^{2+}	8.29 [0.0091]	4.05 ± 0.241	51.1
6	0.90-36	Zn^{2+}	6.85 [0.0012]	4.50 ± 0.741	34.3
7	1.1-36	Cu^{2+}	3.95 [0.017]	1.55 ± 0.0391	60.7
8	0.80-68	Fe^{2+}	3.18 [0.0098]	1.52 ± 0.370	52.2
9	0.38-60	Ni^{2+}	1.30 [0.0015]	0.657 ± 0.201	49.5

* These values are the percentage differences between the K_{assoc} determined between the Thordarson and B-H methods.

3.4.2 Metal competitive experiments

To confirm the selectivity of **98** towards Hg^{2+} over the other metal ions examined, competitive experiments were carried out in the same medium with different metal ions. In the competitive experiments the metals were used as their perchlorate salts and the stock solutions of **98** (2.01×10^{-5} M) and metals (1.49×10^{-2} M) were prepared in the $\text{CH}_3\text{CN}:\text{CHCl}_3$ (9:1) mixed solvent system. In these experiments, a molar equivalent of Hg^{2+} was added to a solution of the **98**:L (1:1, L = different metals) complex. Upon the additions, the fluorescence emissions of the complex **98**:L were rapidly quenched. These results show that **98** is more selective for Hg^{2+} over the other metal ions tested. Figure 3.12 shows the metal competitive studies for **98** with the different metal ions tested, by the resulting fluorescence emission changes.

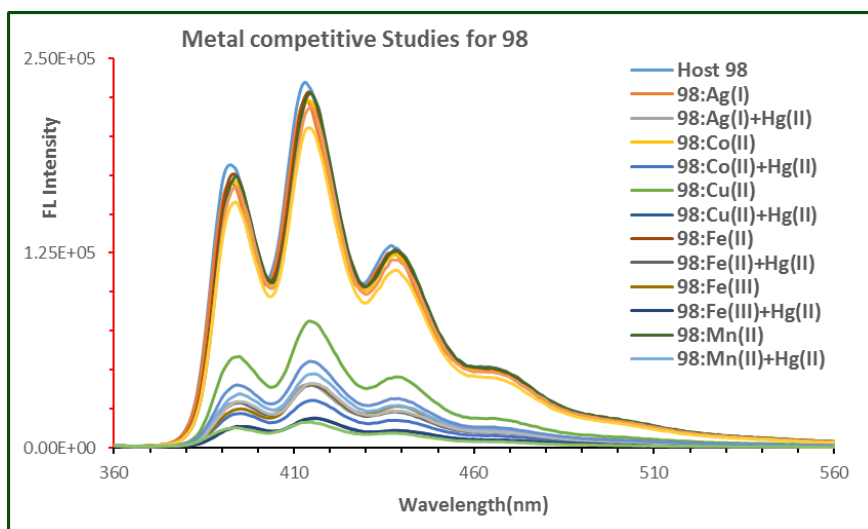


Figure 3.12 Metal competitive studies for receptor **98** with different metal ions.

Figure 3.13 shows the specific competitive studies of the fluorescence emission quenching of the **98**:Ag⁺ and **98**:Co²⁺ (1:1) complexes upon addition of 1 eq. of Hg²⁺ ion.

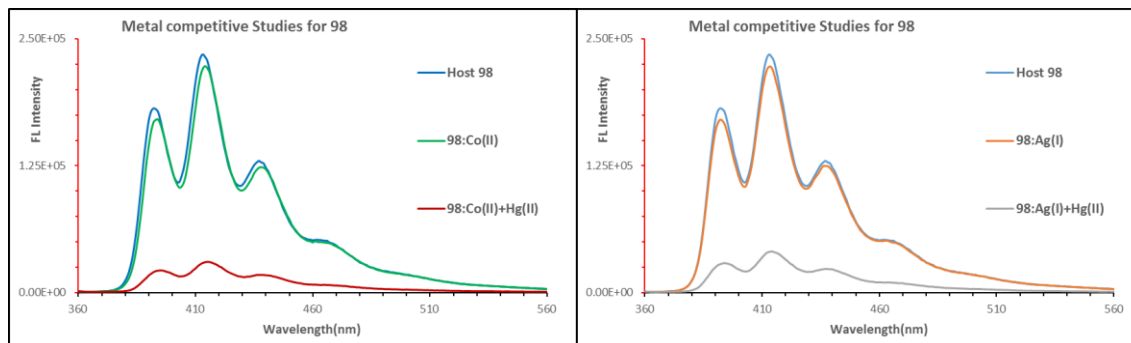


Figure 3.13 Metal competitive studies for receptor **98** with Co²⁺ and Ag⁺ metal ions.

Unlike other metals, in the presence of Zn²⁺ or Cd²⁺, **98** showed an *enhancement* of the fluorescence emissions. Upon addition of a molar equivalent of Hg²⁺ to each of the respective solutions the fluorescence emissions of the **98**:Zn²⁺ and the **98**:Cd²⁺ complexes were rapidly quenched as shown in Figure 3.14.

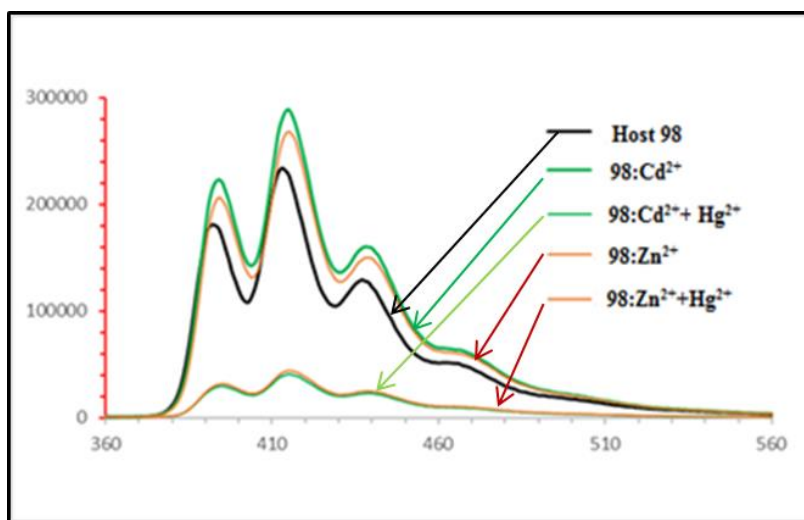


Figure 3.14 Metal competitive studies for receptor **98** with Cd²⁺ and Zn²⁺.

3.4.3 Complexation studies of **98** using ^1H -NMR spectroscopy

In order to support the mode of the complex formation between **98** and Hg^{2+} , ^1H -NMR titration experiments were carried out (0.0 to 2.0 eqs of $\text{Hg}(\text{ClO}_4)_2$) as shown in Figure 3.15. A stock solution of the host molecule **98** (2.51×10^{-3} M) was prepared in a $\text{CD}_2\text{Cl}_2:\text{CD}_3\text{CN}$ (1:4, v/v) solvent mixture that was found to be suitable for the complexation studies by ^1H -NMR spectroscopy. Upon interaction of **98** with aliquots of 1.98×10^{-1} M $\text{Hg}(\text{ClO}_4)_2$ in the same solvent system, downfield chemical shifts were observed for one of the anthracene-*H* signals, namely from δ 8.68 to 8.80 ppm ($\Delta\delta = +0.12$); for the triazole-*H* signals, from δ 7.20 to 8.11 ppm ($\Delta\delta = +0.91$); for the two Ar-*H* protons, from δ 6.58 to 6.88 ppm ($\Delta\delta = +0.30$) and 6.31 to 6.81 ppm ($\Delta\delta = +0.50$); for the anthracene-triazole-bridge- CH_2 - signal, from δ 6.56 to 6.84 ppm ($\Delta\delta = +0.28$); and for the calix- OCH_2 -triazole signal from δ 4.91 to 5.03 ppm ($\Delta\delta = +0.12$). No significant changes were observed in the remaining regions of the NMR spectrum, suggesting that the Hg^{2+} interacts with the region of the calix[4]arene **98** lower rim and the anthracenyl moiety (with in the N_2O_2 core formed by the two calix-OH and two nitrogens of the triazoles). Since the original interpretation of these results additional experiments are being conducted in the Georghiou laboratory. These experiments are designed to more definitively establish the precise mechanism for the observed NMR changes noted.

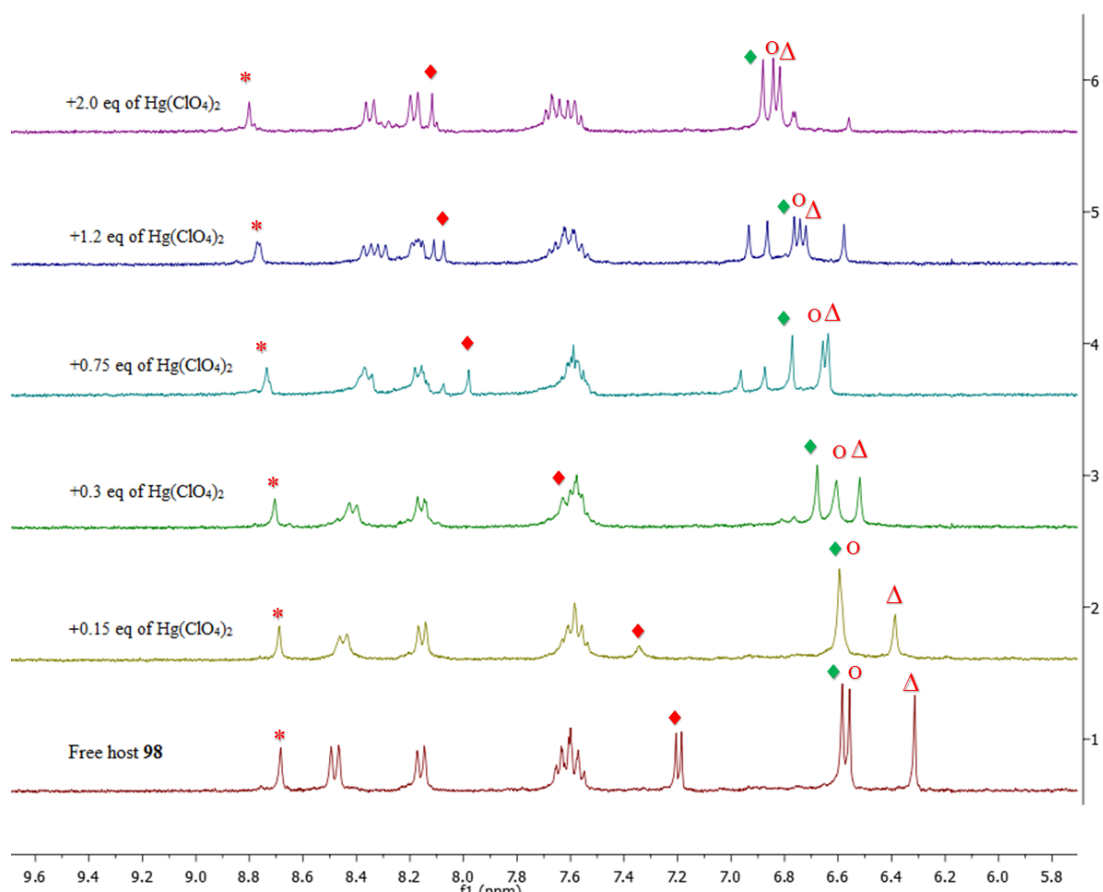


Figure 3.15 Partial ^1H NMR (300 MHz) spectra of **98** with $\text{Hg}(\text{ClO}_4)_2$ in a $\text{CD}_3\text{CN}:\text{CD}_2\text{Cl}_2$ (4:1, v/v) at 298K; *, \blacklozenge , O, \triangle , and \blacklozenge denoted the anthracene-*H*, triazole-*H*, triazole- CH_2 -anthracene, and Ar-*H* protons respectively.

To better understand the binding properties of receptor **98** with Hg^{2+} , DFT calculations were also carried out with the assistance of Dr. Shofiur Rahman in the Georghiou lab.

3.4.4 Computational studies

The individual structures in the gas-phase were fully geometry-optimized using Gaussian 09³⁸ at the B3LYP level of DFT using the lanl2dz basis set. Significant conformational changes were observed for the triazole ring protons of **98** in its Hg^{2+}

complex. The conformational changes for **98** upon complexation with Hg^{2+} ion (1:1 complex) can be seen in Figure 3.16. The N---N distance between the triazole nitrogen atoms decreases from 9.560 to 3.233 Å for N5-N12 and from 9.939 to 3.243 Å for N6-N13. The distance changes are summarized in Table 3.02. The H---H distance between the triazole hydrogen atoms increases from 3.830 to 8.260 Å for H116-H183. The nitrogen atoms therefore move inwards and the hydrogen atoms move outwards upon complexing with the Hg^{2+} ion.

Table 3.02 Selected interatomic distances of triazole nitrogen atoms and hydrogen atoms in the complex of **98**: Hg^{2+} optimized at B3LYP/lanl2dz Level (Distances in Å).

Parameter Distance (Å)	N ₅ -N ₁₂	N ₆ -N ₁₃	H ₁₁₆ -H ₁₈₃	Hg ²⁺ -N ₆	Hg ²⁺ -N ₁₃	Hg ²⁺ -O ₄₁	Hg ²⁺ -O ₅₈
Free host 98	9.560	9.939	3.830	-	-	-	-
98 complex with Hg^{2+}	3.233	3.243	8.260	2.236	2.471	2.036	2.311

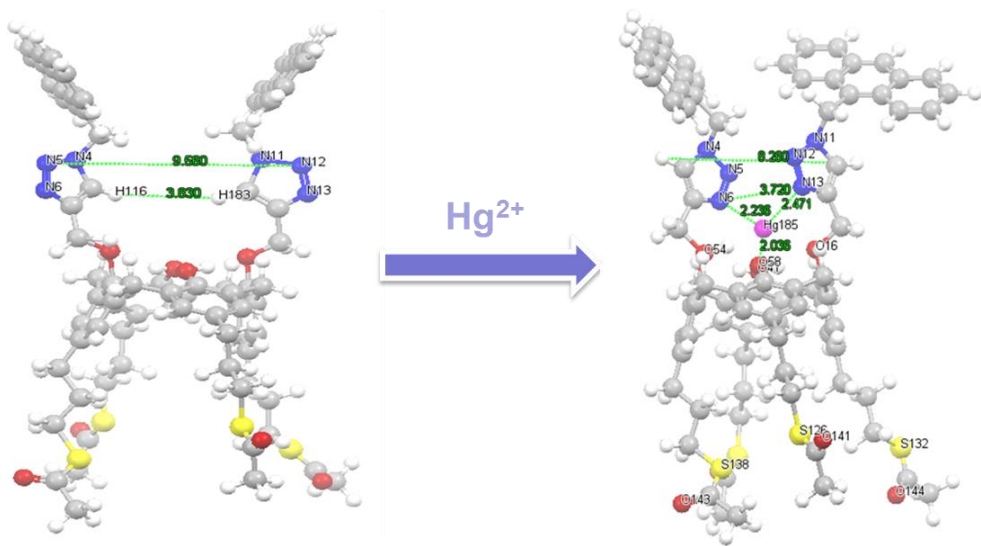


Figure 3.16 *Left*: the optimized (ball-and-stick) structure of free receptor **98**; *right*: the optimized (ball-and-stick) structure of **98**: Hg^{2+} complex.

Comparison of the fluorescence results of **98** with the simpler receptors **103a/b** and the microcantilever studies of **98** are currently on-going.

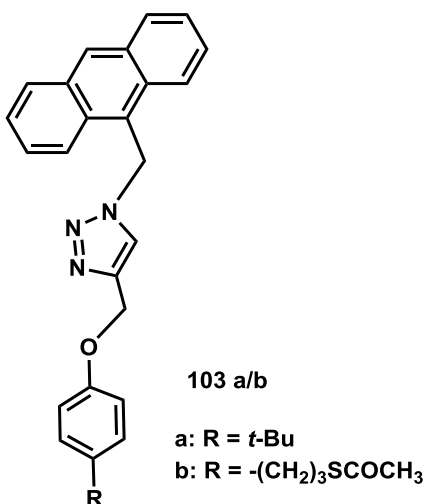


Figure 3.17 Structures of receptors **103a/b**.

3.5 Synthesis and complexation properties of triazole-based pyrene-appended calix[4]arene **99**

In order to test for different metal ion selectivity, the next designed bimodal calix[4]arene was the bis(pyrenyl)-capped triazole-based **99** (Scheme 3.05). Complexation studies of **99** were undertaken with various metal ions. Pyrenes, as previously indicated, are one of the most useful fluorogenic probes due to their efficient excimer formation and emission.³⁹ Host molecules having more than one pyrenyl group exhibit intramolecular excimer emission by two different mechanisms. One mechanism results from π - π stacking of the pyrene rings in the free state. The other mechanism is due to the interaction of a ground-state pyrene (Py) unit with an excited-state pyrene (Py*) unit.⁴⁰

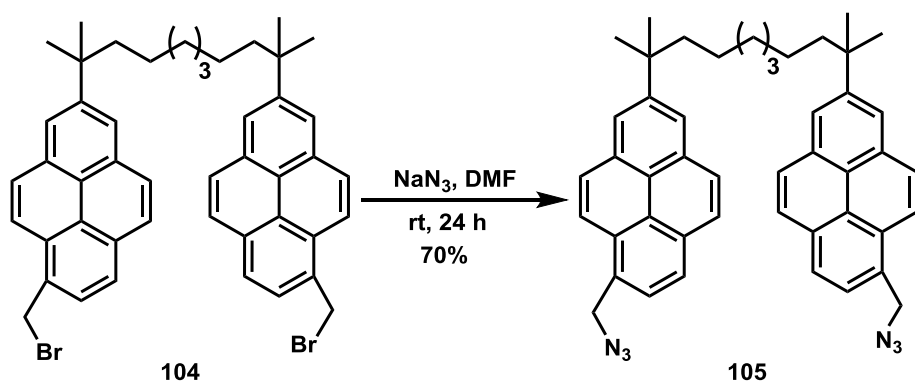
A variety of pyrene-linked triazole-modified calixarenes have previously been reported as fluorescent chemosensors. Cho *et al.*²⁷ reported the pyrenyl-appended calix[2]triazole[2]arene **97** (Figure 3.03) as a bimodal fluorescent ionophore for Zn²⁺ and Fe²⁺ ions. As described previously, pyrene-linked triazole-modified hexahomotrioxacalix[3]arenes **92** and **93** as fluorescent chemosensors for Pb²⁺ were reported by Yamato's group.²² Park *et al.*⁴¹ reported a pyrenyl-appended triazole-based calix[4]arene as a fluorescent sensor for Zn²⁺ and Cd²⁺.

In the current project, a bis(pyrene)-linked triazole-modified calix[4]arene **99** was targeted to determine its binding properties with selected metal ions. In the synthetic approach used for **99**, the intermediate compound **104** has previously been synthesized and used as an intermediate in the synthesis of 1,1,*n,n*-tetramethyl[*n*](2,11)teropyrenophane (*n* = 9) by the Bodwell group, at Memorial University.⁴²

3.5.1 Synthesis of triazole-based pyrene-appended calix[4]arene **99**

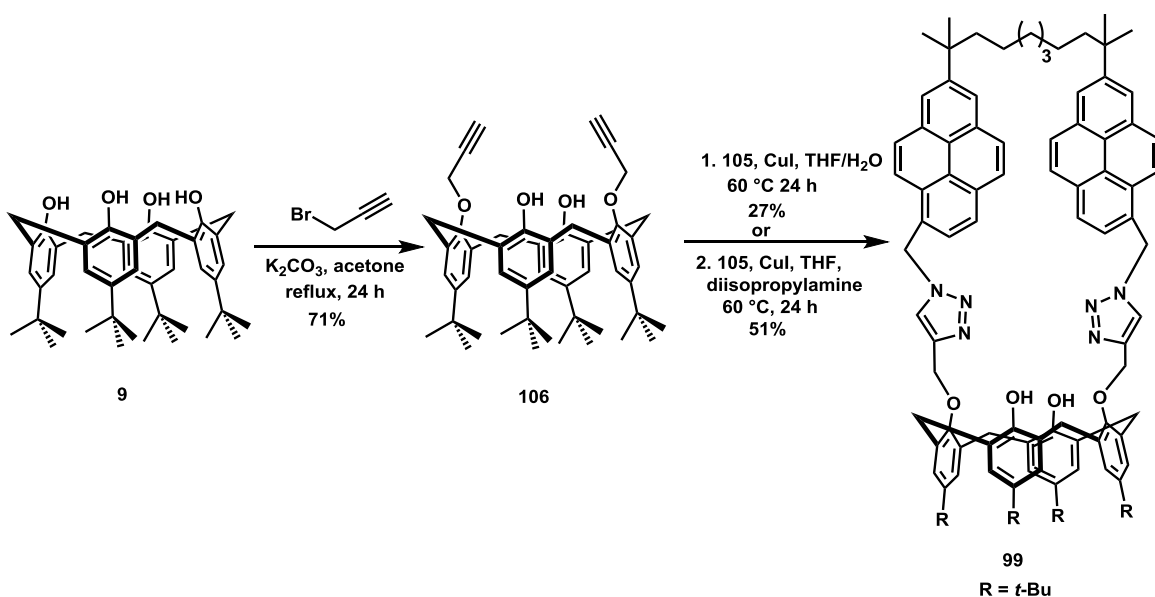
The synthesis of the bis(azidomethyl) intermediate **105** is outlined in Scheme 3.04. Reaction of the bis(bromomethyl) compound **104** with sodium azide in DMF afforded the corresponding azido compound **105** in 70% yield.³² Synthesis of 5,11,17,23-tetra-*tert*-butyl-25,26,27,28-tetrahydroxycalix[4]arene **9** previously described in Chapter 2, which was used as the starting compound for the synthesis of bimodal calix[4]arene **99** as shown in Scheme 3.05. Alkylation of **9** employing the reported conditions of Rao and co workers³² with propargyl bromide in the presence of K₂CO₃ in dry acetone at room temperature, however, did not produce **106**. Nevertheless, the reaction conditions were

modified by using the same reagents, but heating the reaction mixture under reflux conditions for 24 h, to afford the dipropargyl intermediate **106** in 71% yield.



Scheme 3.04 Synthesis of bis(azidomethyl) intermediate **105**.

The CuAAC reaction between the dipropargyl intermediate **106** with the bis(azidomethyl) intermediate **105** was conducted under CuI catalysis³³ in a THF/H₂O (2:1) mixed solvent system with stirring at 60 °C for 24 h afford the bis(pyrene)-linked triazole-based calix[4]arene **99** as a pale yellow solid in 27% yield.



Scheme 3.05 Synthesis of a new bimodal calix[4]arene **99**.

The yield was improved by performing the reaction under CuI catalysis by in THF/diisopropylamine at 60 °C for 24 h to afford **99** in 51% yield.

3.5.2 Characterization of bimodal calix[4]arene **99**

The newly-synthesized compound **99** was characterized by using ^1H and ^{13}C NMR spectroscopy and mass spectrometry. The formation of the 1,2,3-triazole rings was apparent in **99** from the appearance of the triazole-*H* signal as a two-proton singlet at δ 7.65 ppm. The other four-proton singlet was affected by the triazole unit and it was observed at δ 6.13 ppm (pyrene- CH_2 -triazole) and its corresponding ^{13}C chemical shift is at δ 44.6 ppm. The four-proton singlet at δ 4.88 ppm corresponds to the $-\text{OCH}_2$ -triazole linker and the corresponding ^{13}C chemical shift at δ 69.1 ppm. The ^1H NMR spectrum of **99** suggested that the calix[4]arene unit is in a *cone* conformation since the proton chemical shifts of the bridging $-\text{CH}_2-$ groups appeared as a pair of four-proton AB doublets at δ 4.02 and 3.07 ppm ($J = 13.2$ Hz). The corresponding ^{13}C chemical shift was at δ 38.8 ppm. Also, the ^1H NMR shows eight downfield signals for **99**: four of each appear as singlets at δ 6.65 and 6.90 ppm, corresponding to the calix[4]arene Ar-*H* protons. The signal at δ 7.07 ppm is due to the hydroxyl groups of **99** which appear as a singlet. The multiplet at δ 8.00-8.06 ppm, the singlet signal at δ 7.90 ppm, two doublets at δ 7.85 and 7.78 ppm correspond to the pyrene moiety. The tethered twenty-six protons appeared in the δ 1.01-1.74 ppm region. The two singlet signals at δ 0.86 and 1.24 ppm are related to the *t*-Bu groups. APCI-LC/MSD MS confirmed the expected molecular mass of **99**, showing a signal at m/z : 1420.9 $[\text{M}+1]^+$.

3.6 Complexation studies with **99**

Complexation studies with **99** were conducted using UV-vis, fluorescence and ¹H-NMR spectroscopic techniques. All of the metal ion salts were used as their perchlorates in the complexation studies and were purchased from Alfa Aesar in >99 % purity. High-purity spectral grade CDCl₃ and CD₃CN were purchased from Cambridge Isotope Laboratories.

3.6.1 Complexation studies using fluorescence spectroscopy

The association constants (K_{assoc}) determined for the complexation between **99** and the metal ions examined were based on the fluorescence data and were calculated by using the two different methods^{34,35} previously described in section 3.4.1.1. The stock solutions of **99** (2.02×10^{-5} M) and the metal salts (1.51×10^{-2} M) were prepared in a CH₃CN:CHCl₃ (9:1) mixed solvent system. The binding properties of **99** toward the selected metal ions were investigated by the fluorescence changes upon addition of the perchlorate salts of a wide range of cations. On excitation at 330 nm, the maximum absorption wavelength of the pyrene in compound **99** displayed both monomer and excimer emissions in the 340-600 nm range. Figure 3.18 shows the fluorescence spectrum of **99** in CH₃CN:CHCl₃ (9:1) solvent at the excitation wavelength of 330 nm.

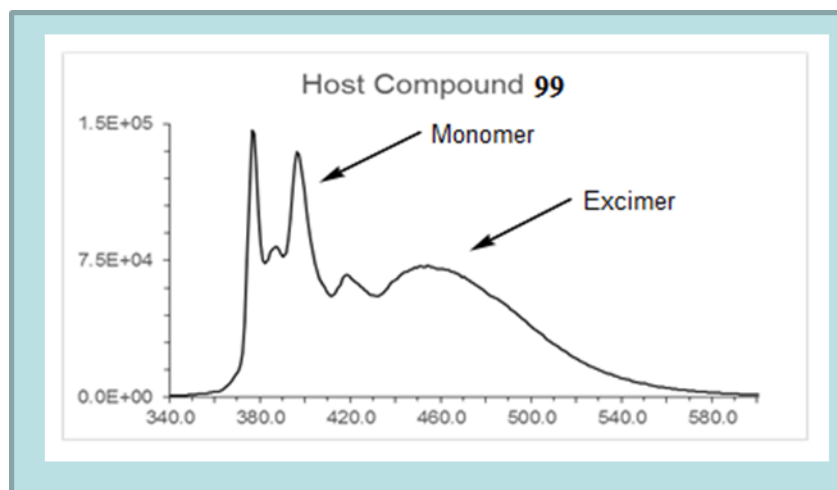


Figure 3.18 Fluorescence spectrum of **99**. The excitation wavelength λ_{exc} is 330 nm.

The excimer emission in **99** is caused by an intramolecular interaction (π - π interaction) between the two pyrene units.⁴⁰ Changes in the fluorescence emissions were noticed upon adding the metal ions as a result of complexation which occurs between the host **99** and the guest metal ions. The cationic guests that were investigated were Na^+ , K^+ , Ba^{2+} , Mg^{2+} , Ca^{2+} , Ag^+ , Co^{2+} , Cd^{2+} , Fe^{2+} , Fe^{3+} , Cu^{2+} , Hg^{2+} , Pb^{2+} , Zn^{2+} , Ni^{2+} and Mn^{2+} ions, all of which were used as their respective perchlorate salts in a $\text{CH}_3\text{CN}:\text{CHCl}_3$ (9:1) mixed solvent. Figure 3.19 shows the fluorescence changes of both the monomer and excimer of **99** which were obtained upon addition of 1 molar equivalents of the perchlorate salts of the individual metal cations. Unlike other metals, in the presence of Cd^{2+} or Zn^{2+} , receptor **99** showed a change in such a manner that an enhancement of monomer emission and a decline of the excimer emission were selectively observed as compared to the other metals. Upon addition of 1 molar equivalent of Hg^{2+} , or Fe^{3+} or Cu^{2+} , drastic quenching of the fluorescence in both the monomer and excimer emissions

of **99** was seen. Upon addition of 1 molar equivalents of Fe^{2+} , Pb^{2+} , Co^{2+} , Mn^{2+} , Ni^{2+} and Ag^+ quenching of both monomer and excimer emissions of **99** were observed. Na^+ , K^+ , Ba^{2+} , Mg^{2+} , Ca^{2+} showed no significant spectral changes of either monomer or excimer emissions.

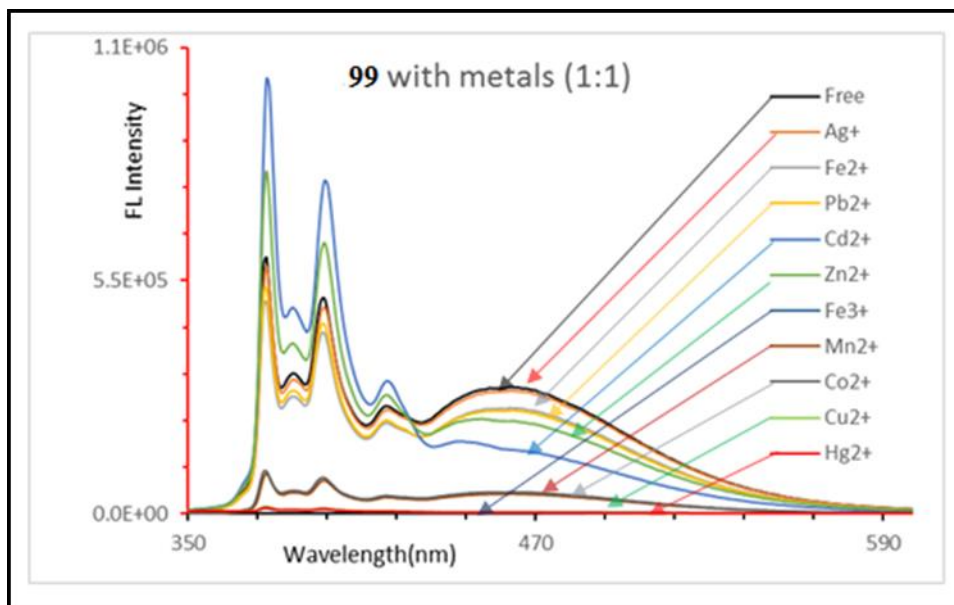


Figure 3.19 Fluorescence spectra of **99** upon addition of 1 molar equivalent of various metal ions. The excitation wavelength is $\lambda_{\text{exc}}=330$ nm.

Figure 3.20 shows the fluorescence titration experiments conducted for the receptor **99** with $\text{Zn}(\text{ClO}_4)_2$. The changes of fluorescence intensity of **99** revealed that, the monomer emissions gradually increased and excimer emissions gradually decreased as the concentration of Zn^{2+} was increased from 0.30-21 molar equivalents. Association constants were calculated using both Pall Thordarson's and the modified Benesi-Hildebrand methods as previously described. The association constant for the **99**: Zn^{2+}

complex was $2.17 \pm 0.404 \times 10^4 \text{ M}^{-1}$ using the modified Benesi-Hildebrand method, as shown in Figure 3.21.

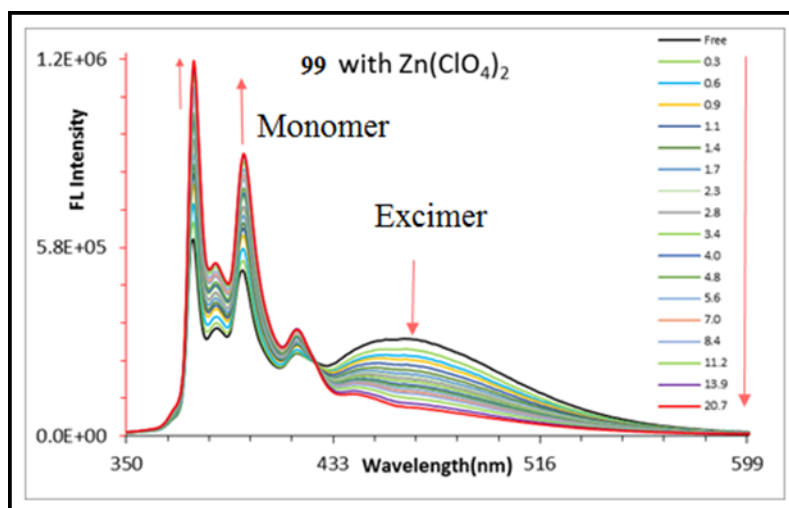


Figure 3.20 Fluorescence spectra of **99** upon addition of Zn^{2+} (0.30-21 eq) in acetonitrile/chloroform (v/v= 9:1) solutions. $\lambda_{\text{exc}} = 330 \text{ nm}$.

Using Pall Thordarson's global fit method for the entire spectra, the calculated association constant for **99**: Zn^{2+} complex is $2.84 \times 10^4 \text{ M}^{-1}$ as shown in Figure 3.22.

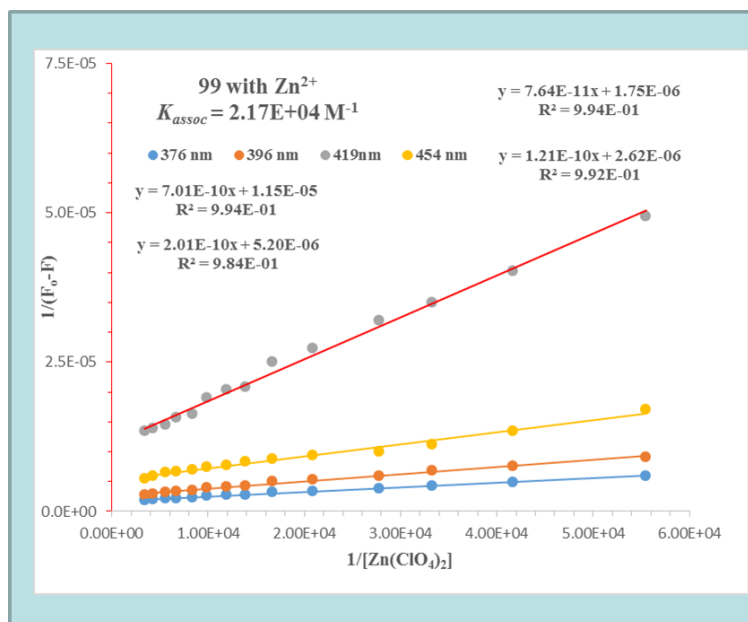
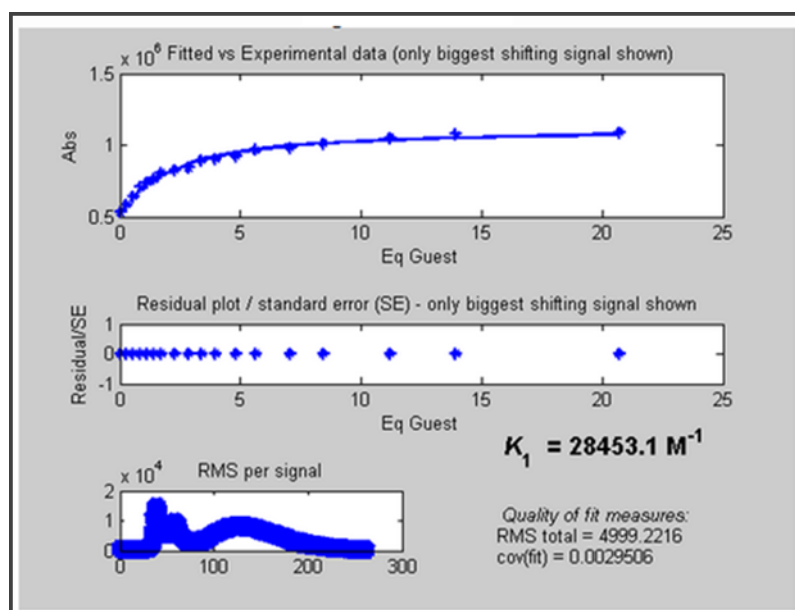


Figure 3.21 Benesi-Hildebrand plots of $1/(F_0-F)$ versus $1/[Zn(ClO_4)_2]$ for **99** upon titration with Zn^{2+} . The linear fits showed 1:1 complexation between **99** and Zn^{2+} . The association constants were calculated for the changes at the 376 nm, 396 nm, 419 nm and 454 nm wavelengths.



$$K = 2.84 \times 10^4 \text{ M}^{-1}$$

Figure 3.22 Screen-capture output showing 1:1 binding model for **99** with Zn^{2+} ,^{35b} using Thordarson's method.

Figure 3.23 shows the fluorescence titration experiments conducted for the receptor **99** with $\text{Cd}(\text{ClO}_4)_2$ salt. The changes of the fluorescence intensity of **99** revealed that, the monomer emission gradually increased, and that the excimer emission gradually decreased as the concentration of Cd^{2+} ion increased from 0.30-21 molar equivalents. The average association constant for the **99**: Cd^{2+} complex was calculated to be $5.26 \pm 0.695 \times 10^4 \text{ M}^{-1}$ by the Benesi-Hildebrand method as shown in Figure 3.24.

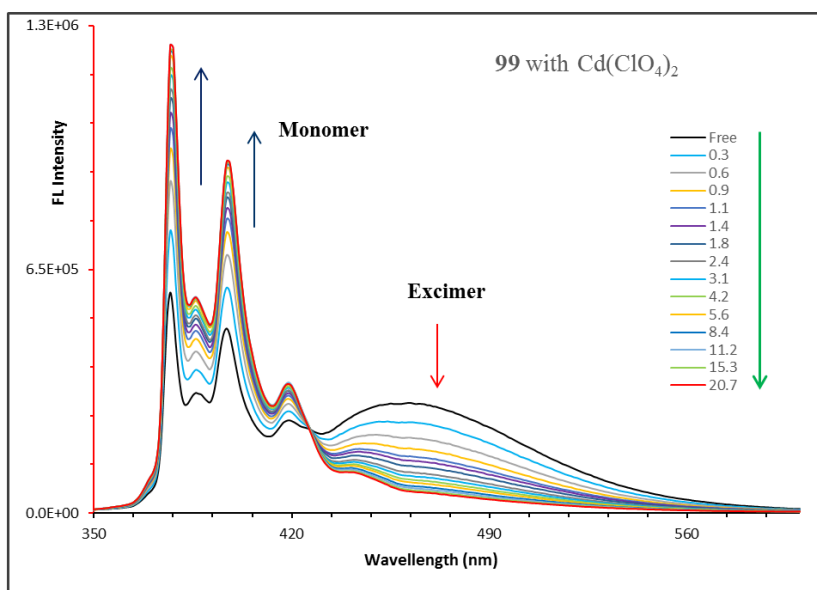


Figure 3.23 Fluorescence spectra of **99** upon addition of Cd^{2+} (0.30-21 eq) in acetonitrile/chloroform (v/v= 9:1) solutions. $\lambda_{exc} = 330 \text{ nm}$.

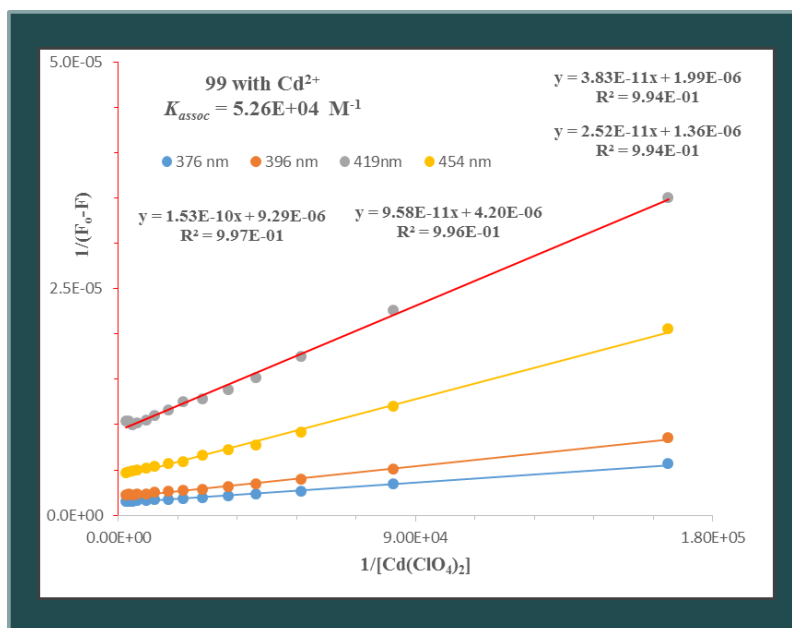
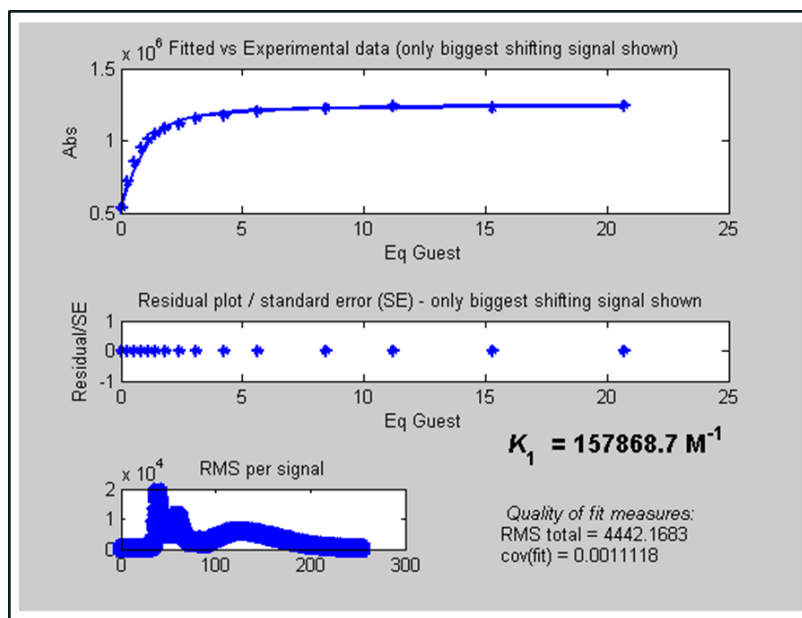


Figure 3.24 Benesi-Hildebrand plots of $1/(F_0-F)$ versus $1/[Cd(ClO_4)_2]$ for **99** upon titration with Cd^{2+} . The linear fits showed 1:1 complexation between **99** and Cd^{2+} . The individual association constants were calculated for the changes at the 376 nm, 396 nm, 419 nm and 454 nm wavelengths.

Using Thordarson's method, the calculated association constant for **99**: Cd^{2+} complex is $1.58 \times 10^5 M^{-1}$ is shown in Figure 3.25, and is significantly different from the previous result.



$$K = 1.58 \times 10^5 \text{ M}^{-1}$$

Figure 3.25 Screen-capture output showing 1:1 binding model for **99** with Cd^{2+} , ^{35b} using Thordarson's method.

Figure 3.26 shows the fluorescence titration experiments conducted for **99** with $\text{Fe}(\text{ClO}_4)_3$. Both monomer and excimer emissions of **99** are gradually decreased as the concentration of Fe^{3+} was increased from 0.057-1.7 molar equivalents. The average association constant for the **99**: Fe^{3+} complex was calculated to be $9.21 \pm 2.48 \times 10^4 \text{ M}^{-1}$ using the Benesi-Hildebrand method as shown in Figure 3.27.

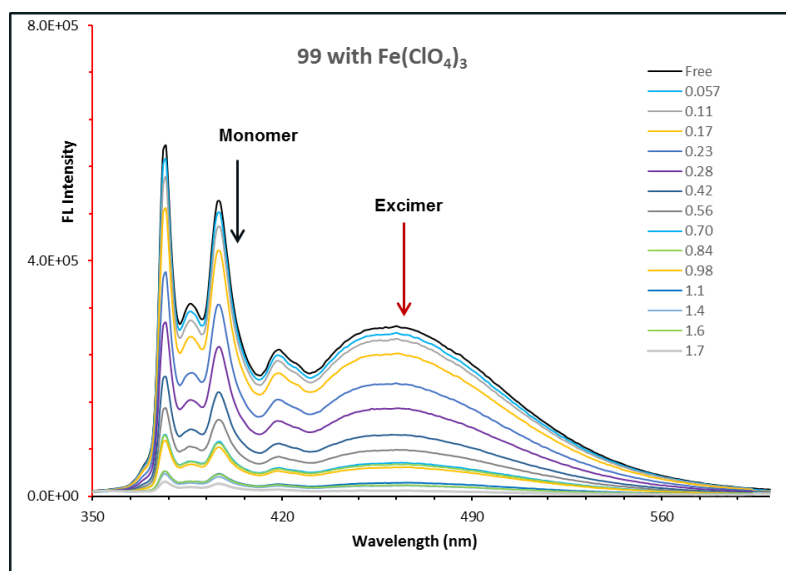


Figure 3.26 Fluorescence spectra of **99** upon addition of Fe^{3+} (0.057-1.7 eq) in acetonitrile/chloroform (v/v= 9:1) solutions. λ_{exc} = 330 nm.

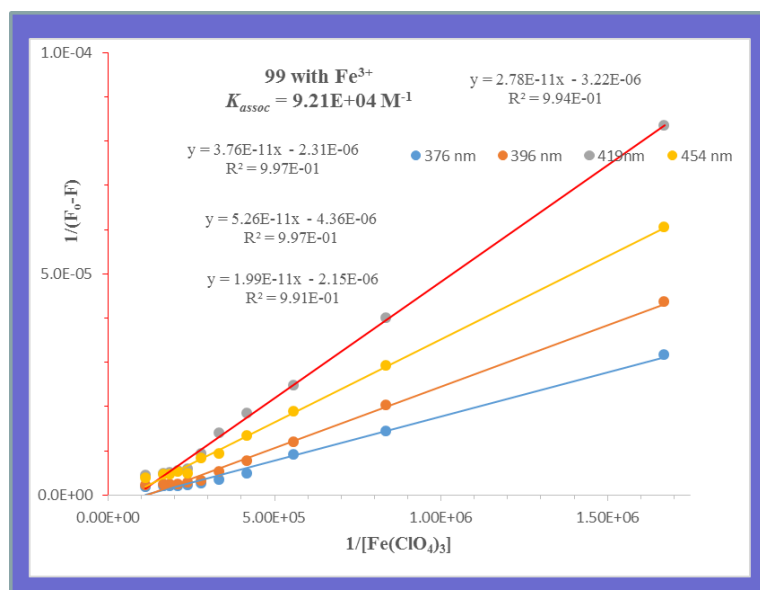


Figure 3.27 Benesi-Hildebrand plots of $1/(F_0-F)$ versus $1/[\text{Fe}(\text{ClO}_4)_3]$ for **99** upon titration with Fe^{3+} . The linear fits showed 1:1 complexation between **99** and Fe^{3+} . The individual association constants were calculated for the changes at the 376 nm, 396 nm, 419 nm and 454 nm wavelengths.

Thordarson's method afforded an association constant of $9.48 \times 10^5 \text{ M}^{-1}$ for **99**: Fe^{3+} , as shown in Figure 3.28, again a significantly higher (90.2%) value than that obtained in the B-H treatment, but the covariance of fit value of 0.046 is not as good as previous values, most probably due to the fact that quenching occurred with only very small amount of added Fe^{3+} .

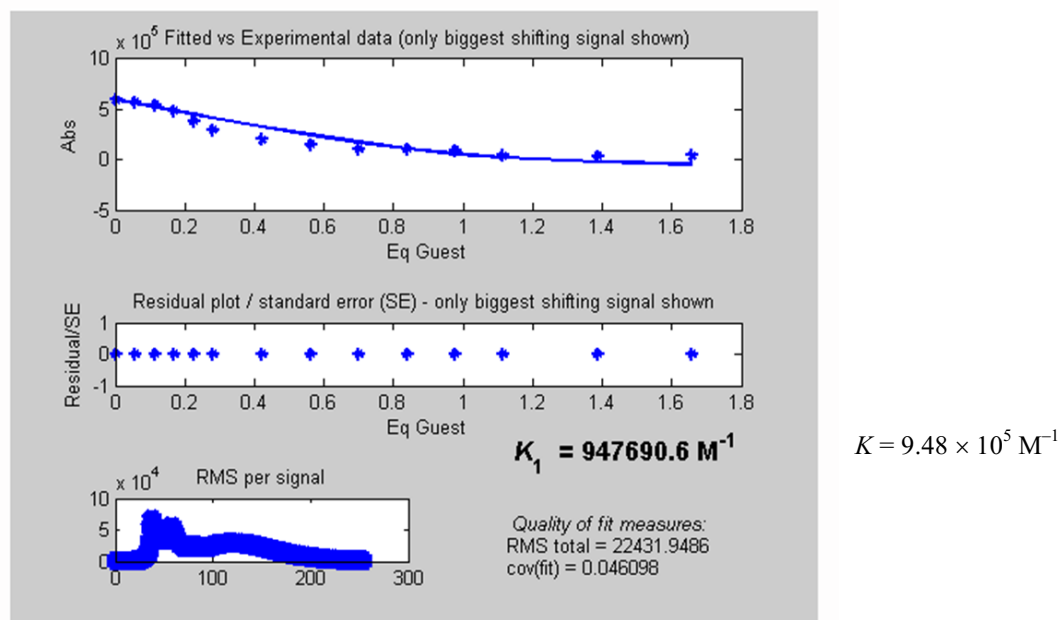


Figure 3.28 Screen-capture output showing 1:1 binding model for **99** with Fe^{3+} ,^{35b} using Thordarson's method.

Based on the fluorescence studies therefore, it can be concluded that the new bimodal calix[4]arene **99** is highly selective toward Fe^{3+} and Cd^{2+} .

3.6.1.1 Comparison of the association constants of receptor **99** with metal ions

Figure 3.29 shows that the association constants determined for all of the complexes using the two methods^{34,35} and it is clear that the complexation between **99** and Fe^{3+} ion

shows the largest K value of $9.48 \times 10^5 \text{ M}^{-1}$ based upon the observed changes measured for the fluorescence intensities.

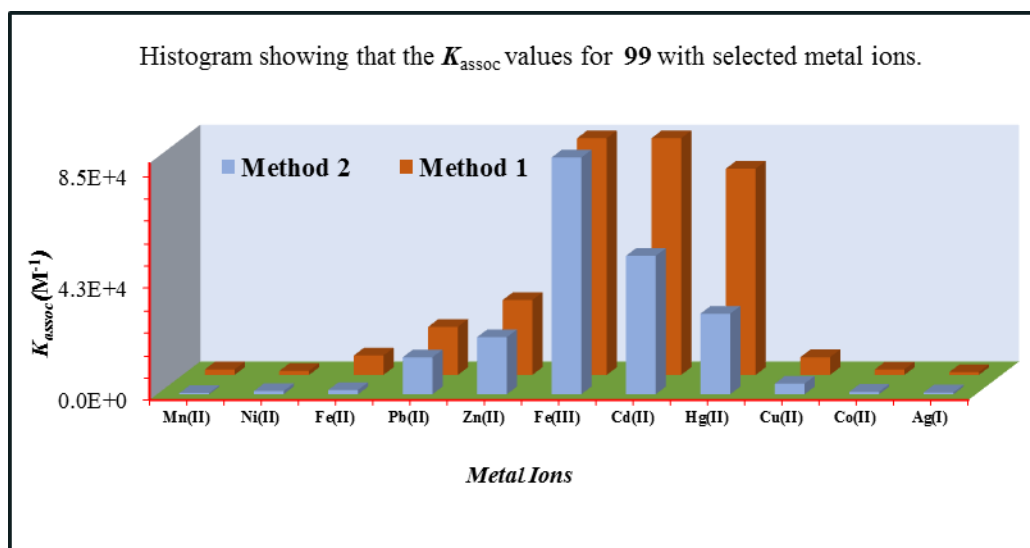


Figure 3.29 Histogram showing the association constant (K_{assoc}) values for receptor **99** with different metal ions determined by the two different methods.

Table 3.03 is a summary of the calculated binding constants for the **99** with selected metal ions as their perchlorate salts, using the two computational methods. Based on these binding constant values it is concluded that **99** is more selective for Fe^{3+} and Cd^{2+} among the ions examined. Note that in general, the Thordarson model afforded higher (i.e. 21-90%). K_{assoc} values and should be more reliable than the Benesi-Hildebrand calculated values since the entire spectra were analyzed in the former case and did not need an arbitrary selection of which data to be analyzed by the Benesi-Hildebrand approach.

Table 3.03 Comparison of calculated binding constants for **99** with selected metal perchlorate salts in 9:1 CH₃CN:CHCl₃ using the Thordarson and Benesi-Hildebrand (B-H) methods.

Entry	M ⁿ⁺ mol eq.	M ⁿ⁺	Thordarson (1) (M ⁻¹) x 10 ³ [cov(fit)]	Benesi-Hildebrand (2) (M ⁻¹) x 10 ³ [r ² > 0.99]	*Δ _{1-2/1} %
1	1.4-27	Mn ²⁺	2.10 [0.017]	0.440 ± 0.0286	79.0
2	0.57-53	Ni ²⁺	1.50 [0.0042]	1.18 ± 0.30	21.3
3	0.85-21	Pb ²⁺	18.3 [0.0027]	14.0 ± 0.210	23.5
4	0.30-10	Fe ²⁺	7.36 [0.0199]	1.61 ± 0.270	78.1
5	0.30-21	Zn ²⁺	28.4 [0.0029]	21.7 ± 0.404	23.6
6	0.057-1.7	Fe ³⁺	948 [0.046]	92.1 ± 0.248	90.2
7	0.30-21	Cd ²⁺	158 [0.0011]	52.6 ± 0.0695	66.7
8	0.080-0.56	Hg ²⁺	78.4 [0.059]	30.6 ± 2.25	61.0
9	0.84-11	Cu ²⁺	6.72 [0.0075]	4.04 ± 0.701	36.3
10	0.57-40	Co ²⁺	2.08 [0.0032]	0.910 ± 0.0801	56.2
11	0.71-27	Ag ⁺	1.03 [0.035]	0.667 ± 0.0811	35.2

* These values are the percentage differences between the K_{assoc} determined between the Thordarson and B-H methods.

3.6.2 Complexation studies of **99** using ¹HNMR spectroscopy

In order to support the mode of the complex formation between **99** and Cd²⁺, ¹HNMR titration experiments were carried out. A stock solution of **99** (2.51×10^{-3} M) was prepared in a CD₂Cl₂:CD₃CN (1:4, v/v) solvent mixture found to be suitable for the complexation study using ¹HNMR. Upon interaction of **99** with aliquots of 1.98×10^{-1} M

$\text{Cd}(\text{ClO}_4)_2$ in the same solvent, the triazole-*H* signal at δ 7.66 ppm was shifted downfield and merged with the signals of the pyrene moiety, which appeared as a broad signal. The two Ar-*H* protons at δ 7.00 and 6.91 ppm merged together to form a broad signal at δ 7.04 ppm. The other triazole unit singlet at δ 6.20 ppm (pyrene- CH_2 -triazole), shifted downfield and appeared as a broad signal at δ 6.25 ppm. The four-proton signal at δ 4.68 ppm which corresponds to the - OCH_2 -triazole linker, shifted upfield and appeared as a broad signal at δ 4.51 ppm. One of the pair of AB doublets at δ 3.90 ppm ($J = 12.9$ Hz) shifted upfield and appeared as a broad signal at δ 3.66 ppm and the other AB doublet at 3.06 ppm ($J = 12.9$ Hz) shifted downfield and appeared as a broad signal at 3.10 ppm. In the titration experiments of **99** with $\text{Cd}(\text{ClO}_4)_2$ the spectra quickly showed broad signals which were due to Cd^{2+} more strongly interacting with the triazole groups of **99** (Figure 3.30).

^1H -NMR titration experiments were also carried out for the complexation of **99** with Zn^{2+} ion as shown in Figure 3.31. A stock solution of the host molecule **99** (2.51×10^{-3} M) was prepared in the $\text{CD}_2\text{Cl}_2:\text{CD}_3\text{CN}$ (1:4, v/v) solvent mixture. Upon interaction of **99** with $\text{Zn}(\text{ClO}_4)_2$, the two-proton triazole-*H* signal at δ 7.66 ppm shifted only slightly downfield to δ 7.68 ppm. The two Ar-*H* protons at δ 6.98 and 6.90 ppm were shifted downfield to δ 6.99 and 6.91 ppm, respectively. The other four-proton triazole singlet at δ 6.20 ppm (pyrene- CH_2 -triazole), shifted downfield to δ 6.25 ppm. The other four-proton singlet at δ 4.68 ppm corresponding to the - OCH_2 -triazole linker, shifted upfield to δ 4.46 ppm. One of the pair of the AB doublets at δ 3.90 ppm ($J = 12.6$ Hz) was shifted upfield to δ 3.64 ppm and the other at 3.06 ppm ($J = 12.6$ Hz) was shifted upfield to 3.01 ppm

(Figure 3.31). The extent of the $^1\text{H-NMR}$ chemical shift changes is in agreement with the association constants ($\text{Cd}^{2+} > \text{Zn}^{2+}$) calculated from the fluorescence spectrometry results, suggesting that Cd^{2+} more strongly interacts with the triazole group of **99** than does Zn^{2+} .

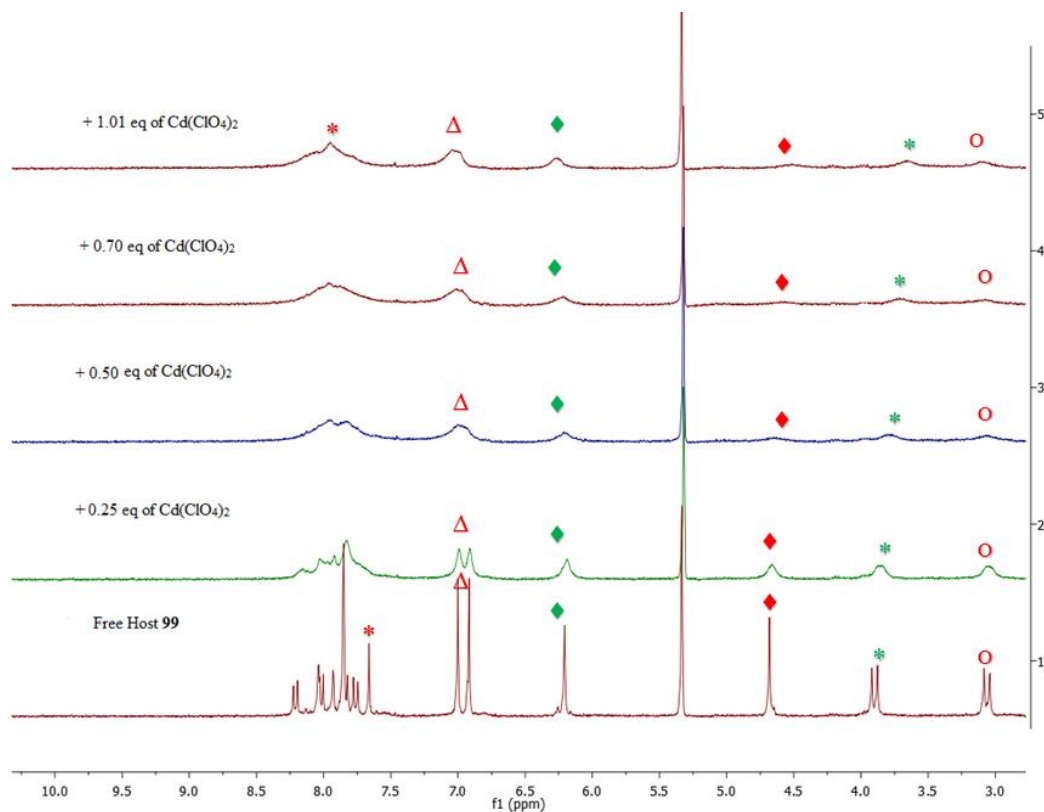


Figure 3.30 Partial $^1\text{H-NMR}$ (300 MHz) spectra of **99** with $\text{Cd}(\text{ClO}_4)_2$ in a $\text{CD}_3\text{CN}:\text{CD}_2\text{Cl}_2$ (4:1, v/v) at 298K; *, Δ, ◆, ♦, * and ○ denoted the triazole- H , Ar- H protons, pyrene- CH_2 -triazole, - OCH_2 -triazole and AB pair of doublets respectively.

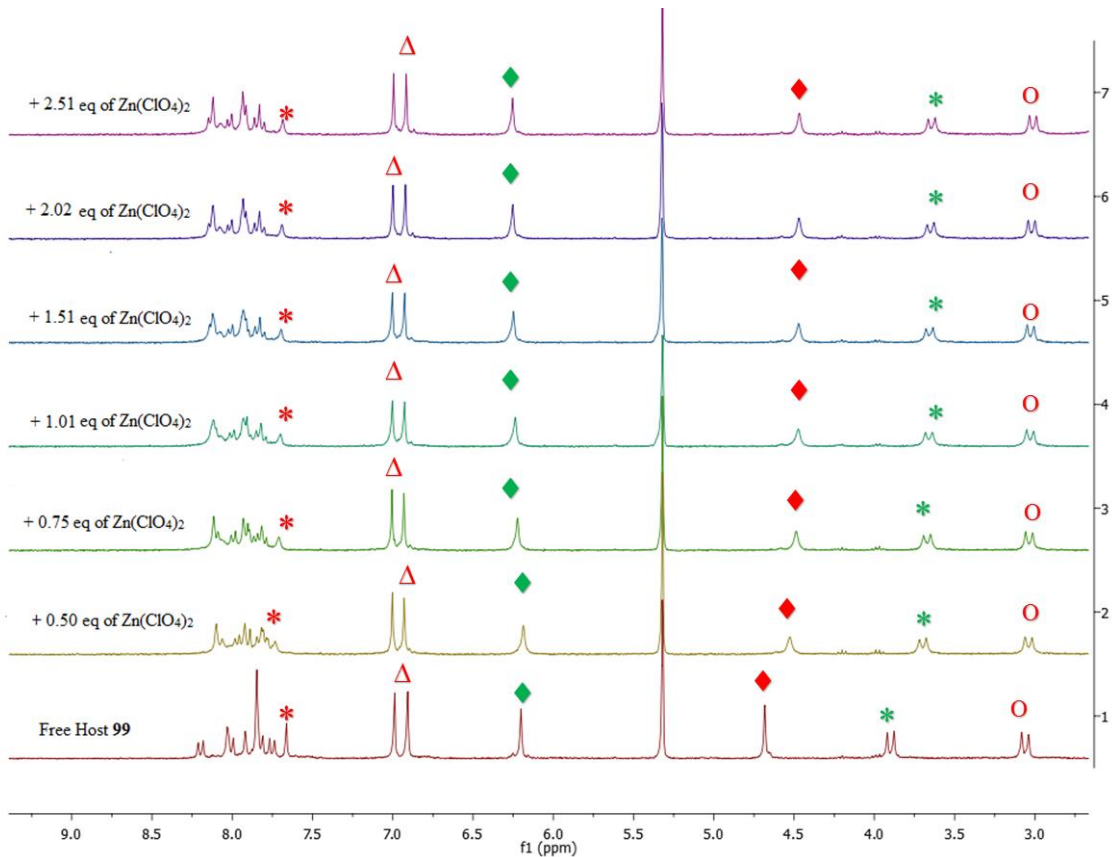


Figure 3.31 Partial ¹H NMR (300 MHz) spectra of **99** with Zn(ClO₄)₂ in a CD₃CN:CD₂Cl₂ (4:1, v/v) at 298K; *, Δ, ◆, ◆, * and ○ denoted the triazole-*H*, Ar-*H* protons, pyrene-CH₂-triazole, -OCH₂-triazole and AB pair of doublets respectively.

Detailed DFT computational studies of the complexation of these different metal salts with **99** with solvent corrections are currently on-going.

3.7 Conclusions

A new bimodal triazole-bridged anthracene-appended calix[4]arene derivative **98** has been synthesized and characterized. The upper rim of the **98** was functionalized with a thioacetate functional group which allows the calixarene to form a stable SAM onto a Au surface (currently on-going work in the Beaulieu Laboratories). Complexation studies

and association/binding constants of this new receptor **98** with different metal ions were investigated by UV-vis, fluorescence and ^1H NMR spectroscopic techniques. Metal ion competitive experiments were also investigated. The fluorescence studies proved that calix[4]arene **98** shows high binding selectivity for Hg^{2+} and Fe^{3+} over the other metal ions tested, as indicated by the significant fluorescence quenching in their titration spectra. The Job plots supported the formation of 1:1 complex formations between **98** and Hg^{2+} or Fe^{3+} , and **98** is therefore an effective and sensitive fluorescent chemosensor for these ions in particular.

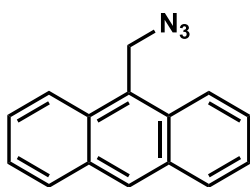
A new bimodal triazole-bridged pyrene-appended calix[4]arene **99** has also now been synthesized and characterized. Using this receptor complexation studies were also undertaken with various metal ions including the calculation of the association/binding constants for the complexes using two methods (i.e. Thordarson and B-H methods) for comparison. Binding of Cd^{2+} and Zn^{2+} occurs as demonstrated by an enhanced monomer and declining excimer emission fluorescence spectral changes. On the other hand, upon addition of Fe^{3+} or Hg^{2+} , and several other metal ions tested, quenching of both monomer and excimer emission of **99** was observed. Calix[4]arene derivative **99** selectively binds to Fe^{3+} and Cd^{2+} ions and is thus an effective fluorescent chemosensor. Crystals of **99** have been submitted to single X-ray diffraction determination but at the time of writing this Chapter, the structure had not been solved.

3.8 Experimental section

All reagents used for the synthesis of functionalized calix[4]arenes **98** and **99** and reagents used in the complexation studies were purchased from Sigma-Aldrich or Alfa Aesar. ^1H NMR spectra were recorded at either 300 or 500 MHz, as noted, and the ^{13}C -NMR spectra at 75.4, MHz. Mass spectra were measured on an APCI-LC/MSD Trap instrument. Complexation studies of the calix[4]arenes **98** and **99** were conducted using UV-vis, fluorescence and ^1H NMR spectroscopic techniques. All the metal ion salts (perchlorates) were used in the complexation studies were purchased from Alfa Aesar in >99 % purity.

3.8.1 Experimental

9-(Azidomethyl)anthracene (**101**).³²

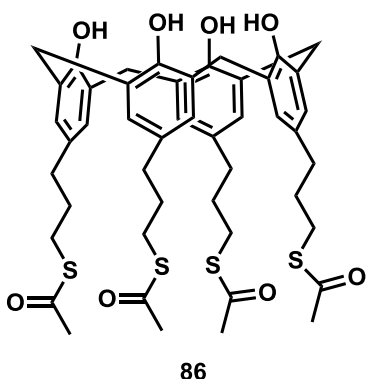


101

A mixture of 9-(chloromethyl)anthracene **100** (1.12 g, 4.94 mmol) and sodium azide (0.641 g, 9.88 mmol) was prepared in 20 mL of anhydrous DMF. The resulting solution was stirred for 24 h at room temperature. After completion of the reaction, saturated brine solution (25 mL) was added to the reaction mixture, the precipitated solid was filtered off and washed with water (20 mL) to yield 9-(azidomethyl)anthracene **101** as a yellow solid (0.810 g, 70%, m.p. 80.0-81.2 °C). ^1H NMR (CDCl_3 , 300 MHz): δ 8.50 (s, 1H, anthracene-*H*), 8.28 (d, 2H, anthracene-*H*, $J = 8.7$ Hz), 8.04 (d, 2H, anthracene-*H*, $J = 8.7$ Hz), 7.61–7.47 (m, 4H, anthracene-*H*), 5.32 (s, 2H, $-\text{CH}_2$). ^{13}C NMR (CDCl_3 , 75.4

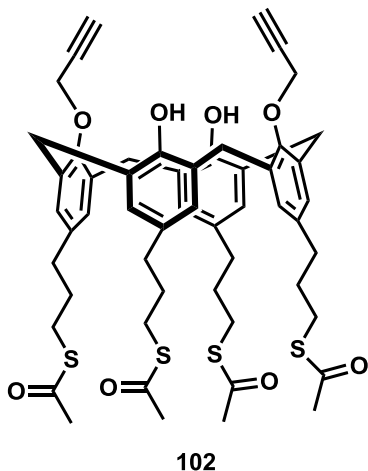
MHz): δ 131.4, 130.7, 129.3, 129.0, 126.9, 125.8, 125.2, 123.5, 46.4. APCI(+) MS (m/z): 191.1 $[M-N_3]^+$.

5,11,17,23-Tetrakis(3-propylthioacetate)-25,26,27,28-tetrahydroxycalix[4]arene (86).



The synthesis of 5,11,17,23-tetrakis(3-propylthioacetate)-25,26,27,28-tetrahydroxycalix[4]arene (**86**) is described in Chapter 2.

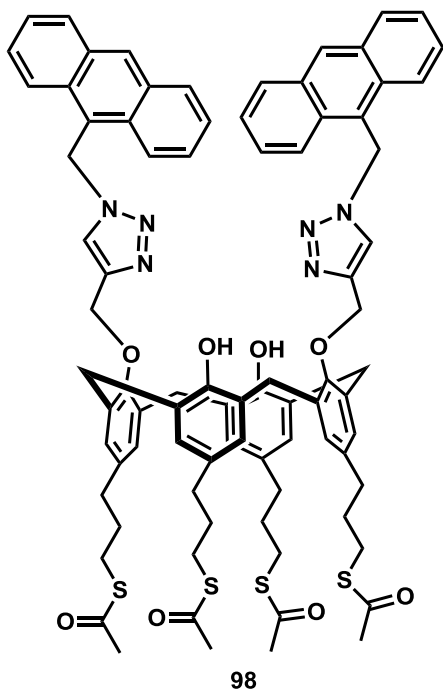
5,11,17,23-Tetrakis(3-propylthioacetate)-25,27-dihydroxy-26,28-dipropargyl calix[4]arene (102).



A mixture of calix[4]arene **86** (0.55 g, 0.62 mmol) and K_2CO_3 (0.171 g, 1.24 mmol) in acetone (30 mL) was heated at reflux for 1 h. Propargyl bromide was added to the reaction mixture, which was then heated at reflux for 24 h. After cooling to room temperature, the reaction mixture was neutralized with aqueous 1.0 M HCl and then extracted with ethyl acetate (3×50 mL), washed with water (2×50 mL). The separated organic layer was dried over anhydrous $MgSO_4$ and the solvent was removed using a rotary evaporator. The residue was subjected to column chromatography (silica gel, 75:25 hexanes: ethyl acetate) to yield 5,11,17,23-tetrakis(3-

propylthioacetate)-25,27-dihydroxy-26,28-dipropargyl calix[4]arene (**102**) as a colourless oil. (0.42 g, 71%). ¹H-NMR (CDCl₃, 300 MHz): δ 6.98 (s, 2H, Ar-OH), 6.85 (s, 4H, Ar-H), 6.63 (s, 4H, Ar-H), 4.75 (d, 4H, -OCH₂, *J* = 2.4 Hz), 4.34 (d, 4H, Ar-CH₂, *J* = 13.2 Hz), 3.31 (d, 4H, Ar-CH₂, *J* = 13.2 Hz), 2.86 (t, 4H, CH₂S-, *J* = 7.2 Hz), 2.66-2.58 (m, 4H, CH₂S-, 4H, ArCH₂CH₂CH₂S-), 2.56 (t, 2H, *J* = 2.4 Hz, -C≡CH), 2.36-2.32 (m, 4H, ArCH₂CH₂CH₂S-), 2.34 (s, 6H, -SCOCH₃), 2.30 (s, 6H, -SCOCH₃), 1.86 (quint, 4H, -CH₂CH₂CH₂S-, *J* = 7.5 Hz), 1.62 (quint, 4H, -CH₂CH₂CH₂S-, *J* = 7.5 Hz). ¹³C-NMR (CDCl₃, 75.4 MHz): δ 195.9, 195.8, 151.0, 149.8, 137.9, 133.4, 131.5, 128.8, 128.4, 128.2, 63.3, 45.8, 36.5, 34.0, 33.9, 31.9, 31.3, 30.8, 30.7, 30.6, 28.6, 28.4. APCI(+) MS (*m/z*): 965.3 [M+1]⁺.

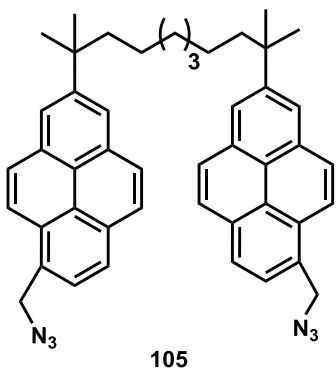
5,11,17,23-Tetrakis(3-propylthioacetate)-25,27-dihydroxy-26,28-di(1,2,3-triazol-1-methylantracene)calix[4]arene (98).



Copper iodide (0.061 g, 0.32 mmol) was added to 5,11,17,23-tetrakis(3-propylthioacetate)-25,27-dihydroxy-26,28-dipropargylcalix[4]arene (**102**) (0.31 g, 0.32 mmol) and 9-(azidomethyl) anthracene (**101**) (0.072 g, 0.32 mmol) in 20 mL of THF/H₂O (2:1) and the reaction mixture was heated at 60 °C for 24 h. The reaction mixture was diluted with ethyl acetate (25 mL), and washed with water (15 mL) and brine (15 mL). The organic layer was

separated, dried over MgSO_4 and filtered. The solvent was removed using a rotary evaporator and the residue was subjected to column chromatography (silica gel, hexanes:ethyl acetate 70:30) to yield 5,11,17,23-tetrakis(3-propylthioacetate)-25,27-dihydroxy-26,28-di(1,2,3-triazol-1-methylanthracene)calix[4]arene (**98**) as a pale yellow solid (0.31 g, 69%, m.p. 112.8-113.9 °C). $^1\text{H-NMR}$ (CDCl_3 , 300 MHz) δ 8.39 (s, 2H, anthracenyl-*H*), 8.18 (d, 4H, anthracenyl-*H*, $J = 8.1$ Hz), 7.96 (d, 4H, anthracenyl-*H*, $J = 8.1$ Hz), 7.49–7.41 (m, 8H, anthracenyl-*H*), 7.23 (s, 2H, triazole-*H*), 6.83 (s, 2H, Ar-*OH*), 6.57 (s, 4H, Ar-*H*), 6.40 (s, 4H, anthracene- CH_2 -triazole), 6.34 (s, 4H, Ar-*H*), 4.75 (s, 4H, $-\text{OCH}_2$), 3.59 (d, 4H, Ar- CH_2 , $J = 12.9$ Hz), 2.86 (t, 4H, CH_2S -, $J = 7.2$ Hz), 2.77 (d, 4H, Ar- CH_2 , $J = 12.9$ Hz), 2.60 (t, 4H, CH_2S -, $J = 7.2$ Hz), 2.51 (t, 4H, Ar $\text{CH}_2\text{CH}_2\text{CH}_2\text{S}$ -, $J = 7.2$ Hz), 2.35 (s, 6H, $-\text{SCOCH}_3$), 2.30 (s, 6H, $-\text{SCOCH}_3$), 2.17 (t, 4H, Ar $\text{CH}_2\text{CH}_2\text{CH}_2\text{S}$ -, $J = 7.2$ Hz), 1.84 (quint, 4H, $-\text{CH}_2\text{CH}_2\text{CH}_2\text{S}$ -, $J = 7.5$), 1.51 (quint, 4H, $-\text{CH}_2\text{CH}_2\text{CH}_2\text{S}$ -, $J = 7.5$). $^{13}\text{C-NMR}$ (CDCl_3 , 75.4 MHz): δ 195.9, 195.8, 150.6, 149.9, 137.5, 133.0, 131.2, 131.1, 130.6, 129.8, 129.4, 128.5, 128.1, 127.6, 127.4, 125.2, 124.0, 123.0, 71.1, 46.4, 34.0, 31.4, 31.3, 30.7, 30.6, 28.6, 28.4. APCI(+) MS (m/z): 1431.6 $[\text{M}+1]^+$.

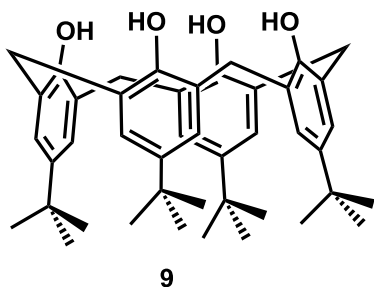
2,10-Bis[6-(azidomethyl)pyren-2-yl]-2,10-dimethylundecane (**105**).



A mixture of 2,10-bis(6-(bromomethyl)pyren-2-yl)-2,10-dimethylundecane⁴² (**104**) (0.31 g, 0.42 mmol) and sodium azide (0.651 g, 4.02 mmol) was prepared in 15 mL of anhydrous DMF. The resulting solution was stirred for 24 h

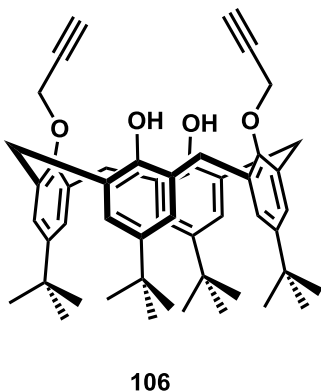
at room temperature. After completion of the reaction, saturated brine solution (25 mL) was added to the reaction mixture. The precipitated solid was filtered off and washed with water (20 mL) to yield 2,10-bis(6-(azidomethyl)pyren-2-yl)-2,10-dimethylundecane (**105**) as a yellow solid (0.212 g, 70%, m.p. 138.9-140.2 °C). ¹H-NMR (300 MHz, CDCl₃) δ 8.22 (d, 2H, *J* = 9.3 Hz), 8.14–8.10 (m, 8H), 8.02 (d, 4H, *J* = 10.8 Hz), 7.92 (d, 2H, *J* = 7.5 Hz), 5.01 (s, 4H), 1.78–1.73 (m, 4H), 1.50 (s, 12H), 1.06–1.00 (m, 10H); ¹³C-NMR (CDCl₃, 75.4 MHz): δ 148.1, 131.6, 130.9, 130.5, 129.0, 128.6, 128.1, 128.0, 127.1, 127.0, 124.9, 124.4, 123.5, 123.3, 122.8, 122.5, 53.1, 45.1, 38.2, 30.2, 29.5, 24.7; APCI(+) MS (*m/z*): 624.3 [M–N₅]⁺.

5,11,17,23-Tetra-*tert*-butyl-25,26,27,28-tetrahydroxycalix[4]arene (9).



The *p-tert*-butylcalix[4]arene **9** was synthesized from *p-tert*-butylphenol **77** according to the procedure described in Chapter 2.

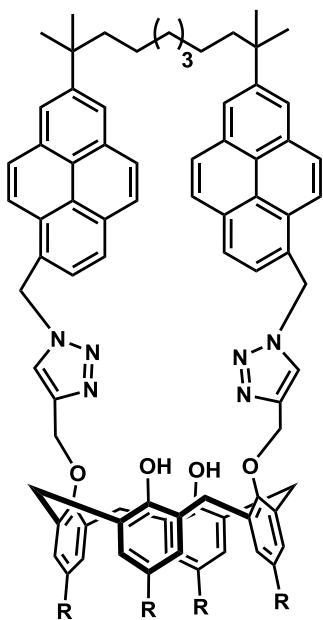
5,11,17,23-Tetra-*tert*-butyl-25,27-dihydroxy-26,28-dipropargylcalix[4]arene (106).³²



A mixture of 5,11,17,23-tetra-*tert*-butyl-25,26,27,28-tetrahydroxycalix[4]arene (**9**) (0.51 g, 0.78 mmol) and K₂CO₃ (0.242 g, 1.57 mmol) was heated at reflux for 1 h in acetone (30 mL). Propargyl bromide (0.191 g, 1.57 mmol) was added to the reaction mixture and then heated at reflux for 24 h.

After cooling to room temperature, the reaction mixture was neutralized with aqueous 1.0 M HCl and then extracted with ethyl acetate (3 × 50 mL), washed with water (2 × 50 mL). The separated organic layer was dried over anhydrous MgSO₄ and the solvent was removed using a rotary evaporator. The residue was subjected to column chromatography (silica gel, 75:25 hexanes: ethyl acetate) to yield 5,11,17,23-tetra-*tert*-butyl-25,27-dihydroxy-26,28-dipropargyl calix[4]arene (**106**) as a colourless solid (0.401 g, 71%, m.p. 222.0-223.3 °C) ¹H-NMR (CDCl₃, 300 MHz): δ 7.07 (s, 4H, ArH), 6.72 (s, 4H, ArH), 6.50 (s, 2H, Ar-OH), 4.74 (d, 4H, *J* = 2.4 Hz, -OCH₂), 4.37 (d, 4H, Ar-CH₂, *J* = 13.2 Hz), 3.33 (d, 4H, Ar-CH₂, *J* = 13.2 Hz), 2.53 (t, 2H, -C≡CH, *J* = 2.4 Hz), 1.30 (s, 18H, *t*-Bu), 0.89 (s, 18H, *t*-Bu). ¹³C-NMR (CDCl₃, 75.4 MHz): δ 150.4, 149.5, 147.2, 141.6, 132.6, 128.0, 125.5, 125.0, 78.8, 63.3, 33.9, 33.8, 32.0, 31.7, 30.9. APCI(+) MS (*m/z*): 725.4 [M+1]⁺.

5,11,17,23-Tetra-*tert*-butyl-25,27-dihydroxy-26,28-bis[1,2,3-triazol-1-methyl(2,10-bis(6-pyren-2-yl)-2,10-dimethylundecane)]calix[4]arene (99).



99
R = *t*-Bu

Copper iodide (0.041 g, 0.21 mmol) was added to a mixture of 5,11,17,23-tetra-*tert*-butyl-25,27-dihydroxy-26,28-dipropargyl calix[4]arene (**106**) (0.15 g, 0.21 mmol), diisopropylamine (20 μL) and 2,10-Bis(6-(azidomethyl)pyren-2-yl)-2,10-dimethylundecane (**105**) (0.14 g, 0.21 mmol) in 20 mL of THF/H₂O (2:1). The reaction mixture was heated at 60 °C for 24 h and was diluted with ethyl acetate (25 mL),

and washed with water (15 mL) and brine (15 mL). The organic layer was separated and dried over MgSO₄ and filtered. The solvent was removed using a rotary evaporator and the residue was subjected to column chromatography (silica gel, hexanes: ethyl acetate 60:40) to yield 5,11,17,23-tetra-*tert*-butyl-25,27-dihydroxy-26,28-di[1,2,3-triazol-1-methyl(2,10-bis(6-pyren-2-yl)-2,10-dimethylundecane)]calix[4]arene (**99**) as a yellow solid (0.14 g, 51%, m.p. 205.8-207.2 °C). ¹H-NMR (CDCl₃, 300 MHz): δ 8.06–8.00 (m, 8H), 7.90 (s, 4H), 7.85 (d, 2H, *J* = 9.3 Hz), 7.77 (d, 2H, *J* = 7.8 Hz), 7.65 (s, 2H, triazole-*H*), 7.07 (s, 2H, Ar-*OH*), 6.90 (s, 4H, Ar-*H*), 6.65 (s, 4H, Ar-*H*), 6.13 (s, 4H, pyrene-CH₂-triazole), 4.88 (s, 4H, -OCH₂), 4.02 (d, 4H, Ar-CH₂, *J* = 13.2 Hz), 3.07 (d, 4H, Ar-CH₂, *J* = 13.2 Hz), 1.74–1.68 (m, 4H), 1.47 (s, 12H), 1.24 (s, 18H, *t*-Bu), 1.02–0.95 (m, 6H), 0.94–0.89 (m, 4H), 0.86 (s, 18H, *t*-Bu). ¹³C-NMR (CDCl₃, 75.4 MHz): δ 150.4, 149.5, 148.0, 147.0, 144.2, 141.4, 132.6, 131.6, 130.9, 130.3, 128.9, 128.7, 128.3, 127.6, 127.2, 126.9, 126.7, 125.5, 124.9, 124.8, 123.6, 123.5, 122.6, 121.8, 69.1, 52.1, 44.6, 38.2, 33.8, 33.7, 31.9, 31.7, 30.9, 29.5, 29.2, 28.1, 24.1. APCI(+) MS (*m/z*): 1420.9 [M+1]⁺.

3.9 References

- (a) de Silva, A. P.; Gunaratne, H. Q. N.; Gunnlaugsson, T.; Huxley, A. J. M.; McCoy, C. P.; Rademacher, J. T.; Rice, T. E. *Chem. Rev.* **1997**, *97*, 1515-1566.
(b) Czarnik, A. W. *Chem. Biol.* **1995**, *2*, 423-428. (c) Kim, J. S.; Quang, D. T. *Chem. Rev.* **2007**, *107*, 3780-3799.
- Joseph, R.; Rao, C. P. *Chem. Rev.* **2011**, *111*, 4658-4702.

3. (a) Ji, H.-F.; Brown, G. M.; Dabestani, R. *Chem. Commun.* **1999**, 609-610. (b) Bu, J.-H.; Zheng, Q.-Y.; Chen, C.-F.; Huang, Z.-T. *Org. Lett.* **2004**, *6*, 3301-3303. (c) Kim, H. J.; Kim, J. S. *Tetrahedron Lett.* **2006**, *47*, 7051-7055.
4. (a) Aoki, I.; Sakaki, T.; Shinkai, S. *J. Chem. Soc., Chem. Commun.* **1992**, 730-732. (b) Leray, I.; Lefevre, J.-P.; Delouis, J.-F.; Delaire, J.; Valeur, B. *Chem. Eur. J.* **2001**, *7*, 4590-4598. (c) Choi, J. K.; Kim, S. H.; Yoon, J.; Lee, K.-H.; Bartsch, R. A.; Kim, J. S. *J. Org. Chem.* **2006**, *71*, 8011-8015. (d) Schazmann, B.; Alhashimy, N.; Diamond, D. *J. Am. Chem. Soc.* **2006**, *128*, 8607-8614. (e) Castellano, R. K.; Craig, S. L.; Nuckolls, C.; Rebek, J. Jr. *J. Am. Chem. Soc.* **2000**, *122*, 7876-7882.
5. Bell, T. W.; Hext, N. M. *Chem. Soc. Rev.* **2004**, *33*, 589-598.
6. Chio, Y. W.; Park, G. H.; Na, Y. J.; Jo, H. Y.; Lee, S. A.; You, G. R.; Kim, C. *Sens. Actuators, B.* **2014**, *193*, 343-352.
7. Matzanke, B. F.; Muller-Martzanke, G.; Raymond, K. N. *Iron Carriers and Iron Proteins*; VCH Publishers: New York, 1989; Vol. 5.
8. Touati, D. *Arch. Biochem. Biophys.* **2000**, *373*, 1-6.
9. (a) Boening, D. W. *Chemosphere* **2000**, *40*, 1335-1351. (b) Zheng, W.; Aschner, M.; Ghersi-Egea, J. F. *Toxicol. Appl. Pharmacol.* **2003**, *192*, 1-11.
10. (a) Wen, S.; Zeng, T.; Liu, L.; Zhao, K.; Zhao, Y.; Liu, X.; Wu, H. C. *J. Am. Chem. Soc.* **2011**, *133*, 18312-18317. (b) Liu, X.; Tang, Y.; Wang, L.; Zhang, J.; Song, S.; Fan, C.; Wang, S. *Adv. Mater.* **2007**, *19*, 1662-1662. (c) Gu, Z.; Zhao,

- M. X.; Sheng, Y. W.; Bentolila, L. A.; Tang, Y. *Anal. Chem.* **2011**, *83*, 2324-2329. (d) Hu, J. M.; Li, C. H.; Liu, S. Y. *Langmuir* **2010**, *26*, 724-729.
11. Lin-Fu, J. S. Lead Poisoning. A Century of Discovery and Rediscovery. In *Human Lead Exposure*; Needleman, H. L. Ed.; Lewis Publishing: Boca Raton, FL. 1992.
12. (a) Kozłowski, H.; Klos, A. J.; Brasun, J.; Gaggelli, E.; Valensin, D.; Valensin, G. *Coord. Chem. Rev.* **2009**, *253*, 2665-2685. b) Duruibe, J. O.; Ogwuegbu, M. O.; Egwurugwu, J. N. *Int. J. Phys. Sci.* **2007**, *2*, 112-118.
13. Gupta, V. K.; Jain, A. K.; Khayat, M.; Bhargava, S. K.; Raison, J. R. *Electrochim. Acta.* **2008**, *53*, 5409-5414.
14. (a) Little, C.; Aakre, S. E.; Rumsby, M. G.; Gwarsha, K. *Biochem. J.* **1982**, *207*, 117-121. (b) Walker, K. W.; Bradshaw, R. A. *Protein Sci.* **1998**, *7*, 2684-2687. (c) Gharehbaghi, M.; Shemirani, F.; Farahani, M. D. *J. Hazard. Mater.* **2009**, *165*, 1049-1055. (d) Memon, S.; Yilmaz, M. *J. Mol. Struct.* **2001**, *595*, 101-109.
15. Murray, C. B.; Noms, D. J.; Bawendi, M. G. *J. Am. Chem. Soc.* **1993**, *115*, 8706-8715.
16. *Cadmium in the Human Environment: Toxicity and Carcinogenicity*; Nordberg, G. F.; Herber, R. F. M.; Alessio, L. Eds.; Oxford University Press: Oxford, UK, 1992.
17. (a) Assaf, S. Y.; Chung, S. H. *Nature* **1984**, *308*, 734-736. (b) Berg, J. M.; Shi, Y. *Science* **1996**, *271*, 1081-1085.

18. (a) Sahin, O.; Yilmaz, M. *Tetrahedron* **2011**, *67*, 3501-3509. (b) Mandolini, L.; Ungaro, R. *Calixarenes in Action*, Imperial College Press, London, 2000. (c) Zhao, J.-L.; Tomiyasu, H.; Ni, X.-L.; Zeng, X.; Elsegood, M. R. J.; Redshaw, C.; Rahman, S.; Georghiou, P. E.; Teat, S. J.; Yamato, T. *Org. Biomol. Chem.* **2015**, *13*, 3476-3483.
19. Kold, H. C.; Finn, M. G.; Sharpless, K. B. *Angew. Chem. Int. Ed.* **2001**, *40*, 2004-2021.
20. Chu, C.; Liu, R. *Chem. Soc. Rev.* **2011**, *40*, 2177-2188.
21. Chang, K.-C.; Su, I.-H.; Senthilvelan, A.; Chung, W.-S. *Org. Lett.* **2007**, *9*, 3363-3366.
22. Ni, X.-L.; Wang, S.; Zeng, X.; Tao, Z.; Yamato, T. *Org. Lett.* **2010**, *12*, 552-555.
23. (a) Araki, K.; Hayashida, H. *Tetrahedron Lett.* **2000**, *41*, 1807-1810. (b) Yamato, T.; Zhang, F. L.; Tsuzuki, H.; Miura, Y. *Eur. J. Org. Chem.* **2001**, 1069-1075. (c) Tsubaki, K.; Morimoto, T.; Otsubo, T.; Fuji, K. *Org. Lett.* **2002**, *4*, 2301-2304.
24. Holm, R. H.; Kennepohl, P.; Solomon, E. I. *Chem. Rev.* **1996**, *96*, 2239-2314.
25. (a) Berg, J. M.; Shi, Y. *Science* **1996**, *271*, 1081-1085. (b) Alberts, I. L.; Nadassy, K.; Wodak, S. J. *Protein Sci.* **1998**, *7*, 1700-1716. (c) Ralph, D. M.; Robinson, S. R.; Campbell, M. S.; Bishop, G. M. *Free Radical Biol. Med.* **2010**, *49*, 649-657.
26. Pathak, R. K.; Hinge, V. K.; Mahesh, K.; Rai, A.; Panda, D.; Rao, C. P. *Anal. Chem.* **2012**, *84*, 6907-6913.

27. Cho, J.; Pradhan, T.; Kim, J. S.; Kim, S. *Org. Lett.* **2013**, *15*, 4058-4061.
28. (a) Rostovtsev, V. V.; Green, L. G.; Fokin, V. V.; Sharpless, K. B. *Angew. Chem., Int. Ed.* **2002**, *41*, 2596-2599. (b) Tornøe, C. W.; Christensen, C.; Meldal, M. *J. Org. Chem.* **2002**, *67*, 3057-3064.
29. (a) Lutz, J.-F. *Angew. Chem. Int. Ed.* **2007**, *46*, 1018-1025. (b) Angell, Y. L.; Burgess, K. *Chem. Soc. Rev.* **2007**, *36*, 1674-1689. (c) Fournier, D.; Hoogenboom, R.; Schubert, U. S. *Chem. Soc. Rev.* **2007**, *36*, 1369-1380. (d) Chan, T. R.; Hilgraf, R.; Sharpless, K. B.; Fokin, V. V. *Org. Lett.* **2004**, *6*, 2853-2855.
30. Ryu, E.-H.; Zhao, Z. *Org. Lett.* **2005**, *7*, 1035-1037.
31. (a) Dondoni, A.; Marra, A. *J. Org. Chem.* **2006**, *71*, 7546-7557. (b) Bew, S. P.; Brimage, R. A.; L'Hermitie, N.; Sharma, S. V. *Org. Lett.* **2007**, *19*, 3713-3716. (c) Marra, A.; Moni, L.; Pazzi, D.; Corallini, A.; Bridi, D.; Dondoni, A. *Org. Biomol. Chem.* **2008**, *6*, 1396-1409.
32. Mummidivarapu, V. V. S.; Hinge, V. K.; Tabbasum, K.; Gonnade, R. G.; Rao, C. P. *J. Org. Chem.* **2013**, *78*, 3570-3576.
33. Chang, K.-C.; Su, I.-H.; Lee, G.-H.; Chung, W.-S. *Tetrahedron Lett.* **2007**, *48*, 7274-7278.
34. (a) Jisha, V. S.; Thomas, A. J.; Ramaiah, D. *J. Org. Chem.* **2009**, *74*, 6667-6673. (b) Bano, S.; Ayaz, M.; Khan, A. A. P.; Siddiqi, K. S. *J. Chem. Eng. Data* **2010**, *55*, 5759-5765.

35. (a) Thordarson, P. *Chem. Soc. Rev.* **2011**, *40*, 1305-1323. (b) www.supramol.com
36. (a) Ojida, A.; Mito-oka, Y.; Inoue, M.-A.; Hamachi, I. *J. Am. Chem. Soc.* **2002**, *124*, 6256-6258. (b) Choi, M.; Kim, M.; Lee, K. D.; Han, K.-N.; Yoon, I.-A.; Chung, H.-J.; Yoon, J. *Org. Lett.* **2001**, *3*, 3455-3457. (c) Chae, M.-Y.; Cherian, X. M.; Czarnik, A. W. *J. Org. Chem.* **1993**, *58*, 5797-5801.
37. Job, P. *Ann. Chim.* **1928**, *9*, 113-203.
38. Zheng, X.; Wang, X.; Yi, S.; Wang, N.; Peng, Y. *J. Comp. Chem.* **2009**, 1458-1468.
39. Briks, J. B. *Photophysics of Aromatic Molecules*; John Wiley: New York, 1970.
40. (a) Kim, S. K.; Bok, J. H.; Bartsch, R. A.; Lee, J. Y.; Kim, J. S. *Org. Lett.* **2005**, *7*, 4839-4842. (b) Kim, S. K.; Lee, S. H.; Lee, J. Y.; Bartsch, R. A.; Kim, J. S. *J. Am. Chem. Soc.* **2004**, *126*, 16499-16506. (c) Choi, J. K.; Kim, S. H.; Yoon, J.; Lee, K. H.; Kim, J. S. *J. Org. Chem.* **2006**, *71*, 8011-8015.
41. Park, S. Y.; Yoon, J. H.; Hong, C. S.; Souane, R.; Kim, J. S.; Matthews, S. E.; Vicens, J. *J. Org. Chem.* **2008**, *73*, 8212-8218.
42. Merner, B. L.; Unikela, K. S.; Dawe, L. N.; Thompson, D. W.; Bodwell, G. J. *Chem. Commun.* **2013**, *49*, 5930-5932.

Chapter 4

Synthesis and Applications Towards Selective Metal Ion Recognition by Calix[4]arene-NHC Derivatives

4.1 Introduction

As described in previous chapters, calix[*n*]arenes have been extensively studied as host molecules in supramolecular chemistry.¹ A great deal of attention has also been directed toward host-guest sensing by calix[*n*]arenes on solid surfaces.² Modification of either or both upper and lower rims allows suitably-functionalized calix[*n*]arenes to be anchored to various substrates and form highly-ordered self-assembled monolayers (SAMs) on solid surfaces.³ SAMs on gold (Au) have significant applications in sensing, drug delivery, microelectronics and surface protection.⁴ Since the first report⁵ of sulfur-based SAMs on gold surfaces, a great variety of applications has been reported. SAMs of thiols (and other sulfur-based head group-containing compounds such as thioacetates, dithiols and disulfides) on Au surfaces have shown a wide range of nanotechnological applications. In general, no suitable alternatives for these thiol-based ligands have been found, even though the thermal and oxidative instability of thiol-based SAMs on gold are significant limitations to their commercial use.⁶ Thiol-based SAMs are stable when stored in an ultra-high vacuum in the absence of light;⁷ degradation has been reported after 1–2 weeks at room temperature in air⁸ and more than 75% of surface thiols are lost by immersion in THF at room temperature for 24 h.⁹ By changes in the nature of the gold

surface, the use of longer-chain thiols, and the use of multidentate sulfur-based ligands, might be expected to yield improvements in stability.¹⁰

Recently, work on *N*-heterocyclic carbene (NHC)-based SAMs on gold surfaces has demonstrated that they exhibit considerably greater resistance to chemical reagents and heat than their thiol-based counterparts. The chemistry of NHCs has developed greatly during the past two decades and a brief introduction to NHCs is presented below.

4.2 *N*-Heterocyclic Carbenes (NHCs)

NHCs, also called “Arduengo”, or “persistent” carbenes, are the most stable types of carbenes. Carbenes are neutral molecules which contain divalent carbon atoms. A carbene has two unshared electrons which are highly reactive. The prototype is methylene (Figure 4.01a) and a schematic representation of a dialkyl carbene is shown in Figure 4.01b.¹¹

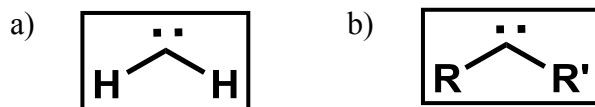


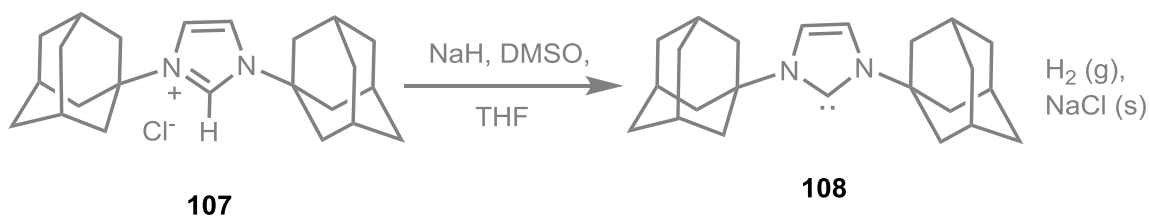
Figure 4.01 Schematic representation of carbenes.

Carbenes are classified into three different types, namely, Fischer, Schrock and persistent carbenes, and NHCs are derived from persistent carbenes. NHCs are stable carbenes which are flanked by two nitrogen atoms and are constrained within a ring (Figure 4.02).¹¹



Figure 4.02 Schematic representation of an NHC.

In the early 1960s the Ofele^{12a} and Wanzlick^{12b,c} groups first investigated the stability and reactivity of NHCs and also their applications as ligands. In 1991 Arduengo and co-workers^{12d} first reported a stable NHC which was flanked by two adamantyl groups and exhibited extraordinary stability and crystalline storability (Scheme 4.01). Due to their stability, NHCs can be readily prepared from commercially-available reagents on the gram scale, and can be stored for long periods and are also derivatizable. NHCs are most frequently prepared by deprotonation of the corresponding azolium salts (pK_a 21-24) with a strong base.¹³



Scheme 4.01 Synthesis of first stable NHC.

NHCs have shown a broad range of applications in different research areas such as in transition-metal catalysis, organocatalysis, drug development and in materials science.¹¹ These ligands have come to replace the well-known phosphorus-based ligands in organometallic and organic reactions. The use of NHCs in the field of material science is of growing interest e.g. for the preparation of light-emissive materials and the coating of

gold surfaces.¹⁴ NHCs have remarkable ability to form strong bonds with metal centers and those complexes show significant catalytic activity in different chemical transformations. Those transformations are olefin metathesis (e.g. Grubbs second-generation metathesis catalyst), carbon-carbon and carbon-nitrogen cross-coupling reactions, hydrosilylation and hydrogenation.^{11,14}

NHCs offer a combination of σ -bond-donating and moderate π back-bonding abilities which make them ligands of choice for transition metals such as Ru(II) and Au(I). The Au-NHC bond strength is estimated to be on the order of 90 kJ mol^{-1} which is stronger than a Au-phosphine bond and double that of Au-sulfur bonds.¹⁵ NHCs are therefore valuable ligands for the protection and functionalization of gold and other metal surfaces. Very few reports are available on studies of NHCs on gold surfaces and their reactivity and stabilization of gold nanoparticles.¹⁶ Some examples of NHCs on gold surfaces are described below.

4.2.1 N-Heterocyclic Carbenes (NHCs) on gold surfaces

Johnson and co-workers¹⁷ reported addressable NHC (ANHC) anchors for gold surfaces. The authors demonstrated the grafting of highly fluorinated polymers from surface-bound NHCs. The species formed by the immobilization of an NHC that contained an ancillary reactive metal alkylidene onto a Au surface can be used to initiate polymerization reactions from the surface. Based on DFT calculations they suggested that the homolytic Au-C bond dissociation energy (BDE) was 280 kJ mol^{-1} , which is 25 kJ mol^{-1} higher than a typical Au-S bond, and also the NHC-Au bond was highly localized

to a single Au atom. This was the first example of gold surface-functionalization with an NHC (Figure 4.03).

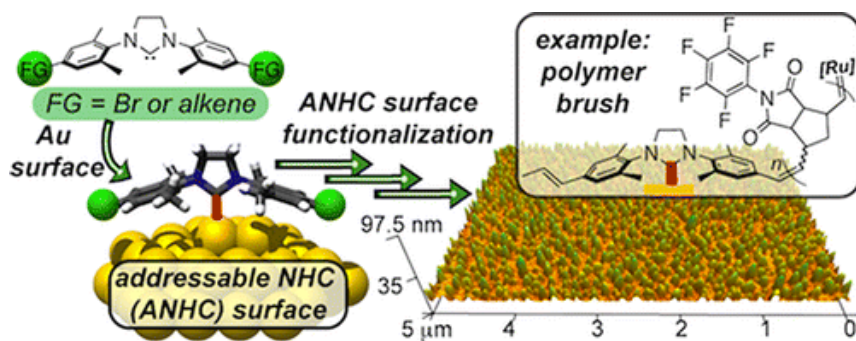


Figure 4.03 Functionalization of gold with ANHCs, reprinted with permission from ref 17.

Crudden and co-workers¹⁸ recently reported NHC-based SAMs on a gold surface. They demonstrated that these SAMs have greater resistance to chemical reagents and heat. The greater stability is due to the strength of the Au-C bond relative that of Au-S bonds and the different mode of bonding for carbon-based NHCs. Once NHCs are bound to the gold surface, they will not be displaced by thiols (or thioethers), and are also stable to high temperatures, pH changes, organic solvents, and electrochemical changes. The NHC ligands are stable and storable for long periods and NHCs can be easily generated from imidazolium precursors. Crudden demonstrated that the chemical derivatization of NHC-Au(111) surfaces could be employed to adjust the properties of NHC-based SAMs. The calculated bonding geometry and also an STM image of NHC on Au(111) surface is shown in Figure 4.04. DFT calculations indicate that the most-stable binding mode was one in which the NHC binds at ‘*atop*’ sites via a single gold-carbon bond (Figure 4.04a).

They reported the calculated bond strength of this bonding mode was 150 kJ mol^{-1} , approximately 25 kJ mol^{-1} stronger than the thiolate–Au bond.¹⁹

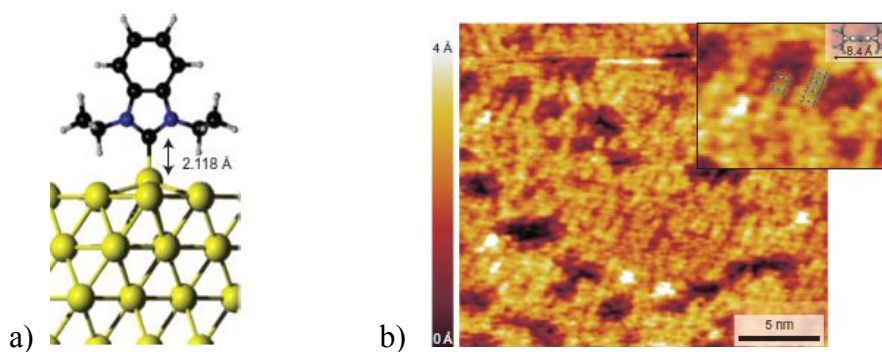


Figure 4.04 a) Bonding geometry of NHC on Au(III) surface. b) An STM image of SAMs of NHC on gold surface, reprinted with permission from ref 18.

Gold nanoparticles (AuNPs) have a wide range of applications in the field of biomedical sciences (imaging or drug delivery) and they are also used for catalytic applications.²⁰ For controlling the morphology of AuNPs, their stability and properties depend upon the nature of the coating agents. NHCs are strong σ -donor ligands which have been used as stabilizing agents for different metallic nanoparticles such as Au, Pd, Ru and Ir, etc.²⁰ NHC-coated AuNPs have been reported by various research groups.^{16,21} The shape, size-distribution and stability of these nanoparticles depend upon the structure of the NHC ligands and also upon the reaction conditions used.

Richeter and co-workers²² recently reported the reactivity of AuNPs towards NHCs generated *in situ* from a benzimidazolium salt which leads to the formation of bis-carbene Au(I) complexes. For interpretation of the reactivity of AuNPs toward NHCs they used

powder XRD and solid-state NMR techniques were used. Figure 4.05 shows the structures of the molecules and Au(I) complex that were used in Richeter's studies.

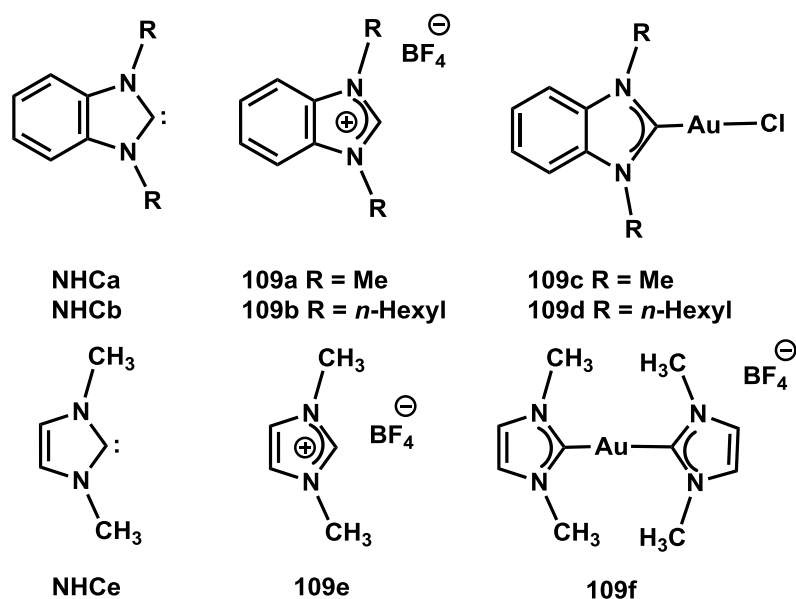
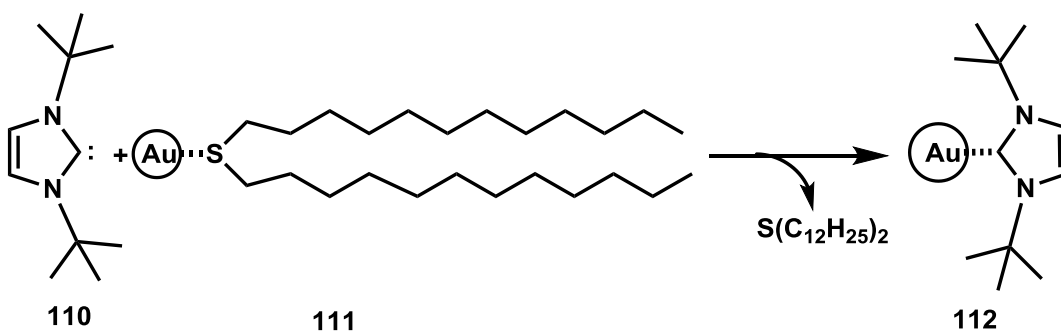


Figure 4.05 Structures of the molecules and Au(I) complexes studied by Richeter.

The NHC-coated AuNPs were synthesized either by reducing Au-NHC complexes or by replacing the ligands at the AuNPs surface by NHCs. Vignolle *et al.*²³ reported the synthesis of AuNPs by reduction of NHC-AuCl complexes. They demonstrated that the nature of the substituents on the NHC ligand was responsible for the control of the NP size. NPs with a diameter of ~ 2 nm were obtained when a bulky substituent was present on the NHC ligand, whereas NPs with a diameter of ~ 6-7 nm were formed when long alkyl chain substituents were attached to the NHC. High quality NPs were obtained with the use of 9-BBN as a reducing agent, which ultimately led to their self-assembly into 3D superlattices. Based on these studies, the authors reported that NHCs possess desirable properties as capping agents for AuNP stabilization.

Chechik, Fairlamb and co-workers^{16a} reported the preparation of NHC coated AuNPs by a ligand exchange reaction. These NPs were reported to have limited stability in solution. A spontaneous irreversible aggregation of nanoparticles leads to the formation of NHC-metal complexes. The synthesis of NHC-protected AuNPs is shown in Scheme 4.02. Bis-*tert*-butylimidazol-2-ylidene **110** was synthesized by the deprotonation of the corresponding imidazolium salt using KO^tBu as the base. The ligand **110** was then reacted with the thioether-protected AuNPs **111** to afford a NHC-protected AuNPs **112**. Carbene synthesis and ligand exchange reactions were carried out under inert atmosphere in a glove box. The authors suggested that in catalytic processes the NHC-coated nanoparticles will leach mononuclear NHC-metal complexes.



Scheme 4.02 Synthesis of NHC-protected AuNPs.

4.3 Objectives of the work reported in this Chapter

In order to test for metal ion selectivity with the sensing layers needed for the different microcantilevers (MCLs) envisioned in the multi-MCL instrument being designed by L.Y. Beaulieu's group at Memorial University, the newly designed

calix[4]arene-NHC derivative **113** (Figure 4.06) which incorporates a “crown-ether” component was undertaken.

In this Chapter the synthesis and applications toward selective metal ion recognition by calix[4]arene-NHC derivative **113** will be presented. The bimodal calix[4]arene **113** is functionalized with two different groups, one of which consists of a 1,3 bridged “crown-5” and the other 1,3 bridged “NHC” moiety. The resulting NHC enables the calix[4]arene **113** to form a stable self-assembled monolayer (SAM) onto the Au surface of a microcantilever. In addition to the solid Au surface study of this calix[4]arene **113**, work aimed at the synthesis of **113**-coated AuNPs was undertaken.

4.4 Results and discussion

Recent work on NHC-based SAMs on gold surfaces, their reactivity and their stabilization of AuNPs has demonstrated the greater stability of Au-C bonds relative to Au-sulfur bonds.¹⁵⁻¹⁸ In this project the synthesis of bimodal calix[4]arene-NHC derivative **113** (Figure 4.06) was targeted for its use in sensing layers on Au-coated microcantilevers (MCLs) and for selective binding of various metal ions. Also targeted were comparative studies with thioacetate-bearing calix[4]arene **72** (Page 87, Scheme 2.08) which forms a SAM on a Au-coated MCL.

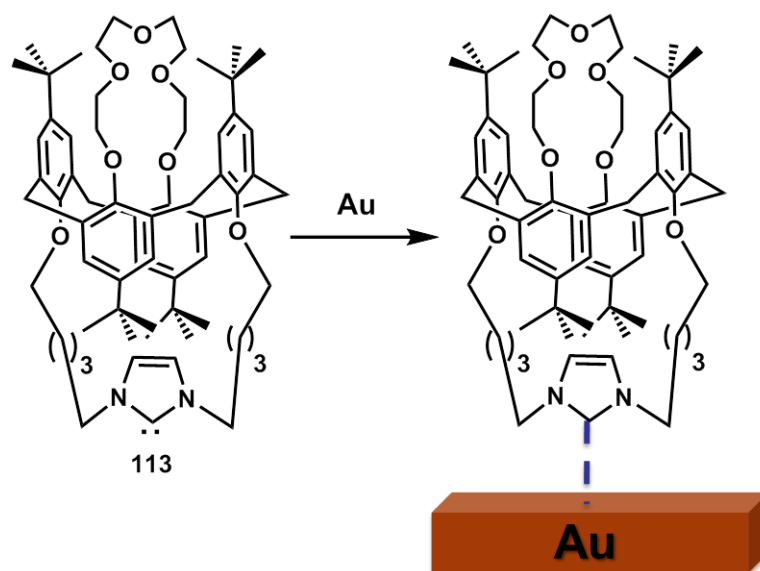
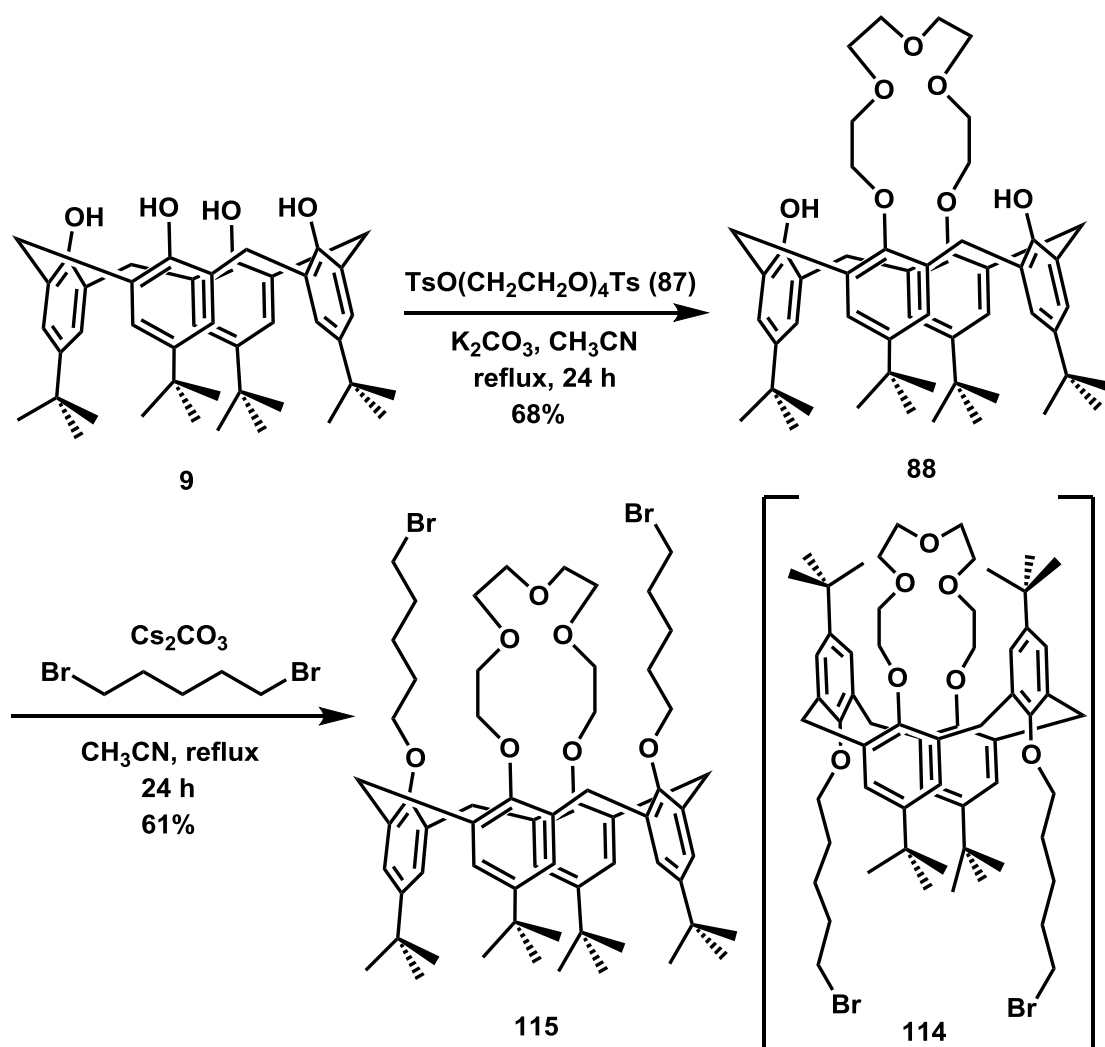


Figure 4.06 Structure of targeted new calix[4]arene-NHC derivative **113**.

4.4.1 Synthesis and applications towards a new bimodal calix[4]arene-NHC derivative **113**

The synthetic procedure for the required dibromo intermediate **115** which would lead to **113**, is outlined in Scheme 4.03. The synthetic strategy involves *p*-*tert*-butylcalix[4]arene **9** as the starting compound, which was synthesized from *p*-*tert*-butylphenol (**77**) according to the procedure of Gutsche *et al.*^{24a} A substitution reaction of calix[4]arene **9** with tetraethyleneglycol ditosylate **87** using K_2CO_3 as base in CH_3CN gave **88** in 68% yield.^{24b} The reaction of calix[4]arene **88** with 1,5-dibromopentane in the presence of K_2CO_3 in CH_3CN at reflux for 24 h provided the *cone*-conformer of dibromo intermediate **115** in 61% yield. From the published literature on transformations of bimodal calix[4]arenes^{24c} it was anticipated that formation of the *1,3-alternate* conformer **114** would result which would give the desired NHC **113**. However, the major product

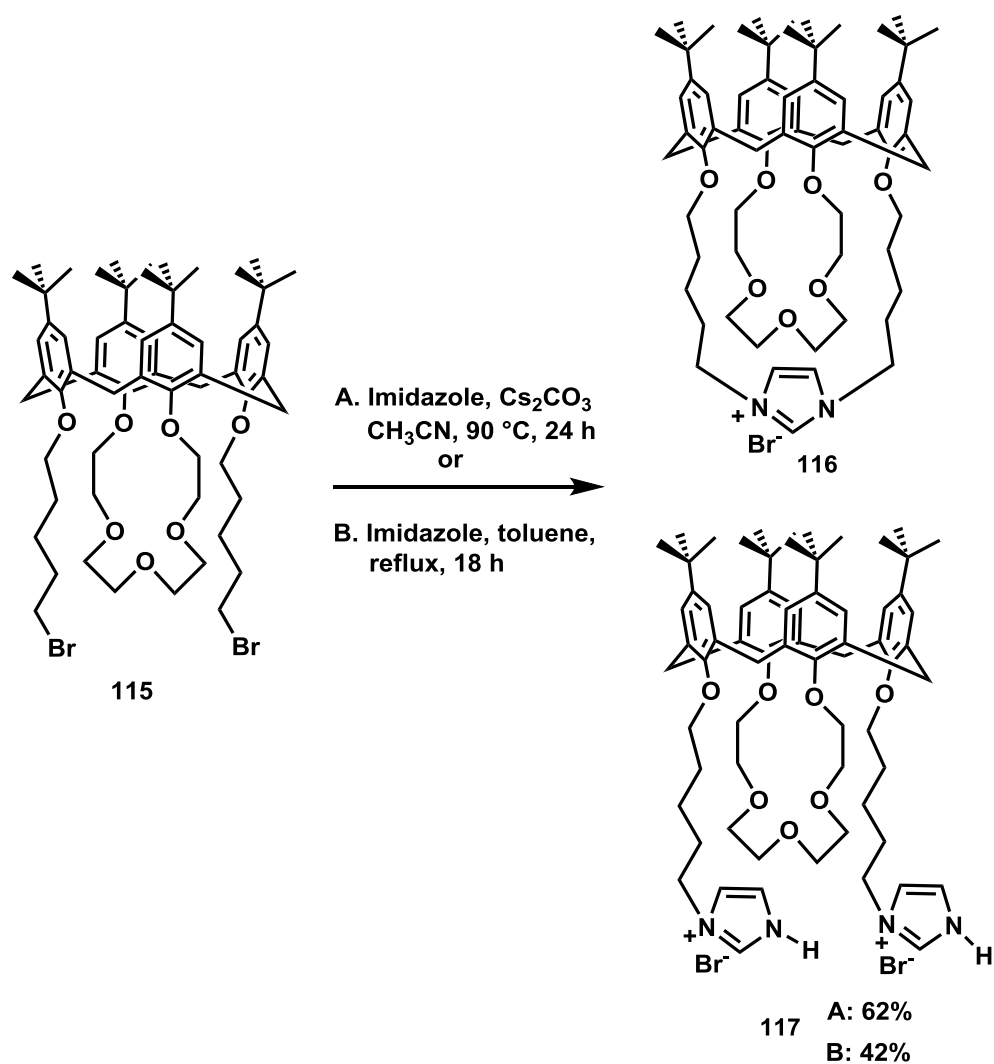
obtained from this transformation was instead found to be the corresponding *cone*-conformer **115**. The $^1\text{H-NMR}$ spectrum of **115** clearly indicated that the calix[4]arene unit is in a *cone* conformation since the proton chemical shifts of the bridging $-\text{CH}_2-$ groups appeared as a pair of AB doublets at δ 4.33 and 3.14 ppm ($J = 12.0$ Hz) and the corresponding ^{13}C chemical shift was observed at δ 34.0 ppm. The *tert*-butyl groups (36H) appear as two singlets at δ 1.34 and 0.80 ppm.



Scheme 4.03 Synthesis of dibromo intermediate **115**.

Nevertheless, the conversion of *cone*-conformer of dibromo intermediate **115** to the corresponding 1,3-bridged-imidazole compound **116** was attempted using the different procedures reported by Crudden *et al.*¹⁸ and Nigra *et al.*²⁵ Reaction of **115** with imidazole in the presence of Cs₂CO₃ in CH₃CN at 90 °C for 24 h afforded diimidazole derivative **117** in 62% yield. Alternatively, the reaction of **115** with imidazole in dry toluene at reflux for 18 h afforded **117** in 42% yield as outlined in Scheme 4.04. From the both procedures the desired 1,3-bridged imidazole **116** however, was not obtained.

The ¹H-NMR spectrum of **117** suggested that the calix[4]arene unit is in a *cone* conformation since the proton chemical shifts of the bridging -CH₂- groups appeared as a pair of AB doublets at δ 4.30 and 3.13 ppm ($J = 12.0$ Hz) and the corresponding ¹³C chemical shift was observed at δ 34.1 ppm. The *tert*-butyl groups (36H) appear as two singlets at δ 1.34 and 0.80 ppm.



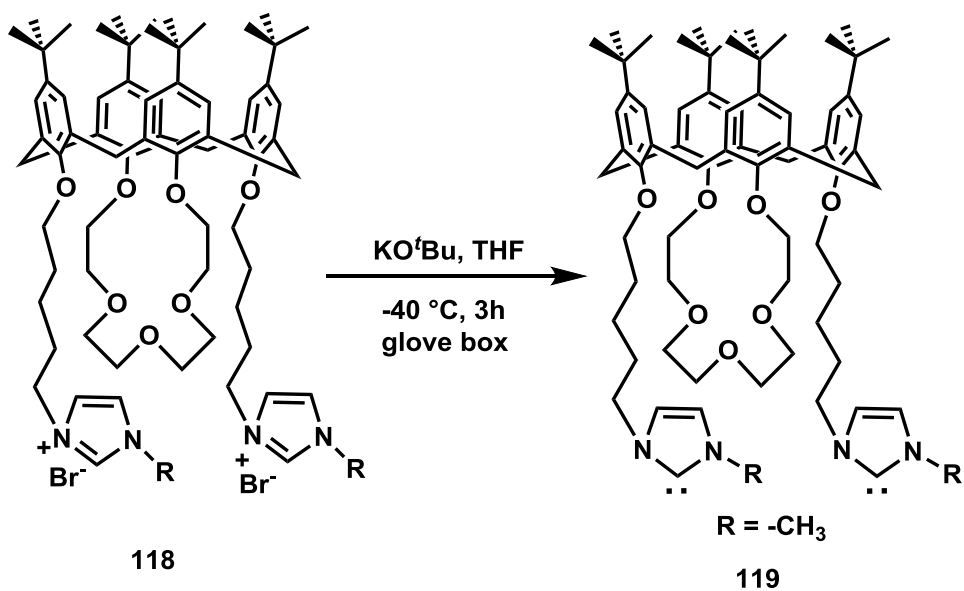
Scheme 4.04 Synthesis of imidazole compound **117**

4.4.1.1 Attempted generation of a dicarbene from calix[4]arene **117**

The generation of the carbene from the corresponding imidazole of **117** was conducted using Crudden's¹⁸ methodology. Generation of carbene was carried out under inert atmosphere conditions in glove box by using KO^tBu as base. In the case of **117**, the de-protonation occurs at N-H of the corresponding imidazolium salt since that bond has a pK_a of ~6 whereas that for the C-H is ~20. Consequently, it is not possible to generate a

carbene from **117** and instead, alkylation of NH groups is needed. *N*-alkyl or *N*-aryl protected imidazoles are therefore needed for the generation of the NHC carbenes functionality. Synthesis of the corresponding bis-*N*-methylimidazole calix[4]arene derivative **118** and the subsequent generation of the dicarbene **119** from **118** were still ongoing at the time of the writing of this thesis.

Fevre *et al*²⁶ reported the imidazolium hydrogen carbonates as alternative sources for generation of NHCs. The generation of NHCs from the imidazolium hydrogen carbonates according to Fevre's methodology is also currently ongoing in our laboratory.



Scheme 4.05 Proposed synthesis of calix[4]arene-NHC derivative **119**.

4.4.2 Preparation of Gold Nanoparticles (AuNPs)

As described earlier, AuNPs have a wide range of applications and there is interest in their size- and shape- dependent properties. AuNPs in particular have been stabilized by a variety of surfactants, polymers and dendrimers.²⁷ A major development in the area was the use of thiols as AuNPs stabilizers. Arduini *et al.*²⁸ reported the recognition of quaternary ammonium cations by calix[4]arene derivatives **120a** and **120b** supported on AuNPs (Figure 4.07). These derivatives supported on monolayer protected gold clusters (MPCs) show a remarkable binding efficiency towards quaternary ammonium salts in apolar solvents.

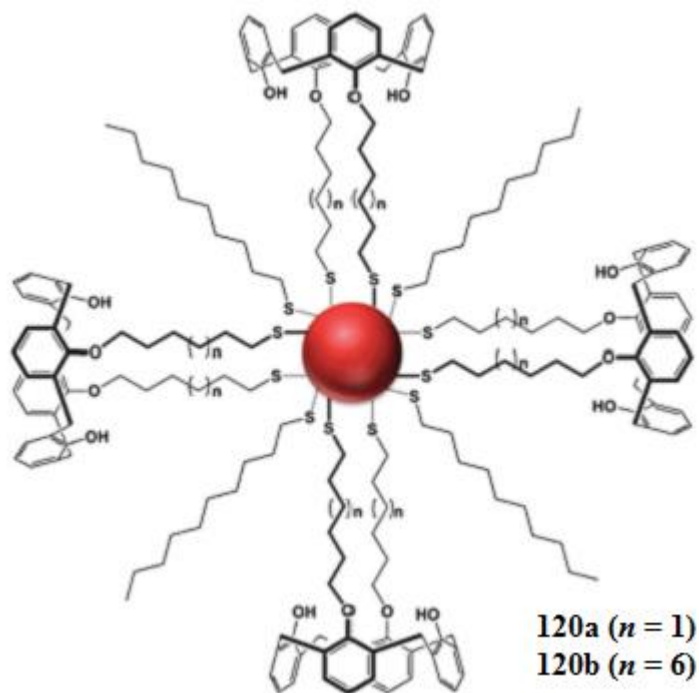


Figure 4.07 Schematic representation of gold MPCs functionalized with calix[4]arenes **120a** ($n = 1$) and **120b** ($n = 6$), reprinted with permission from ref 28.

Tshikhudo *et al.*²⁹ reported the molecular recognition by calix[4]arene **121a** modified AuNPs in aqueous solution. A schematic representation of calix[4]arene modified AuNPs is shown in Figure 4.08. The authors introduced a simple route for the preparation of water-soluble calix[4]arene functionalized gold MPCs. Citrate-stabilized gold nanoparticles were treated with a 2:1 mixture of the stabilizing ligand (1-sulfanylundec-11-yl) tetraethylene glycol **121b** and 25,27-bis(11-thio-1-oxyundecan)-26,28-dihydroxycalix[4]arene (**121c**) in a THF/water mixed solvent system to give the calix[4]arene **121a** modified AuNPs. The authors demonstrated that in an aqueous environment the modified calix[4]arene **121a** retains its molecular recognition properties.

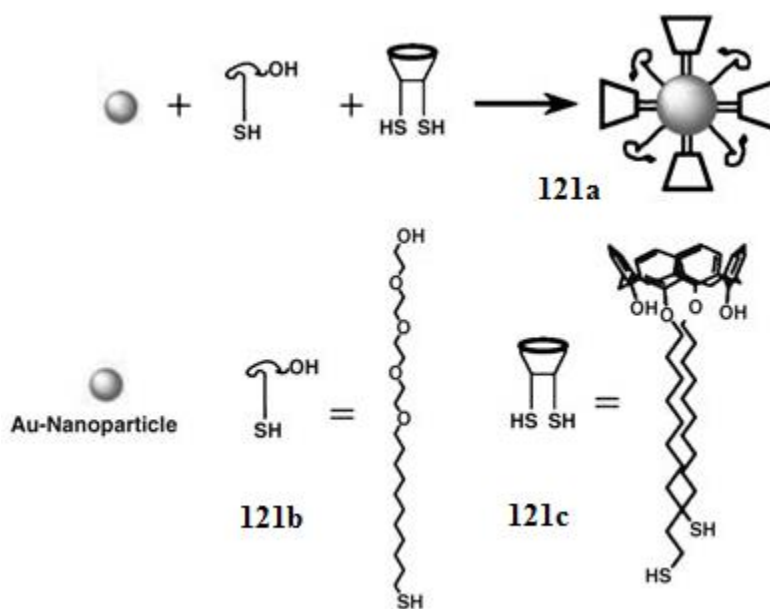
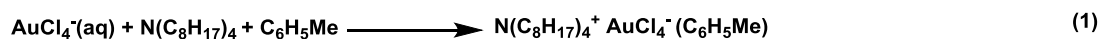


Figure 4.08 Schematic representation of the stabilization and functionalization of AuNPs with **121b** and **121c**, reprinted with permission from ref 29.

In the current project, based on Arduini's procedure²⁸ dodecanethiol stabilized MPCs were synthesized using the following molar ratios of reagents: $\text{HAuCl}_4 \cdot 3\text{H}_2\text{O}$: *n*-

$C_{12}H_{25}SH$: $(n-C_8H_{17})_4N^+Br^-$: $NaBH_4 = 1 : 3 : 3 : 20$. These AuNPs were grown in a two-phase system (liquid-liquid), in which the $AuCl_4^-$ was transferred from aqueous solution to organic solution (toluene) using tetraoctylammonium bromide as a phase-transfer catalyst and reduced with aqueous $NaBH_4$ in the presence of dodecanethiol ($C_{12}H_{25}SH$). Upon addition of the reducing agent, the colour of the organic phase changed from orange to deep brown within a few seconds. The overall reaction is summarized by Equations (1) and (2):



The reaction conditions determine the ratio of thiol to gold, *i.e.* the ratio n/m .

4.5 Conclusions

A new imidazole calix[4]arene derivative **117** has been synthesized and characterized. Since it is not possible to generate the carbenes from **117**, the synthesis of the corresponding *N*-methylimidazole calix[4]arene **118** and the attempts at the generation of dicarbene from the corresponding **118** remain to be conducted. An alternative approach for the synthesis of calix[4]arene **113** and the corresponding di-*tert*-butyl analogues are also currently ongoing in our laboratory.

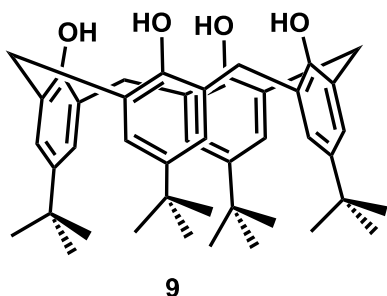
4.6 Experimental section

All reagents used for the synthesis of calix[4]arene derivatives **117** and reagents used in the preparation of AuNPs were purchased from Sigma-Aldrich or AlfaAesar and were used as supplied. 1H -NMR spectra were recorded at either 300 or 500 MHz, as noted, and

the ^{13}C -NMR spectra at 75.4 MHz as noted. Mass spectra were recorded using an APCI-LC/MSD Trap instrument.

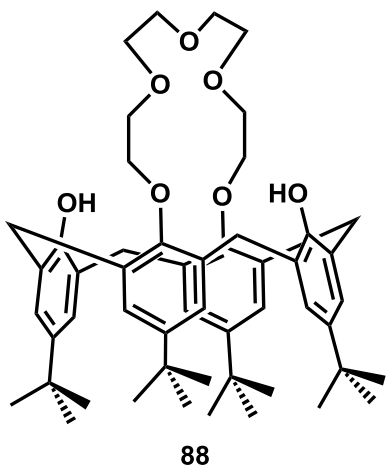
4.6.1 Experimental

5,11,17,23-Tetra-*tert*-butyl-25,26,27,28-tetrahydroxycalix[4]arene (**9**).



p-*tert*-Butylcalix[4]arene **9** was synthesized from *p*-*tert*-butylphenol **77** according to the procedure of Gutsche *et al.*^{24a}

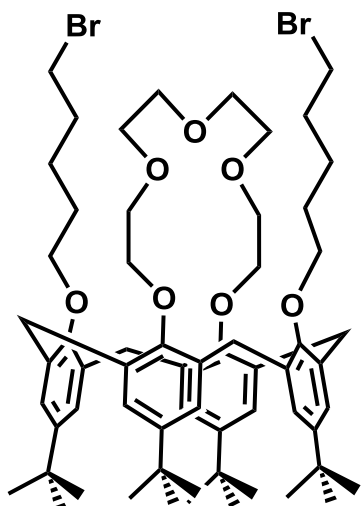
5,11,17,23-Tetra-*tert*-butyl-25,27-crown-[5]-ether-26,28-dihydroxycalix[4]arene (**88**).



A mixture of 5,11,17,23-tetra-*tert*-butyl-25,26,27,28-tetrahydroxycalix[4]arene (**9**) (1.01 g, 1.56 mmol) and K_2CO_3 (0.215 g, 1.56 mmol) in 25 mL of dry CH_3CN was heated at reflux under nitrogen for 1 h. A solution of tetraethyleneglycol ditosylate (0.942 g, 1.87 mmol) in 10 mL of dry CH_3CN was added dropwise and the mixture was refluxed for 48 h. Then, K_2CO_3 was removed by filtration. The residue was extracted with CH_2Cl_2 and water. The separated organic layer was dried over anhydrous MgSO_4 and the solvent was removed using a rotary evaporator. The residue was subjected to column chromatography (silica gel, 70:30 hexanes: ethyl acetate) to yield 5,11,17,23-tetra-*tert*-butyl-25,27-crown-[5]-ether-26,28-dihydroxycalix[4]arene (**88**) (0.85 g, 68%, m.p. 123.7-125.1 $^\circ\text{C}$) as a colourless solid.

$^1\text{H-NMR}$ (CDCl_3 , 300 MHz): $\delta = 7.16$ (s, 2H, ArOH), 7.07 (s, 4H, ArH), 6.74 (s, 4H, ArH), 4.37 (d, $J = 12.9$ Hz, 4H, ArCH₂), 4.07 (s, 8H, OCH₂), 3.97 (t, $J = 5.7$ Hz, 4H, OCH₂), 3.84 (t, $J = 5.7$ Hz, 4H, OCH₂), 3.29 (d, $J = 12.9$ Hz, 4H, ArCH₂), 1.31 (s, 18H, *t*-Bu), 0.91 (s, 18H, *t*-Bu). $^{13}\text{CNMR}$ (CDCl_3 , 75.4 MHz): $\delta = 150.8$, 149.8, 146.8, 141.2, 132.5, 127.8, 125.4, 124.9, 71.1, 70.9, 70.4, 33.9, 33.8, 31.7, 31.3, 31.0. APCI(+) MS (m/z): 807.1 [M+1]⁺.

5,11,17,23-Tetra-*tert*-butyl-25,27-crown-[5]-ether-26,28-bis(5-bromo-1-pentoxy)-calix[4]arene (115).

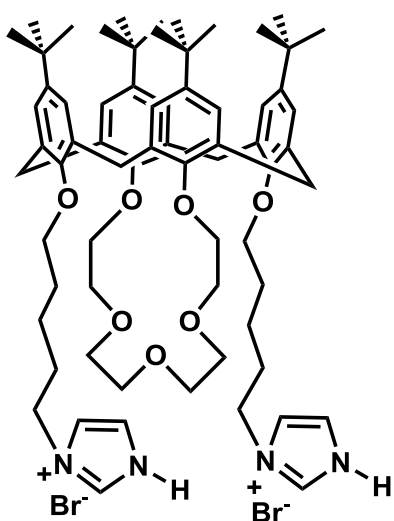


115

A mixture of 5,11,17,23-tetra-*tert*-butyl-25,27-crown-[5]-26,28-dihydroxycalix[4]arene (**88**) (0.25 g, 0.31 mmol), Cs₂CO₃ (0.40 g, 1.2 mmol) and 1,5-dibromopentane (0.16 mL, 1.2 mmol) in dry CH₃CN (15 mL) was heated at reflux under nitrogen for 24 h. After cooling to room temperature, the reaction mixture was neutralized with aqueous 1.0 M HCl and then extracted with ethyl acetate (3 × 50 mL), washed with water (2 × 50 mL). The separated organic layer was dried over anhydrous MgSO₄ and the solvent was removed using a rotary evaporator. The residue was subjected to column chromatography (silica gel, 75:25 hexanes: ethyl acetate) to yield 5,11,17,23-tetra-*tert*-butyl-25,27-crown-[5]-ether-26,28-bis(5-bromo-1-pentoxy)calix[4]arene (**115**) (0.21 g, 61%, m.p. 184.1-185.6 °C) as a colourless solid. $^1\text{HNMR}$ (CDCl_3 , 300 MHz): δ 7.12 (s, 4H, ArH), 6.43 (s, 4H, ArH), 4.35–4.16 (m, 12H, ArCH₂, –OCH₂), 3.81–3.71 (m, 12H, ArOCH₂, –OCH₂), 3.48 (t, $J = 6.0$ Hz, 4H, CH₂Br), 3.14 (d, $J = 12.0$ Hz, 4H, ArCH₂), 2.03–1.92 (m, 8H, –

CH₂CH₂CH₂-), 1.68–1.59 (m, 4H, -CH₂CH₂CH₂-), 1.34 (s, 18H, *t*-Bu), 0.80 (s, 18H, *t*-Bu). ¹³C-NMR (CDCl₃, 75.4 MHz): δ = 154.9, 152.2, 145.1, 144.1, 135.3, 131.6, 125.5, 124.5, 75.5, 72.5, 71.1, 70.4, 34.1, 33.6, 32.8, 31.7, 31.1, 30.9, 29.6, 25.0. APCI(+) MS (*m/z*): 1106.2 [M+1]⁺.

5,11,17,23-Tetra-*tert*-butyl-25,27-crown-[5]-ether-26,28-bis(1-[5-{3-imidazolium}]pentoxy)calix[4]arene (117).



117

To a suspension of imidazole (3.1 mg, 0.045 mmol) and Cs₂CO₃ (29.0 mg, 0.090 mmol) in CH₃CN (2.0 mL) was added 5,11,17,23-tetra-*tert*-butyl-25,27-crown-[5]-ether-26,28-bis(5-bromo-1-pentoxy)-calix[4]arene (**115**) (50.0 mg, 0.045) in CH₃CN (2mL). The reaction mixture was heated at reflux under nitrogen atmosphere for 24 h. After cooling to room temperature, the reaction mixture was evaporated in *vacuo* and the residual solid was triturated and sonicated in diethyl ether (2 × 5.0 mL), which was then decanted off. Subsequent drying under vacuum to yield 5,11,17,23-tetra-*tert*-butyl-25,27-crown-[5]-ether-26,28-bis(1-[5-{3-imidazolium}]pentoxy)calix[4]arene (**117**) (30.0 mg, 62%, m.p. 157.2-158.8 °C) as a colourless solid. ¹H-NMR (CDCl₃, 300 MHz): δ 7.49 (s, 2H), 7.12 (s, 4H, *ArH*), 7.06 (s, 2H), 6.93 (s, 2H), 6.43 (s, 4H, *ArH*), 4.33–4.20 (m, 12H, *ArCH*₂, -OCH₂), 4.00 (t, *J* = 6.0 Hz, 4H, CH₂N), 3.78–3.69 (m, 12H, *ArOCH*₂, -OCH₂), 3.13 (d, *J* = 12.0 Hz, 4H, *ArCH*₂), 2.01–1.83 (m, 8H, -CH₂CH₂CH₂-), 1.57–1.47 (m, 4H, -CH₂CH₂CH₂-), 1.34 (s, 18H, *t*-Bu), 0.80 (s, 18H, *t*-Bu). ¹³C-NMR (CDCl₃, 75.4 MHz): δ = 154.8, 152.1,

145.2, 144.2, 137.1, 135.2, 131.6, 129.5, 125.6, 124.5, 118.8, 75.3, 72.5, 72.2, 71.1, 70.3, 46.9, 34.1, 33.6, 31.7, 31.2, 31.1, 30.9, 29.9, 23.5. APCI(+) MS (m/z): 1081.2 $[M+1]^+$.

Preparation of gold nanoparticles stabilized with dodecanethiol.²⁸

An aqueous solution of hydrogen tetrachloroaurate (HAuCl_4) (0.21 g, 0.50 mmol) in 50 mL water was mixed with a solution of tetraoctyl ammonium bromide (0.82 g, 1.5 mmol) in 100 ml of toluene at room temperature. The two-phase mixture was stirred until the tetrachloroaurate was transferred into the organic layer. *n*-Dodecanethiol (0.31 g, 1.5 mmol) was then added to the organic layer and then 20 ml of an aqueous solution of NaBH_4 (0.41 g, 10 mmol) was added. After stirring for 3 h, the organic layer was separated and the solvent was evaporated under vacuum. Methanol (50 mL) was added to the residue and the mixture was kept for 2 h at $-20\text{ }^\circ\text{C}$. A dark precipitate of the nanoparticles formed this was filtered and washed with methanol ($2 \times 10\text{ mL}$) and the residue was dried under high vacuum and stored under argon at $-20\text{ }^\circ\text{C}$. For future work synthesis and applications of calix[4]arene **119** supported on AuNPs will be carried out in our laboratory.

4.7 References

1. Gutsche, C. D.; *Calixarenes an Introduction*, 2nd ed.; Royal Society of Chemistry: Cambridge, 2008.
2. Kim, H. J.; Lee, M. H.; Mutihac, L.; Vicens, J.; Kim, J. S. *Chem. Soc. Rev.* **2012**, *41*, 1173–1190.

3. (a) Zhang, S.; Echegoyen, L. *Tetrahedron Lett.* **2003**, *44*, 9079–9082. (b) Schemidtchen, F. P.; Berger, M. *Chem. Rev.* **1997**, *97*, 1609–1646. (c) Zhang, S.; Echegoyen, L. *Langmuir* **2006**, *22*, 10732–10738. (d) Cormode, D. P.; Evans, A. J.; Davis, J. J.; Beer, P. D. *Dalton Trans.* **2010**, *39*, 6532–6541.
4. (a) Gates, B. D.; Xu, Q.; Stewart, M.; Ryan, D.; Willson, C. G.; Whitesides, G. M. *Chem. Rev.* **2005**, *105*, 1171–1196. (b) Love, J. C.; Estroff, L. A.; Kriebel, J. K.; Nuzzo, R. G.; Whitesides, G. M. *Chem. Rev.* **2005**, *105*, 1103–1169. (c) Drechsler, U.; Erdogan, B.; Rotello, V. M. *Chem. Eur. J.* **2004**, *10*, 5570–5579.
5. Nuzzo, R. G.; Allara, D. L. *J. Am. Chem. Soc.* **1983**, *105*, 4481–4483.
6. (a) Leff, D. V.; Brandt, L.; Heath, J. R. *Langmuir* **1996**, *12*, 4723–4730. (b) Gittins, D. I.; Caruso, F. *Angew. Chem. Int. Ed.* **2001**, *40*, 3001–3004. (c) Vericat, C.; Vela, M. E.; Benitez, G.; Carro, P.; Salvarezza, R. C. *Chem. Soc. Rev.* **2010**, *39*, 1805–1834.
7. Noh, J.; Kato, H. S.; Kawai, M.; Hara, M. *J. Phys. Chem. B* **2006**, *110*, 2793–2797.
8. (a) Li, Y.; Huang, J.; McIver, R. T.; Hemminger, J. C. *J. Am. Chem. Soc.* **1992**, *114*, 2428–2432. (b) Schoenfish, M. H.; Pemberton, J. E. *J. Am. Chem. Soc.* **1998**, *120*, 4502–4513.
9. Schlenoff, J. B.; Li, M.; Ly, H. *J. Am. Chem. Soc.* **1995**, *117*, 12528–12536.

10. (a) Tam-Chan, S.-W.; Biebuyck, H. A.; Whitesides, G. M.; Jeon, N.; Nuzzo, R. G. *Langmuir* **1995**, *11*, 4371–4382. (b) Yang, G.; Amro, N. A.; Starkewolfe, A. B.; Liu, G.-Y. *Langmuir* **2004**, *20*, 3995–4003.
11. (a) Frémont, P. de.; Marion, N.; Nolan, S. P. *Coord. Chem. Rev.* **2009**, *253*, 862–892. (b) Hindi, K. M.; Panzner, M. J.; Tessier, C. A.; Cannon, C. L.; Youngs, W. *J. Chem. Rev.* **2009**, *109*, 3859–3884.
12. (a) Öfele, K. *J. Organomet. Chem.* **1968**, *12*, 42–43. (b) Wanzlick, H.-W. *Angew. Chem. Int. Ed.* **1962**, *1*, 75–80. c) Wanzlick, H.-W.; Schonherr, H.-J. *Angew. Chem. Int. Ed.* **1968**, *7*, 141–142. d) Arduengo III, A. J.; Harlow, R. L.; Kline, M. *J. Am. chem. Soc.* **1991**, *113*, 361–363.
13. Herrmann, W. A.; Kocher, C. *Angew. Chem. Int. Ed.* **1997**, *36*, 2162–2187.
14. a) Mercks, L.; Albrecht, M. *Chem. Soc. Rev.* **2010**, *39*, 1903–1912. b) Li, K.; Cheng, G.; Ma, C.; Guan, X.; Kwok, W.-M.; Chen, Y.; Lu, W.; Che, C.-M. *Chem. Sci.* **2013**, *4*, 2630–2644.
15. Pyykko, P.; Runeberg, N. *Chem. Asian J.* **2006**, *1*, 623–628.
16. (a) Hurst, E. C.; Wilson, K.; Fairlamb, I. J. S.; Chechik, V. *New J. Chem.* **2009**, *33*, 1837–1840. (b) Serpell, C. J.; Cookson, J.; Thompson, A. L.; Brown, C.M.; Beer, P. D. *Dalton Trans.* **2013**, *42*, 1385–1393. (c) Huang, R. T. W.; Wang, W. C.; Yang, R. Y.; Lu, J. T.; Lin, I. J. B. *Dalton Trans.* **2009**, *38*, 7121–7131. (d) Weidner, T. *Aust. J. Chem.* **2011**, *64*, 1177–1179.

17. Zhukhovitskiy, A. V.; Marvros, M. G.; Voorhis, T. V.; Johnson, J. A. *J. Am. Chem. Soc.* **2013**, *135*, 7418–7421.
18. Crudden, M. C.; Horton, H. J.; Ebralidze, I.; Zenkina, O. V.; McLean, A. B.; Drevniok, B.; She, Z.; Kraatz, H.-B.; Mosey, N. J. Seki, T.; Keske, E. C.; Leake, J. D.; Rousina-Webb, A.; Wu, G. *Nat. Chem.* **2014**, *6*, 409–414.
19. (a) Nuzzo, R. G.; Dubois, L. H.; Allara, D. L. *J. Am. Chem. Soc.* **1990**, *112*, 558–569. (b) Lavrich, D. J.; Wetterer, S. M.; Bernasek, S. L.; Scoles, G. *J. Phys. Chem. B* **1998**, *102*, 3456–3465.
20. (a) Lara, P.; Rivada-Wheelaghan, O.; Conejero, S.; Poteau, R.; Philippot, K.; Chaudret, B. *Angew. Chem. Int. Ed.* **2011**, *50*, 12080–12084. (b) Ranganath, K. V. S.; Kloesges, J.; Schafer, A. H.; Glorius, F. *Angew. Chem. Int. Ed.* **2010**, *49*, 7786–7789.
21. Ling, X.; Schaeffer, N.; Roland, S.; Pileni, M.-P. *Langmuir* **2013**, *29*, 12647–12656.
22. Rodriguez-Castillo, M.; Laurencin, D.; Tielens, F.; Lee, A. V.; Clement, S.; Guari, Y.; Richeter, S. *Dalton Trans.* **2014**, *43*, 5978–5982.
23. Vignolle, J.; Tilley, T. D. *Chem. Commun.* **2009**, 7230–7232.
24. (a) Gutsche, C. D.; Iqbal, M. *Org. Synth.* **1990**, *68*, 234–236. (b) Chailap, B.; Tuntulani, T. *Org. Biomol. Chem.* **2012**, *10*, 3617–3625.

25. Nigra, M. M.; Yeh, A. J.; Okrut, A.; Dipasquale, A. G.; Yeh, S. W.; Solovyov, A.; Katz, A. *Dalton Trans.* **2013**, *42*, 12762–12771.
26. Fevre, M.; Pinaud, J.; Leteneur, A.; Gnanou, Y.; Vignolle, J. *J. Am. Chem. Soc.* **2012**, *134*, 6776–6784.
27. (a) Shan, J.; Tenhu, H. *Chem. Commun.* **2007**, 4580–4598. (b) Kuo, C.-H.; Chiang, T.-F.; Chen, L.-J.; Huang, M. H. *Langmuir* **2004**, *20*, 7820–7824.
28. Arduini, A.; Demuru, D.; Pochini, A.; Secchi, A. *Chem. Commun.* **2005**, 645–647.
29. Tshikhudo, T. R.; Demuru, D.; Wang, Z.; Brust, M.; Secchi, A.; Arduini, A.; Pochini, A. *Angew. Chem. Int. Ed.* **2005**, *44*, 2913–2916.

Chapter 5

Synthesis and applications of sulfonated calix[4]naphthalene derivatives

5.1 Introduction

As highlighted previously in this thesis, calix[*n*]arenes are among the most extensively studied class of organic host molecules in supramolecular chemistry.¹ The lower and upper rims of calixarenes can be modified to produce a variety of derivatives, many of which have been used in molecular recognition studies.¹ Most of the calix[*n*]arenes however, are insoluble in water. Functionalization with polar groups such as sulfonate, carboxylate or phosphate groups, *etc.* can make them water soluble. Arduni *et al.*² reported the first water-soluble calix[4]arene by functionalization of the lower rim with carboxylate groups. Shinkai and co-workers³ synthesized *p*-sulfonatocalix[*n*]arenes, which are more water-soluble and form aqueous solution-state complexes with metal cations, organic cations and neutral molecules. The structures of *p*-sulfonatocalix[*n*]arenes (*n* = 4, 6) are shown in Figure 5.01. Since then, water-soluble *p*-sulfonatocalix[*n*]arenes have been shown to possess a wide range of biochemical properties⁴ and can form complexes with amino acids, active pharmaceutical ingredients, nucleobases, peptides and proteins.⁵

Atwood *et al.*⁶ have shown the activity of different *p*-sulfonatocalix[*n*]arenes as chloride channel blockers. Hwang *et al.*⁷ patented a method of treatment of infection by enveloped viruses such as influenza, HIV and herpes simplex with calix[*n*]arenes having sulfonate, carboxylate or phosphate polar groups. *p*-Sulfonatocalix[*n*]arenes and their

reported the first synthesis of *peri*-tetrasulfonatotetrahydroxy calix[4]naphthalene¹³ **124** (Figure 5.02) in 15% yield. These water soluble calix[4]naphthalene, however, failed to show any complexation properties although the study was rather limited.

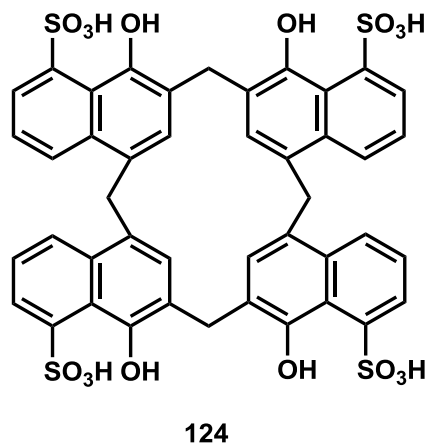


Figure 5.02 Structure of *peri*-tetrasulfonatotetrahydroxycalix[4]naphthalene **124**.

In 1989, Poh and coworkers¹⁴ first reported the highly water-soluble sulfonatocalix[4]naphthalene **125** which is known as cyclotetrachromotropanylene (–CTCTTM) (Figure 5.03). Similar to calix[*n*]arenes and **124** it has a hydrophobic cavity and the hydrophilic sulfonate groups which enables it to be highly water-soluble. Poh's group¹⁵ published several host-guest complexation studies using **125** with various guests such as metal cations, amino acids, polycyclic aromatic hydrocarbons, phenols, and alcohols. The structure of **125** however, was not unequivocally established by Poh's group, since other cyclic oligomers could also be consistent with the data they reported.

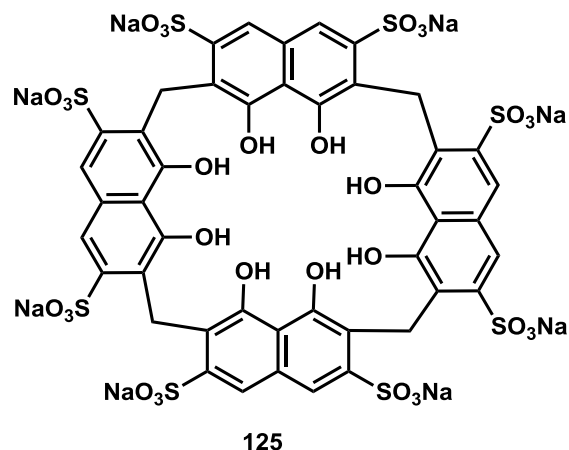


Figure 5.03 Structure of cyclotetrachromotropylene **125**.

Noble metal nanoparticles (NPs), especially of silver and gold, have attracted attention due to their remarkable chemical, optical, and electrical properties.¹⁶ A detailed description of silver nanoparticles and their applications are presented below. Since some of the research reported in this thesis incorporated NPs and dealt with single-walled carbon nanotubes. These will be briefly reviewed in later sections.

5.2 Silver nanoparticles and their applications

Nanoparticles (NPs) have a wide range of applications in medicine, catalysis, environmental remediation, cosmetics and biomedical devices, *etc.*¹⁷ These applications are due to the fact that nanometer-scale (i.e. NP) materials have significantly different properties when compared to the bulk material. Metallic nanoparticles show size- and shape-dependent properties, which are responsible for a variety of applications. Control over the size and shape of the nanoparticle is an important task. Many research groups have reported the synthesis of different nanoscale materials. A specific shape and size

distribution is achieved with different synthetic methods, reducing agents and stabilizers.¹⁷ Metallic nanoparticles can be prepared in two ways; one is by a chemical approach in which the metal ions in a solution are reduced using different conditions leading to the formation of nanoparticles. The other way is by a physical approach that includes several methods such as condensation, evaporation and laser ablation.¹⁸

Silver nanoparticles (AgNPs) have also attracted more interest in academic and industrial applications due to their unique biological, chemical and physical properties and also their ease of production and cost efficiency. These nanoparticles have a wide range of applications in catalysis, biosensors, biomolecular detection, diagnostics and photography, etc.¹⁹ AgNPs show antibacterial, anti-inflammatory and antitumor properties, and these materials have also been modified by using various macrocycles, including calixarenes, crown ethers and cyclodextrins, which are used as hosts in the molecular recognition of different substrates.²⁰ Several methods have been reported for the synthesis of AgNPs; for example, reduction of silver metal ions in solution, thermal decomposition of silver compounds, chemical and photoreduction in reverse micelles and recently, bio- or green synthesis. The most commonly used method to synthesize stable and different-shaped nanoparticles in water is by the chemical reduction of silver metal salts. Commonly employed reducing agents include sodium borohydride, hydrazine, ascorbic acid, ammonium formate and hydroxylamine hydrochloride. A biosynthetic method as an alternative approach for the synthesis of some nanoparticles employs either biological microorganisms such as yeast, bacteria, fungi or some plant extracts.^{19c} Characterization of nanoparticles is very important to understand and control nanoparticle

synthesis and their potential applications. Different techniques which can be used for characterization include transmission electron microscopy (TEM), scanning electron microscopy (SEM), atomic force microscopy (AFM), X-ray photoelectron spectroscopy (XPS), Fourier transform infrared spectroscopy (FTIR), powder X-ray diffractometry (XRD), dynamic light scattering (DLS) and UV-vis spectroscopy. These techniques can be used to determine the different parameters such as shape, particle size, crystallinity, pore size and surface area.^{18,20,21}

Li's^{19b} group demonstrated the application of *p*-sulfonatocalix[*n*]arene-capped noble metal nanoparticles. Li and Xiong²² also reported the molecular recognition of water-soluble *p*-sulfonatocalix[4]arene-modified AgNPs towards several pesticides such as iprodione, thiabendazole, acetamiprid, optunal and methomyl in aqueous solutions. Based on TEM images, the modified silver nanoparticles are highly dispersed and uniform in aqueous solution (approx. diameter is 8.0 nm). After the addition of pesticides to the modified AgNP solutions, a color change from yellow to red can be observed, as well as increases in the absorbance for the reaction of the pesticide optunal with *p*-sulfonatocalix[4]arene-modified AgNPs (Figure 5.04). The *p*-sulfonatocalix[4]arene binds to the aromatic and amino groups of optunal by non-covalent interactions such as π - π interactions, cation- π interactions or electrostatic forces. Li and Xiong reported that *p*-sulfonatocalix[4]arene-modified AgNPs could therefore be used as a colorimetric sensor for optunal.

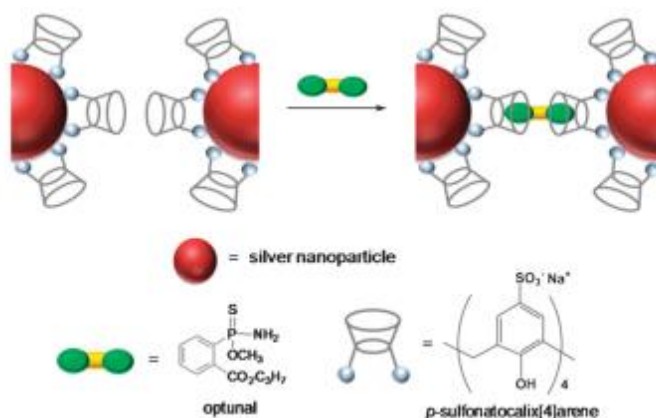


Figure 5.04 Schematic representation of the optunal-induced aggregation of *p*-sulfonatocalix[4]arene modified AgNPs, reprinted with permission from ref 20.

Coleman's group²³ later reported the selective complexation of nucleotides and nucleosides, and also the complexation of active pharmaceutical ingredients, micellar behaviour and serum albumins using *p*-sulfonatocalix[4]arene-capped silver nanoparticles.

5.3 Single-walled carbon nanotubes (SWNTs)

In 1991 S. Iijima discovered carbon nanotubes (CNTs) as a new allotrope of carbon.²⁴ Since then, research in this field has exploded. In the last two decades CNTs have been reported in a wide range of applications in medicinal chemistry and in materials science.²⁵ CNTs are helical tubular-shaped carbon nanomaterials and which were initially observed as a byproduct of fullerene synthesis. These nanotubes consist of graphene sheets which are rolled up into tubes (cylindrical shape), and the lengths of these CNTs are measured in micrometers, and with diameters up to 100 nm. Depending on the extent of layer formation, CNTs can be named as either single-walled carbon

nanotubes (SWNTs), double-walled CNTs, or multi-walled carbon nanotubes (MWNTs), examples of which are shown in Figure 5.05.²⁵

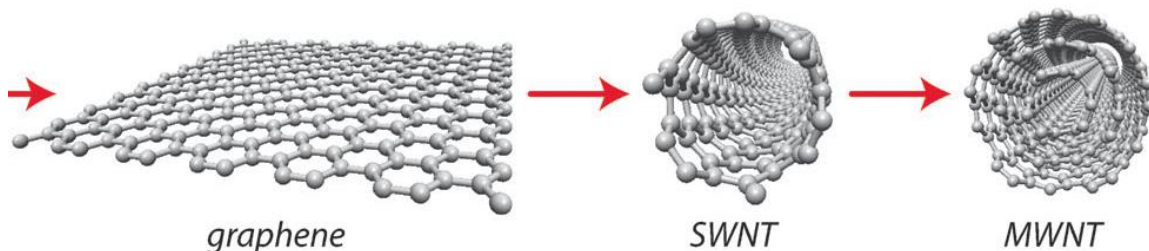


Figure 5.05 Schematic representation of SWNTs and MWNTs, reprinted with permission from ref 25f.

In particular, due to their unique physical and chemical properties²⁶ SWNTs have gained much interest from researchers over the past two decades. Many research groups have reported a wide range of applications using suspensions of these nanotubes in organic or aqueous media.²⁶ SWNTs can be considered as nanowires with exceptional electrical, thermal, mechanical and electronic properties. The structure of these nanotubes can be characterized by the angles in which a “graphene” sheet is rolled up. The various types of SWNTs are referred to as “zigzag”, “armchair” and “chiral” nanotubes, which are defined based on the chiral vector (C_h) of the graphene lattice (Figure 5.06). The side-walls of SWNTs have hexagonal networks of carbon atoms with sp^2 hybridization and their end-caps contain hexagonal, as well as pentagonal carbon networks.²⁵ Based on the arrangements of the hexagon rings on the outer surface, the carbon nanotubes are categorized as either “metallic” or “semiconducting”. SWNTs can interact with one another to form strong bundles with highly complex architectures in the solid state, and

due to this reason, it is very difficult to dissolve/disperse them in organic or aqueous solvents. Lack of solubility is a great limitation toward the application of nanotubes and to overcome this barrier, various chemical functionalization methods have been developed. In order to improve the poor solubility of SWNTs, the most powerful approaches are covalent and noncovalent modifications. The covalent functionalization approach involves the attachment of various functional groups onto the conjugated surface of the nanotubes by chemical reactions.

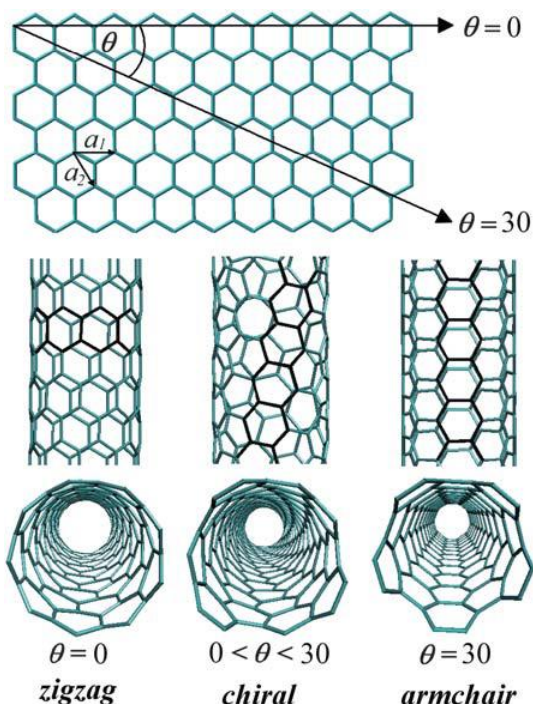


Figure 5.06 Schematic representation of three different types of SWNTs based on the angle of chiral vector of graphene lattice, reprinted with permission from ref 25g.

Many methods have been reported for producing carbon nanotubes. Some commercially available SWNTs are actually named after their methods of formation; examples are CoMoCAT (cobalt-molybdenum-catalyzed) and HiPCO (high pressure CO

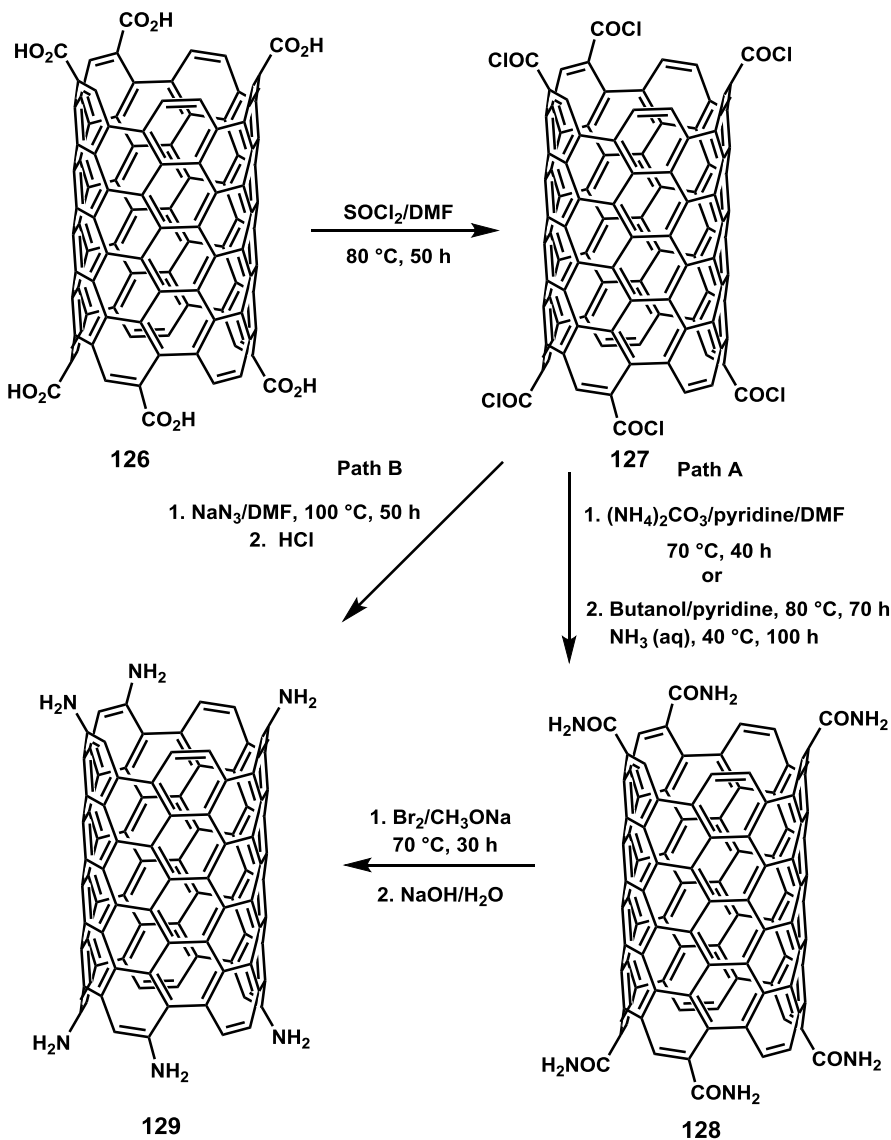
disproportionation) nanotubes. These nanotubes have been used in different areas of research, for example, gas storage, biosensors, fibers, organic solar cells, medicinal chemistry, solar energy conversion, conductive textiles, selective recognition of chemical substances.^{25,26,27} However the preparation of SWNTs with specific length, chirality and other parameters is still a challenge. Several research groups are working on the synthesis of structurally-uniform SWNTs.^{28, 29}

5.3.1 Covalent functionalization of SWNTs.

Chemical functionalization of SWNTs, especially side-wall functionalization is known to provide species which show different applications and increased solubility of the carbon nanotubes,³⁰ but also alter their electronic properties.³¹ In contrast to the side-wall chemistry of SWNTs, the chemistry at the open ends has been limited to various substitution reactions on carboxylic acid groups. Among the various reaction conditions, oxidation (in nitric acid)³² is one of the most widely-studied methods for SWNT functionalization, which can be induced at the tips or at defects in the nanotube side-walls to generate the carboxylic acid groups. By varying the limited functional groups, the properties of covalently functionalized SWNTs can be greatly altered.

Gromov *et al.*³³ reported the multi-step synthesis of the covalent amino-functionalized SWNT **129**. The authors performed the chemical transformation of SWNTs, edge-terminated with carboxylic groups to amino groups directly attached to the tube open ends. For the synthesis of amino-SWNT **129**, two different reaction paths were used, as shown in Scheme 5.01. The first path involves the Hofmann rearrangement of amides (Path A), whereas the second path involves the Curtius reaction of the carboxylic

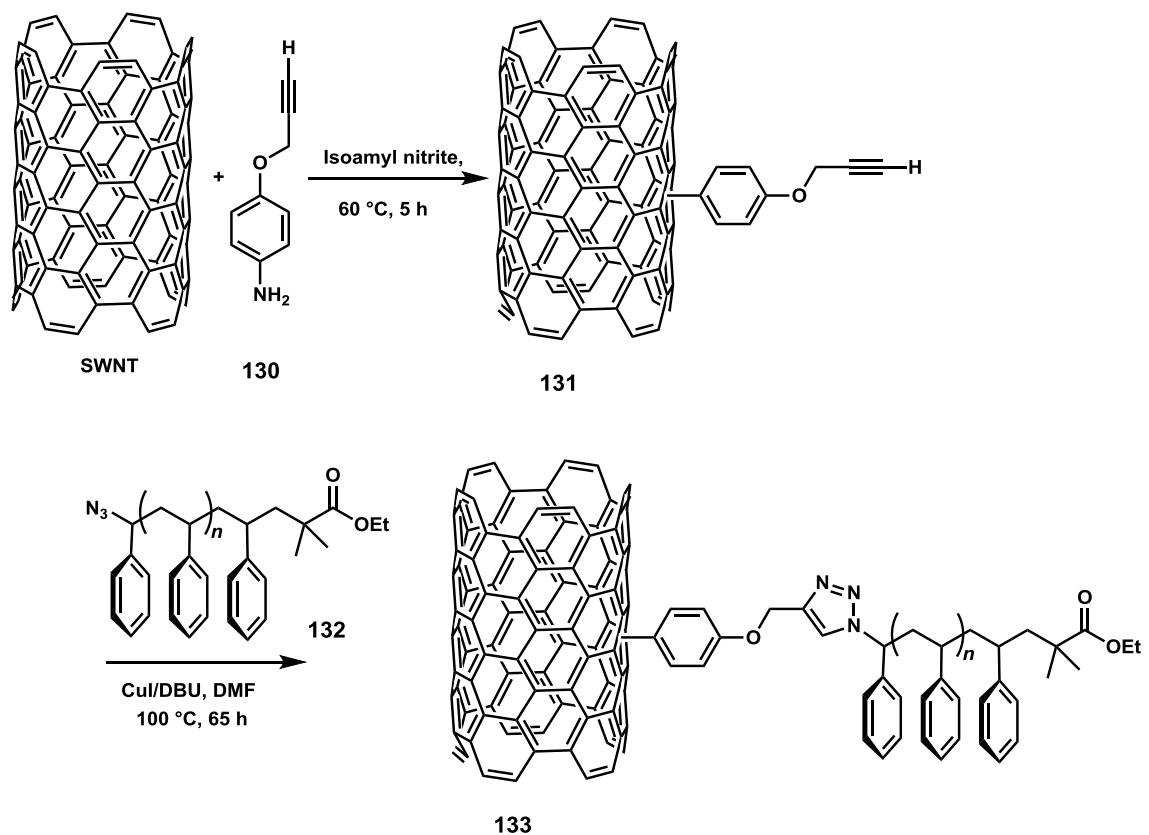
acid chlorides with sodium azide (Path B). This is the first reported application of the Hofmann rearrangement of amides and Curtius rearrangement of carboxylic acid azides in carbon nanotube chemistry.



Scheme 5.01 Synthesis of amino-functionalized SWNT **129**.

Adronov's group³⁴ reported the covalent functionalization of SWNTs with polystyrene **133** using the Cu(I)-catalyzed [3+2] Huisgen cycloaddition (–Click

chemistry” or CuAAC reaction) between alkyne-functionalized SWNTs e.g. **131** and azido-polystyrenes e.g. **132** as shown in Scheme 5.02. The resulting polystyrene functionalized SWNTs **133** exhibited high solubility in organic solvents such as THF, CHCl₃ and CH₂Cl₂.



Scheme 5.02 Synthesis of polystyrene-functionalized SWNT **133**.

Palacin *et al.*³⁵ reported the novel synthesis of two SWNTs functionalized with zinc porphyrin electron donor-acceptor conjugates **134** and **135** (Figure 5.07). The authors demonstrated that “click chemistry” is an efficient reaction for SWNT functionalization and very mild conditions were applied between alkyne-functionalized SWNTs and the

zinc porphyrin azide counterparts. SWNTs-Zn-P^{'''} conjugates **134** and **135** were found to have good solubility in organic solvents. Based on steady-state and time-resolved spectroscopic measurements the formation of reduced SWNT and oxidized Zn-P^{'''} species after photoexcitation were revealed.

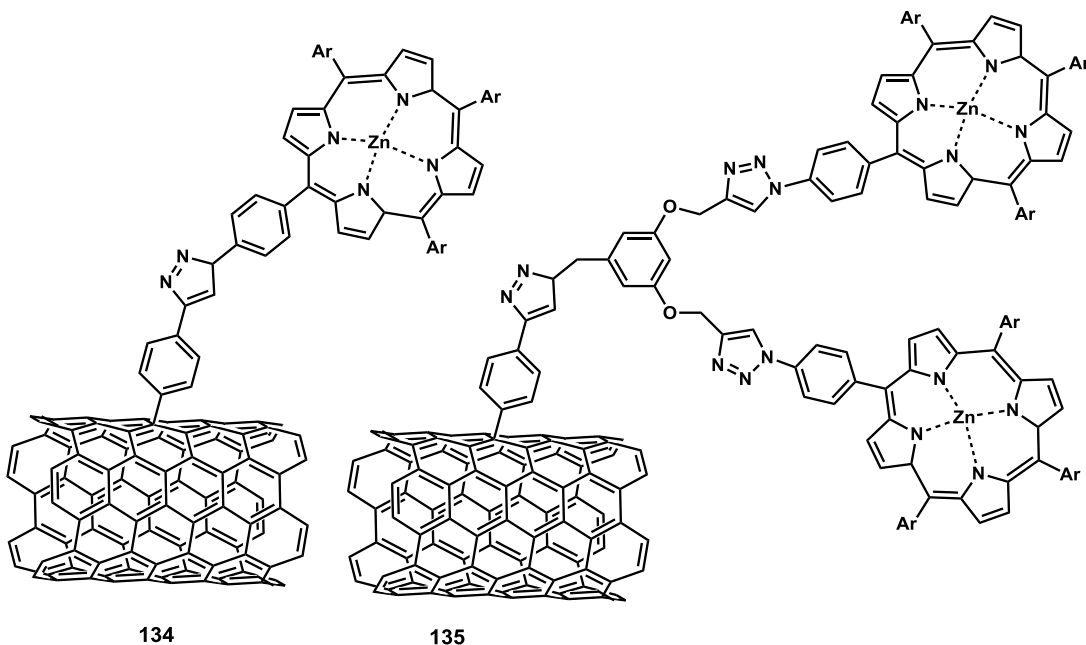


Figure 5.07 Structures of SWNTs functionalized with zinc-porphyrin conjugates **134** and **135**.

Although covalent functionalization of SWNTs is an effective approach for dispersing nanotube bundles, it has some disadvantages. In this approach, the chemical reactions occur on the surfaces of the nanotubes and can cause structural damage, thereby affecting their optical and electronic properties.³⁶ On the other hand, a noncovalent functionalization approach has advantages over the covalent approach since it does not require any chemical reactions to be performed on the surface of the nanotube. A description of noncovalent functionalization of SWNTs is presented below.

5.3.2 Noncovalent functionalization of SWNTs.

Among the various methods which have been reported, noncovalent functionalization of SWNTs with a suitable dispersant is an appealing approach to overcome solubility difficulties. Usually, in the noncovalent approach, the SWNTs can be functionalized through surface binding of macromolecule-based dispersants such as surfactants,^{37a} DNA,^{37b} polymers,^{38a-b} and the adhesion of small molecules^{38c-d} can be used to improve the solubility of SWNTs in various solvents. This approach involves noncovalent adsorption, or wrapping, of different molecules on the surface of the nanotubes by supramolecular forces such as π - π interactions and van der Waals forces, *etc.*²⁵

Moore and Zang *et al.*³⁹ reported the noncovalent functionalization of SWNTs using oligo(*m*-phenyleneethynylene)s (named “*m*PE-13mers”) as shown in Figure 5.08. These oligomers exist in a flexible, unfolded conformation in nonpolar solvents, which causes association between the surface of the oligomers and the SWNTs via intermolecular π - π interactions, resulting in the dispersion of the nanotubes. By increasing the polarity of the solution by the addition of acetonitrile, the oligomers are forced to fold into rigid helical structures, due to the conformational changes in the oligomers which disrupts the surface π - π stacking with the SWNTs. As a result, the oligomers dissociate from the nanotubes and dissolve back into the solution. The authors concluded that these foldable oligomers can be used for the purification of SWNTs.

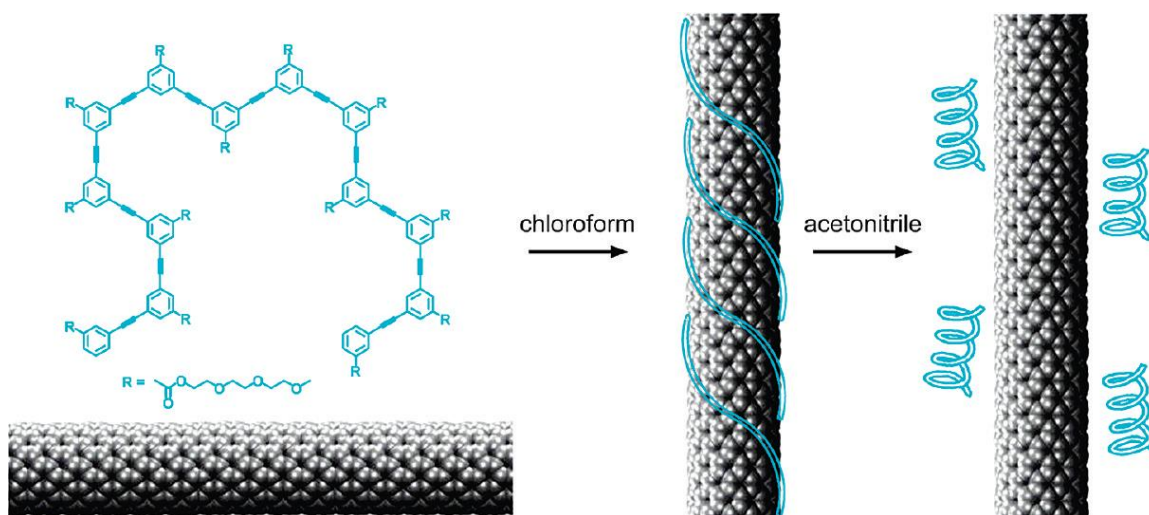


Figure 5.08 Solution process for dispersion and release of SWNTs by *mPE-13*, reprinted with permission from ref 39.

Zhao's group⁴⁰ reported that a tetrathiafulvalene (TTFV)-phenylacetylene folding polymer **136** exhibited the property of reversibly dispersing and releasing SWNTs in organic solvents under the control of redox or pH stimuli (Figure 5.09). The authors demonstrated that the wrapping mode facilitates the interaction between TTFV-polymer **136** and SWNTs leads to the dispersion of individual small-diameter tubes, while the adhesion mode works for large-diameter tubes and produces TTFV-polymer/SWNTs sol-gels. Since the TTFV unit is known to be able to undergo *cis-to-trans* structural changes, the switching behavior of TTFV has therefore been utilized to allow for controllable dispersion and releasing of SWNTs in solution.

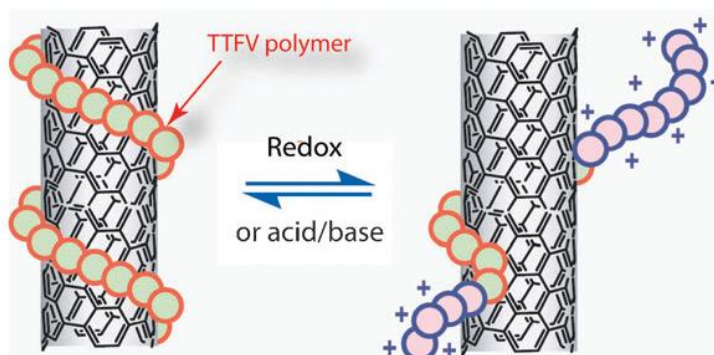
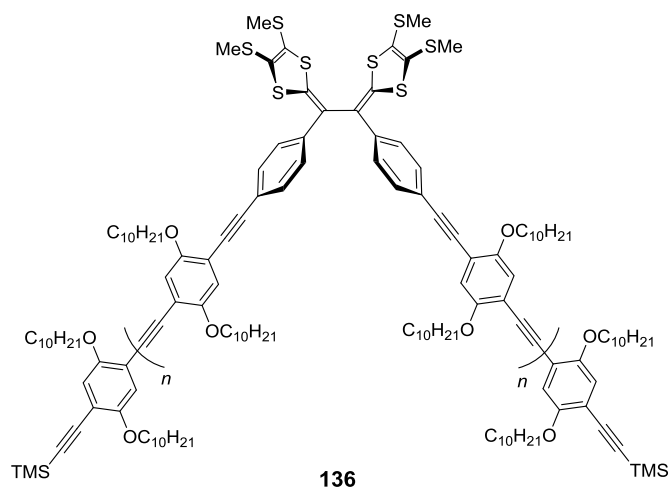


Figure 5.09 *Top*: Molecular structure of polymer **136**. *Bottom*: Reversible wrapping and unwrapping of SWNTs by a TTFV polymer, reprinted with permission from ref. 40.

Smalley and coworkers⁴¹ reported a detailed study on the application of various surfactants toward the dispersion of HiPCO^{41b} SWNTs into water. The surfactants examined included sodium alkyl allylsulfosuccinate, sodium dodecyl sulfonate (SDS), sodium dodecylbenzene sulfonate (SDBS), and the sodium salt of polystyrenesulfonate (PSS). Tummala *et al.*⁴² conducted several studies elaborating upon the use of SDS for dispersing SWNTs into aqueous solutions. The presence of planar aromatic cyclic structures (*e.g.* flavin mononucleotide) however has also been presumed to be an

essential component for the observed dispersive effectiveness of SWNTs. Recently Martin and Guldi and co-workers⁴³ used the planar aromatic 11,11,12,12-tetracyano-9,10-anthraquinodimethane (TCAQ) derivatized onto a water-soluble dendron to solubilize SWCNTs in water.

Application of SWNTs in electronic devices requires their separation based on diameter and chirality.^{44a} The usage of nanotubes in composites and therapeutics also requires homogeneous dispersions in organic, aqueous and cellular environments.^{44b,c} Hence, research on separating and dispersing SWNTs continues to attract the interest of the scientific community. Various research groups have reported the application of different surfactants capable of dispersing SWNTs in organic and aqueous media.^{25, 26}

5.4 Objectives of the work reported in this Chapter

In this Chapter the focus is on the synthesis and applications of some sulfonated calix[4]naphthalene derivatives. The three calix[4]naphthalenes that were synthesized and studied were *peri*-sulfonatocalix[4]naphthalene **124**, diacetoxyoxa calix[4]naphthalenesultone **137** and cyclotetrachromotrolylene **125**. In a collaborative project with Anthony Coleman's group at the University of Lyon, these naphthalene derivatives were shown to be capable of capping and stabilizing silver nanoparticles and also to possess molecular recognition properties with nucleobases and certain amino acids. Along with these properties, cyclotetrachromotrolylene **125** which was first reported by Poh and co-workers was also characterized using ¹H-NMR diffusion coefficient measurements with the assistance of Dr. Celine Schneider at MUN. The water-soluble **125** was shown to be capable of selectively dispersing SWNTs into the

aqueous phase. The resulting supramolecular complexes, in a collaborative project with Zhao's group at Memorial University and Adronov's group at McMaster University, were characterized by UV-Vis-NIR analysis. The dried aggregates were examined by Atomic Force Microscopy (AFM) and Raman spectroscopy. The results of these projects highlighted the diverse properties of these calix[4]naphthalenes. The major results obtained from this work have been published in **2014** in the journals *RSC Advances* and *Supramolecular Chemistry*.⁴⁵

5.5 Results and discussion

In order to investigate the supramolecular complexation properties of sulfonated calix[4]naphthalenes, these three derivatives **124**, **125** and **137** (Figure 5.10) were synthesized. As described previously, these supramolecular hosts have deeper, wider and electron-rich cavities as compared to the "classical" calix[4]arenes. As documented earlier also the water-soluble *p*-sulfonatocalix[*n*]arenes are known to possess a wide range of biological properties and also show a variety of applications in molecular recognition studies using calix[4]arene capped silver nanoparticles. Based on these studies, the current investigations were performed using three sulfonated calix[4]naphthalene-capped silver nanoparticles. The synthesis and applications of these sulfonated calix[4]naphthalenes are described in the following sections.

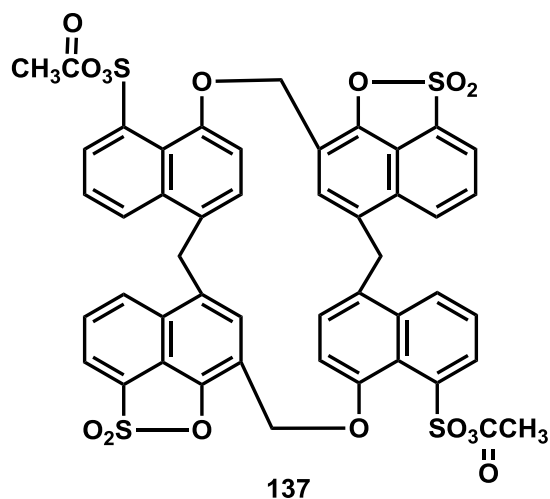
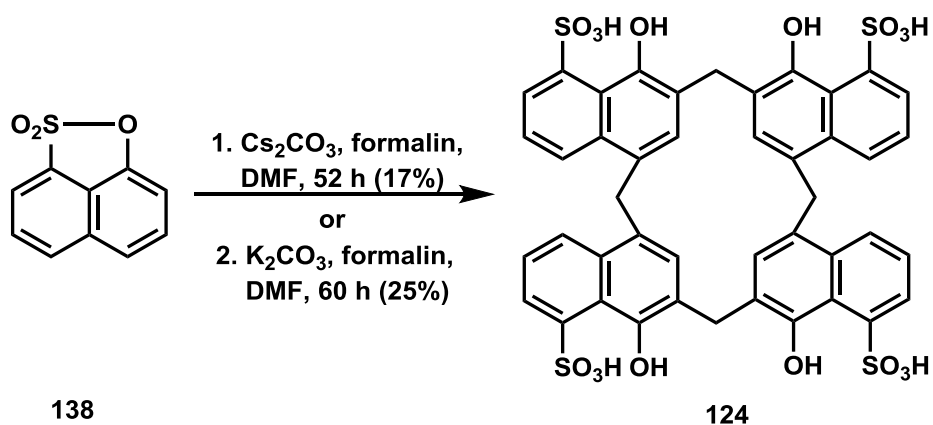


Figure 5.10 Structure of oxacalix[4]naphthalenesultone **137**.

5.5.1 Synthesis of sulfonated calix[4]naphthalene derivatives **124**, **125** and **137**.

The synthesis of *peri*-sulfonatocalix[4]naphthalene **124** is outlined in Scheme 5.03.¹³ Commercially available 1,8-naphthalenesultone (**138**) was used as the precursor compound for cyclooligomerization with formaldehyde. Sultone **138** contains a masked sulfonic acid group, as it is an internal ester of the corresponding 8-hydroxy-1-naphthalenesulfonic acid. Since the five-membered ring is fused at *peri* positions of the naphthalene ring, it is a strained molecule and has some unique chemical properties.⁴⁶ Heating **138** at reflux with Cs₂CO₃ and formalin in DMF for 52 h, followed by acidification and crystallization, affords the cyclic tetramer **124** in 17% yield, following the procedure via a “*hemicalix*[*n*]arene” type pathway previously reported by Georghiou’s group.^{1,13} When K₂CO₃ was used as base instead with the same conditions, **124** was obtained in better, (25%) yield. When **138** was reacted with Cs₂CO₃ and formalin in DMF under microwave heating conditions at 175 °C for 7 h, the reaction only

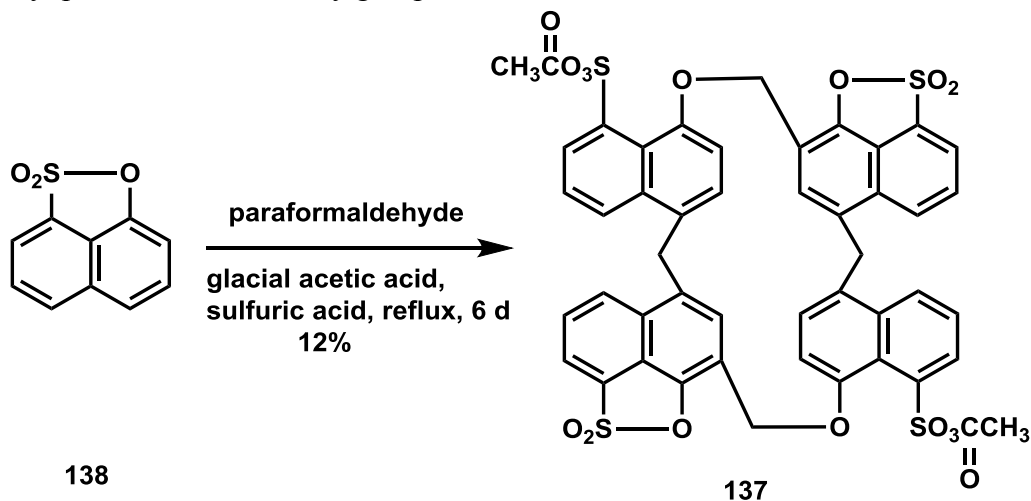
afforded very low (4%) yields. The tetrameric compound **124** was characterized by ^1H and ^{13}C NMR spectroscopy. The ^1H -NMR spectrum shows two sharp singlets at δ 4.45 and 4.01 ppm, which corresponds to the two methylene bridges. As well, two doublets at δ 8.07 and 7.94 ppm and a multiplet at δ 7.30-7.25 ppm correspond to the naphthalene moieties. All ^1H -NMR signals at ambient temperature are sharp and this is indicative therefore of conformational flexibility.



Scheme 5.03 Synthesis of *peri*-sulfonatocalix[4]naphthalene **124**.

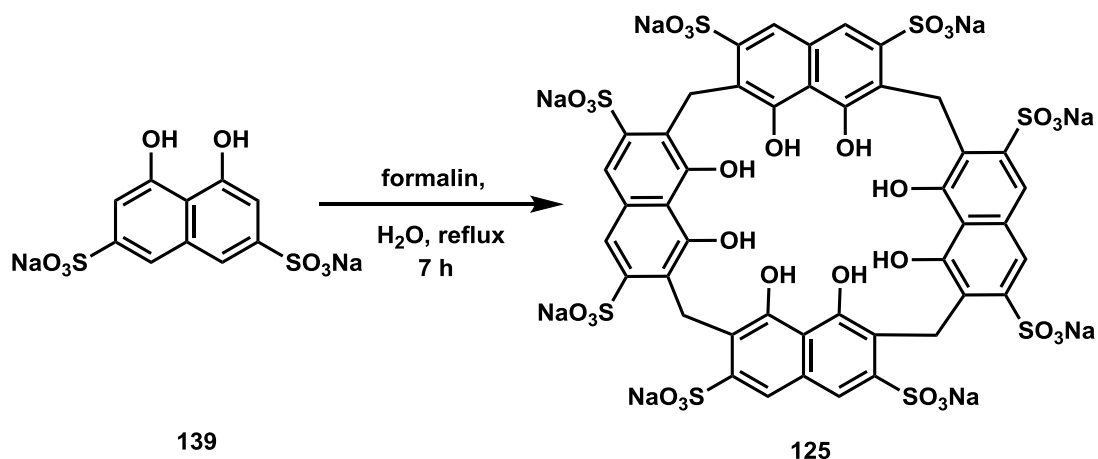
When **138** was heated at reflux under acidic conditions, with paraformaldehyde and sulfuric acid (3%) in glacial acetic acid for 6 days a cyclic condensation product, diacetoxyoxacalix[4]naphthalenesultone (**137**) was formed in 12% yield (Scheme 5.04).¹³ The ^1H -NMR spectrum of **137** reveals two singlets at δ 4.84 and 5.24 ppm, due to the methylene protons and oxymethylene protons and their corresponding ^{13}C chemical shifts were present at δ 33 and 59 ppm respectively. The doublets at δ 7.05 and 7.21 ppm and the singlet at δ 7.32 ppm are due to the “intraannular” aromatic protons. As well, two

doublets at δ 8.24 ppm and 8.14 ppm, and multiplets at δ 8.07-8.04 ppm and 7.90-7.81 ppm correspond to the naphthalene moieties. The singlet at δ 2.04 ppm is due to the methyl protons of the acetoxy groups.



Scheme 5.04 Synthesis of diacetoxyoxacalix[4]naphthalenesultone **137**.

The synthesis of cyclotetrachromotropyrene (**125**) is outlined in Scheme 5.05.¹⁴ In 1989 Poh and co-workers¹⁴ first reported the cyclotetrachromotropyrene (“-CTCT” or **125**) as a “dark red plastic-like product” which was ambiguously characterized. In a subsequent paper,⁴⁷ Poh reported the combustion analysis for the compound consistent with a multi-hydrated form of octasodium **125**. In the current work **125** was synthesized according to the Poh’s procedure,⁴⁷ using 37% w/w formaldehyde solution with disodium salt of chromotropic acid (DSCTA, **139**) in aqueous solution.



Scheme 5.05 Synthesis of cyclotetrachromotrylene **125**.

5.5.1.1 Characterization of cyclotetrachromotrylene (“CTCT” or **125**)

Compound **125** was characterized by ¹H- and ¹³C-NMR spectroscopy. The ¹HNMR spectrum of **125** shows eight aromatic protons (Ar-*H*) appearing as singlet at δ 8.05 ppm and the bridging -CH₂- groups appeared as a singlet at δ 4.88 ppm. However, the data could just as easily be accounted for by other larger cyclic oligomeric products which could be potentially formed between DSCTA and formaldehyde. To better characterize the molecular structure of CTCT, the freshly prepared product was subjected to diffusion ¹HNMR analysis⁴⁸ in addition to routine spectroscopic characterizations. The diffusion curve (Figure 5.11) conducted and analyzed by Dr. Celine Schneider at MUN, shows the decay of the peak intensity of the protons of the naphthalene ring -C_{Naphth}H (δ = 7.99 ppm) as a function of the gradient strength.^{45b} Based upon this curve, the diffusion coefficient was calculated to be $2.79 \times 10^{-10} \text{ m}^2 \cdot \text{s}^{-1}$, which corresponds to a “sphere” having a hydrodynamic radius⁴⁹ of 7.14 Å. This radius is consistent with a hydrated form

of an ellipsoidal CTCT according to our molecular modeling,⁵⁰ and it does not match the sizes of any higher order cyclic oligomers. In further support, after hydrogen ion exchange of **125** to the resultant corresponding CTCT octasulfonic acid, ion-trap LC/MS analysis run in the negative mode was conducted to reveal the expected molecular ion $[M]^-$ at m/z 1327.8 and the $[M-2H]^{2-}$ at m/z 662.9.

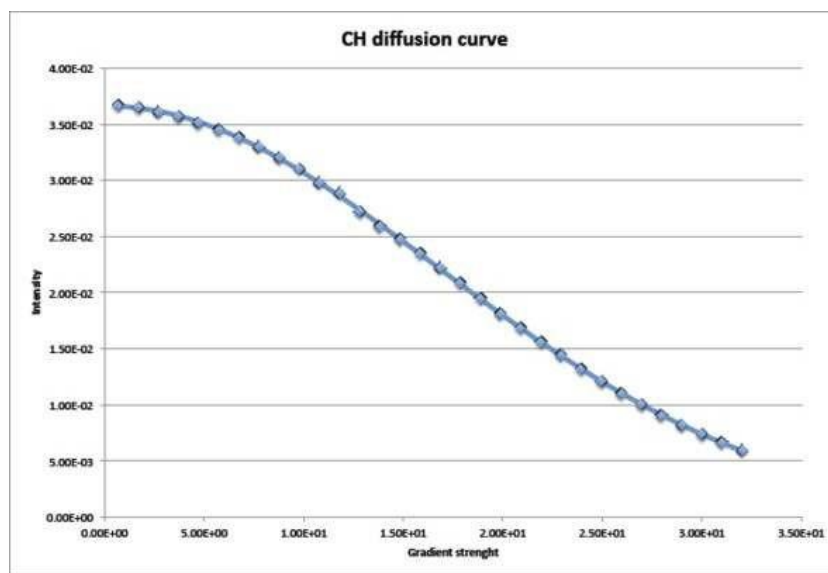


Figure 5.11 ^1H -NMR diffusion spectroscopic curve ($r^2 = 0.999$) based upon the analysis of the chemical shift changes for the naphthalene ring $-\text{C}_{\text{Naphth}}\text{H}$ protons.

5.5.2 Complexation studies of calix[4]naphthalenes **124**, **125** and **137**

In a collaborative project with Coleman's group at the University of Lyon, the naphthalene derivatives **124**, **125** and **137** were shown to be capable of capping and stabilizing silver nanoparticles, and also to possess molecular recognition properties with regard to nucleobases and certain amino acids. The corresponding capped nanoparticles were prepared using the method in which the relevant calix[4]naphthalene was mixed

with silver nitrate in deionised water and then treated with sodium borohydride. The nanoparticles were characterized by dynamic light scattering (DLS) and zeta potentials. The sizes of the nanoparticles and their zeta potentials indicate that the ~16 and ~24 nm diameter nanoparticles prepared from **124** and **137**, respectively, are not similar, and those prepared from **125**, which were ~40 nm are about twice as large. With regard to their zeta potentials, as expected, the nanoparticles prepared from **124** and **125** which contain sulfonic acid groups show more strongly negative potentials than those from **137**. All three derivatives in de-ionized water show strong absorptions with λ_{max} 390–410 nm for their plasmon resonances. The spectra remain unchanged after 24 h showing that the nanoparticles are stable in the aqueous solutions. In the case of the hybrid nanoparticles using **125** as the capping agent, a small ligand-associated peak is observed at 540 nm (Table 5.01). The UV-vis spectra of all three nanoparticles are shown in Figure 5.12.

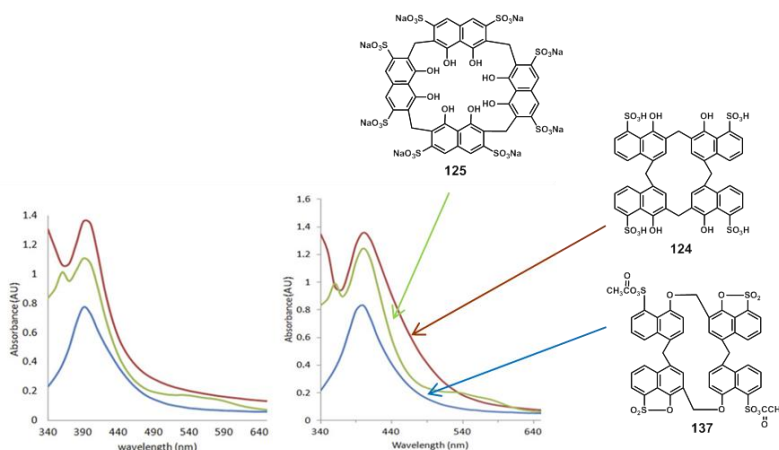


Figure 5.12 UV-vis spectra of the three nanoparticles. *Left*: after 1 h; *right*: after 24 h, red curve (-) is **124:AgNP**, blue curve (-) is **137:AgNP** and green curve (-) is **125:AgNP**.^{45a}

Table 5.01 The wavelengths and intensities of the plasmon resonance band after 1 and 24 h for the three nanoparticle systems.

Entry	System	After 1 h Wavelength [nm]	After 24 h Wavelength [nm]	After 1 h Absorbance [AU]	After 24 h Absorbance [AU]
1	124:AgNP	390	400	1.373	1.195
2	137:AgNP	390	400	0.765	0.756
3	125:AgNP	390	410	1.095	1.106

5.5.2.1 Molecular recognition studies

Molecular recognition of the nucleobases by the calix[4]naphthalene-capped silver nanoparticles were conducted in the same manner as in the work reported by Coleman's group using *p*-sulfonatocalix[4]arene-capped silver nanoparticles.⁵¹ The molecular recognition studies with amino acids followed Li's procedures.^{19a}

5.5.2.1.1 With nucleobases

Figures 5.13-5.15 show the spectra obtained after 1 and 24 h in each case after mixing each of the respective calixnaphthalene-capped nanoparticles with adenine, cytosine, guanine, thymine, and uracil nucleobases (Tables 5.02 and 5.03). The λ_{max} of the plasmon resonance bands after 1 h were in the range of 390–430 nm for the three systems. For the nanoparticles capped with **124** (Figure 5.13), interactions exist with adenine, cytosine and guanine after 1 h, the λ_{max} of the plasmon resonance band shifted to 420 (blue), 410 (green) and 430 (purple) nm. After 24 h there were no changes in the resonance bands that may be ascribed to aggregation in these cases. For the hybrid nanoparticles capped with **137** there were no significant shifts in the wavelength of the

plasmon resonance bands after 1 or 24 h (Figure 5.14). However, in the case of guanine only is there an absence of aggregation bands after 1 h. With adenine the aggregation band appears at 510 nm, for thymine and cytosine at 590 nm, and for uracil, a band appears at 600 nm. The situation changes strongly after 24 h: only for thymine, cytosine and uracil, there were aggregation bands; for adenine the band has weakened, suggesting that a de-aggregation process occurs.

In the case of the nanoparticles capped with **125**, only for adenine and guanine, was there a significant shift in the plasmon resonance band after 1 h (Figure 5.15).

The above can be compared with the situation for the nanoparticles capped with *p*-sulfonatocalix[4]arene, where after 24 h, strong aggregation behaviour was observed with guanine, uracil and thymine, and with adenine precipitation was also observed.

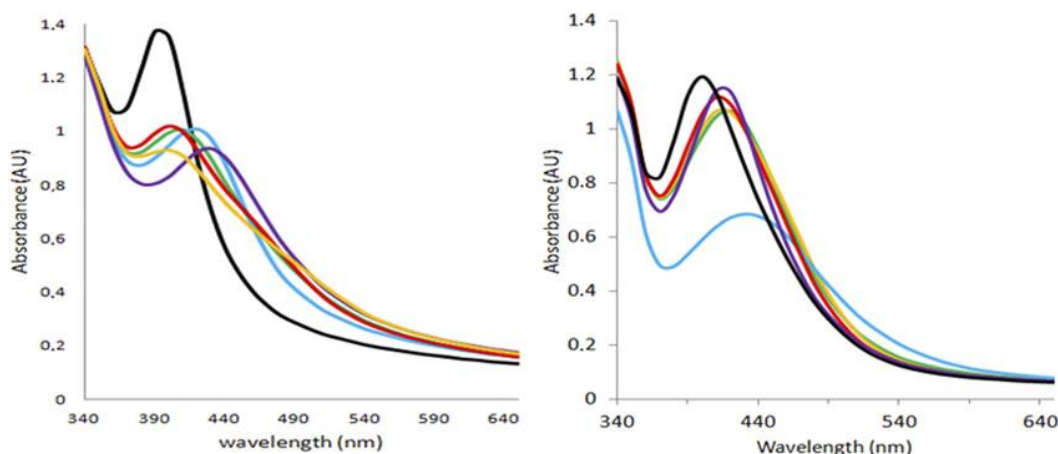


Figure 5.13 UV-vis spectra of **124:Ag** NP mixed with nucleobases: red (–) with thymine; blue (–) with adenine; green (–) with cytosine; purple with guanine; yellow (–) with uracil. *Left*: after 1 h; *right*: after 24 h. Black (–) is **124:Ag** NP in de-ionised water.^{45a}

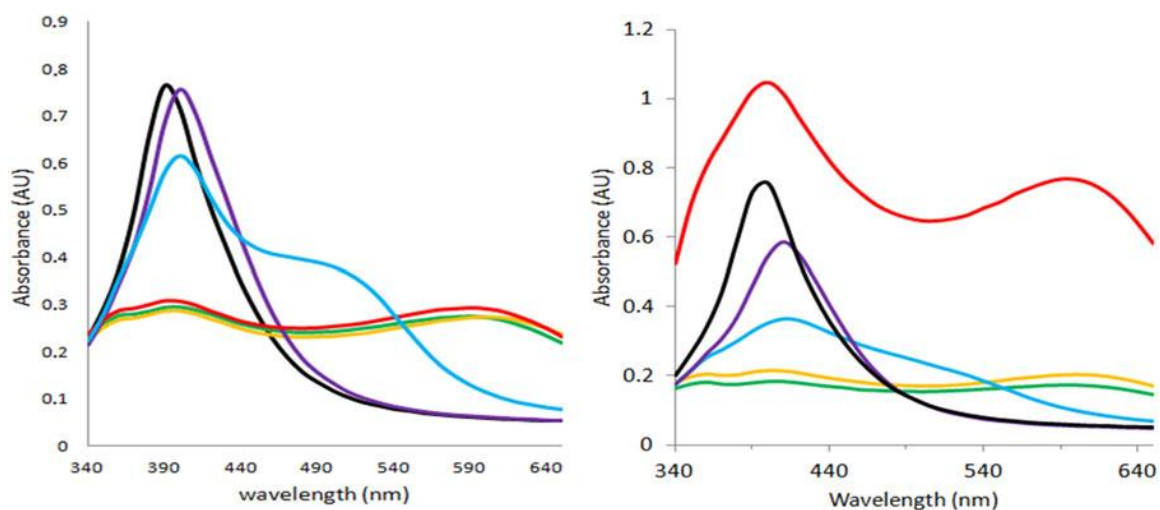


Figure 5.14 UV-vis spectra of **137:Ag** NP mixed with nucleobases: red (–) with thymine; blue (–) with adenine; green (–) with cytosine; purple (–) with guanine; yellow (–) with uracil. *Left*: after 1 h; *right*: after 24 h. Black (–) is **137:Ag** NP in de-ionised water.^{45a}

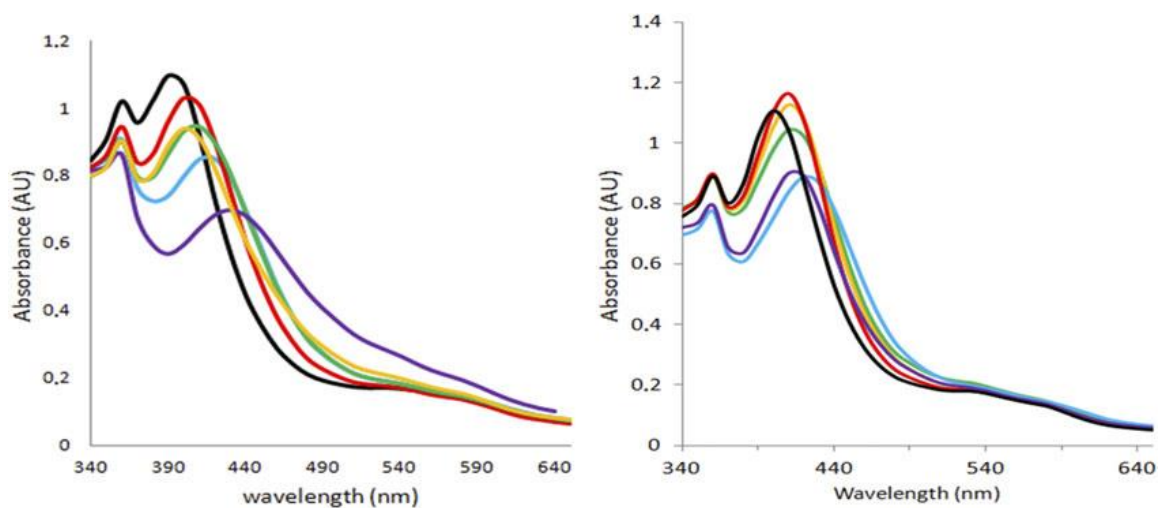


Figure 5.15 UV-vis spectra of **125:Ag** NP mixed with nucleobases: red (–) with thymine; blue (–) with adenine; green (–) with cytosine; purple (–) with guanine; yellow (–) with uracil. *Left*: after 1 h; *right*: after 24 h. Black (–) is **125:Ag** NP in de-ionised water.^{45a}

Table 5.02 Summary of plasmon resonance and aggregation spectral data for the nucleobase-hybrid nanoparticle interactions after 1 h.^{45a}

Nucleobase-NPs interactions	Wavelength [nm]	Absorbance [AU]	Wavelength [nm]	Absorbance [AU]
124:AgNPs				
Adenine	420	1.008	----	----
Thymine	400	1.018	----	----
Cytosine	410	1.007	----	----
Guanine	430	0.936	----	----
Uracil	400	0.929	----	----
Water	390	1.373	----	----
137:AgNPs				
Adenine	410	0.616	510	0.367
Thymine	390	0.308	590	0.293
Cytosine	400	0.294	590	0.274
Guanine	400	0.755	----	----
Uracil	390	0.286	600	0.273
Water	390	0.765		
125:AgNPs				
Adenine	420	0.851	540	0.182
Thymine	410	1.01	540	0.171
Cytosine	410	0.945	540	0.183
Guanine	430	0.698	540	0.266
Uracil	400	0.939	540	0.197
Water	390	1.095	540	0.198

5.5.2.1.2 With amino acids

The UV–vis spectra (Figures 5.16–5.18) obtained after 1 h and 24 h in each case are shown after each of the respective calixnaphthalene-capped nanoparticles were mixed with eight different amino acids namely, aspartate, asparagine, phenylalanine, alanine, tryptophan, histidine, lysine and arginine. The recognition behaviour of the calix[4]naphthalene-capped Ag-nanoparticles with respect to the amino acids tested was quite different from that seen with the nucleobases and are shown in Tables 5.04 and

5.05. Only with the nanoparticles capped with **137** (Figure 5.17) was there a significant interaction with four of the amino acids tested.

Table 5.03 Summary of plasmon resonance and aggregation spectral data for the nucleobase-hybrid nanoparticle interactions after 24 h.^{45a}

Nucleobase-NPs interactions	Wavelength [nm]	Absorbance [AU]	Wavelength [nm]	Absorbance [AU]
124:AgNPs				
Adenine	430	0.685	----	----
Thymine	410	1.115	----	----
Cytosine	420	1.065	----	----
Guanine	410	1.138	----	----
Uracil	410	1.065	----	----
Water	400	1.195	----	----
137:AgNPs				
Adenine	410	0.363	----	----
Thymine	400	1.048	590	0.767
Cytosine	400	0.184	600	0.173
Guanine	410	0.586	----	----
Uracil	400	0.214	600	0.203
Water	400	0.756		
125:AgNPs				
Adenine	420	0.889	540	0.190
Thymine	410	1.163	540	0.174
Cytosine	410	1.043	540	0.195
Guanine	410	0.902	540	0.181
Uracil	410	1.128	540	0.181
Water	410	1.106	540	0.186

In contrast to *p*-sulfonatocalix[*n*]arenes, there is no significant interaction observed for lysine with **137**.⁵² With histidine and arginine, aggregation bands at 590 and 610 nm, respectively, are seen after 1 h (Table 5.04) accompanied by precipitation of the arginine system after 24 h (Table 5.05). In contrast to the *p*-sulfonatocalix[*n*]arene-capped nanoparticles,⁵¹ both tryptophan and phenylalanine are associated with interaction and

aggregation behaviours. None of the other amino acids showed any significant interaction or aggregation with the three calix[4]naphthalene-AgNPs.

Table 5.04 Summary of plasmon resonance and aggregation spectral data for the amino acid-hybrid nanoparticle interactions after 1 h.^{45a}

Amino acid-NPs interactions	Wavelength [nm]	Absorbance [AU]	Wavelength [nm]	Absorbance [AU]
124:AgNPs				
Aspartate	400	1.274	----	----
Asparagine	390	1.262	----	----
Phenylalanine	400	1.314	----	----
Alanine	400	1.324	----	----
Tryptophan	400	1.229	----	----
Histidine	390	0.978	----	----
Lysine	400	1.426	490	0.484
Arginine	400	1.129	----	----
Water	390	1.373	----	----
137:AgNPs				
Aspartate	400	0.219	----	----
Asparagine	390	0.712	----	----
Phenylalanine	390	0.687	510	0.229
Alanine	390	0.795	----	----
Tryptophan	390	0.602	510	0.309
Histidine	390	0.233	590	0.218
Lysine	390	0.823	----	----
Arginine	400	0.302	610	0.277
Water	390	0.765	----	----
125:AgNPs				
Aspartate	390	1.270	540	0.172
Asparagine	390	1.128	540	0.179
Phenylalanine	400	1.065	540	0.171
Alanine	390	1.095	540	0.174
Tryptophan	400	0.996	540	0.179
Histidine	400	0.993	540	0.168
Lysine	400	1.102	540	0.167
Arginine	400	1.103	540	0.160

Table 5.05 Summary of plasmon resonance and aggregation spectral data for the amino acid-hybrid nanoparticle interactions after 24 h.^{45a}

Amino acid-NPs interactions	Wavelength [nm]	Absorbance [AU]	Wavelength [nm]	Absorbance [AU]
124:AgNPs				
Aspartate	400	0.904	----	----
Asparagine	400	0.242	----	----
Phenylalanine	400	1.258	----	----
Alanine	400	1.225	----	----
Tryptophan	410	1.265	----	----
Histidine	400	1.143	----	----
Lysine	400	1.410	----	----
Arginine	410	1.380	----	----
Water	400	1.195	----	----
137:AgNPs				
Aspartate	400	0.344	----	----
Asparagine	400	0.730	----	----
Phenylalanine	400	0.667	530	0.164
Alanine	410	0.670	----	----
Tryptophan	400	0.624	530	0.225
Histidine	400	0.368	580	0.259
Lysine	400	0.842	----	----
Arginine	400	0.184	----	----
Water	400	0.756	----	----
125:AgNPs				
Aspartate	400	1.196	540	0.172
Asparagine	400	1.129	540	0.182
Phenylalanine	410	1.109	540	0.184
Alanine	400	1.119	540	0.182
Tryptophan	410	1.049	540	0.202
Histidine	410	1.087	540	0.176
Lysine	400	1.271	540	0.168
Arginine	410	1.173	540	0.182
Water	400	1.106	540	0.174

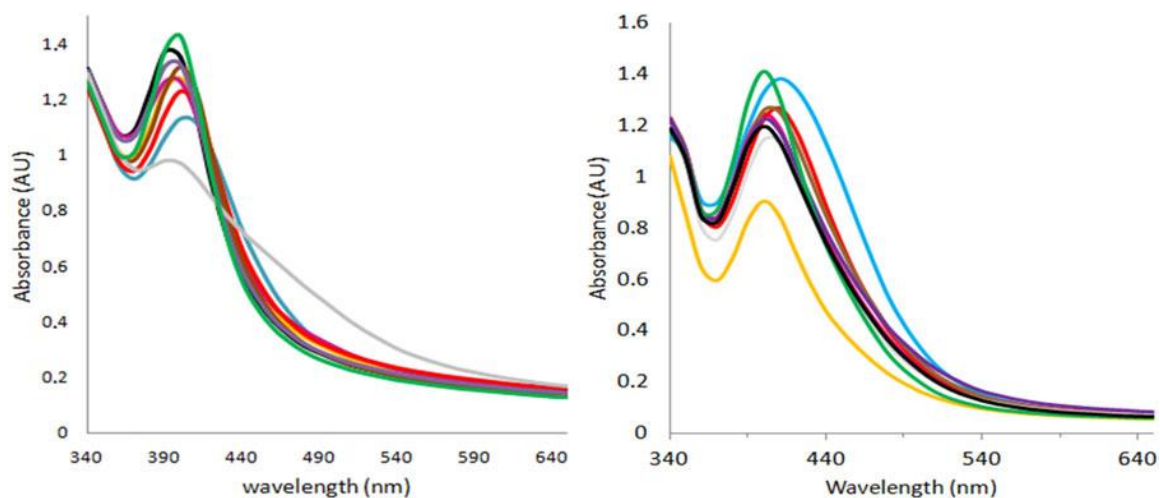


Figure 5.16 UV-vis spectra of **124:Ag** NP mixed with amino acids: red (–) with tryptophan; blue (–) with arginine; green (–) with lysine; purple (–) with alanine; yellow (–) with aspartate; fuchsia (–) with asparagine; brown (–) with phenylalanine; grey (–) with histidine. *Left*: after 1 h; *right*: after 24 h. Black (–) is **124:Ag** NP in de-ionised water.^{45a}

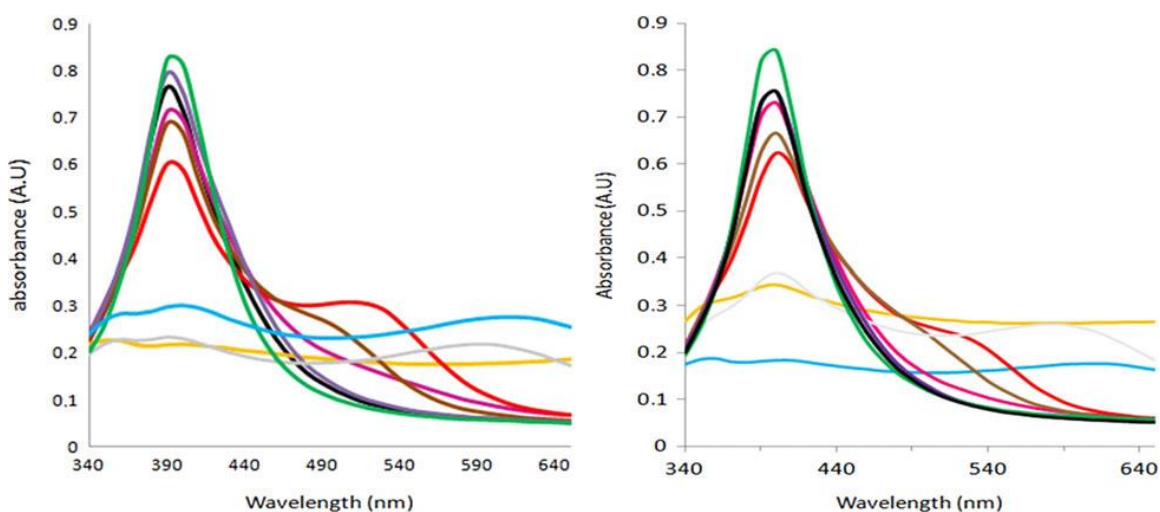


Figure 5.17 UV-vis spectra of **137:Ag** NP mixed with amino acids: red (–) with tryptophan; blue (–) with arginine; green (–) with lysine; purple (–) with alanine; yellow (–) with aspartate; fuchsia (–) with asparagine; brown (–) with phenylalanine; grey (–) with histidine. *Left*, after 1 h; *right*, after 24 h. Black (–) is **137:Ag** NP in de-ionised water.^{45a}

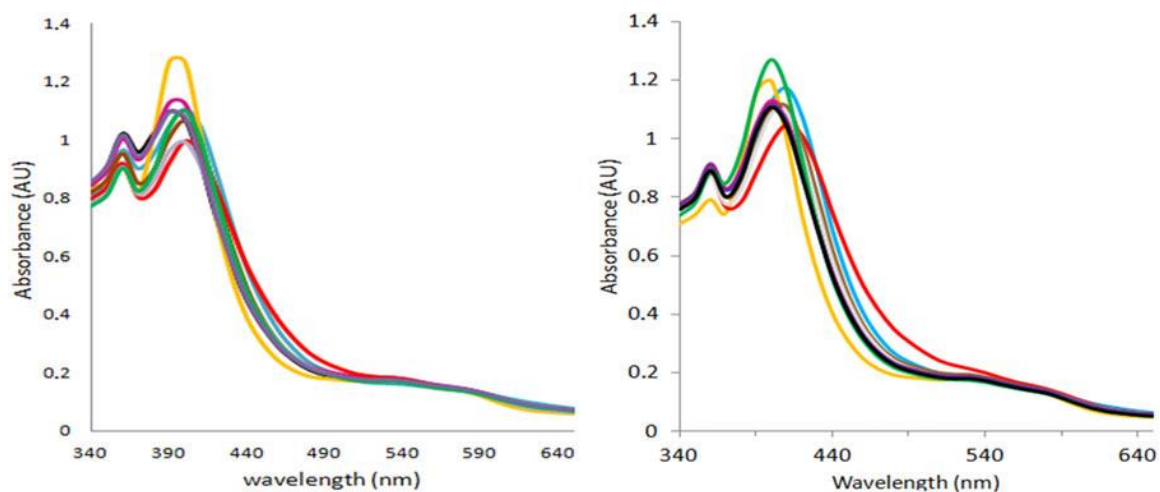


Figure 5.18 UV-vis spectra of **125:Ag** NP mixed with amino acids: red (–) with tryptophan; blue (–) with arginine; green (–) with lysine; purple (–) with alanine; yellow (–) with aspartate; fuchsia (–) with asparagine; brown (–) with phenylalanine; grey (–) with histidine. *Left*, after 1 h; *right*, after 24 h. Black (–) is **125:Ag** NP in de-ionised water.

The differences in behaviour between the three naphthalenic calix[4]arene-capped nanoparticles suggests that the capping mechanism is different with **137**, which has a larger cavity for complexation with the nucleobases and amino acids observed and was capable of even complexing with tryptophan.

5.5.3 Dispersion of SWNTs into aqueous solutions using “CTCT” or **125**

In another collaborative project with Zhao’s group at Memorial University and Adronov’s group at McMaster University, compound **125** was shown to be capable of selectively dispersing SWNTs into the aqueous phase. Since the molecular structure of **125** contains a large π -system as well as polar hydroxyl and sulfonate groups, it should have sufficient non-covalent binding potential as a supramolecular host for various π -conjugated molecules. In the meantime, it is also reasonable to hypothesize that **125** could interact with the surfaces of SWNTs through π - π interactions. The two types of

commercially-available SWNTs, CoMoCAT and HiPCO SWNTs were used in the dispersion studies and the characterization of the resulting SWNT–**125** supramolecular complexes using various analytical methods.

Dispersions of SWNTs with **125** in water were then conducted through a general ultrasonication procedure described as follows: SWNTs (0.8 mg) and **125** (0.5 mg) were added in 1.0 mL of deionized water. The mixture was sonicated for 30 min and then subjected to centrifugation for another 30 min. The resulting supernatant was subjected to UV-Vis-NIR spectral analysis. Figure 5.19 shows the photographic image of **125** and the dispersion of CoMoCAT SWNTs in aqueous solution. The discussion which follows is taken from the published work which appeared in *RSC Advances*.^{45b}

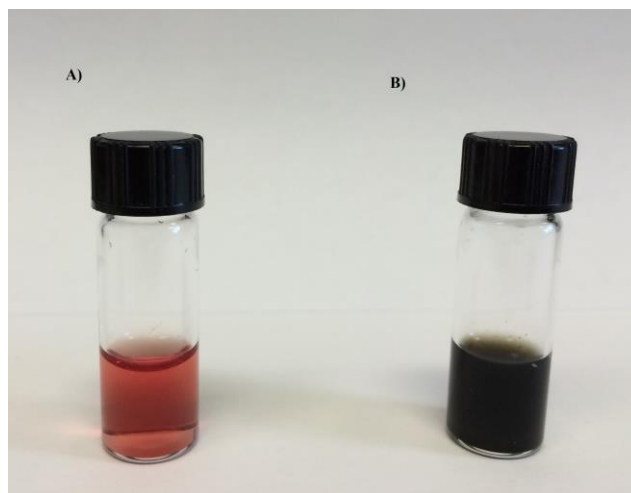


Figure 5.19 Photographic image of the solutions of (A) Free **125** (B) **125** was mixed with CoMoCAT SWNTs after sonication for 30 min.

Figure 5.20 shows the UV-Vis-NIR spectra of SWNT suspensions in aqueous **125** solutions. In Figure 5.19A the prominent absorption band centered at $\sim 1000\text{ cm}^{-1}$ is that

of the characteristic absorption of (6,5) SWNTs. As the CoMoCAT sample is known to consist of mainly semiconducting tubes, such as (6,5), (7,5), (7,6), (8,3), and (8,4) tubes, the results shown in Figure 5.20A clearly indicate a selectivity for (6,5) chirality by **125**. In the case of dispersion of HiPCO SWNTs with **125**, reasonably resolved absorption bands are observed in the Vis- NIR region as disclosed in Figure 5.20B. The bands which emerged in the range of 920 to 1400 nm are due to the semiconducting S_{11} transitions, while the bands from 620 to 920 nm are assigned to metallic M_{11} and semiconducting S_{22} transitions. Overall, the UV-Vis-NIR analysis confirms that **125** is capable of dispersing SWNTs in the aqueous phase.

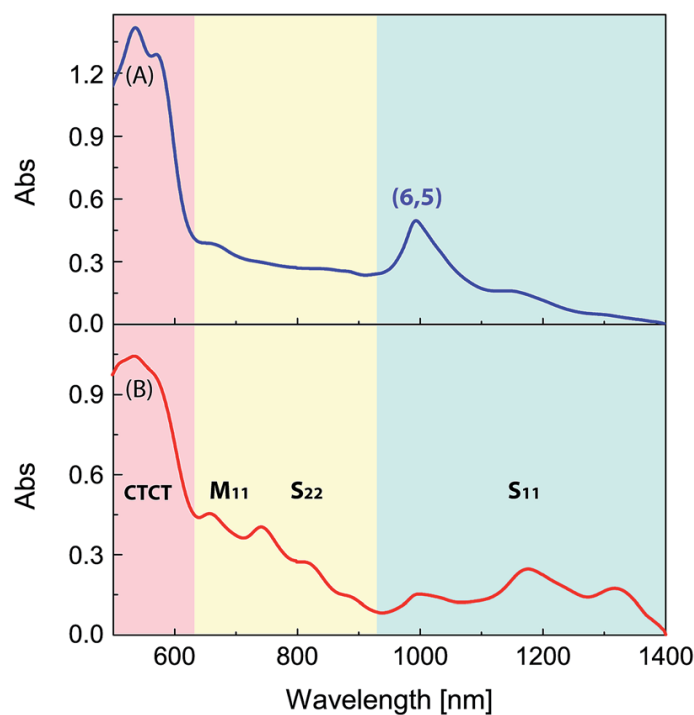


Figure 5.20 UV-Vis-NIR spectra: (A) CoMoCAT and (B) HiPCO nanotubes diffusion dispersed by **125** in aqueous solutions.^{45b}

To confirm the UV-Vis-NIR observations, the **125**–SWNT suspensions were then examined using Raman spectroscopy.³⁶ Figure 5.21A shows the Raman spectra of CoMoCAT and HiPCO SWNTs before and after dispersed with **125**. As shown in Figure 5.20A, the CoMoCAT nanotubes dispersed with **125** show a much weaker D-band than the raw sample, indicating that the dispersion results in better-quality tubes. It is also worth noting that the metallic G⁻ band is considerably reduced after dispersion, which suggests that **125** is selective for semiconducting tubes. In the radial breathing mode (RBM) region,⁵³ three major bands are observed at 231, 266 and 302 cm⁻¹ for the raw CoMoCAT sample, corresponding to nanotubes with different diameters. After dispersion, only the band at 266 cm⁻¹ remains, significantly, whereas the other two bands diminish substantially. The Raman data clearly shows that **125** is selective towards nanotubes with certain diameters. It has been known that the RBM frequency is inversely proportional to the diameter of a nanotube as described by the equation: $\omega = 223.5/d + 12.5$, where ω is the RBM frequency in cm⁻¹ and d is the nanotube diameter in nm. The CoMoCAT nanotubes selectively dispersed by **125** are estimated to have an average diameter of 0.88 nm. Similar results can be seen in the dispersion of HiPCO nanotubes in Figure 5.21B. In the RBM region, the raw HiPCO nanotubes give a number of bands at 201, 210, 220, 229, and 266 cm⁻¹. After dispersion, only the band at 266 cm⁻¹ appears to be the major one, while the others diminish considerably.

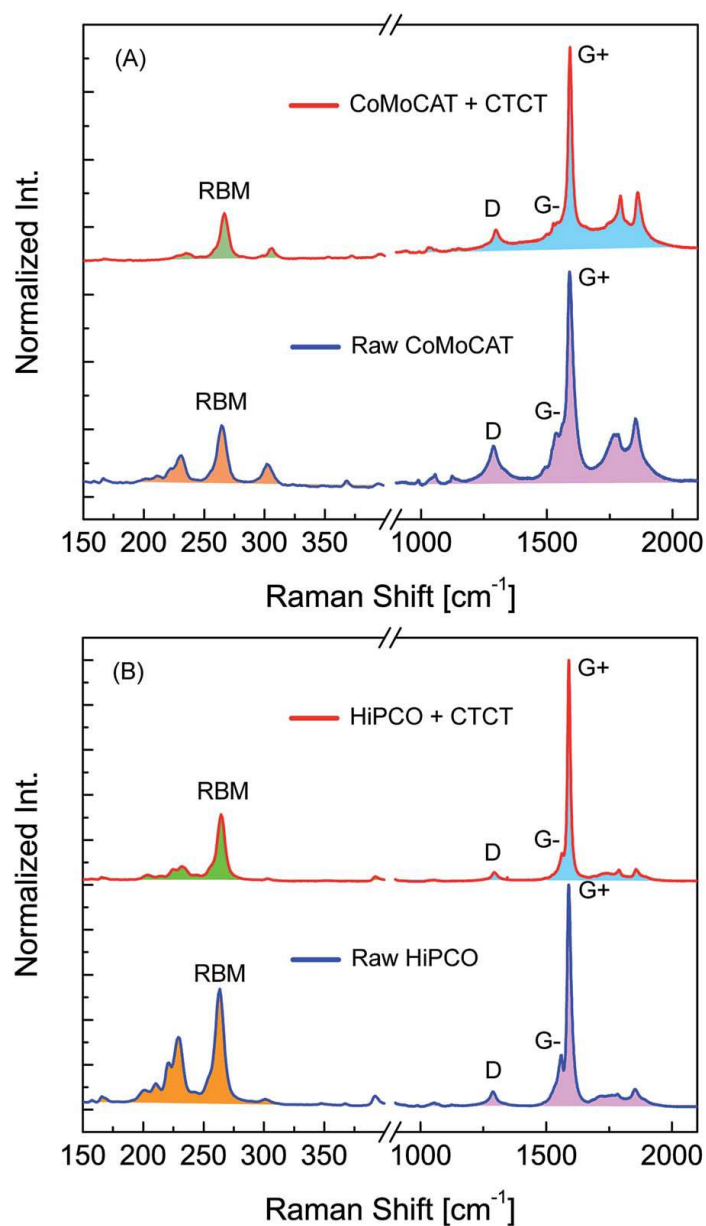


Figure 5.21 Raman spectra comparing the SWNTs before and after being dispersed with **125** in water. (A) CoMoCAT nanotubes (B) HiPCO nanotubes. Excitation wavelength: 785 nm.^{45b}

To characterize the supramolecular interactions between **125** and SWNTs in the solid state, suspensions of SWNTs were drop-cast on a freshly cleaved mica surface for atomic force microscopic (AFM) analysis. Figure 5.22 shows the 3-D AFM images of the

supramolecular self-assemblies of **125** and CoMoCAT SWNTs on surface. The AFM results clearly show that **125** and nanotubes strongly aggregate together to exhibit somewhat “worm-like” morphologies.

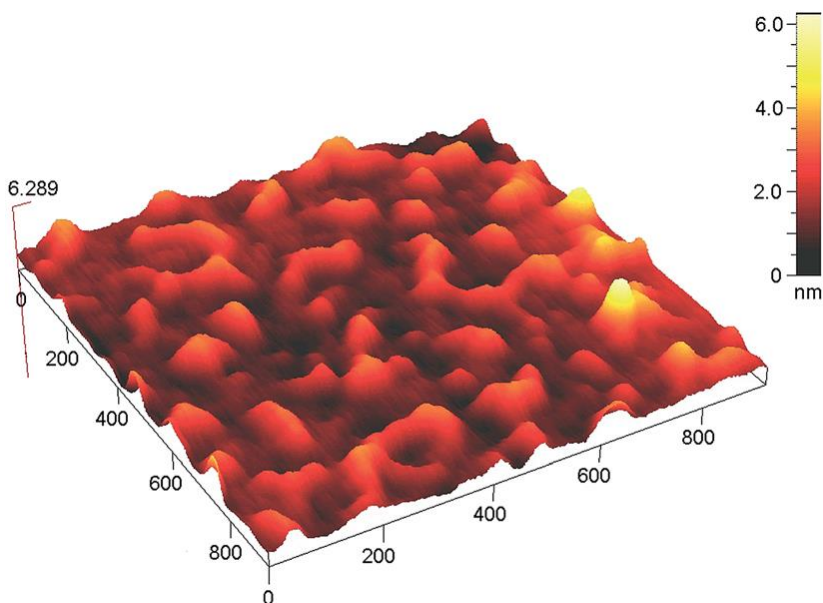


Figure 5.22 AFM image showing the supramolecular assemblies of **125** and CoMoCAT SWNT drop-cast onto mica.^{45b}

To further understand the interactions between **125** and SWNTs at the molecular level, molecular modeling studies were conducted. The complexes of **125** and SWNTs were simulated by the molecular mechanics (MM) method using the MMFF force field implemented in Spartan'10 software. Figure 5.23 illustrates a possible mode in which **125** molecules could interact with representative SWNTs. In this representation, the **125** molecules are shown in a “one” shaped conformation in which the naphthyl groups are bound to the SWNTs *via* intimate π -stacking, with the sulfonate groups on the opposite sides which can become hydrated with the water molecules but also with neighboring

similarly **125** bound SWNTs. The modeling results are consistent with the AFM analysis in that nanotubes still remain in small bundles when dispersed in the aqueous phase.

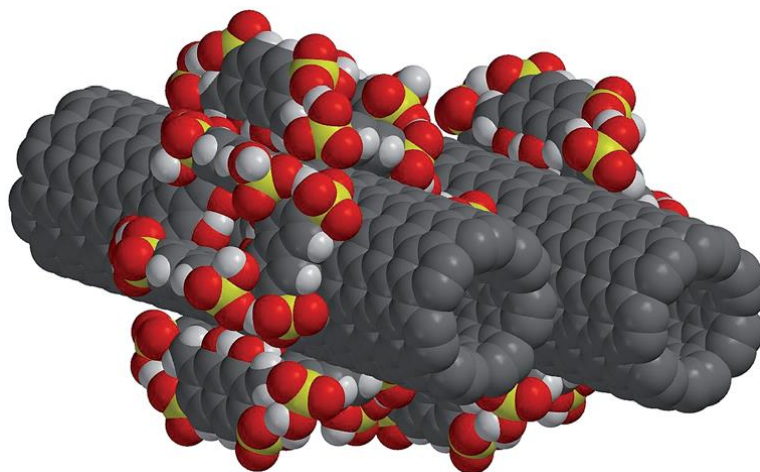


Figure 5.23 Spartan'10-generated molecular modeling (MMFF) showing a putative mode of binding between **125** molecules and two SWNTs. Water molecules are not shown for simplicity.^{45b}

5.5.4 Complexation studies of “CTCT” or **125** with C_{60}

Fukami *et al.*⁵⁴ developed a C_{60} solubilization method involving mechanochemically co-grinding the C_{60} with cycloamyloses. Deguchi *et al.*⁵⁵ found that C_{60} particles as small as 20 nm were readily produced by grinding the C_{60} in an agate mortar, the resulting nanoparticulate C_{60} being successfully dispersed in water with or without the support of a surfactant such as sodium dodecylsulfate.

Depending on the nature of the functional groups on their upper or lower rims calix[*n*]arenes have been used as cavitands which can bind C_{60} thereby rendering them soluble in water, Raston's group⁵⁶ reported that *p*-sulfonatocalix[4]arene was effective in solubilising both fullerenes C_{60} and C_{70} in water under certain conditions. It is well-

known that complementarity of size and shape of the cavity of calix[*n*]arenes relative to the fullerenes is an important factor for supramolecular complexation to occur. Higher analogues of calixarenes and calix[4]naphthalene can therefore form such host–guest complexes. Based on Raston’s procedure complexation studies of **125** with C₆₀ were conducted. The 10:1 molar ratio of **125** relative to C₆₀ was mixed together by mechanical grinding in an agate mortar and pestle for 40 min. Deionized water (5 mL) was added to solubilize the reaction mixture. After a further grinding of the slurry for 5 min, the slurry was sonicated for 30 min and then subjected to centrifugation for 60 min. The resulting supernatant was filtered through a cotton plug and subjected to ¹³C-NMR analysis at 25 °C in a 9:1 H₂O:D₂O solvent mixture. Figure 5.24 (top) shows that the ¹³C-chemical shift at δ 143.2 ppm, corresponding to the C₆₀ signal which indicates that **125** can solubilize C₆₀ into water. For further evidence of complexation, UV-vis experiments and solid state studies are currently underway.

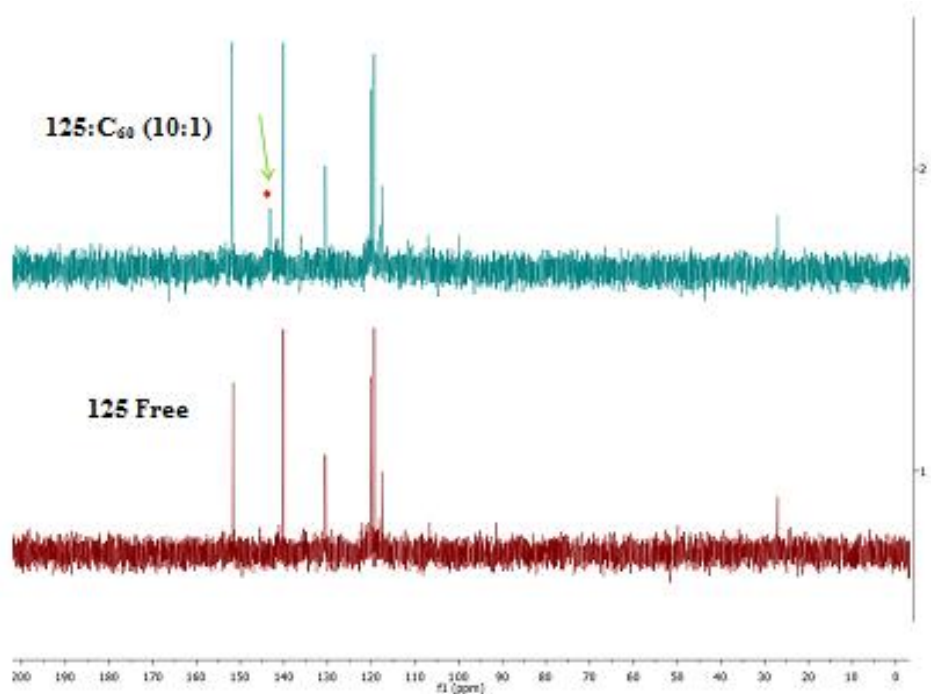


Figure 5.24 ^{13}C -NMR (75.4 MHz) spectra of **125** and complex with C_{60} in D_2O at 298K; \blacklozenge ” denoted the C-13 signal of C_{60} .

5.6 Conclusions

The three sulfonated calix[4]naphthalenes *peri*-sulfonatocalix[4]naphthalene **124**, cyclotetrachromotropyene **125**, and diacetoxycalix[4]naphthalenesultone **137** were synthesized. All were found to be capable of capping and stabilizing silver nanoparticles. For the nanoparticles capped with **137**, however, complexation of both nucleobases and certain amino acids occurs. Of particular interest is the selective complexation of the aromatic amino acids phenylalanine and tryptophan.

125 which is a water-soluble cyclic tetramer formed by the cyclocondensation of formaldehyde with disodium salt of 4,5-dihydroxy-2,7-naphthalenedisulfonic acid

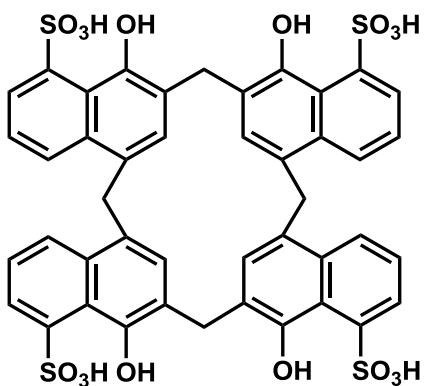
(DSCTA) synthesized in our labs was found to be capable of selectively dispersing SWNTs into the aqueous phase. The resulting supramolecular complexes in aqueous solution were characterized by UV-Vis-NIR analysis, while the dried aggregates were examined by Raman spectroscopy and atomic force microscopy (AFM). The synthesized **125** which was additionally characterized in aqueous solution by diffusion ^1H -NMR spectroscopy was found to show significant selectivity in dispersing CoMoCAT and HiPCO SWNTs in water, although this dispersion appears to be comprised of small bundles of SWNTs rather than individual tubes. This discloses a new approach to process and/or enrich SWNTs in the aqueous phase, and it could be useful in the applications of nanoelectronic and nanobiological systems.

5.7 Experimental section

All reagents used for the synthesis of three sulfonated calix[4]naphthalenes **124**, **125** and **137** and reagents used in the complexation studies were purchased from Sigma-Aldrich or AlfaAesar. ^1H -NMR spectra were recorded at either 300 or 500 MHz, as noted, and the ^{13}C -NMR spectra at 75.4, MHz as noted. Mass spectra were conducted on an APCI-LC/MSD Trap and MALDI instruments.

5.7.1 Experimental

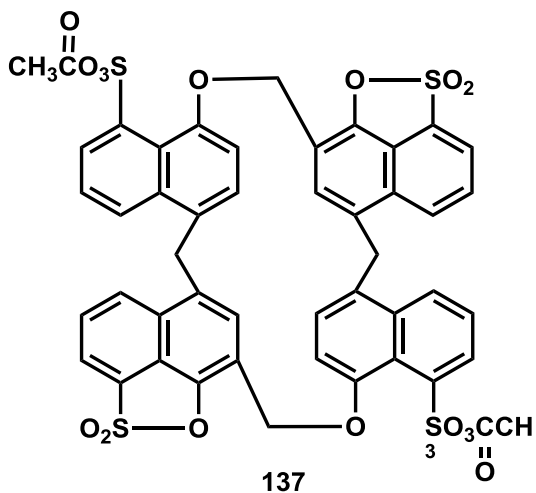
peri-Sulfonatocalix[4]naphthalene **124**¹³



124

To a solution of 1,8-naphthalenesultone **138** (2.06 g, 10.1 mmol) in DMF (10 mL) under N₂ were added formalin (37% w/w formaldehyde solution, 0.70 mL, 8.6 mmol) and Cs₂CO₃ (2.01 g, 6.13 mmol) in water (3 mL). The reaction mixture was refluxed for 52 h and then cooled to room temperature, then poured into 5% hydrochloric acid (30 mL). The reaction mixture was left in refrigerator for 1d. A white precipitate formed that was filtered and washed with deionized water until the washings were neutral to pH paper. The crude product was crystallized from 95% ethanol to yield *peri*-sulfonatocalix[4]naphthalene **124** as a colourless powder (1.41 g, 15%). Alternatively, K₂CO₃ was used as base under the same conditions to afford **124** in 25% yields, m.p. 256.2-275.1 °C. ¹HNMR (DMSO-*d*₆, 300 MHz): δ 12.3 (s, 4H), 8.07 (d, 4H, *J* = 9.0 Hz), 7.94 (d, 4H, *J* = 9.0, Hz), 7.30–7.25 (m, 4H), 6.61 (s, 4H), 4.45 (s, 4H), 4.00 (s, 4H). ¹³CNMR (DMSO-*d*₆, 75.4 MHz): δ 149.3, 141.5, 132.6, 129.8, 126.7, 125.9, 125.2, 123.7, 123.1, 120.3, 35.1, 29.6. MALDI (*m/z*): 1056.9 [M+3K]⁺.

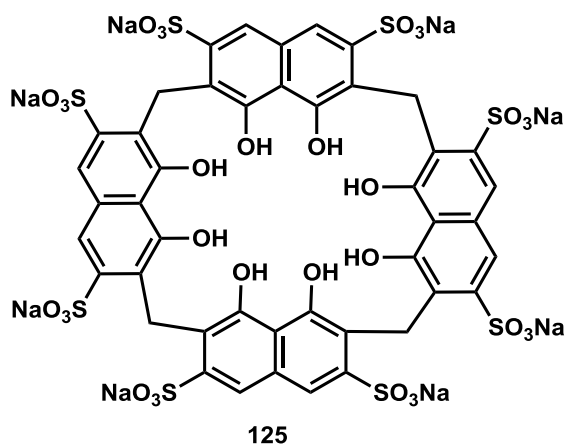
Diacetoxyoxacalix[4]naphthalenesultone **137** ¹³



To a solution of 1,8-naphthalene sultone **138** (3.91 g, 18.9 mmol) and paraformaldehyde (2.4 g, 80 mmol) in glacial acetic acid (100 mL) was added concentrated sulfuric acid (3.0 mL). The clear solution was refluxed for 6 d. After being cooled to room temperature, the reaction solution was poured onto crushed ice.

The obtained grey precipitate was extracted with dichloromethane (3 × 75 mL), washed with water (2 × 50 mL). The separated organic layer was dried over anhydrous MgSO₄ and the solvent was removed using a rotary evaporator. The residue was subjected to column chromatography (silica gel, 80:20 dichloromethane: methanol) to yield diacetoxyoxacalix[4]naphthalenesultone **137** as a colourless solid (0.94 g, 12%) m.p. 265.1-270.2 °C. ¹HNMR (CDCl₃, 300 MHz): δ 8.24 (d, 4H, *J* = 6.1 Hz), 8.14 (d, 4H, *J* = 6.1 Hz), 8.07–8.04 (m, 4H), 7.90–7.81 (m, 4H), 7.32 (s, 2H), 7.21 (d, 2H, *J* = 6.1 Hz), 7.05 (d, 2H, *J* = 6.1 Hz), 5.24 (s, 4H), 4.84 (s, 4H), 2.04 (s, 6H). ¹³CNMR (CDCl₃, 75.4 MHz): δ 170.5, 146.4, 144.2, 130.8, 130.3, 130.1, 130.0, 129.9, 129.7, 129.6, 129.5, 129.3, 129.1, 128.5, 128.3, 122.1, 122.0, 121.2, 120.9, 115.1, 106.4, 59.5, 33.5, 20.7. APCI(+) MS (*m/z*): 1009.2 [M+1]⁺.

Cyclotetrachromotropylenes 125 (“CTCT”)⁴⁸



A stock solution of formaldehyde (4.99 mmol) was prepared by diluting 0.4 mL of 37% w/w formaldehyde solution to 5 mL of distilled water. From the stock solution 1 mL of formaldehyde was added to a solution of the disodium salt of chromotropic acid (DSCTA, **139**) (2.01 g, 4.99 mmol) in 20 mL of distilled water. The reaction mixture was refluxed for 1 h and 1 mL of formaldehyde was added, continued the reflux for 1 h. The addition of formaldehyde was repeated until completion of stock solution. The total time duration of the reaction was refluxed for 7 h, the mixture was then evaporated to dryness on a hot plate to afford a crude product cyclotetrachromotropylenes **125** as a dark purple solid. The crude product was further purified as follows: it was dissolved in a minimum amount of boiling water. Ethanol was added until the solution become cloudy and then the solution was reheated until it becomes a clear. It was then left in a refrigerator overnight. The solution was decanted and the remaining sticky mass was washed with acetone until the product solidified to afford **125**. (2.91 g, 40%) ¹H-NMR (D₂O, 300 MHz): δ 8.05 (s, 4H, Ar-H), 4.88 (s, 4H, Ar-CH₂). ¹³C-NMR (D₂O, 75.4 MHz): δ 151.6, 140.1, 130.5, 120.1, 119.3, 117.5, 27.0. APCI(-) MS (*m/z*): 1327.8 [M-H]⁻ and 662.9 [M-2H]²⁻.

5.8 References

1. (a) Gutsche, C. D.; *Calixarenes an Introduction*, 2nd ed.; Royal Society of Chemistry: Cambridge, 2008. (b) Asfari, Z.; Böhmer, V.; Harrowfield, J.; Vicens, J. *Calixarenes* 2001; Kluwer Academic Press: Dordrecht, 2001.
2. Arduni, A.; Pochini, A.; Reverberi, S.; Ungaro, R. *J. Chem. Soc., Chem. Commun.* **1984**, 981–982.
3. Shinkai, S.; Araki, K.; Arimura, T.; Manabe, O. *J. Chem. Soc., Perkin Trans. 1* **1987**, 2297–2299.
4. (a) Perret, F.; Coleman, A.W. *Chem. Commun.* **2011**, 47, 7303–7319. (b) Danylyuk, O.; Suwinska, K. *Chem. Commun.* **2009**, 5799–5813. (c) Guo, D.-S.; Liu, Y. *Acc. Chem. Res.* **2014**, 47, 1925–1934.
5. Perret, F.; Coleman, A. W. *In Supramolecular Systems in Biomedical Fields*; Schneider, H.-J., Ed.; Royal Society of Chemistry: Cambridge, 2013; Chapter 6, pp 140–163.
6. Atwood, J. L.; Bridges, R. J.; Juneja, R. K.; Singh, A. K. *US Patent* 5489612, 1996.
7. Hwang, K. M.; Qi, Y. M.; Liu, S. Y.; Choy, W.; Chen, J. *US Patent* 5441983, 1995.
8. Lamartine, R.; Tsukada, M.; Wilson, D.; Shirata, A. Antimicrobial activity of calixarenes. *C. R. Chimie* **2002**, 5, 163–169.

9. Hulmes, D. J. S.; Aubert-Foucher, E.; Coleman, A. W. *French Patent* 98.10074, 1998.
10. (a) Selkti, M.; Coleman, A. W.; Nicolis, I.; Douteau-Guevel, N.; Villain, F.; Tomas, A.; de Rango, C. *Chem. Commun.* **2000**, 161–162. (b) Lazar, A.; Da Silva, E.; Navaza, A.; Barbey, C.; Coleman, A. W. *Chem. Commun.* **2004**, 2162–2163.
11. (a) Danylyuk, O.; Monachino, M.; Lazar, A. N.; Suwinska, K.; Coleman, A. W. *J. Mol. Struct.* **2010**, *965*, 116–120. (b) Dupont, N.; Lazar, A. N.; Perret, F.; Danylyuk, O.; Suwinska, K.; Navaza, A.; Coleman, A. W. *Cryst. Eng. Comm.* **2008**, *10*, 975–977.
12. (a) Georghiou, P. E.; Li, Z. *Tetrahedron Lett.* **1993**, *34*, 2887–2889. (b) Georghiou, P. E.; Li, Z. *J. Incl. Phenom. Mol. Recognit. Chem.* **1994**, *19*, 55–66. (c) Georghiou, P. E.; Ashram, M.; Li, Z.; Chaulk, S. G. *J. Org. Chem.* **1995**, *60*, 7284–7289. (d) Georghiou, P. E.; Ashram, M.; Clase, H. J.; Bridson, J. N. *J. Org. Chem.* **1998**, *63*, 1819–1826.
13. Georghiou, P. E.; Li, Z.; Ashram, M. *J. Org. Chem.* **1998**, *63*, 3748–3752.
14. Poh, B.-L.; Lim, C. S.; Khoo, K. S. *Tetrahedron Lett.* **1989**, *30*, 1005–1008.
15. (a) Poh, B.-L.; Koay, L.-S. *Tetrahedron Lett.* **1990**, *31*, 1911–1914. (b) Poh, B.-L.; Seah, L. H.; Lim, C. S. *Tetrahedron* **1990**, *46*, 4379–4386; (c) Poh, B.-L.; Lim, C. S. *Tetrahedron* **1990**, *46*, 3651–3658; (d) Poh, B.-L.; Lim, C. H.; Tan, C. M.; Wong, W. M. *Tetrahedron* **1994**, *49*, 7259–7266. (e) Poh, B.-L.; Tan, C. M.

- Tetrahedron* **1993**, *49*, 9581–9592. (f) Poh, B.-L.; Tan, C. M. *Tetrahedron* **1994**, *50*, 3453–3462. (g) Poh, B.-L.; Tan, C. M. *J. Incl. Phenom. Macrocyclic Chem.* **2000**, *38*, 69–74.
16. (a) Du, B. A.; Li, Z. P.; Liu, C. H. *Angew. Chem. Int. Ed.* **2006**, *45*, 8022–8025. (b) Lioubashevski, O.; Chegel, V. I.; Patolsky, F.; Katz, E.; Willner, I. *J. Am. Chem. Soc.* **2004**, *126*, 7133–7143. (c) Wile, B. M.; Stradiotto, M. *Chem. Commun.* **2006**, 4104–4106.
17. (a) Chadhuri, R. G.; Paria, S. *Chem. Rev.* **2012**, *112*, 2373–2433. (b) Lu, A.-H.; Salabas, E. L.; Schuth, F. *Angew. Chem. Int. Ed.* **2007**, *46*, 1222–1244. (c) De, M.; Ghosh, P. S.; Rotello, V. M. *Adv. Mater.* **2008**, *20*, 4225–4241.
18. Kholoud, M. M.; El-Nour, A.; Eftaiha, A.; Al-Warthan, A.; Ammar, A. A. *Arab. J. Chem.* **2010**, *3*, 135–140.
19. (a) Sun, T.; Seff, K. *Chem. Rev.* **1994**, *94*, 857–870. (b) Xiong, D.; Chen, M. L.; Li, H. *Chem. Commun.* **2008**, 880–882. (c) Hussain, J. I.; Kumar, S.; Hashmi, A. A.; Khan, Z. *Adv. Mat. Lett.* **2011**, *2*, 188–194.
20. Kim, H. J.; Lee, M. H.; Mutihac, L.; Vicens, J.; Kim, J. S. *Chem. Soc. Rev.* **2012**, *41*, 1173–1190.
21. Peters, M. S.; Li, M.; Schrader, T. *Nat. Prod. Commun.* **2012**, *7*, 409–417.
22. Xiong, D.; Li, H. *Nanotechnol.* **2008**, *19*, 465502–465507.

23. (a) Tauran, Y.; Brioude, A.; Shahgaldian, P.; Cumbo, A.; Kim, B. J.; Perret, F.; Coleman, A. W.; Montasser, I. *Chem. Commun.* **2012**, *48*, 9483–9485. (b) Tauran, Y.; Brioude, A.; Kim, B.J.; Perret, F.; Coleman, A. W. *Molecules* **2013**, *18*, 5993–6007.
24. Iijima, S. *Nature* **1991**, *354*, 56–58.
25. (a) Tasis, D.; Tagmatarchis, N.; Bianco, A.; Prato, M. *Chem. Rev.* **2006**, *106*, 1105–1136. (b) Bacon, R. *J. Appl. Phys.* **1960**, *31*, 284–290. (c) Iijima, S.; Ichihashi, T. *Nature* **1993**, *363*, 603–605. (d) Bethune, D. S.; Kiang, C. H.; de Vries, M. S.; Gorman, G.; Savoy, R.; Vazquez, J.; Bevers, R. *Nature* **1993**, *363*, 605–607. (e) Robertson, N.; McGowan, C. A. *Chem. Soc. Rev.* **2003**, *32*, 96–103. (f) Dumitrescu, I.; Unwin, P. R.; Macpherson, J. V. *Chem. Commun.* **2009**, 6886–6901. (g) Galano, A. *Nanoscale* **2010**, *2*, 373–380.
26. (a) *Carbon Nanotubes: Synthesis, Structure, Properties, and Applications*; Dresselhaus, M. S.; Dresselhaus, G.; Avouris, Ph., Eds.; Springer: New York, 2001. (b) Ausman, K. D.; Piner, R.; Lourie, O.; Ruoff, R. S.; Korobov, M. *J. Phys. Chem. B* **2000**, *104*, 8911–8915. (c) Islam, M. F.; Rojas, E.; Bergey, D. M.; Johnson, A. T.; Yodh, A. G. *Nano Lett.* **2003**, *3*, 269–273.
27. (a) Zandonella, C. *Nature* **2001**, *410*, 734–735. (b) So, H.-M.; Won, K.; Kim, Y. H.; Kim, B.-K.; Ryu, B. H.; Na, P. S.; Kim, H.; Lee, J.-O. *J. Am. Chem. Soc.* **2005**, *127*, 11906–11907. (c) Panhuis, M. I. h.; Wu, J.; Ashraf, S. A.; Wallace, G. G. *Synth. Mat.* **2007**, *157*, 358–362.

28. (a) Omachi, H.; Nakayama, T.; Takahashi, E.; Segawa, Y.; Itami, K. *Nat. Chem.* **2013**, *5*, 572–576. (b) Yu, X.; Zhang, J.; Choi, W.; Choi, J.-Y.; Kim, J. M.; Gan, L.; Liu, Z. *Nano Lett.* **2010**, *10*, 3343–3349. (c) Jasti, R.; Bhattacharjee, J.; Neaton, J. B.; Bertozzi, C. R. *J. Am. Chem. Soc.* **2008**, *130*, 17646–17647.
29. Aliev, A. E.; Oh, J.; Kozlov, M. E.; Kuznetsov, A. A.; Fang, S.; Fonseca, A. F.; Ovalle, R.; Lima, M. D.; Haque, M. H.; Gartstein, Y. N.; Zhang, M.; Zakhidov, A. A.; Baughman, R. H. *Science* **2009**, *323*, 1575–1578.
30. (a) Hirsch, A. *Angew. Chem. Int. Ed.* **2002**, *41*, 1853–1859. (b) Bahr, J. L.; Tour, J. M. *J. Mater. Chem.* **2002**, *12*, 1952–1958. (c) Banerjee, S.; Hemray-Benny, T.; Wong, S. *Adv. Mater.* **2005**, *17*, 17–29.
31. (a) Zhao, J.; Park, H.; Han, J.; Lu, J. P. *J. Phys. Chem. B.* **2004**, *108*, 4227–4230. (b) Fagan, S. B.; da Silva, A. J. R.; Mota, R.; Baierle, R. J.; Fazzio, A. *Phys. Rev. B.* **2003**, *67*, 33405–33408.
32. Zhang, J.; Zou, H.; Qing, Q.; Yang, Y.; Li, Q.; Liu, Z.; Guo, X.; Du, Z. *J. Phys. Chem. B.* **2003**, *107*, 3712–3718.
33. Gromov, A.; Dittmer, S.; Svensson, J.; Nerushev, O. A.; Perez-Garcia, S. A.; Licea-Jimenez, L.; Rychwalski, R.; Campbell, E. E. B. *J. Mater. Chem.* **2005**, *15*, 3334–3339.
34. Li, H.; Cheng, F.; Duft, A. M.; Adronov, A. *J. Am. Chem. Soc.* **2005**, *127*, 14518–14524.

35. Palacin, T.; Khanh, H. L.; Joussetme, B.; Jegou, P.; Filoramo, A.; Ehli, C.; Guldi, D. M.; Campidelli, S. P. *J. Am. Chem. Soc.* **2009**, *131*, 15394–15402.
36. (a) Cabana, J.; Martel, R. *J. Am. Chem. Soc.* **2007**, *129*, 2244–2245. (b) Cognet, L.; Tsyboulski, D. A.; Rocha, J.-D. R.; Doyle, C. D.; Tour, J. M.; Weisman, R. B. *Science* **2007**, *316*, 1465–1468.
37. (a) O'Connell, M. J.; Bachilo, S. M.; Huffman, C. B.; Moore, V. C.; Strano, M. S.; Haroz, E. H.; Rialon, K. L.; Boul, P. J.; Noon, W. H.; Kittrell, C.; Ma, J.; Hauge, R. H.; Weisman, R. B.; Smalley, R. E. *Science* **2002**, *297*, 593–596. (b) Zheng, M.; Jagota, A.; Semke, E. D.; Diner, B. A.; McLean, R. S.; Lustig, S. R.; Richardson, R. E.; Tassi, N. G. *Nat. Mater.* **2003**, *2*, 338–342.
38. (a) Star, A.; Stoddart, J. F.; Steuerman, D.; Diehl, M.; Boukai, A.; Wong, E. W.; Yang, X.; Chung, S.-W.; Choi, H.; Heath, J. R. *Angew. Chem. Int. Ed.* **2001**, *40*, 1721–1725. (b) Nakayama-Ratchford, N.; Bangsaruntip, S.; Sun, X.; Welsher, K.; Dai, H. *J. Am. Chem. Soc.* **2007**, *129*, 2448–2449. (c) Chen, R. J.; Zhang, Y.; Wang, D.; Dai, H. *J. Am. Chem. Soc.* **2001**, *123*, 3838–3839. (d) Li, H.; Zhou, B.; Lin, Y.; Gu, L.; Wang, W.; Fernando, K. A. S.; Kumar, S.; Allard, L. F.; Sun, Y.-P. *J. Am. Chem. Soc.* **2004**, *126*, 1014–1015.
39. Zhang, Z.; Che, Y.; Smaldone, R. A.; Xu, M.; Bunes, B. R.; Moore, J. S.; Zang, L. *J. Am. Chem. Soc.* **2010**, *132*, 14113–14117.
40. Liang, S.; Chen, G.; Peddle, J.; Zhao, Y. *Chem. Commun.* **2012**, *48*, 3100–3102.

41. (a) Moore, V. C.; Strano, M. S.; Haroz, E. H.; Hauge, R. H.; Smalley, R. E.; Schmidt, J.; Talmon, Y. *Nano Lett.* **2003**, *3*, 1379–1382. (b) Bronikowski, M. J.; Willis, P. A.; Colbert, D. T.; Smith, K. A.; Smalley, R. E. *J. Vac. Sci. Technol. A.* **2001**, *19*, 1800–1805.
42. Tummala, N. R.; Morrow, B. H.; Resaco, D. E.; Striolo, A. *ACS Nano.* **2010**, *4*, 7193–7204.
43. Romero-Nieto, C.; Garcia, R.; Herranz, M. A.; Rodriguez-Perez, L.; Sanchez-Navarro, M.; Rojo, J.; Martin, N.; Guldi, D. M. *Angew. Chem. Int. Ed.* **2013**, *52*, 10216–10220.
44. (a) Avouris, P.; Chen, Z.; Perebeinos, V. *Nat. Nanotechnol.* **2007**, *2*, 605–615. (b) Mutlu, G. K. M.; Budinger, G. R. S.; Green, A. A.; Urich, D.; Soberanes, S.; Chiarella, S. E.; Alheid, G. F.; McCrimmon, D. R.; Szleifer, I.; Hersam, M. C.; *Nano Lett.* **2010**, *10*, 1664–1670. (c) Calvert, P. *Nature* **1999**, *399*, 210–211.
45. (a) Valluru, G. K.; Georghiou, P. E.; Sleem, H. F.; Perret, F.; Montasser, I.; Grandvoinet, A.; Brolles, L.; Coleman, A. W. *Supramol chem* **2014**, *26*, 561–568. (b) Georghiou, P. E.; Valluru, G. K.; Schneider, C.; Liang, S.; Woolridge, K. Mulla, K.; Adronov, A.; Zhao, Y. *RSC Adv.* **2014**, *4*, 31614–31617.
46. Buglass, A. J.; Tillett, J. G. *In The Chemistry of Sulfonic Acids, Esters and Their Derivatives*, Patai, S., Ed.; Wiley: Toronto 1991.
47. Poh, B.-L.; Tan, C. M.; Loh, C. L. *Tetrahedron* **1993**, *49*, 3849–3856.
48. Cameron, K. S.; Fielding, L. *J. Org. Chem.* **2001**, *66*, 6891–6895.

49. Schultz, S. G.; Solomon, A. K. *J. Gen. Physiol.* **1961**, *44*, 1189–1199.
50. *Spartan'10* molecular modeling program from Wavefunction, Inc., Irvine, CA, USA was used to estimate the molecular volumes of hydrated CTCT structures.
51. Tauran, Y.; Grosso, M.; Brioude, A.; Kassab, R.; Coleman, A. W. *Chem. Commun.* **2011**, *47*, 10013–10015.
52. Selkti, M.; Tomas, A.; Coleman, A. W.; Douteau-Guevel, N.; Nicolis, I.; Villain, F.; de Rango, C. *Chem. Commun.* **2000**, 161–162.
53. For the RBM features: (a) Maultzsch, J.; Telg, H.; Reich, S.; Thomsen, C. *Phys. Rev. B: Condens. Matter Mater. Phys.* **2005**, *72*, 205438. (b) Alvarez, L.; Righi, A.; Guillard, T.; Rols, S.; Anglaret, E.; Laplaze D.; Sauvajol, J. L. *Chem. Phys. Lett.* **2000**, *316*, 186–190. (c) Jorio, A.; Pimenta, M. A.; Souza Filho, A. G.; Saito, R.; Dresselhaus, G.; Dresselhaus, M. S.; *New. J. Phys.* **2003**, *5*, 139.1–139.17.
54. Fukami, T.; Mugishima, A.; Suzuki, T.; Hidaka, S.; Endo, T.; Ueda, H.; Tomono, K. *Chem. Pharm. Bull.* **2004**, *52*, 961–964.
55. Deguchi, S.; Mukai, S.; Tsudome, M.; Horikoshi, K. *Adv. Mater.* **2006**, *18*, 729.
56. Ling, I.; Alias, Y.; Raston, C. L. *New. J. Chem.* **2011**, *35*, 1549–1555.

Chapter 6

6.1 Summary and conclusions

In conclusion, the syntheses of several bimodal upper- and lower-rim functionalized calix[4]arenes and calix[4]naphthalene derivatives have been accomplished. Their complexation properties with some Group 1, 2 and transition metal cation guests were examined.

In the first project, three new bimodal upper- and lower-rim functionalized calix[4]arenes **70**, **71** and **72** were synthesized. The upper rims of **70** and **71** were functionalized with thioacetate groups which allowed the calix[4]arene to form a stable self-assembled monolayer (SAM) onto a Au surface, characterization of which was accomplished by Scanning Tunneling Microscopy (STM). The lower rims of these calix[4]arenes were modified with *O*-methyl and *O*-ethyl ester groups. Microcantilevers functionalized with the bimodal calix[4]arene **70** were capable of detecting calcium ion concentrations as low as 10^{-11} M in aqueous solutions. The thioacetate-bearing calix[4]arene **70** was shown to be a sensitive calcium ion sensor. Also based on $^1\text{H-NMR}$ titration experiments of **70** and **71** with various Group 2 ions, the ester functional groups of **70** and **71** were found to bind selectively to Ca^{2+} ions.

The lower rim of the calix[4]arene **72** is functionalized with two different groups, one of which is a "crown-5" ether type and the other two positions have thioacetate groups. The thioacetate group enables **72** to form a stable SAM onto a Au surface, and

the resulting SAM has been characterized by STM. The “crown-5” group selectively binds to Group 1 ions and forms a sensitive cesium ion MCL sensor. Calix[4]arene **72** was unexpectedly formed preferentially in a *cone* conformation.

In the second project, the syntheses of anthracene- and pyrene-appended triazole-based calix[4]arene derivatives **98** and **99** were accomplished. The lower rim of **98** was functionalized with anthracene-appended triazole moieties and the upper rim was modified with thioacetate functionality which allows the **98** to form a stable SAM on a Au surface. Complexation studies and association/binding constants of **98** with different metal ions were investigated by fluorescence, UV-vis and ¹H-NMR spectroscopic techniques. The fluorescence studies proved that **98** shows high binding selectivity for Hg²⁺ and Fe³⁺ over the other metal ions tested

Using this new bimodal calix[4]arene **99**, complexation studies were also undertaken with various metal ions including the calculation of the association/binding constants for the complexes using two methods (i.e. Thordarson and B-H methods) for comparison. Binding of Cd²⁺ and Zn²⁺ occurs, as demonstrated by an enhanced monomer and declining excimer emission fluorescence spectral changes. On the other hand, upon addition of Fe³⁺ or Hg²⁺, and several other metal ions tested, quenching of both monomer and excimer emission of **99** was observed. Calix[4]arene **99** selectively binds to Fe³⁺ and Cd²⁺ ions and is thus an effective fluorescent chemosensor. The microcantilever studies of **71** and **98** are currently on-going in the Beaulieu Laboratories at MUN.

In the third project, a new imidazole calix[4]arene derivative **117** has been synthesized and characterized. Since it is not possible to generate *N*-heterocyclic carbenes

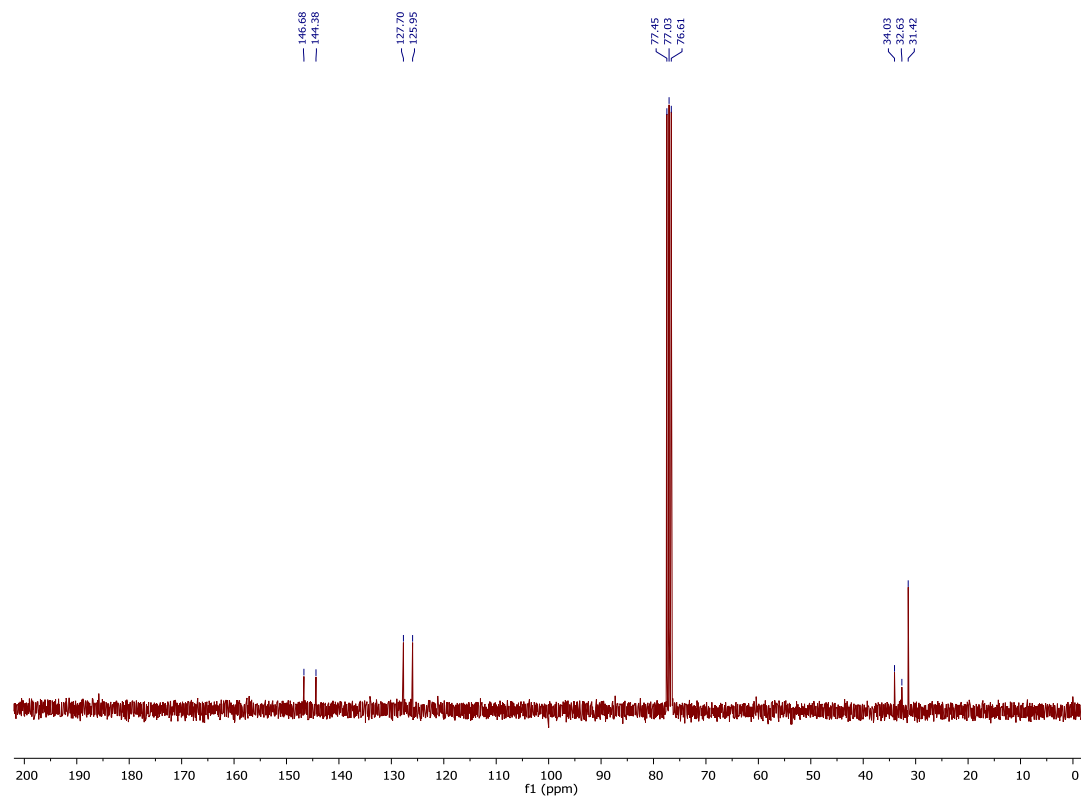
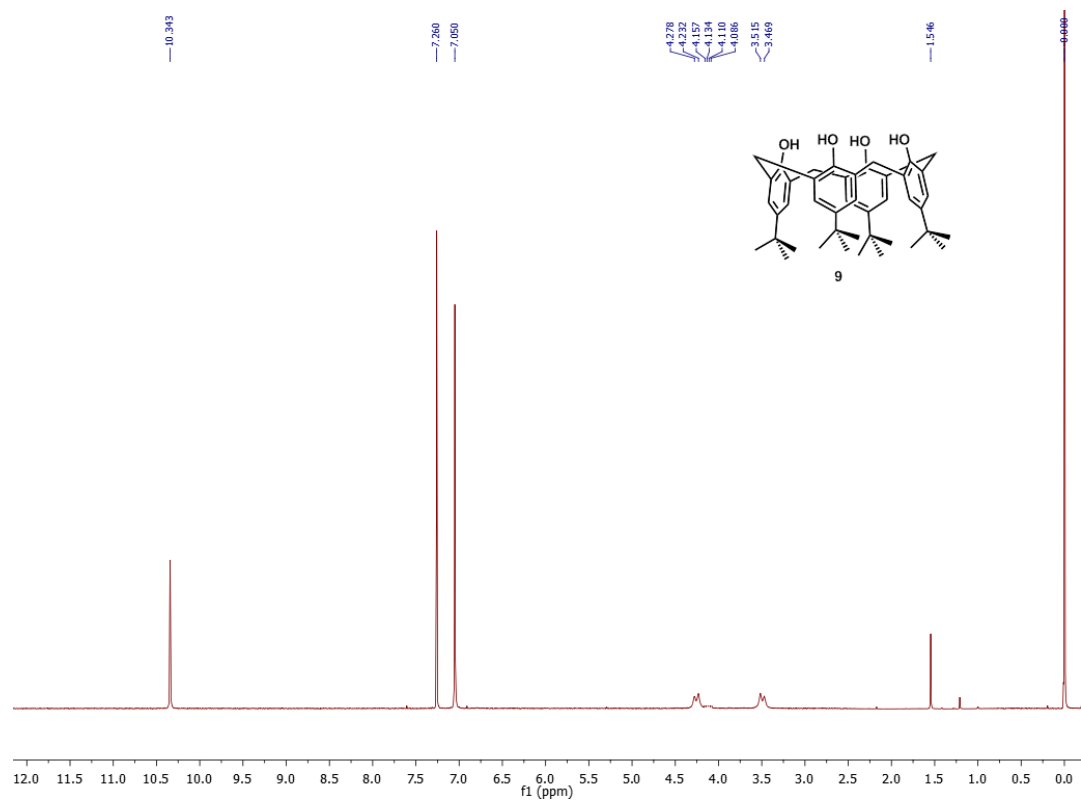
from this compound, the synthesis of the corresponding *N*-methylimidazole calix[4]arene **118** and the attempts at the generation of the corresponding dicarbene from **118** remain to be conducted. An alternative approach for the synthesis of calix[4]arene **113** and the corresponding *de-tert*-butyl analogues are also currently on-going and remain to be explored in future experiments.

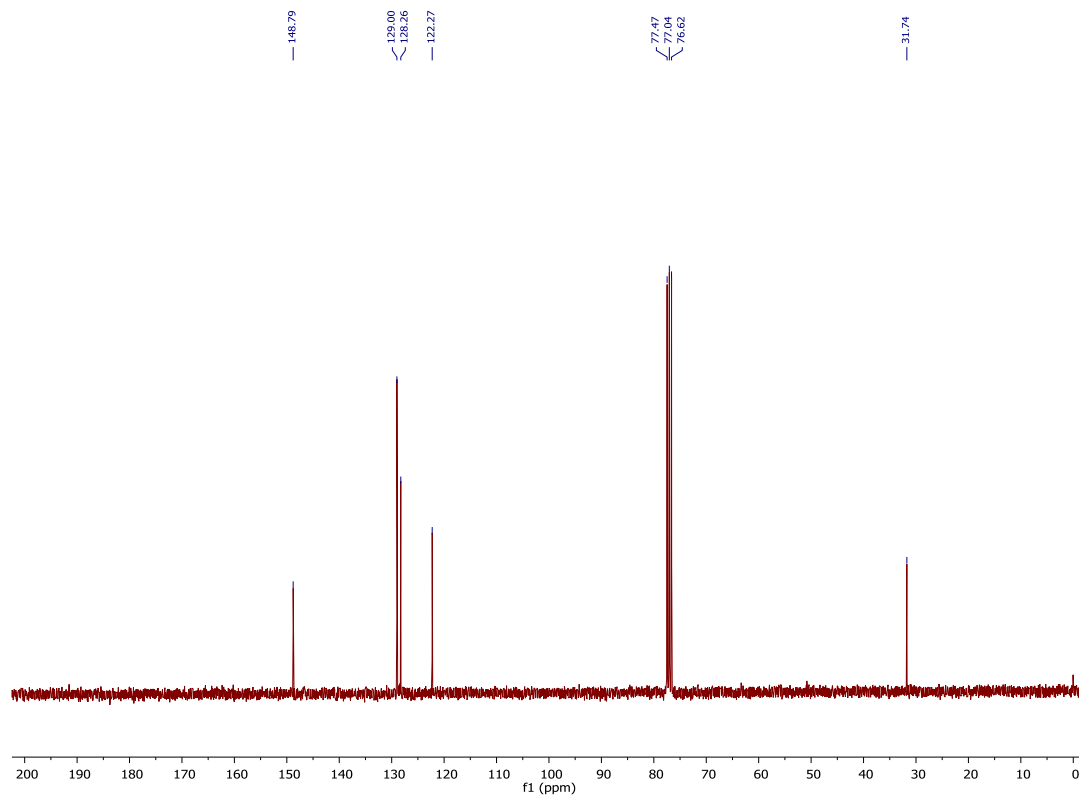
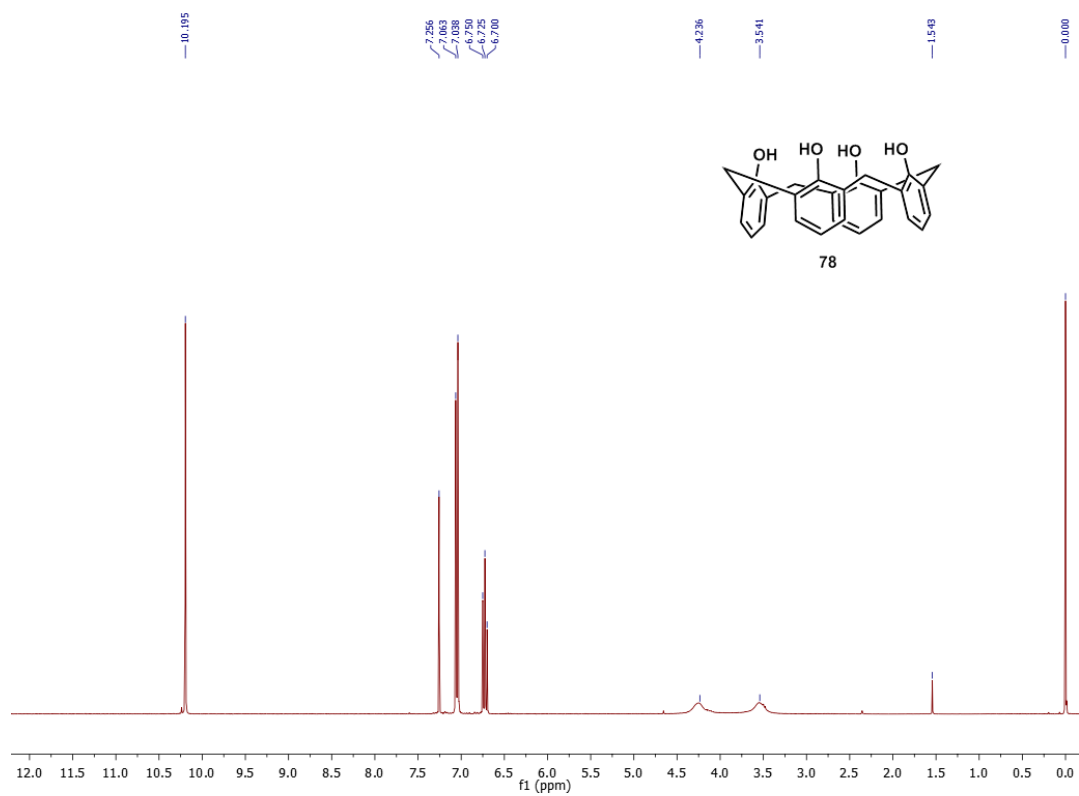
In the fourth project, three sulfonated calix[4]naphthalenes **124**, **125**, and **137** were synthesized. All were found to be capable of capping and stabilizing silver nanoparticles (AgNPs). For the AgNPs capped with **137**, however, complexation of both amino acids and nucleobases occurs. Of particular interest is the selective complexation of the aromatic amino acids tryptophan and phenylalanine. Compound **125** or cyclotetrachromotropylen (–CTCT–) which is a water-soluble cyclic tetramer was found to be capable of selectively dispersing SWNTs into the aqueous phase. The resulting supramolecular complexes in aqueous solution were characterized by UV-Vis-NIR analysis, while the dried aggregates were examined by Raman spectroscopy and atomic force microscopy (AFM). For future work the dispersion of SWNTs using disodium salt of chromotropic acid (DSCTA, **139**) in different solvents will be carried out in collaboration with Dr. Y. Zhao's group at MUN.

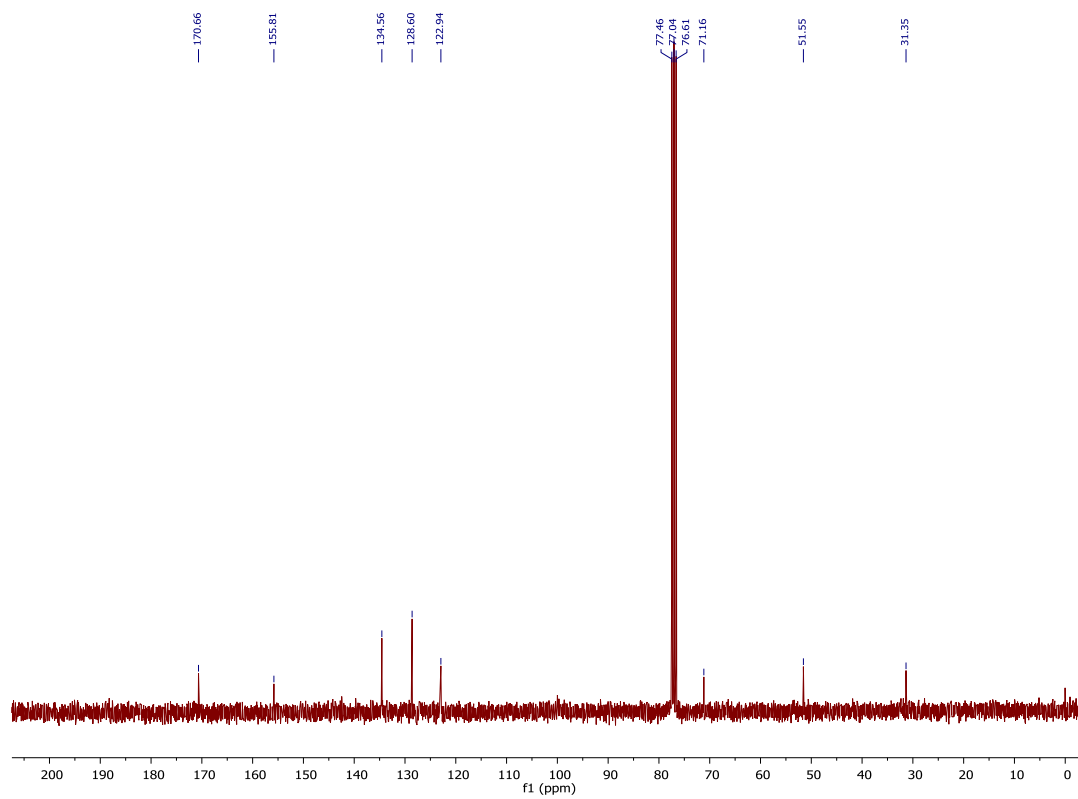
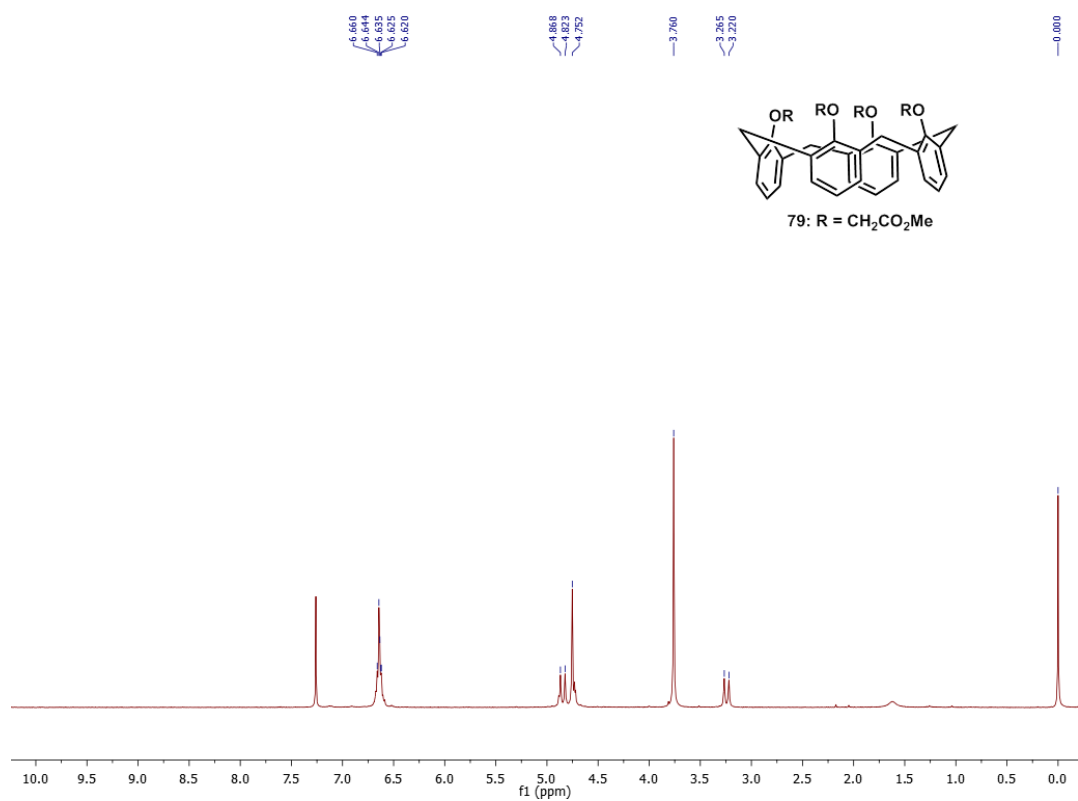
Each Chapter includes brief suggestions/recommendations for future work in the respective projects.

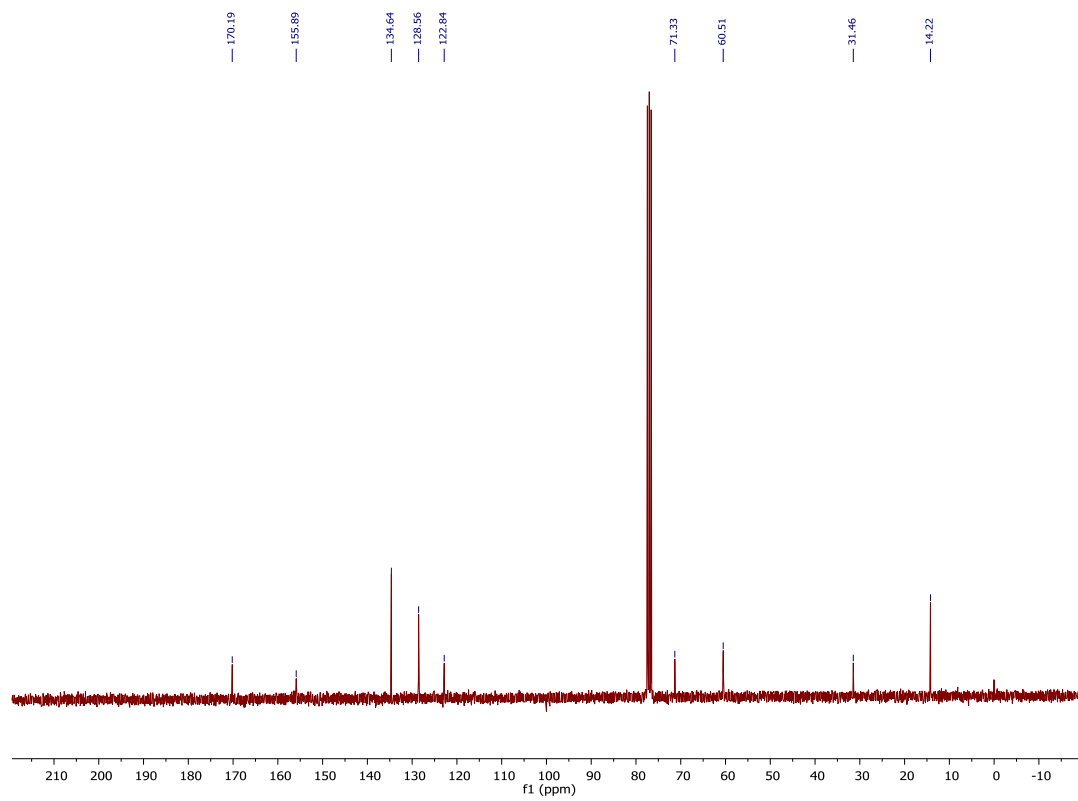
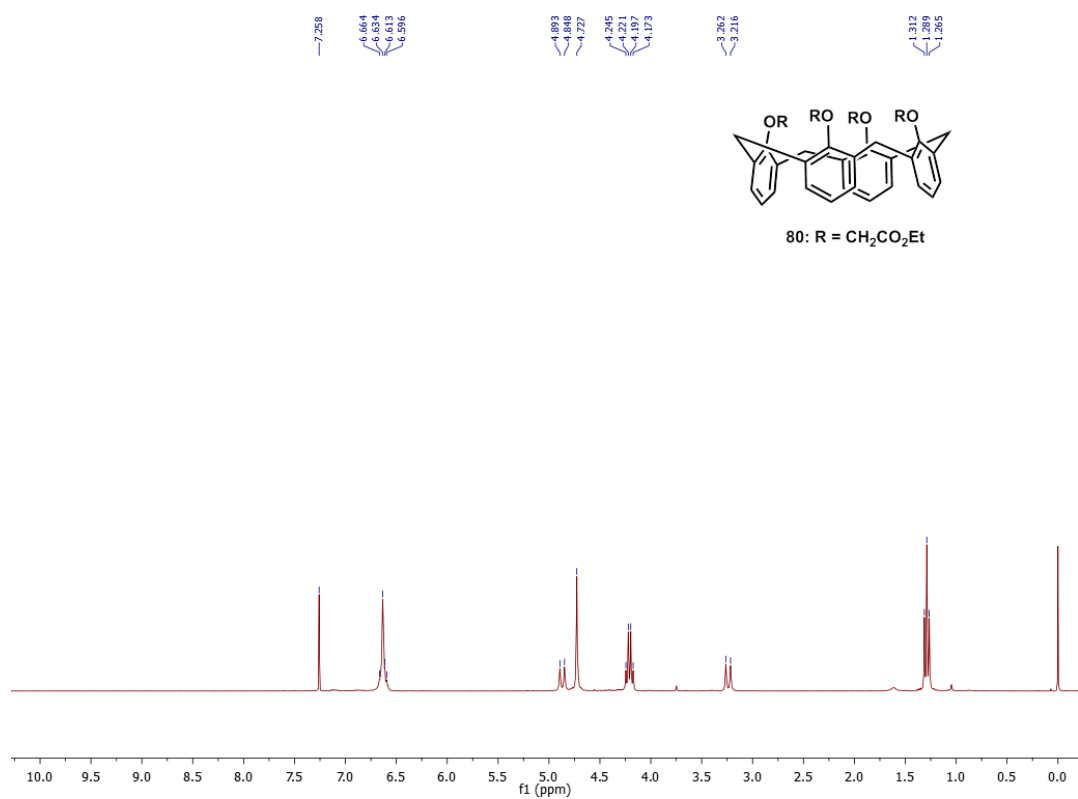
Appendix A

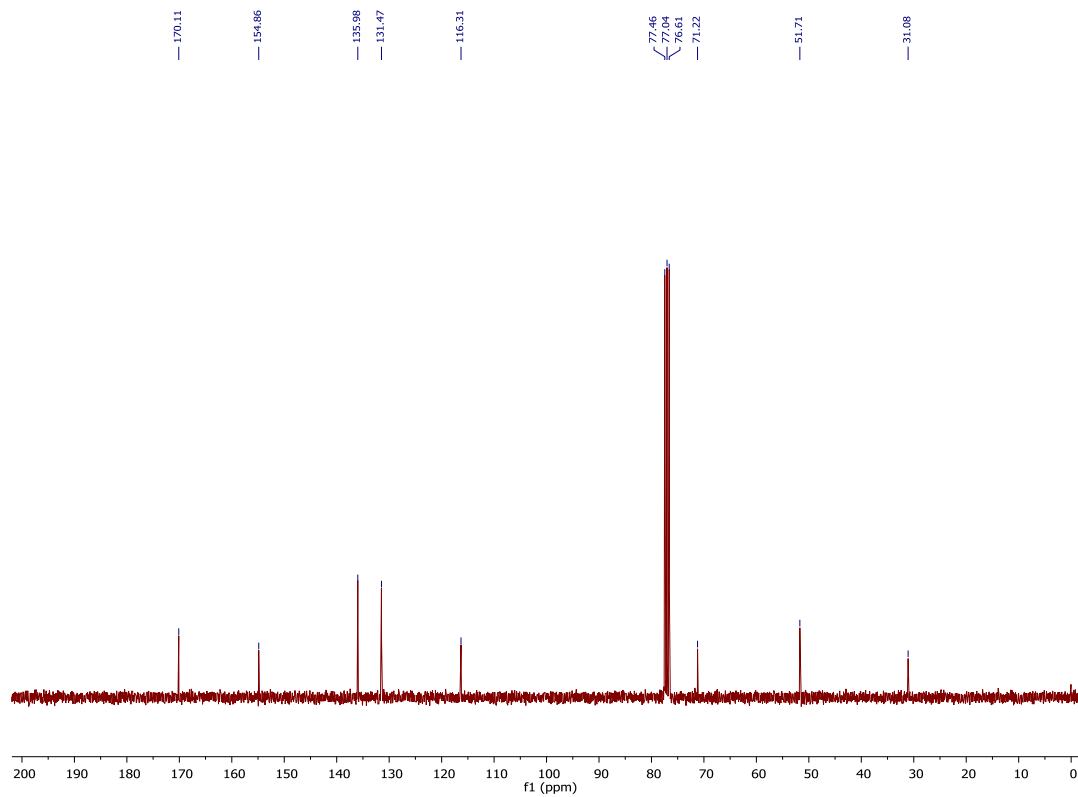
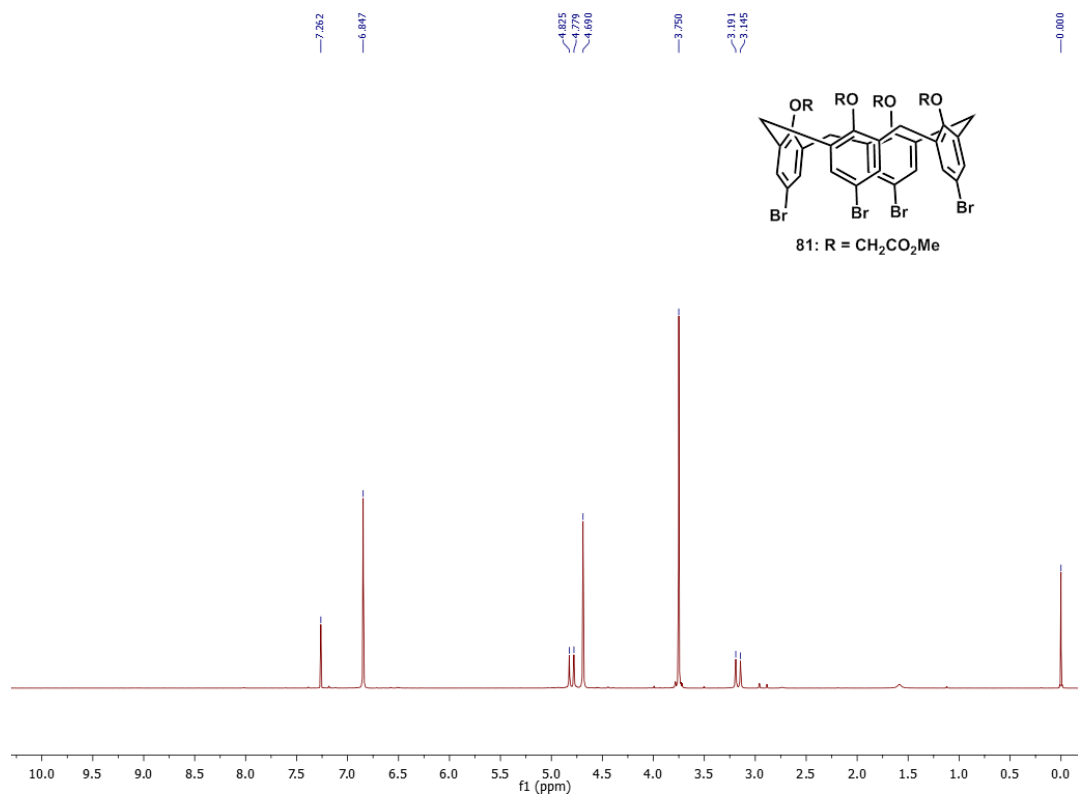
^1H - and ^{13}C -NMR spectra and X-ray crystallographic data
for compounds described in **Chapter 2**

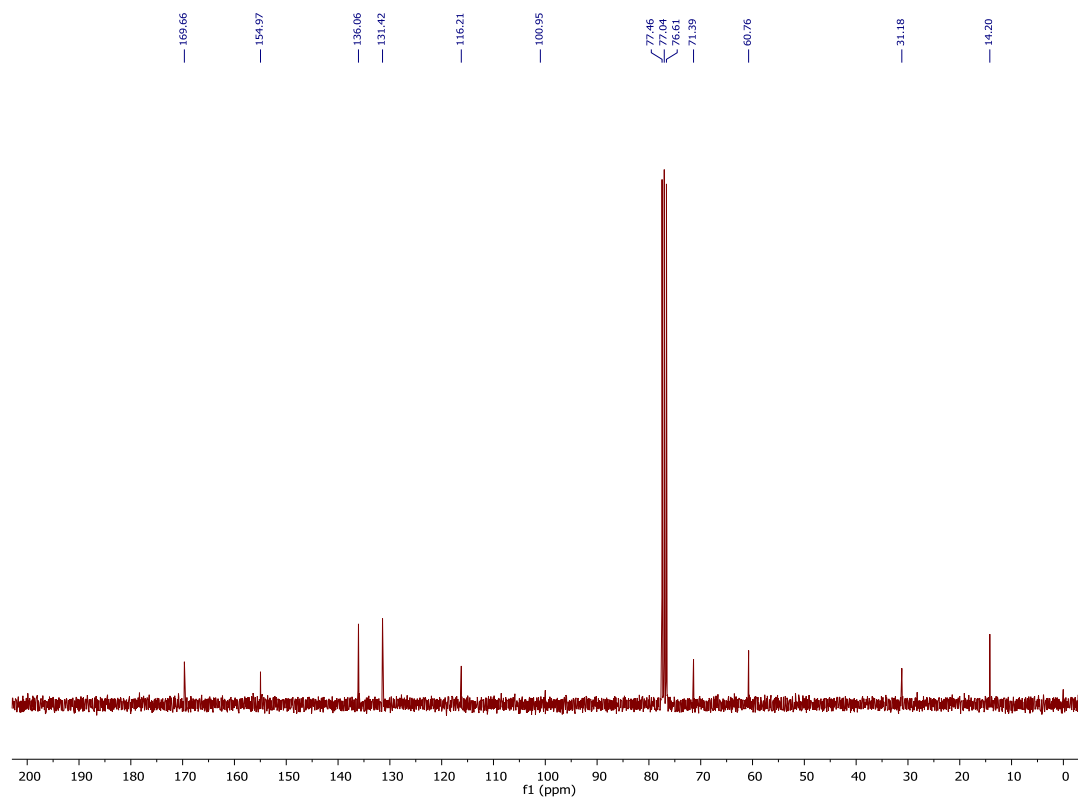
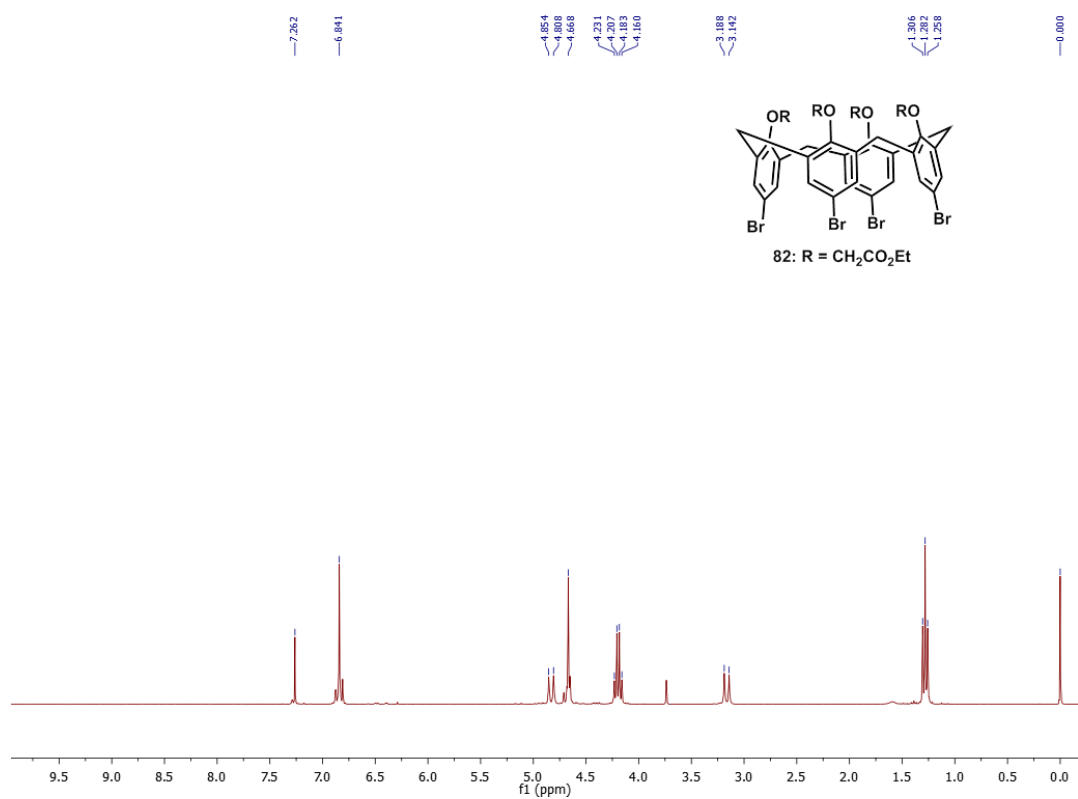


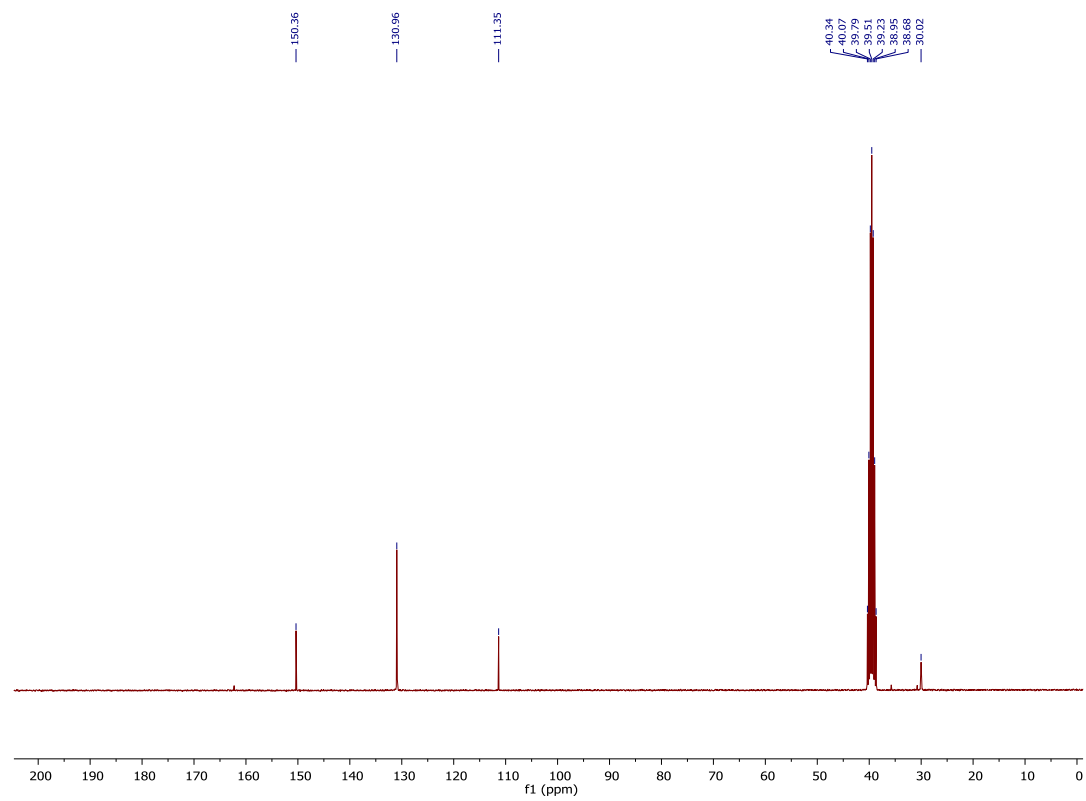
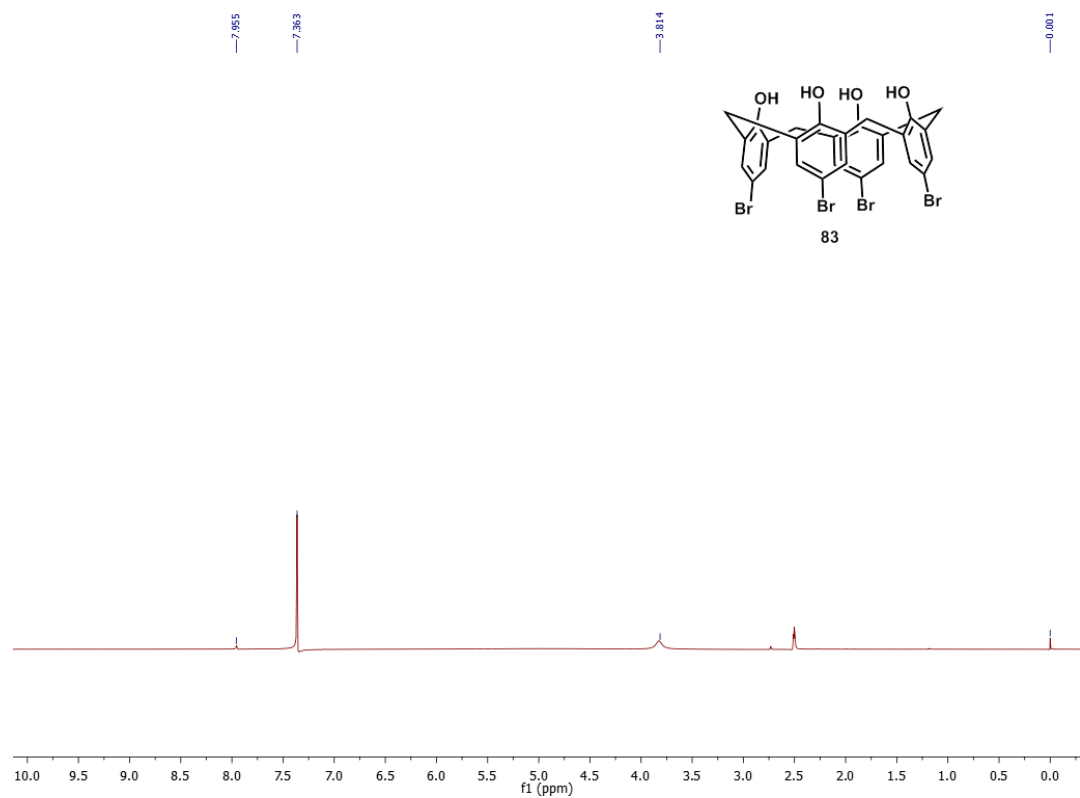


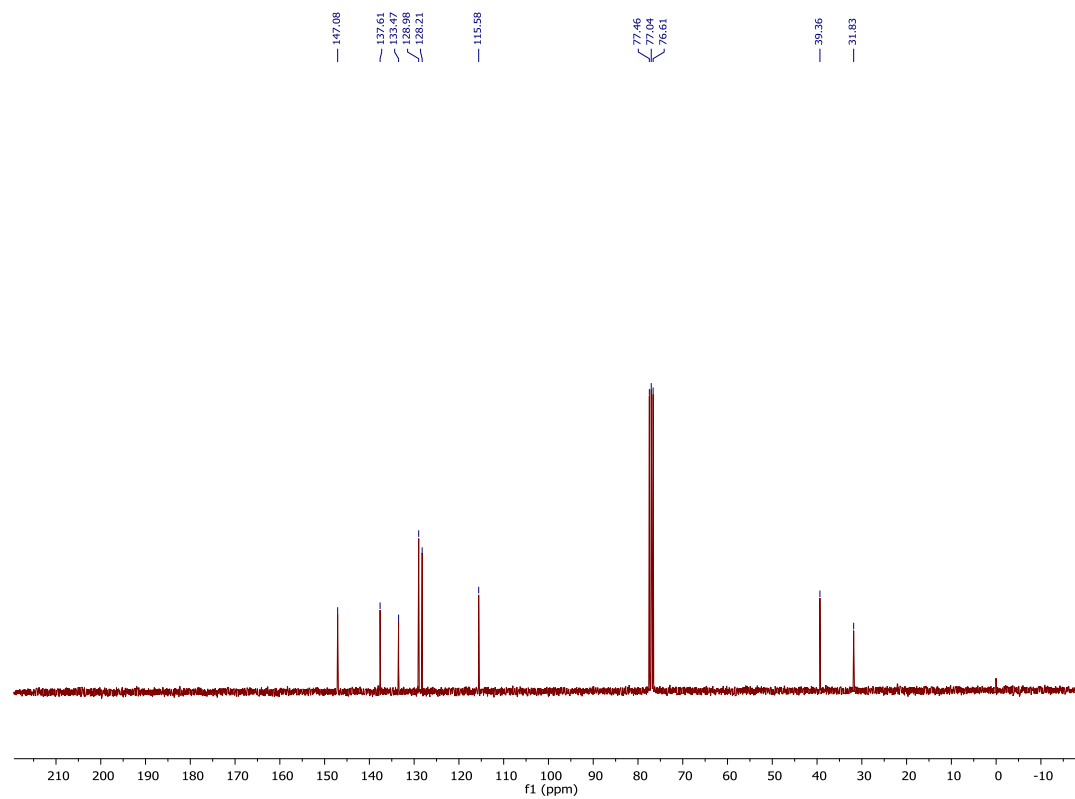
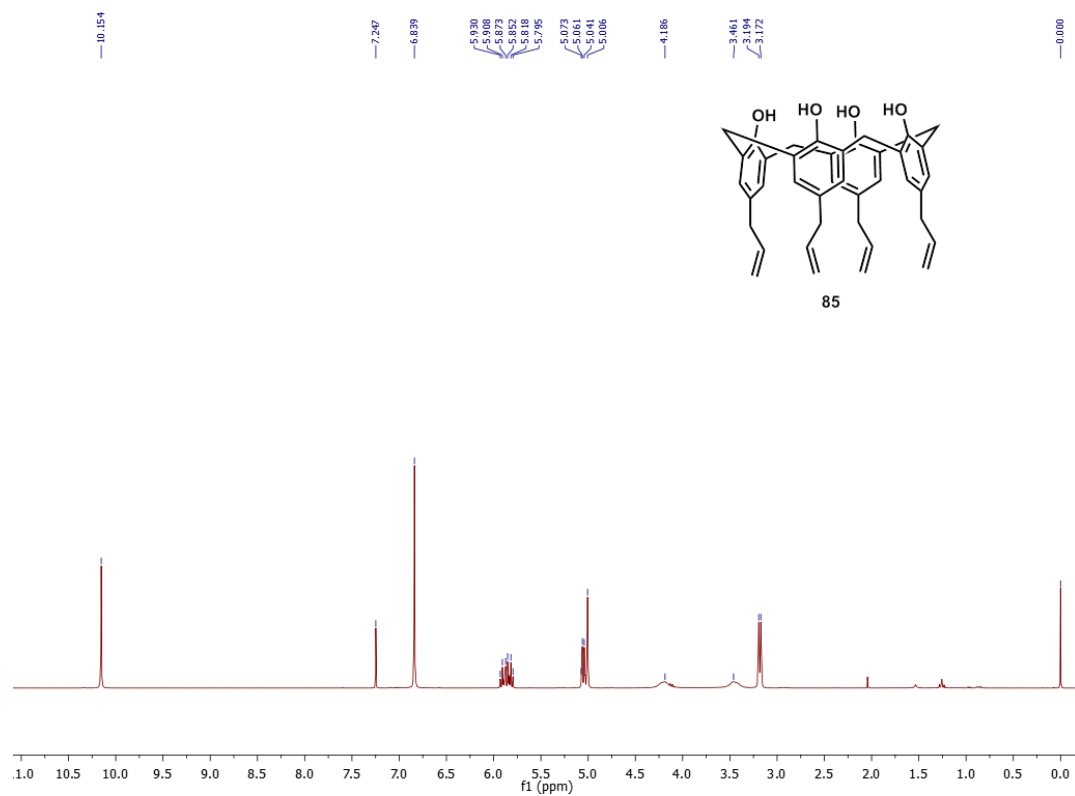


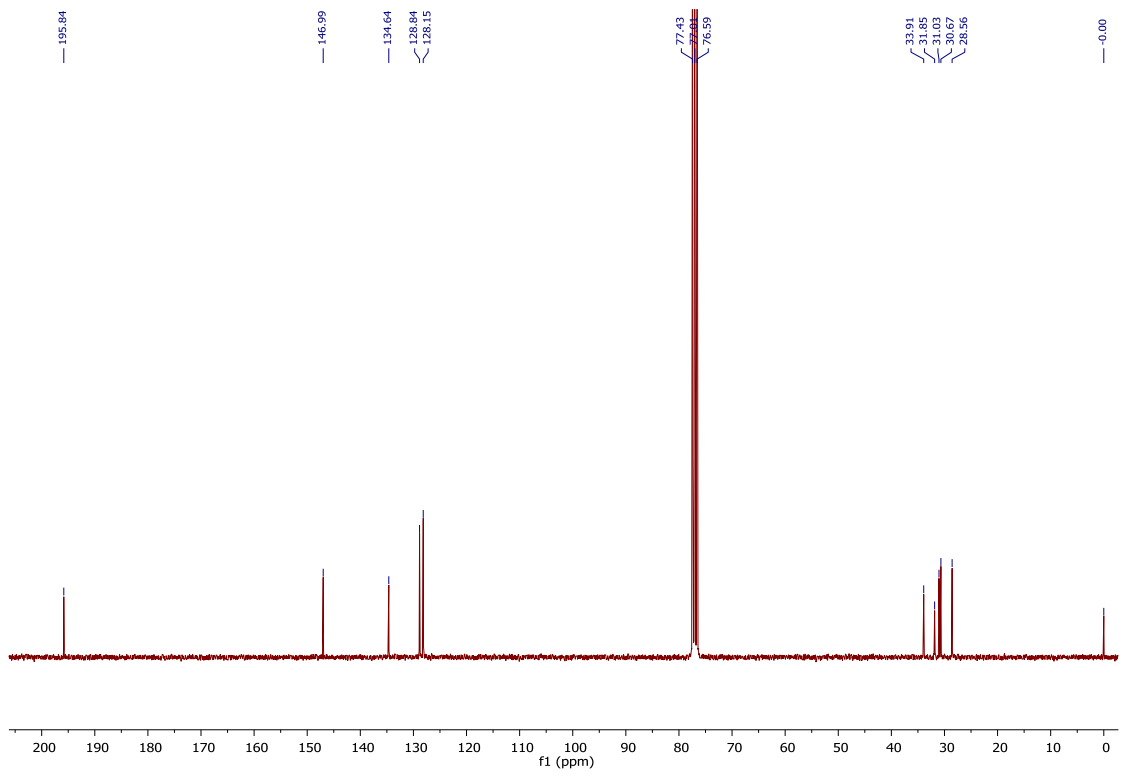
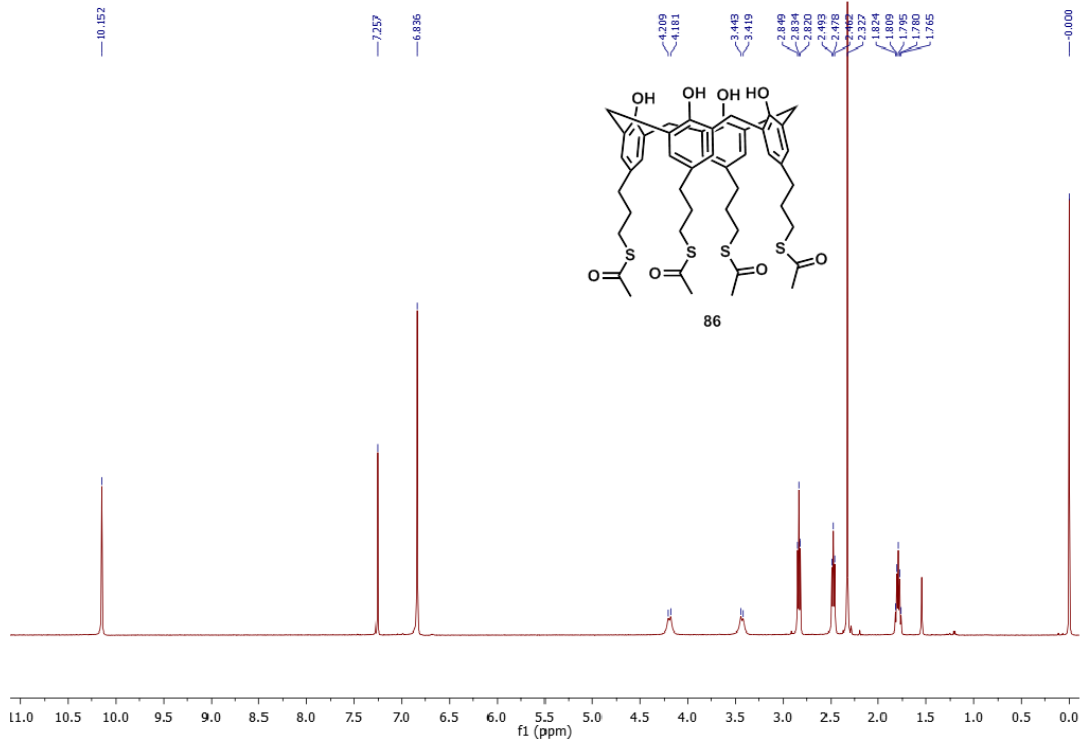


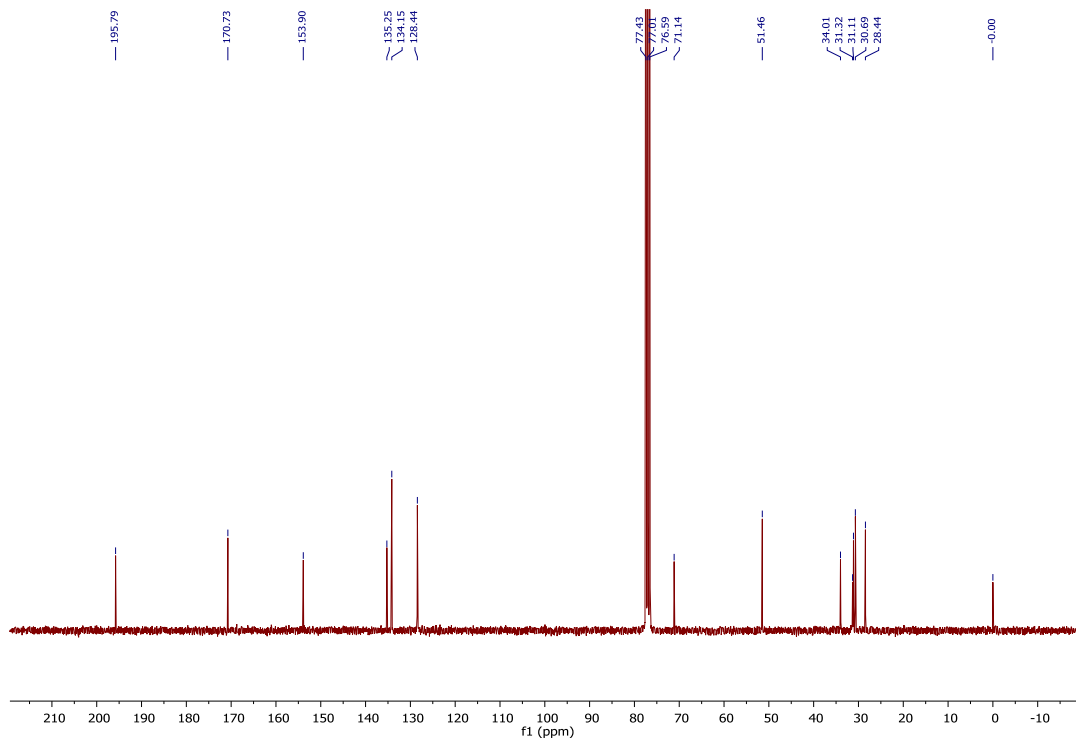
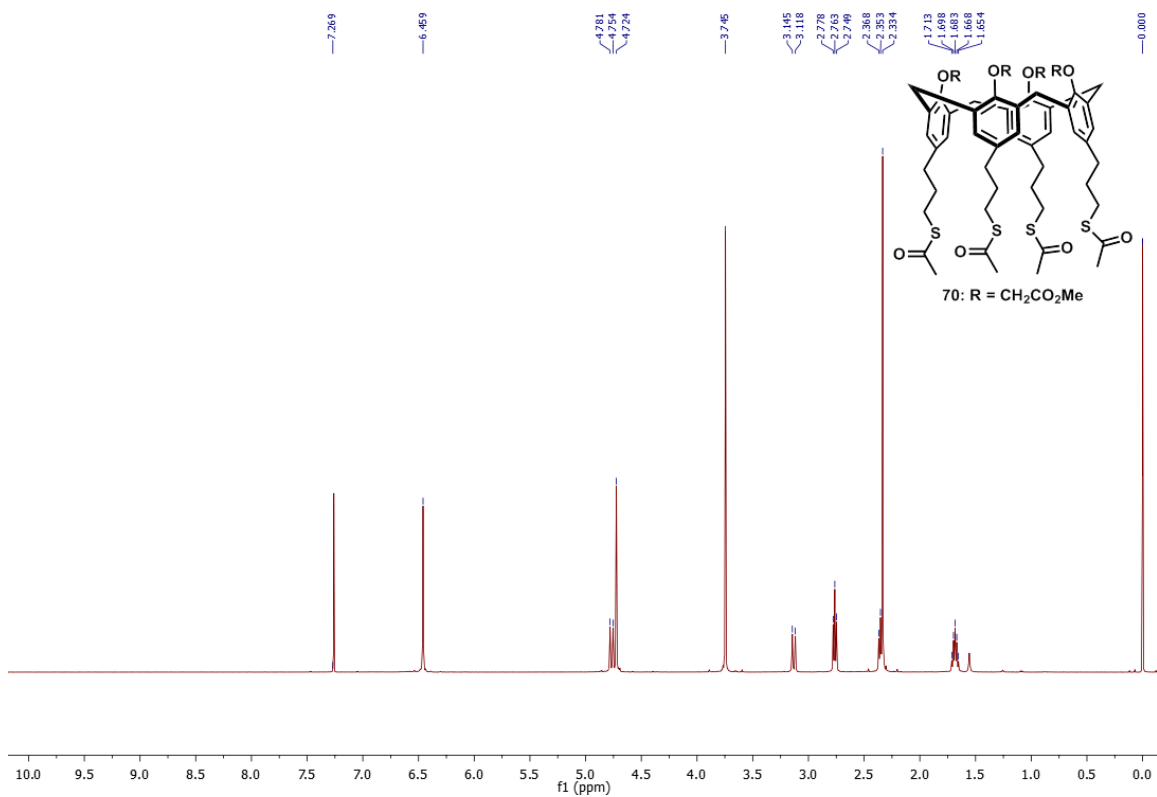


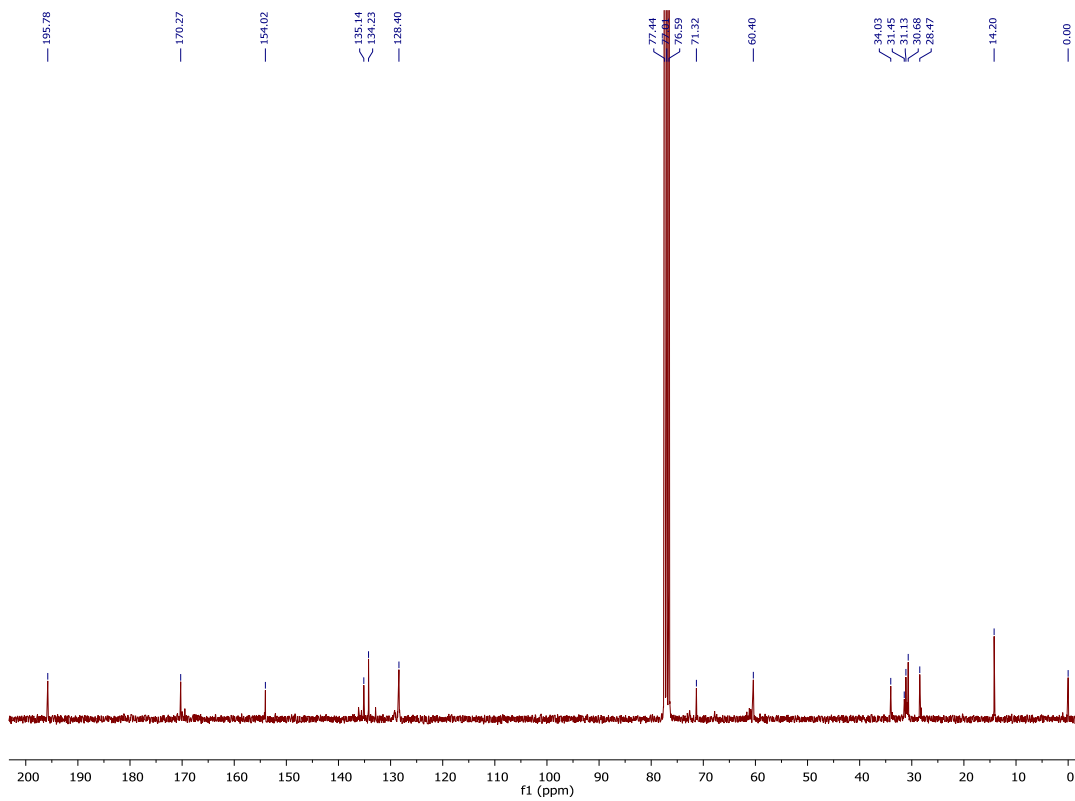
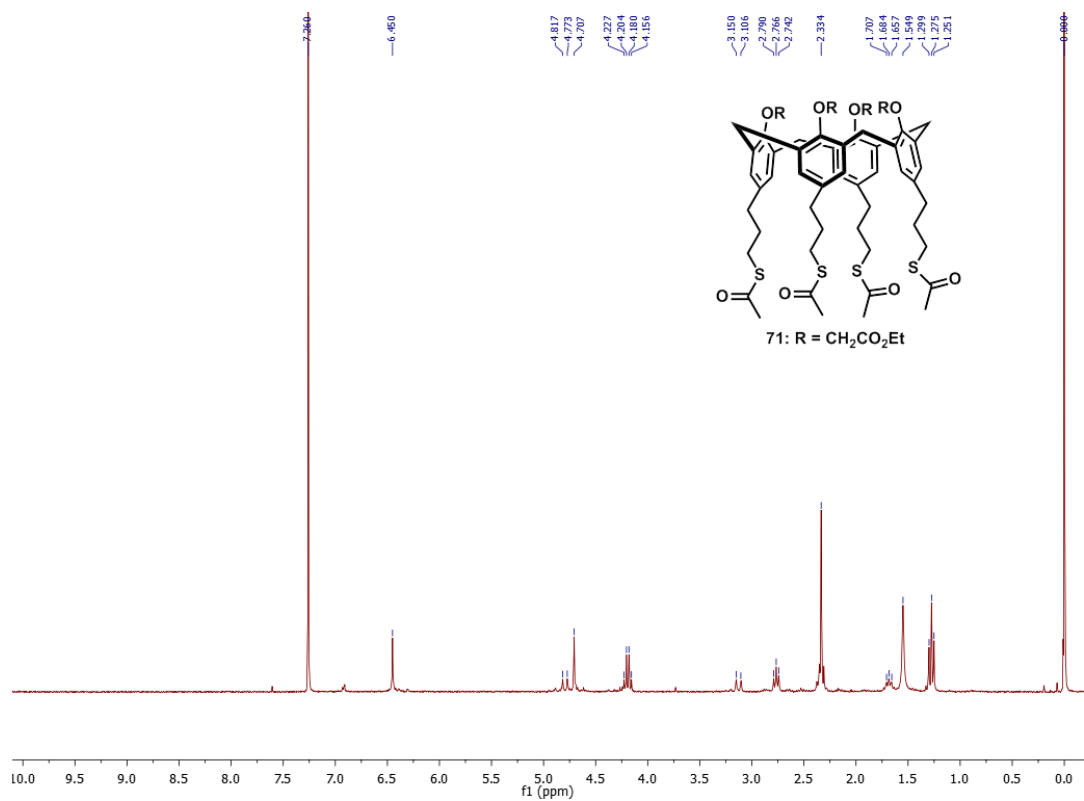


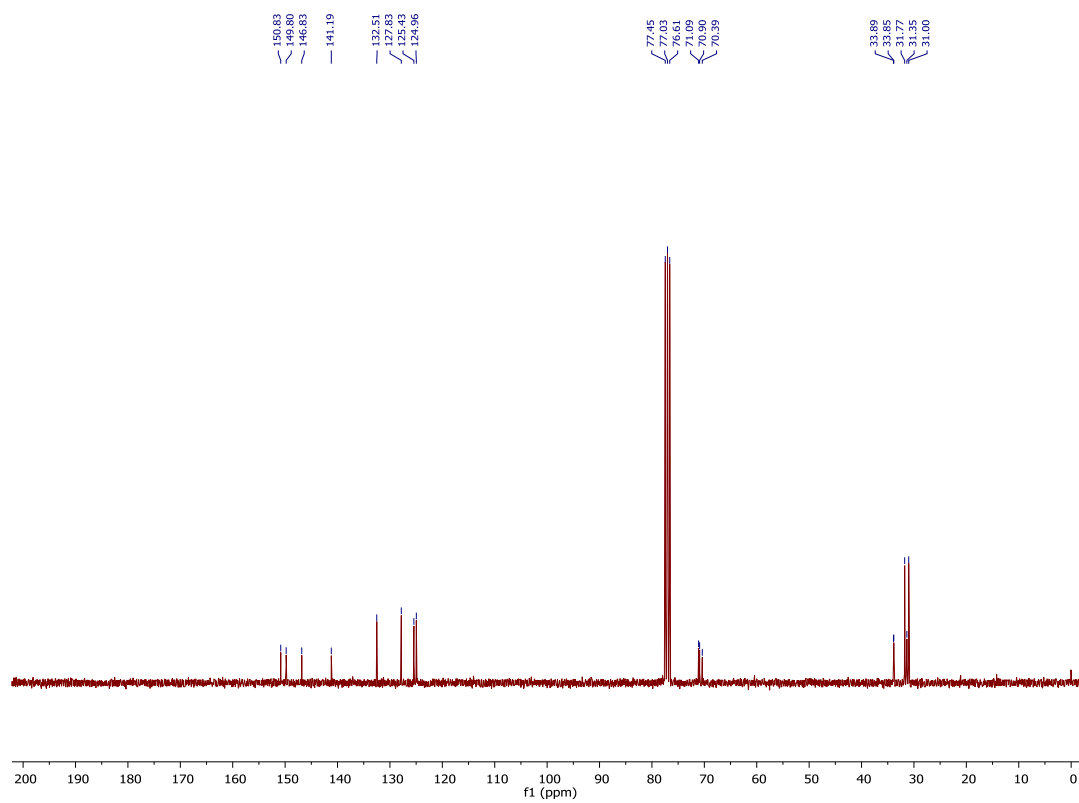
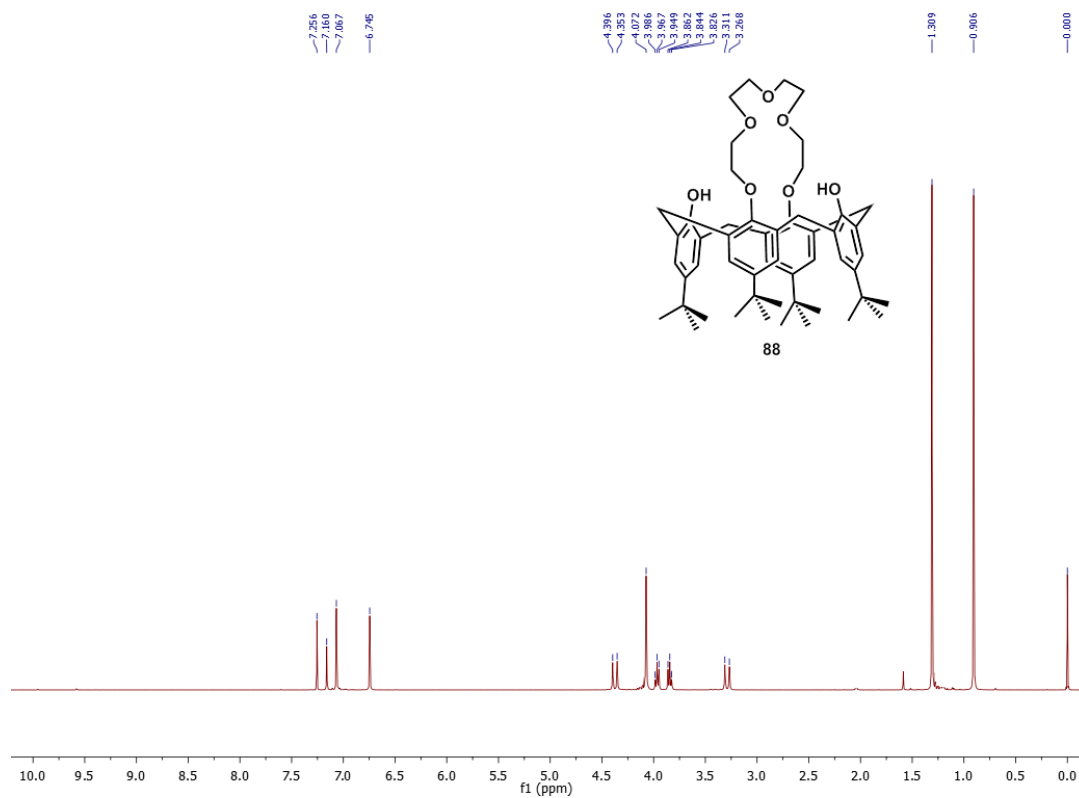


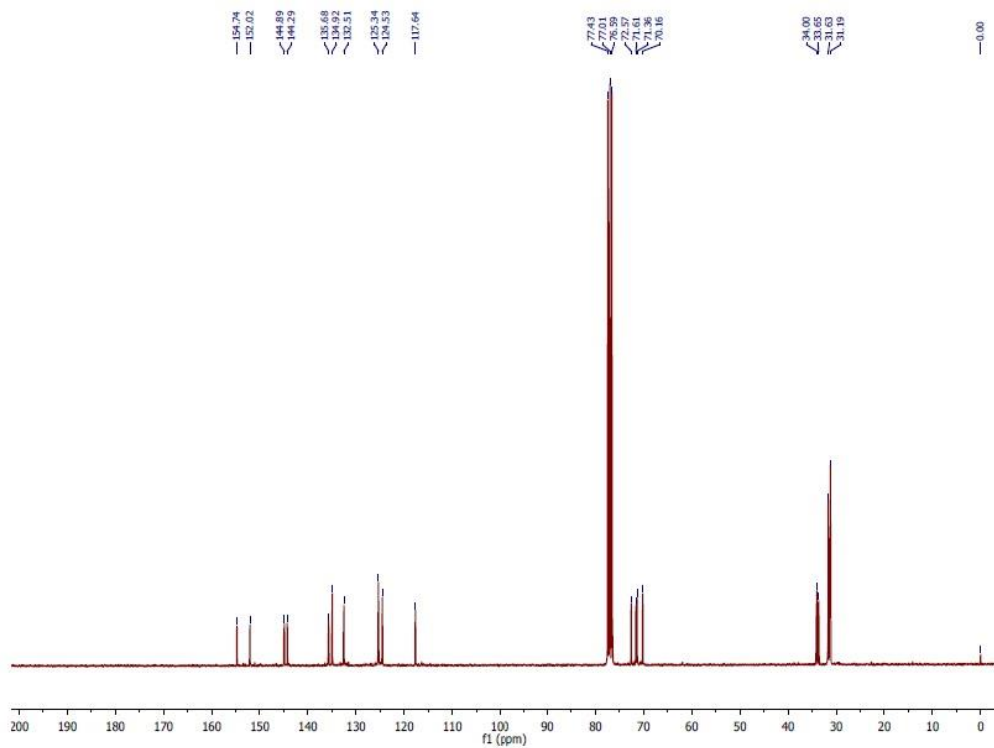
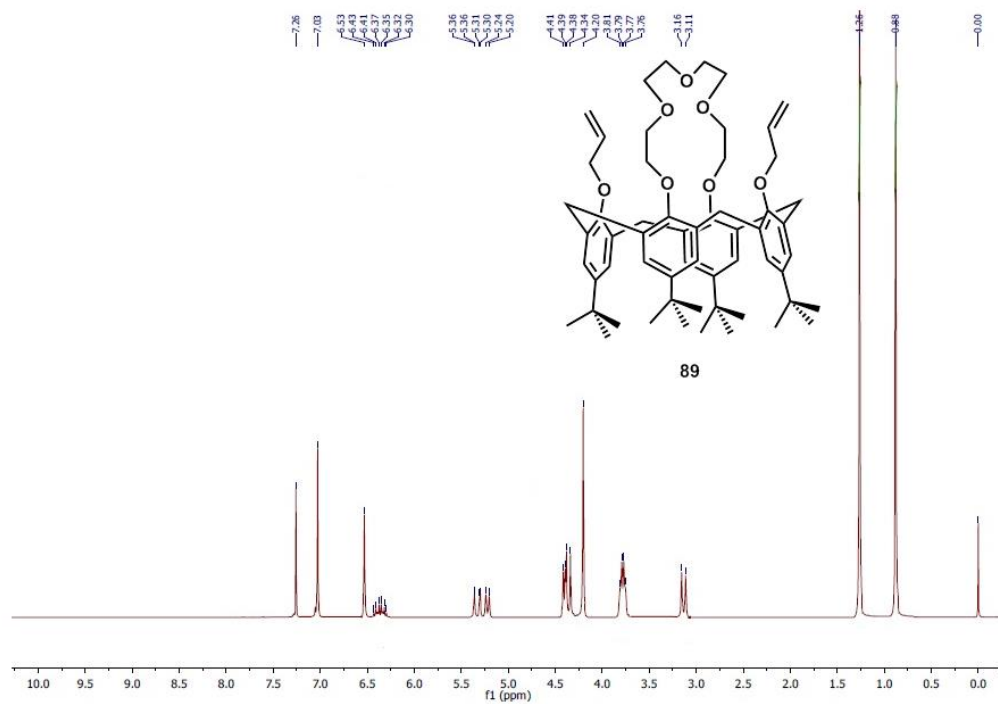


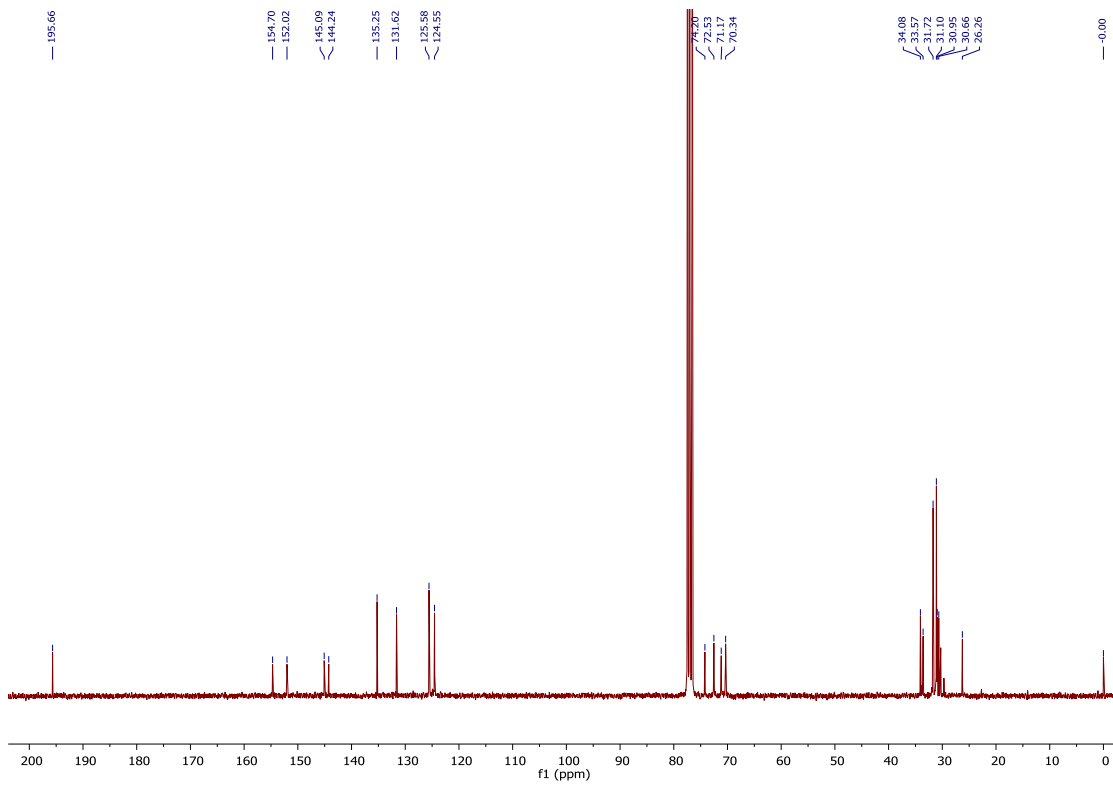
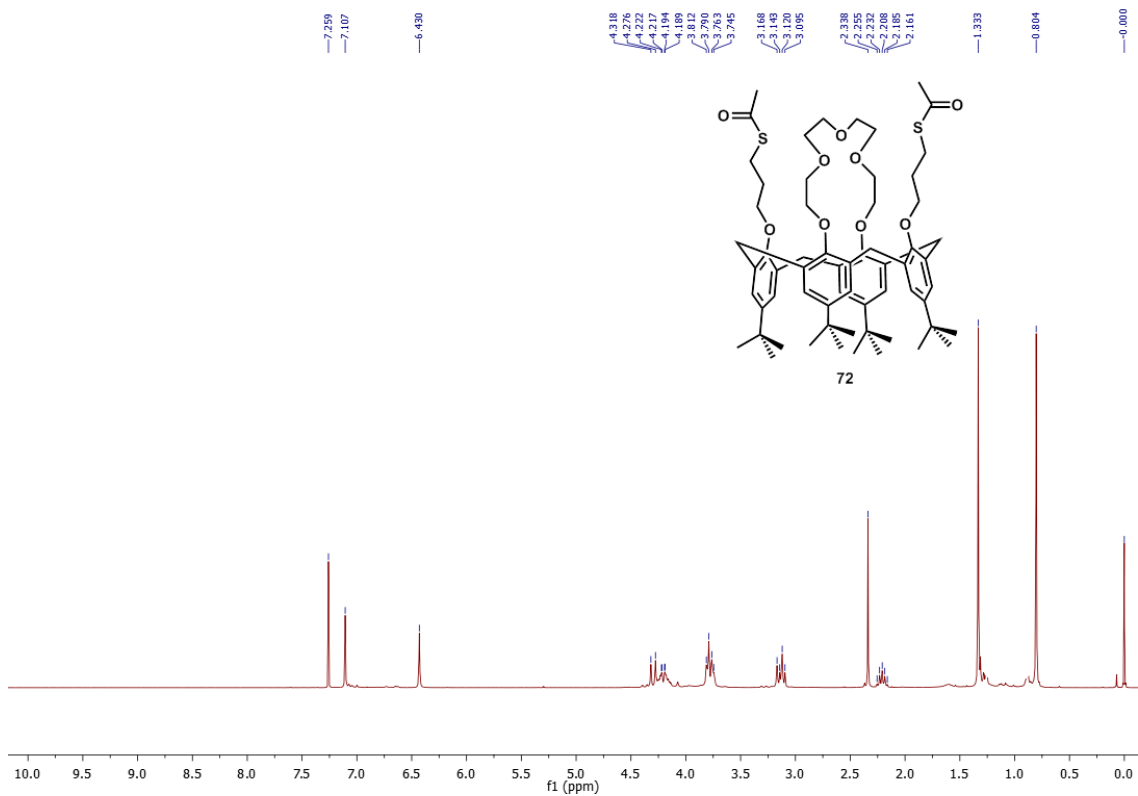












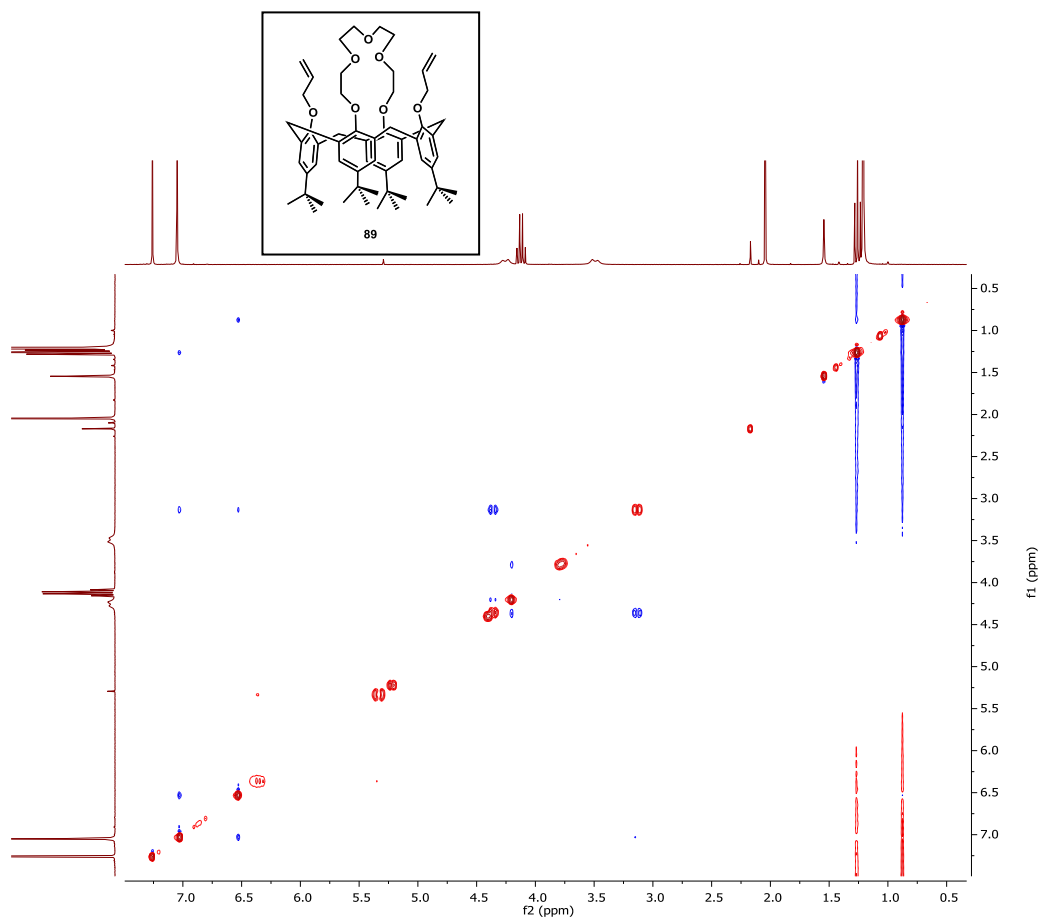


Figure 2.34 2D NOESY spectrum for calix[4]arene **89**.

X-ray crystallographic data for compound 70

Experimental details

Empirical Formula	$C_{60} H_{72} O_{16} S_4$
Formula weight	1177.46
Crystal Color	Colourless crystals
Crystal System	Monoclinic

Bond precision:	C-C = 0.0058 Å	Wavelength = 0.71075
Cell:	a = 22.889(7) b = 13.486(4) c = 21.398(6)	
	Alpha = 90 beta = 113.624(4) gamma = 90	
Temperature	163 K	
	Calculated	Reported
Volume	6052 (3)	6052 (3)
Space group	C 2/c	C 1 2/c 1
Hall group	-C 2yc	-C 2yc
Moiety formula	C ₆₀ H ₇₂ O ₁₆ S ₄	C ₆₀ H ₇₂ O ₁₆ S ₄
Sum formula	C ₆₀ H ₇₂ O ₁₆ S ₄	C ₆₀ H ₇₂ O ₁₆ S ₄
M.wt	1177.46	1177.46
Dx,g cm ⁻³	1.292	1.292
Z value	4	4
Mu (mm ⁻¹)	0.224	0.223
F000	2496.0	2496.0
F000 ^ˆ	2499.22	
h, k, l max	28, 16, 26	28, 16, 26
Nref	6285	6266
Tmin,Tmax	0.961,0.985	0.960,0.991
Tmin ^ˆ	0.939	

Correction method = NUMERICAL

Data completeness = 0.997

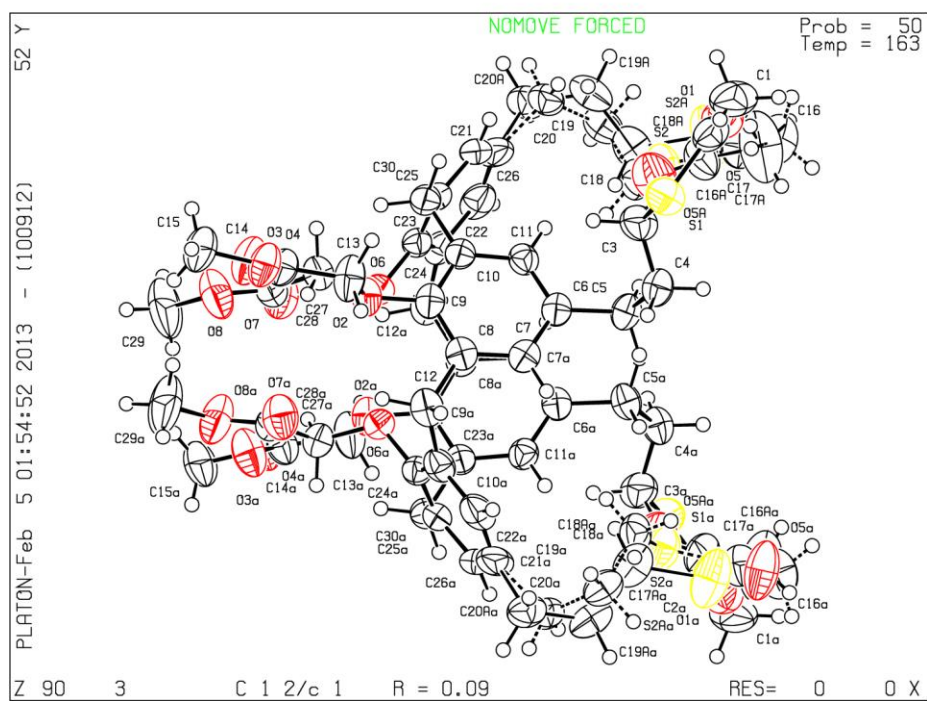
Theta(max) = 26.500

R(reflections) = 0.0944(5422)

wR2(reflections) = 0.2660(6266)

S = 1.126

Npar = 430



X-ray crystallographic data for compound 72

The structure crystallized in the monoclinic space group $P2_1/n$, with three chemically identical molecules in the asymmetric unit ($Z' = 3$, Figure 2.35a). The molecules pack in discrete chains perpendicular to the c -axis (Figure 2.35b), though no significant intermolecular interactions are present. Each molecule adopts a cone-like configuration (Figure 2.35c). The ether chains and bridge exhibited disorder in the crystal structure that was difficult to model, however, this disorder did not indicate the presence of any molecules in the 1,3-*alternate* conformation.

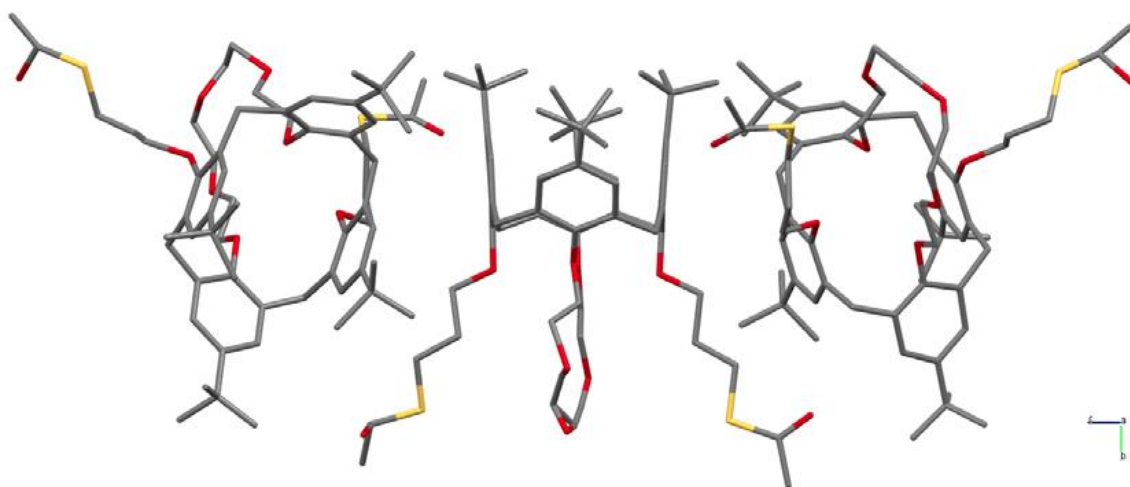


Figure 2.35a The asymmetric unit, represented with capped sticks, containing three chemically identical, but crystallographically independent molecules ($Z' = 3$). H-atoms and minor disorder component omitted for clarity.

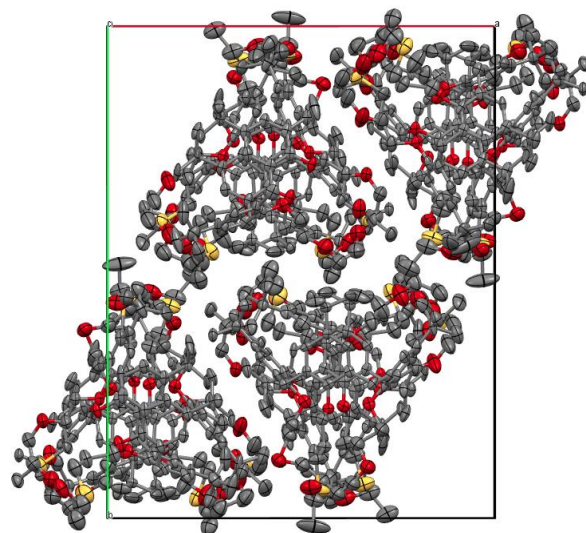


Figure 2.35b Packed unit cell, represented with 30% displacement ellipsoids, looking down the c-axis, showing the discrete chain-like arrangement of molecules in the structure.

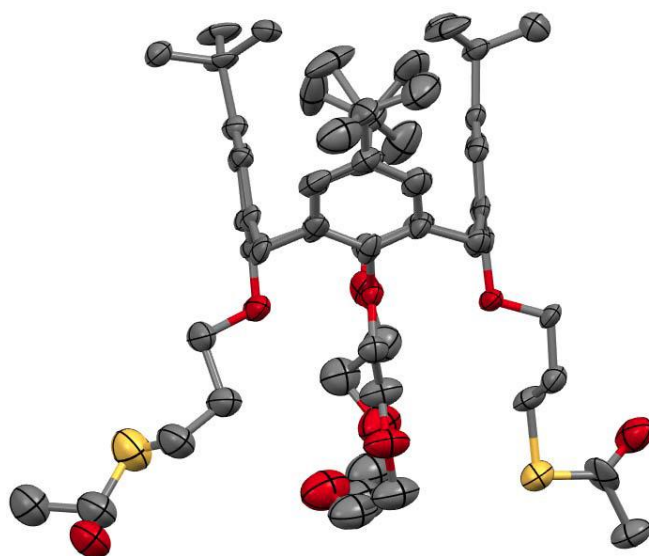


Figure 2.35c One molecule, represented with 30% displacement ellipsoids, showing the cone conformation. H-atoms and minor disorder components omitted for clarity.

Bond precision:	C-C = 0.0191 Å	Wavelength = 1.54178
Cell:	a = 21.9907 (9) b = 27.7429 (14) c = 29.1299 (12)	
	Alpha = 90 beta = 95.471 (3) gamma = 90	
Temperature	100 K	
	Calculated	Reported
Volume	17690.8 (14)	17690.8 (14)
Space group	P 21/n	P 1 21/n 1
Hall group	-P 2yn	-P 2yn
Moiety formula	C61.92 H73 O9 S2, C61.41 H71.71 O8 S2, C62 H69.37 O9 S2	0.33(C61.92 H73 O9 S2), 0.33(C62 H69.37 O9 S2), 0.33(C61.41 H71)
Sum formula	C185.33 H214.08 O26 S6	C62 H88 O9 S2
Mr	3050.03	1041.44
Dx,g cm-3	1.145	1.173
Z value	4	12
Mu (mm-1)	1.233	1.242
F000	6520.2	6768.0
F000'	6546.12	
h, k, l max	21, 26, 28	26, 33, 34
Nref	16459	16373
Tmin,Tmax	0.888, 0.952	Tmin' 0.939

Correction method = Not given

Data completeness = 0.995

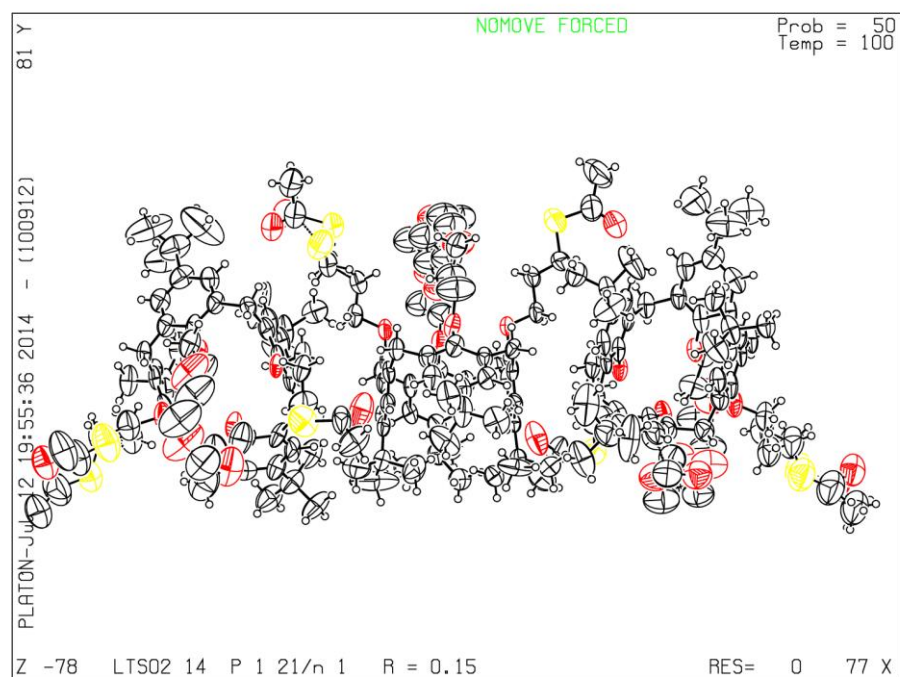
Theta(max) = 47.836

R(reflections) = 0.1519 (8707)

wR2(reflections) = 0.4584 (16373)

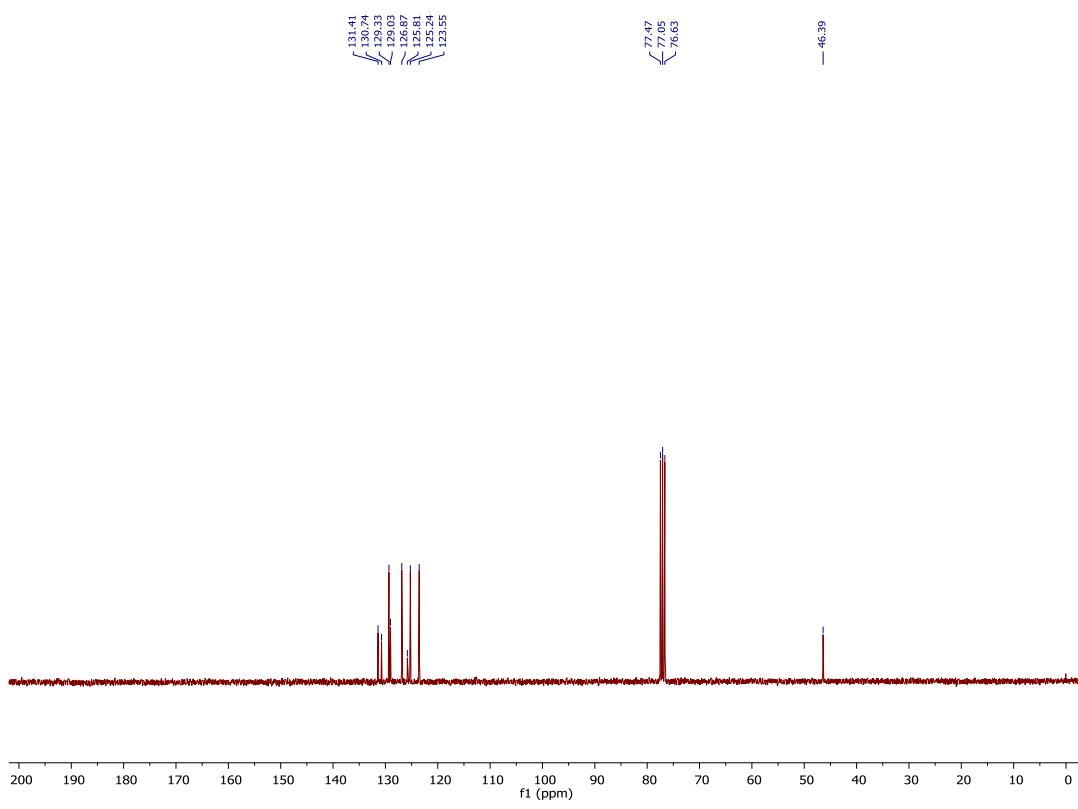
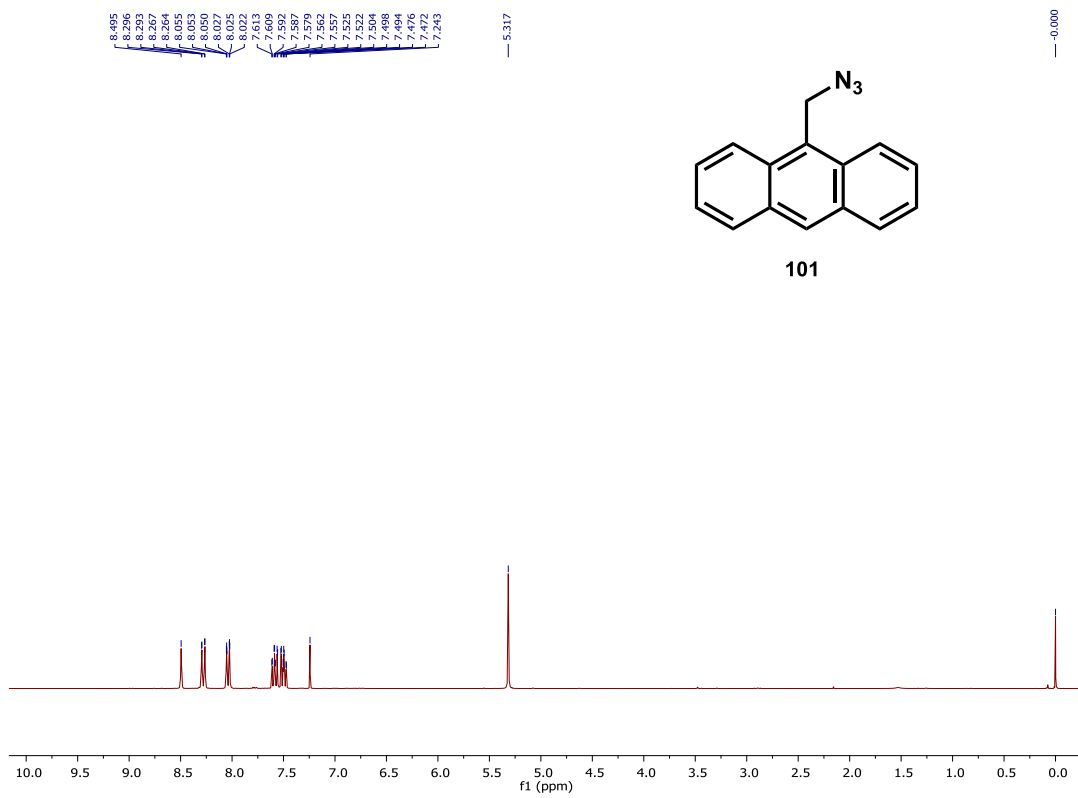
S = 1.595

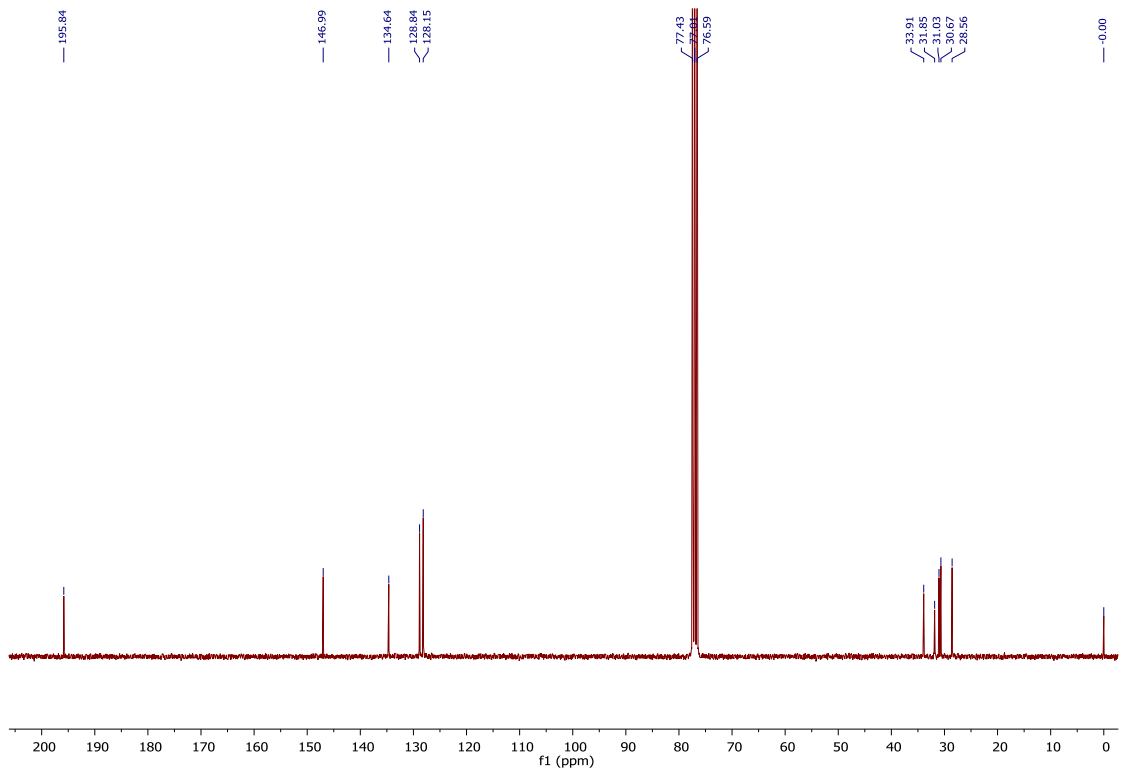
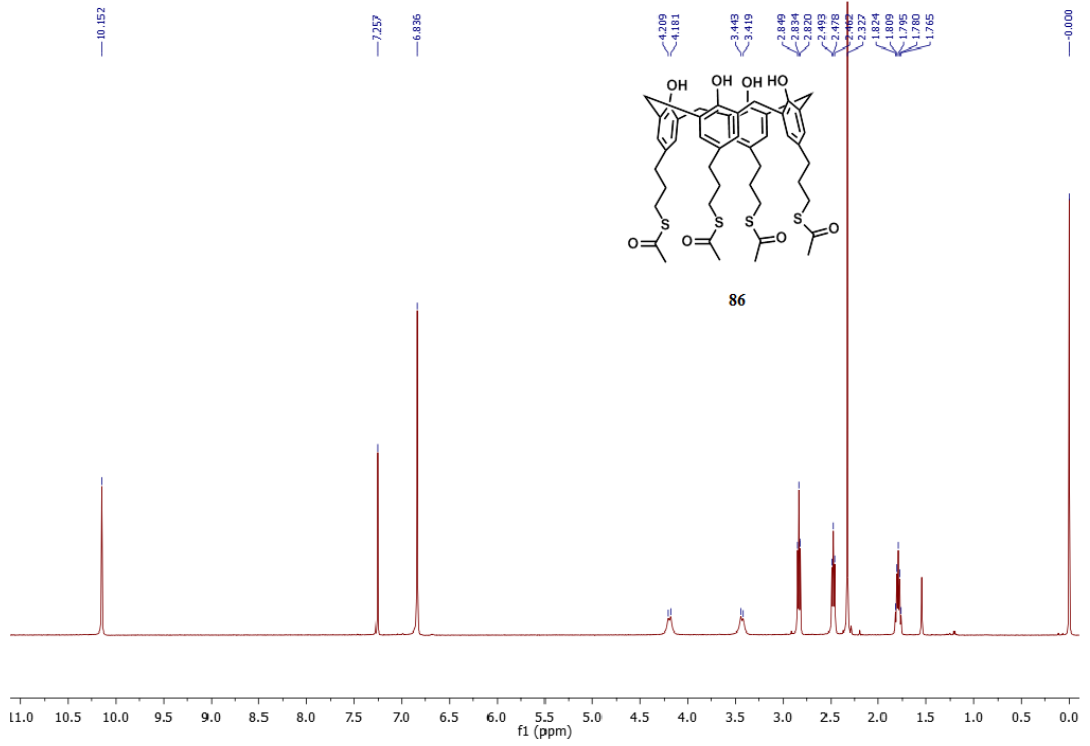
Npar = 2207

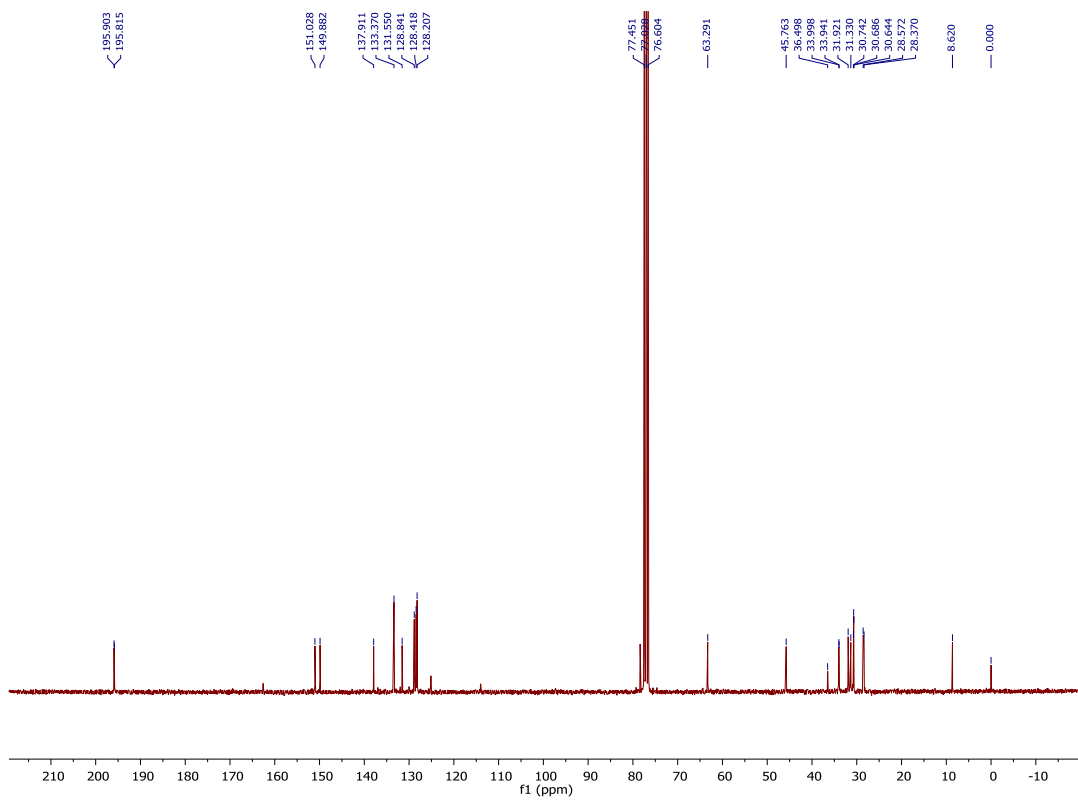
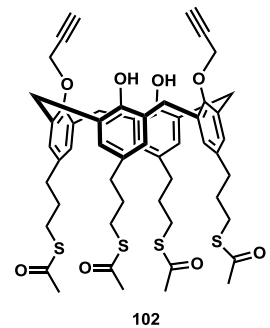
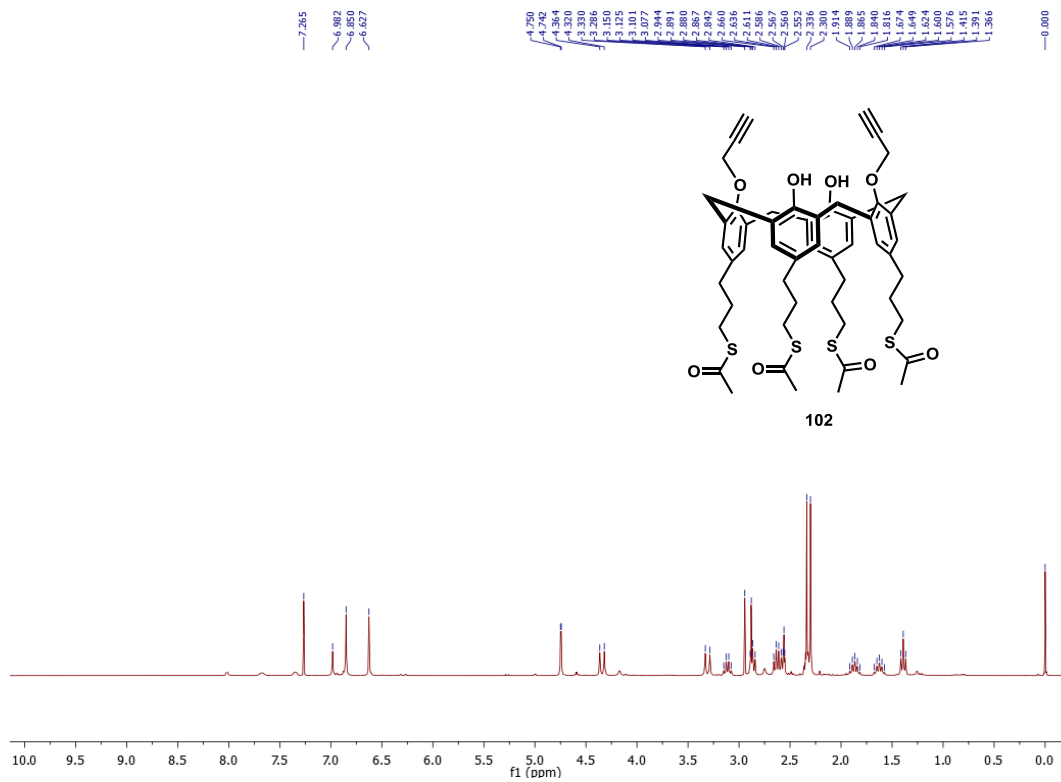


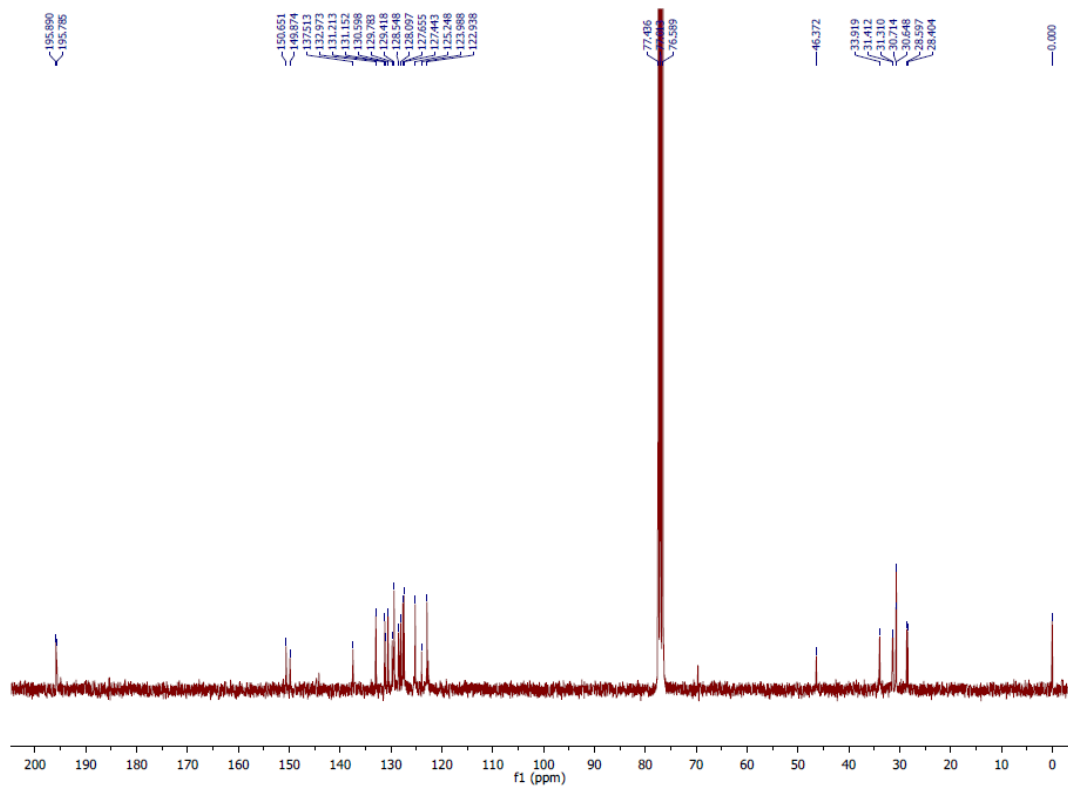
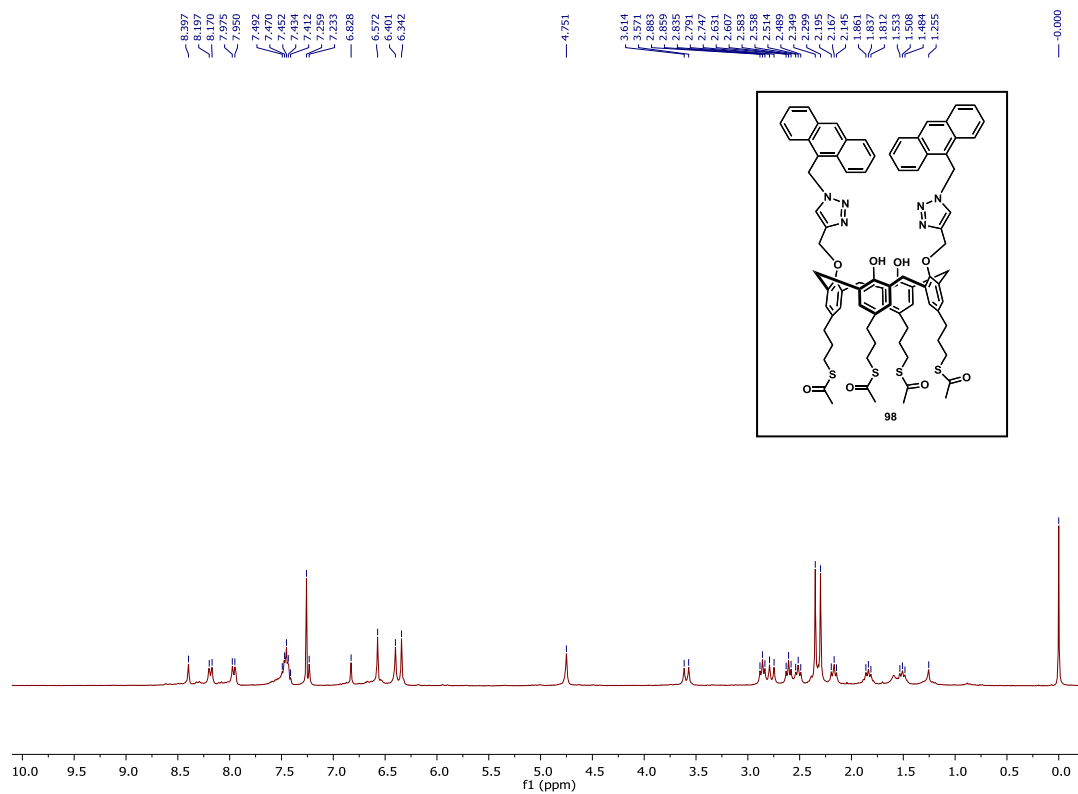
Appendix B

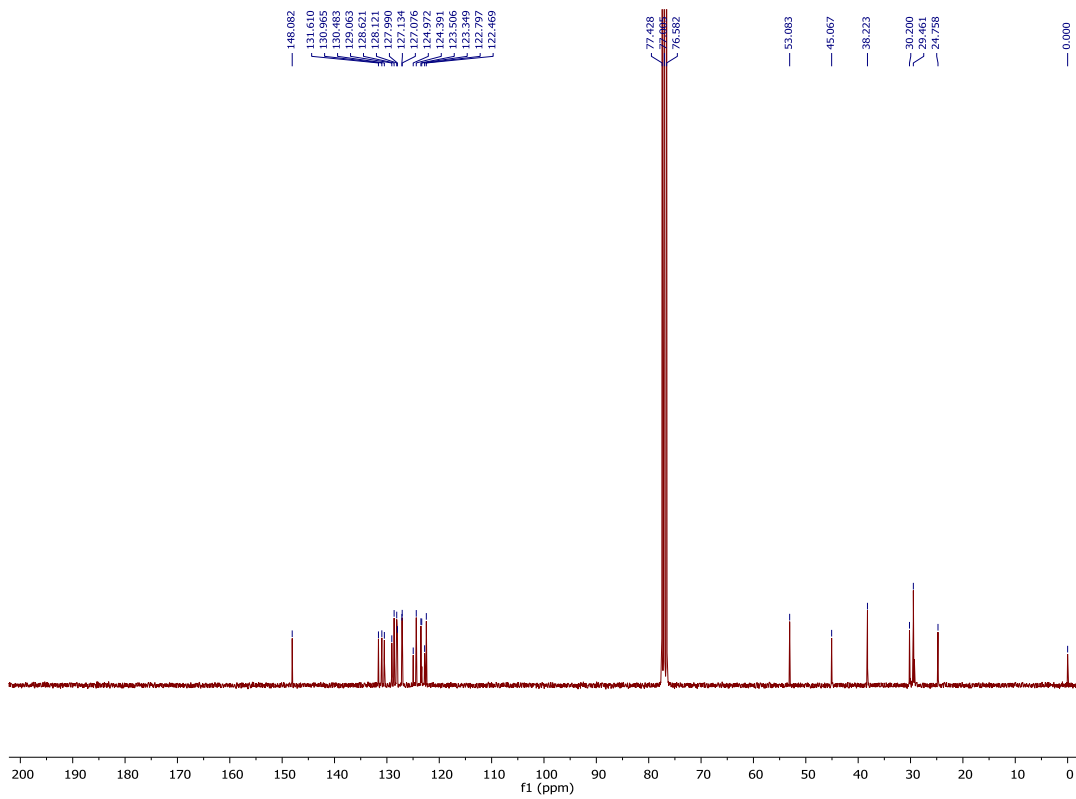
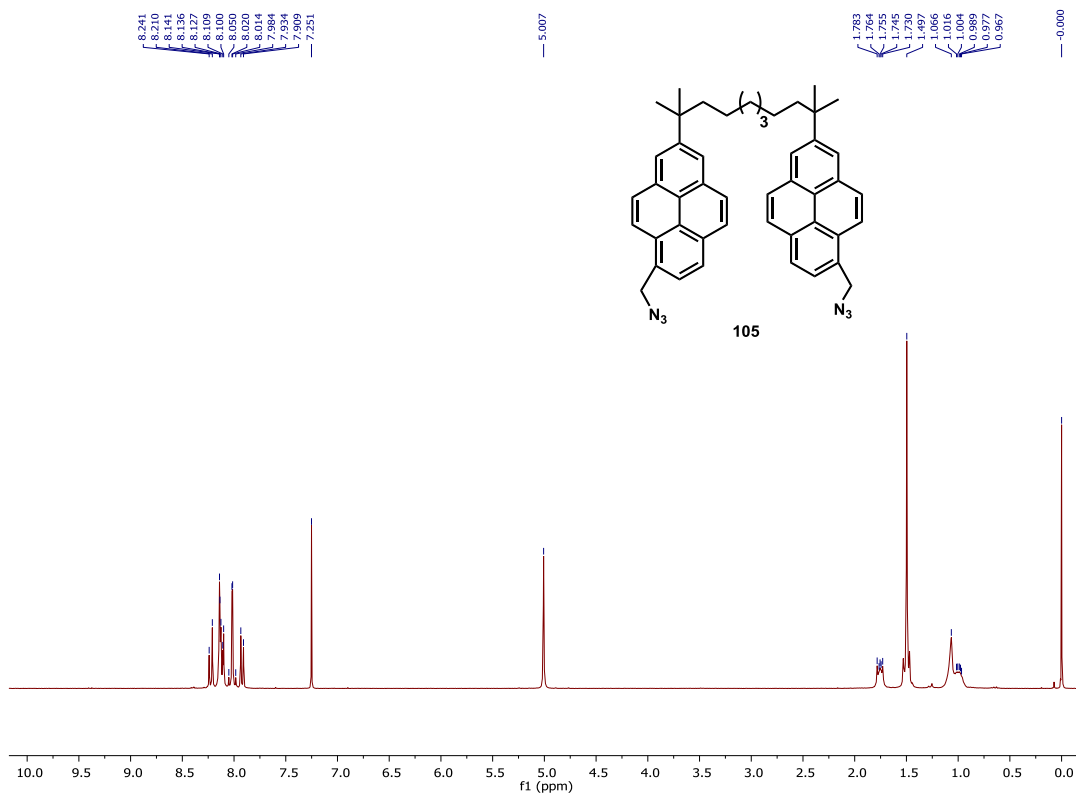
^1H - and ^{13}C -NMR spectra and fluorescence spectra for
compounds described in **Chapter 3**

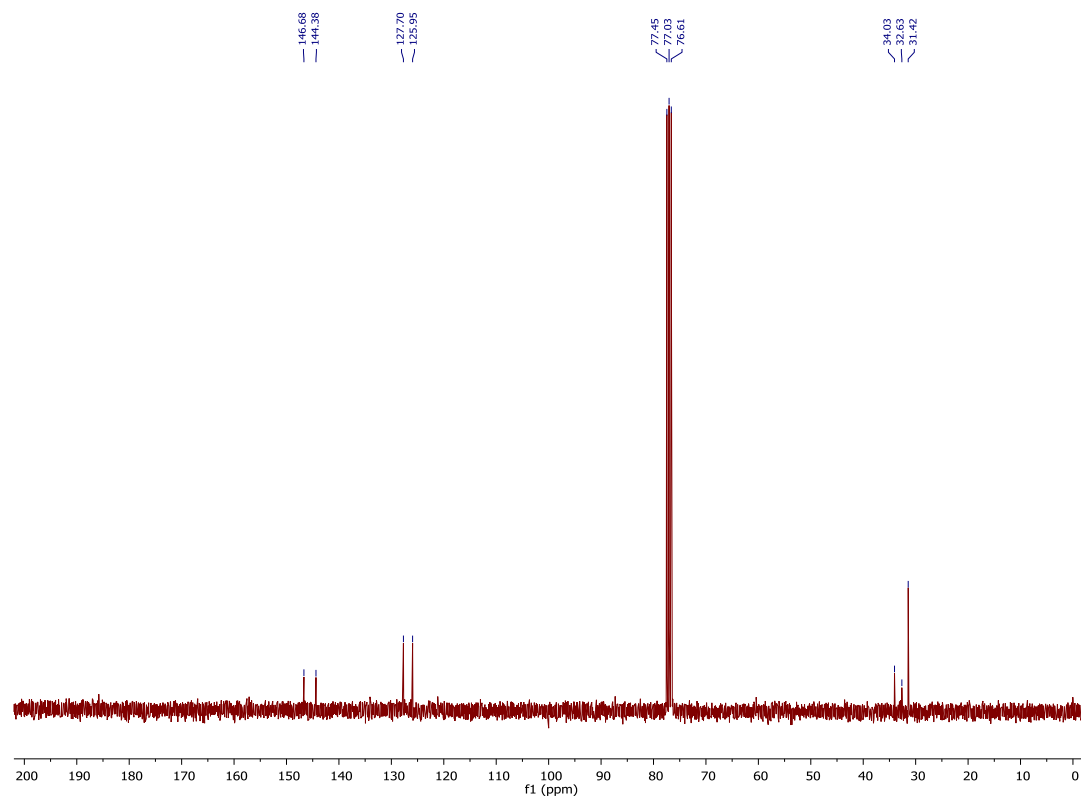
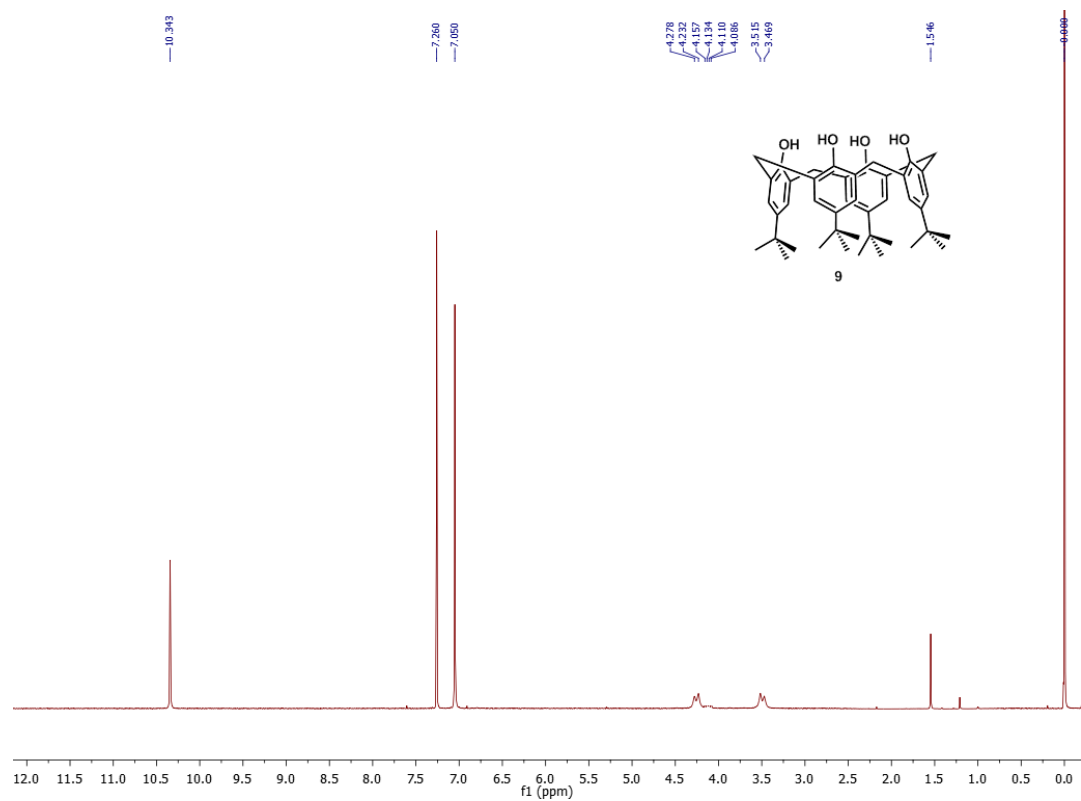


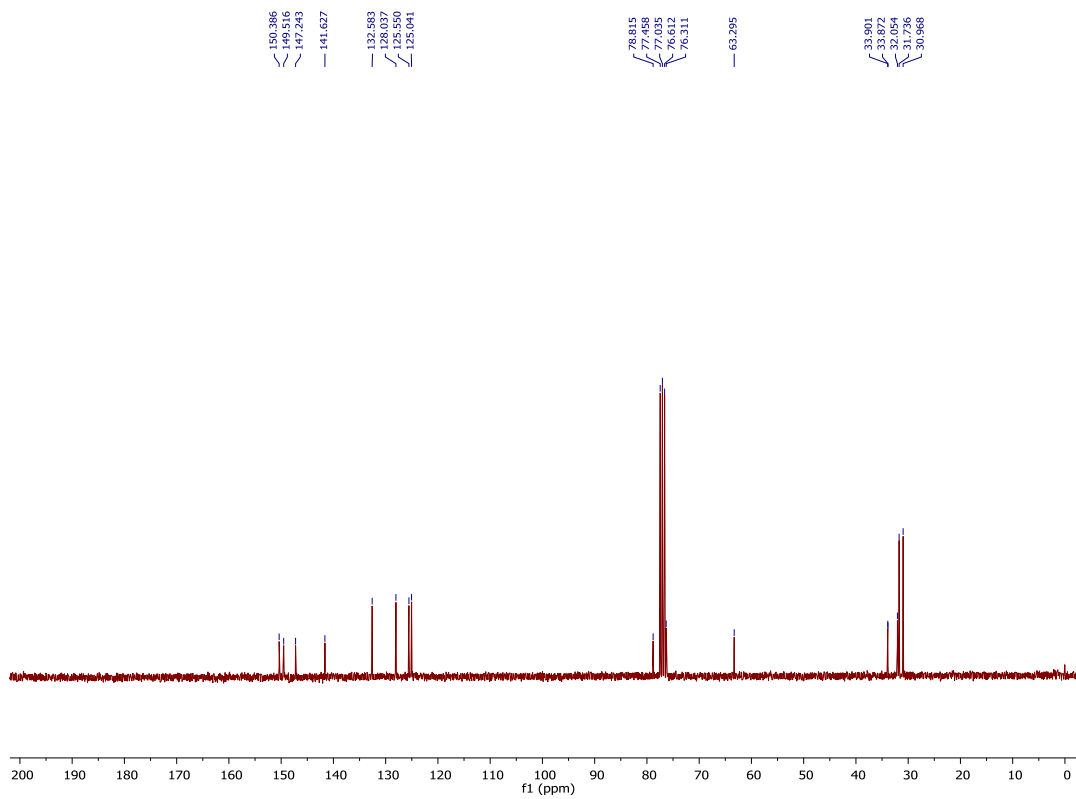
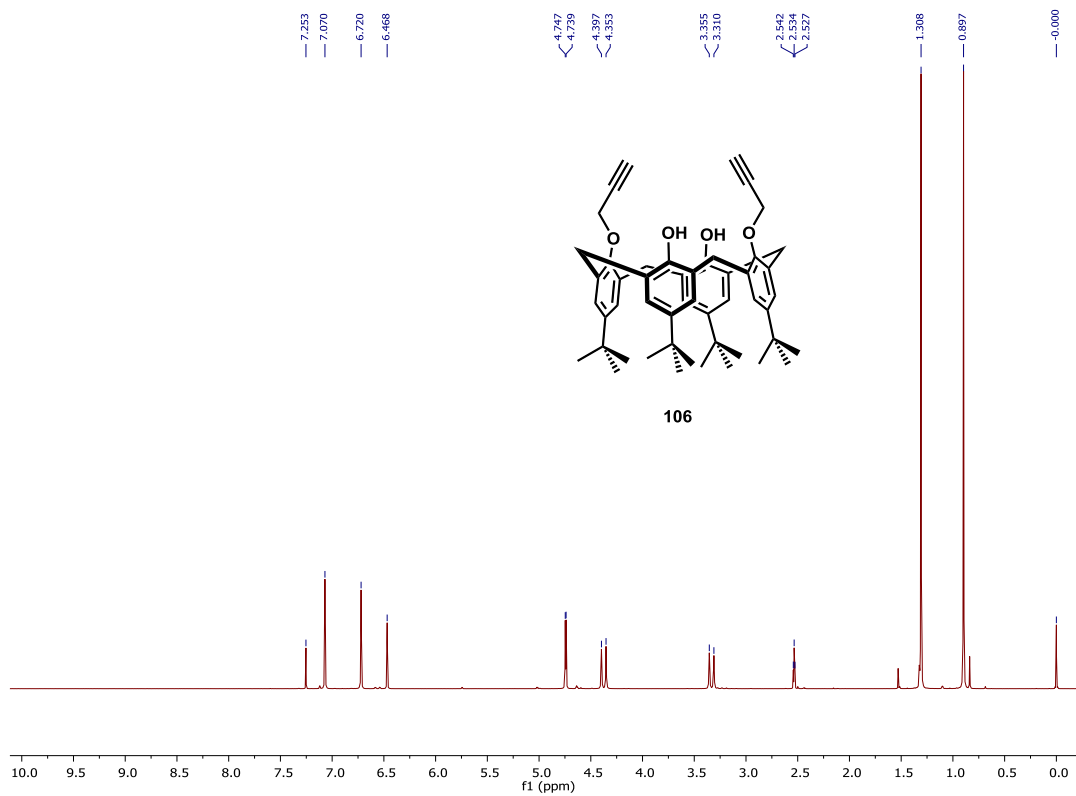


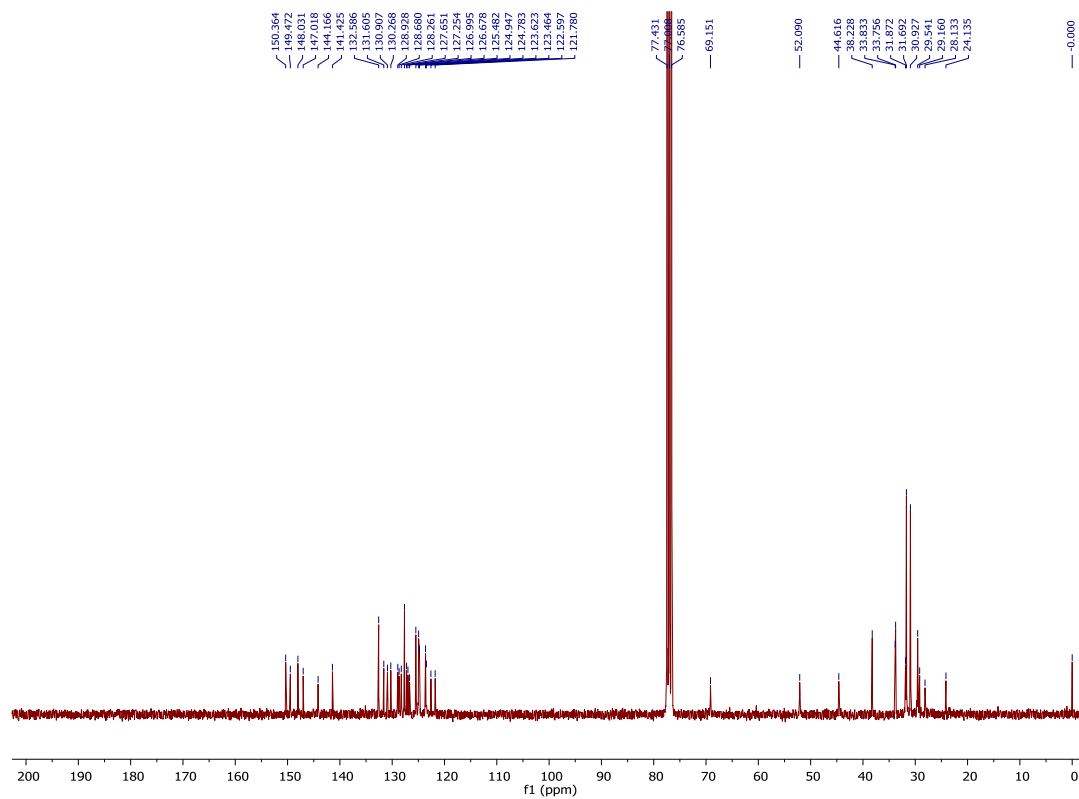
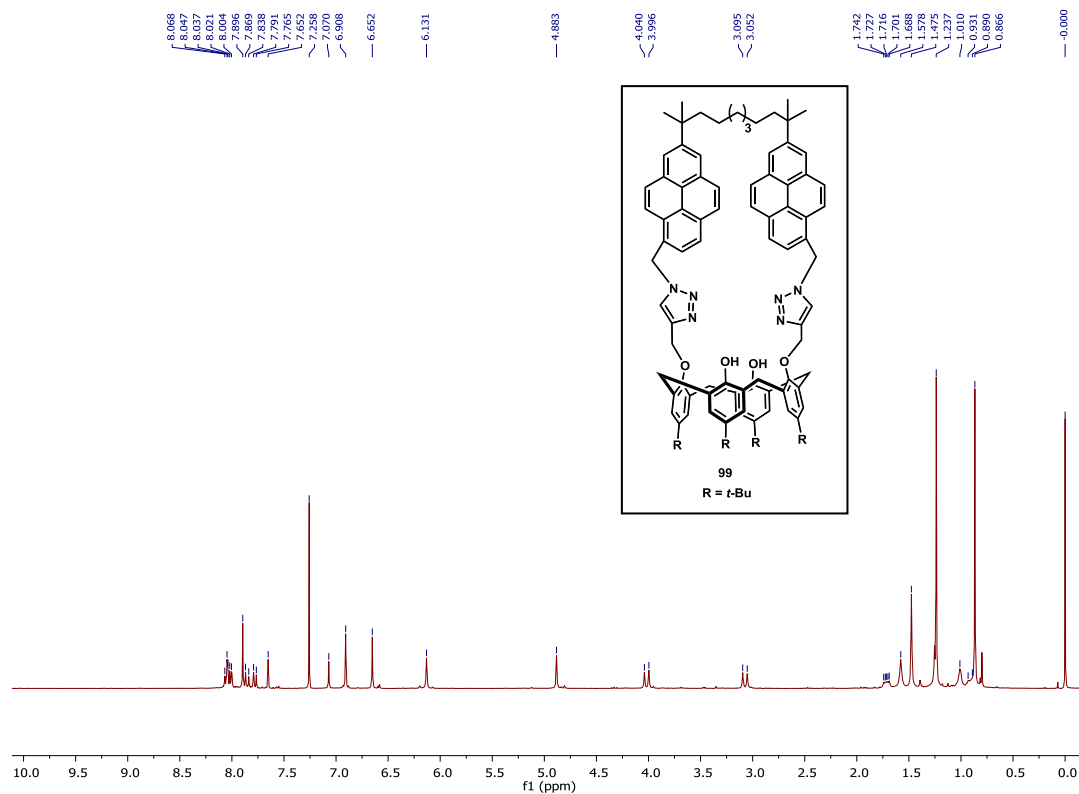












Fluorescence complexation studies of **98** with various metal ions

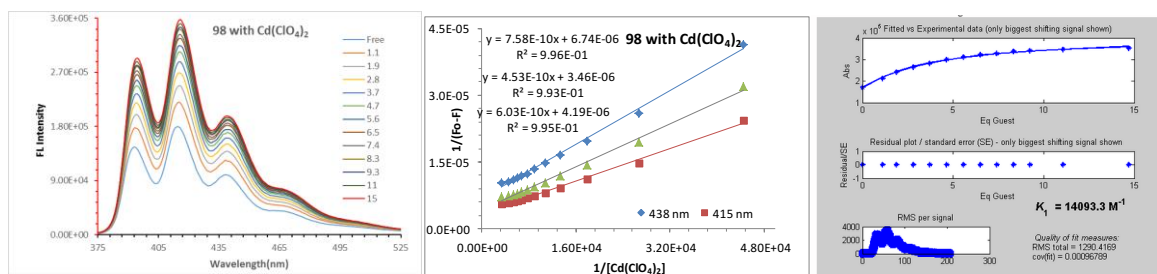


Figure 3.32 *Left*: Fluorescence spectra of **98** upon addition of Cd^{2+} (1.1-15 eq) in acetonitrile/ chloroform ($v/v= 9:1$) solutions. $\lambda_{ex} = 350 \text{ nm}$. *Middle*: Benesi-Hildebrand plot of $1/(F_0-F)$ versus $1/[\text{Cd}(\text{ClO}_4)_2]$ for **98** upon titration with $\text{Cd}(\text{ClO}_4)_2$. The linear fit showed a 1:1 complexation between **98** and Cd^{2+} ions. *Right*: Screen-capture output showing 1:1 binding model for **98** with Cd^{2+} , using Thordarson's method (Ref 35b in Chapter 3).

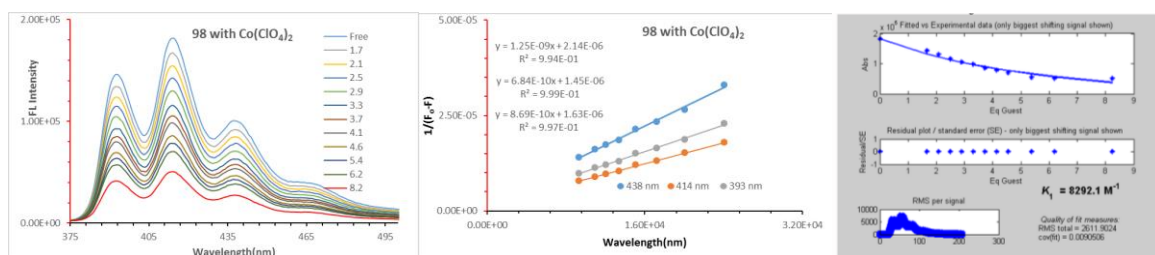


Figure 3.33 *Left*: Fluorescence spectra of **98** upon addition of Co^{2+} (1.7-8.2 eq) in acetonitrile/ chloroform ($v/v= 9:1$) solutions. $\lambda_{ex} = 350 \text{ nm}$. *Middle*: Benesi-Hildebrand plot of $1/(F_0-F)$ versus $1/[\text{Co}(\text{ClO}_4)_2]$ for **98** upon titration with $\text{Co}(\text{ClO}_4)_2$. The linear fit showed a 1:1 complexation between **98** and Co^{2+} ions. *Right*: Screen-capture output showing 1:1 binding model for **98** with Co^{2+} , using Thordarson's method.

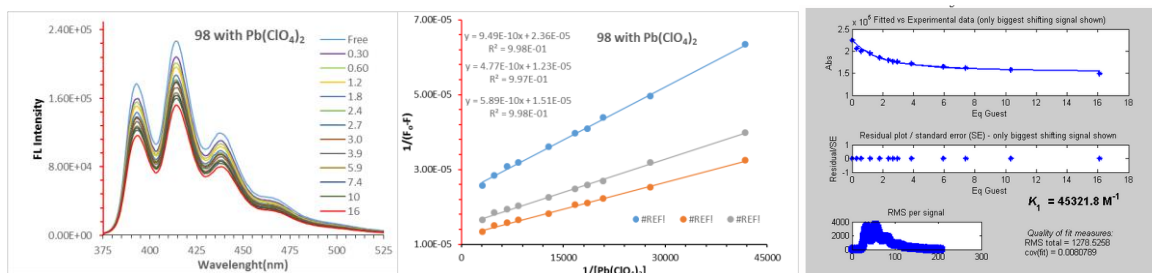


Figure 3.34 *Left*: Fluorescence spectra of **98** upon addition of Pb^{2+} (0.30-16 eq) in acetonitrile/ chloroform ($v/v= 9:1$) solutions. $\lambda_{ex} = 350$ nm. *Middle*: Benesi-Hildebrand plot of $1/(F_o-F)$ versus $1/[\text{Pb}(\text{ClO}_4)_2]$ for **98** upon titration with $\text{Pb}(\text{ClO}_4)_2$. The linear fit showed a 1:1 complexation between **98** and Pb^{2+} ions. *Right*: Screen-capture output showing 1:1 binding model for **98** with Pb^{2+} , using Thordarson's method.

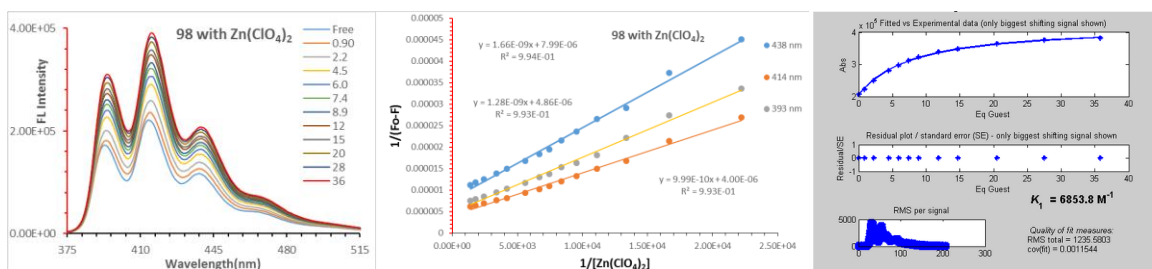


Figure 3.35 *Left*: Fluorescence spectra of **98** upon addition of Zn^{2+} (0.90-36 eq) in acetonitrile/ chloroform ($v/v= 9:1$) solutions. $\lambda_{ex} = 350$ nm. *Middle*: Benesi-Hildebrand plot of $1/(F_o-F)$ versus $1/[\text{Zn}(\text{ClO}_4)_2]$ for **98** upon titration with $\text{Zn}(\text{ClO}_4)_2$. The linear fit showed a 1:1 complexation between **98** and Zn^{2+} ions. *Right*: Screen-capture output showing 1:1 binding model for **98** with Zn^{2+} , using Thordarson's method.

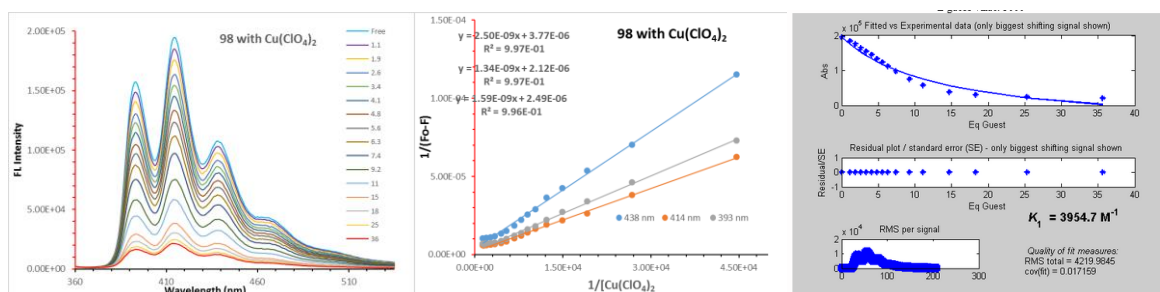


Figure 3.36 *Left*: Fluorescence spectra of **98** upon addition of Cu^{2+} (1.1-36 eq) in acetonitrile/ chloroform ($v/v= 9:1$) solutions. $\lambda_{ex} = 350$ nm. *Middle*: Benesi-Hildebrand plot of $1/(F_o-F)$ versus $1/[\text{Cu}(\text{ClO}_4)_2]$ for **98** upon titration with $\text{Cu}(\text{ClO}_4)_2$. The linear fit showed a 1:1 complexation between **98** and Cu^{2+} ions. *Right*: Screen-capture output showing 1:1 binding model for **98** with Cu^{2+} , using Thordarson's method.

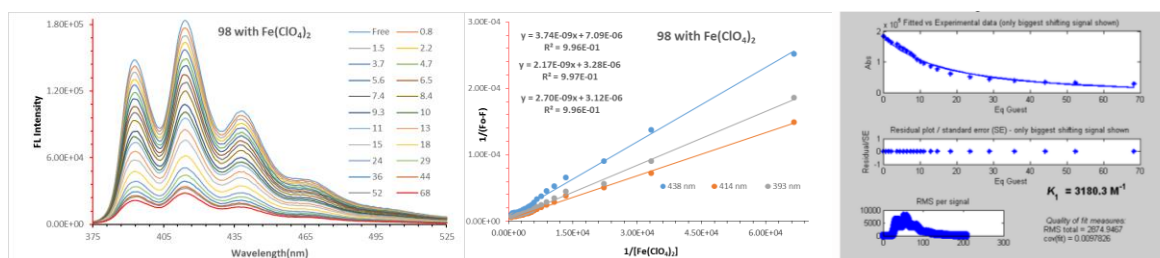


Figure 3.37 *Left*: Fluorescence spectra of **98** upon addition of Fe^{2+} (0.80-68 eq) in acetonitrile/ chloroform ($v/v= 9:1$) solutions. $\lambda_{ex} = 350$ nm. *Middle*: Benesi-Hildebrand plot of $1/(F_o-F)$ versus $1/[\text{Fe}(\text{ClO}_4)_2]$ for **98** upon titration with $\text{Fe}(\text{ClO}_4)_2$. The linear fit showed a 1:1 complexation between **98** and Fe^{2+} ions. *Right*: Screen-capture output showing 1:1 binding model for **98** with Fe^{2+} , using Thordarson's method.

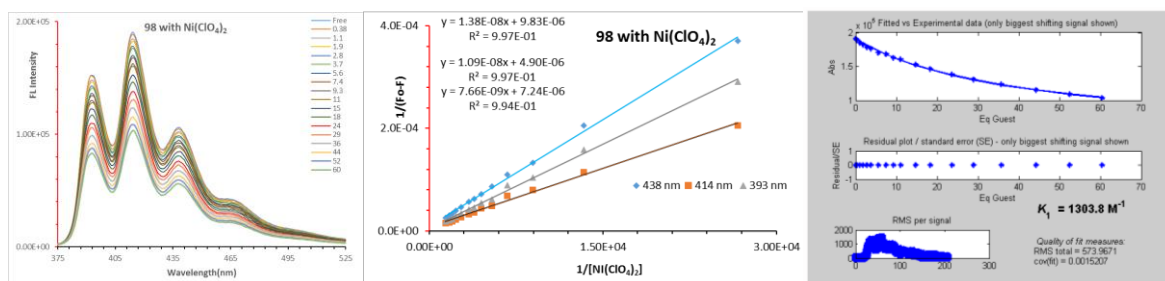


Figure 3.38 *Left*: Fluorescence spectra of **98** upon addition of Ni^{2+} (0.38-60 eq) in acetonitrile/ chloroform ($v/v= 9:1$) solutions. $\lambda_{ex} = 350$ nm. *Middle*: Benesi-Hildebrand plot of $1/(F_0-F)$ versus $1/[\text{Ni}(\text{ClO}_4)_2]$ for **98** upon titration with $\text{Ni}(\text{ClO}_4)_2$. The linear fit showed a 1:1 complexation between **98** and Ni^{2+} ions. *Right*: Screen-capture output showing 1:1 binding model for **98** with Ni^{2+} , using Thordarson's method.

Fluorescence complexation studies of **99** with various metal ions

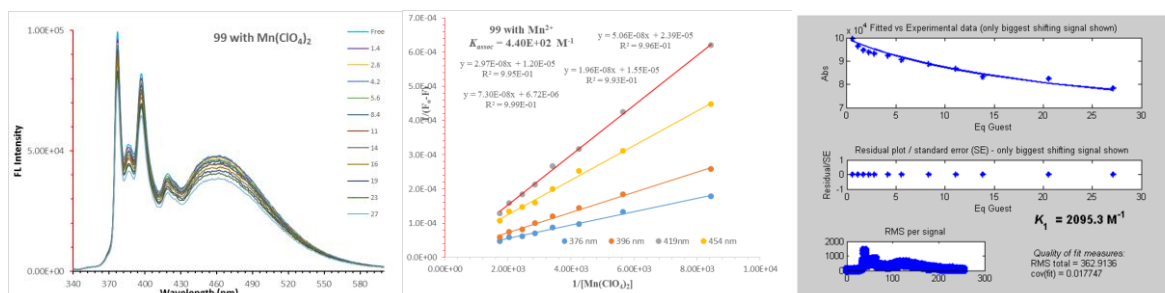


Figure 3.39 *Left*: Fluorescence spectra of **99** upon addition of Mn^{2+} (1.4-27 eq) in acetonitrile/ chloroform ($v/v= 9:1$) solutions. $\lambda_{ex} = 330$ nm. *Middle*: Benesi-Hildebrand plot of $1/(F_0-F)$ versus $1/[\text{Mn}(\text{ClO}_4)_2]$ for **99** upon titration with $\text{Mn}(\text{ClO}_4)_2$. The linear fit showed a 1:1 complexation between **99** and Mn^{2+} ions. *Right*: Screen-capture output showing 1:1 binding model for **99** with Mn^{2+} , using Thordarson's method.

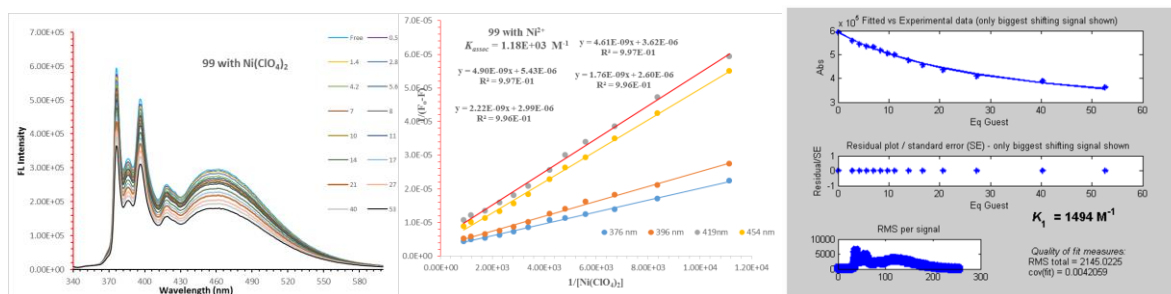


Figure 3.40 *Left*: Fluorescence spectra of **99** upon addition of Ni^{2+} (0.57-53 eq) in acetonitrile/ chloroform (v/v= 9:1) solutions. $\lambda_{\text{ex}} = 330 \text{ nm}$. *Middle*: Benesi-Hildebrand plot of $1/(F_0 - F)$ versus $1/[\text{Ni}(\text{ClO}_4)_2]$ for **99** upon titration with $\text{Ni}(\text{ClO}_4)_2$. The linear fit showed a 1:1 complexation between **99** and Ni^{2+} ions. *Right*: Screen-capture output showing 1:1 binding model for **99** with Ni^{2+} , using Thordarson's method.

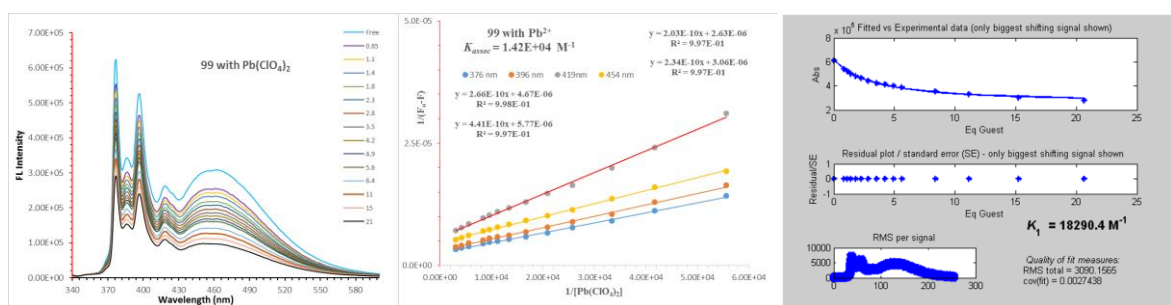


Figure 3.41 *Left*: Fluorescence spectra of **99** upon addition of Pb^{2+} (0.85-21 eq) in acetonitrile/ chloroform (v/v= 9:1) solutions. $\lambda_{\text{ex}} = 330 \text{ nm}$. *Middle*: Benesi-Hildebrand plot of $1/(F_0 - F)$ versus $1/[\text{Pb}(\text{ClO}_4)_2]$ for **99** upon titration with $\text{Pb}(\text{ClO}_4)_2$. The linear fit showed a 1:1 complexation between **99** and Pb^{2+} ions. *Right*: Screen-capture output showing 1:1 binding model for **99** with Pb^{2+} , using Thordarson's method.

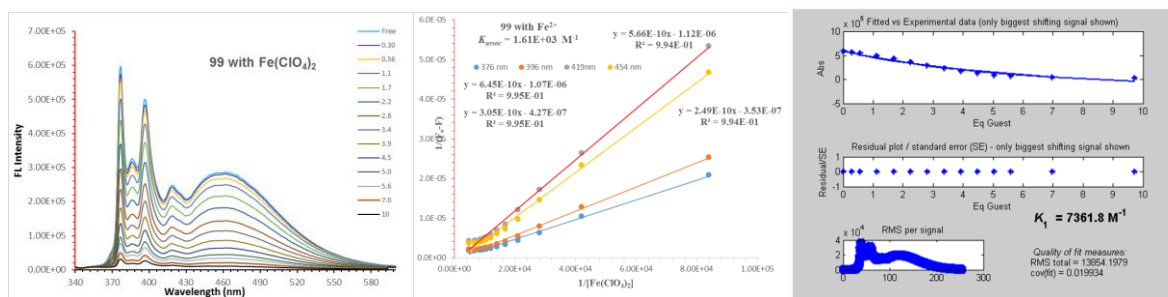


Figure 3.42 *Left*: Fluorescence spectra of **99** upon addition of Fe^{2+} (0.30-10 eq) in acetonitrile/ chloroform (v/v= 9:1) solutions. $\lambda_{ex} = 330$ nm. *Middle*: Benesi-Hildebrand plot of $1/(F_0-F)$ versus $1/[\text{Fe}(\text{ClO}_4)_2]$ for **99** upon titration with $\text{Fe}(\text{ClO}_4)_2$. The linear fit showed a 1:1 complexation between **99** and Fe^{2+} ions. *Right*: Screen-capture output showing 1:1 binding model for **99** with Fe^{2+} , using Thordarson's method.

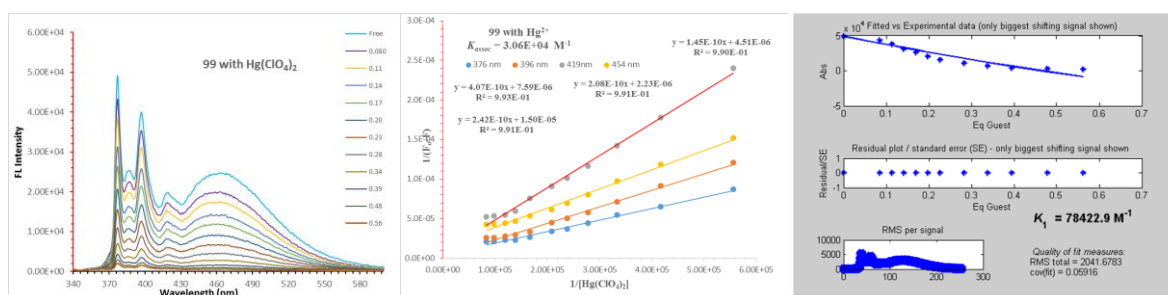


Figure 3.43 *Left*: Fluorescence spectra of **99** upon addition of Hg^{2+} (0.0080-0.56 eq) in acetonitrile/ chloroform (v/v= 9:1) solutions. $\lambda_{ex} = 330$ nm. *Middle*: Benesi-Hildebrand plot of $1/(F_0-F)$ versus $1/[\text{Hg}(\text{ClO}_4)_2]$ for **99** upon titration with $\text{Hg}(\text{ClO}_4)_2$. The linear fit showed a 1:1 complexation between **99** and Hg^{2+} ions. *Right*: Screen-capture output showing 1:1 binding model for **99** with Hg^{2+} , using Thordarson's method.

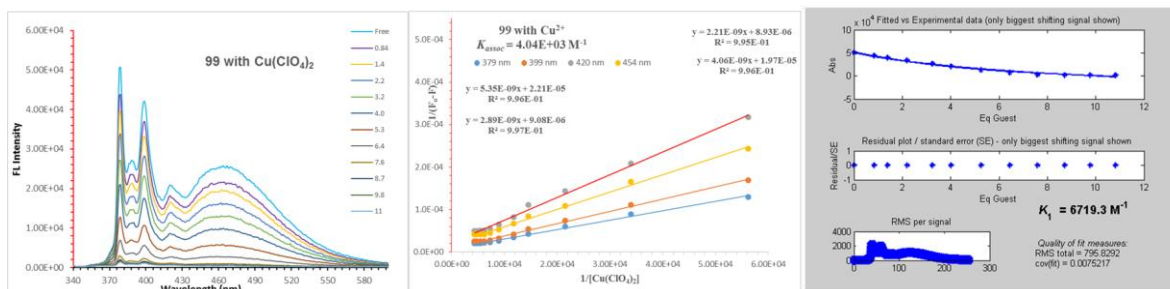


Figure 3.44 *Left*: Fluorescence spectra of **99** upon addition of Cu^{2+} (0.84-11 eq) in acetonitrile/ chloroform (v/v= 9:1) solutions. $\lambda_{\text{ex}} = 330 \text{ nm}$. *Middle*: Benesi-Hildebrand plot of $1/(F_0 - F)$ versus $1/[\text{Cu}(\text{ClO}_4)_2]$ for **99** upon titration with $\text{Cu}(\text{ClO}_4)_2$. The linear fit showed a 1:1 complexation between **99** and Cu^{2+} ions. *Right*: Screen-capture output showing 1:1 binding model for **99** with Cu^{2+} , using Thordarson's method.

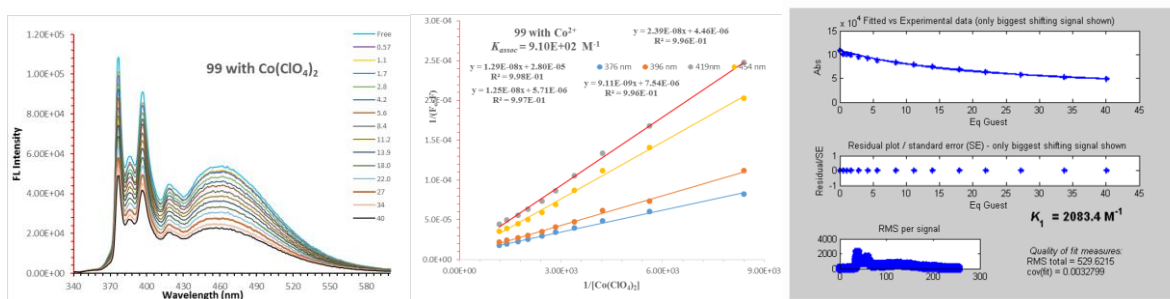


Figure 3.45 *Left*: Fluorescence spectra of **99** upon addition of Co^{2+} (0.57-40 eq) in acetonitrile/ chloroform (v/v= 9:1) solutions. $\lambda_{\text{ex}} = 330 \text{ nm}$. *Middle*: Benesi-Hildebrand plot of $1/(F_0 - F)$ versus $1/[\text{Co}(\text{ClO}_4)_2]$ for **99** upon titration with $\text{Co}(\text{ClO}_4)_2$. The linear fit showed a 1:1 complexation between **99** and Co^{2+} ions. *Right*: Screen-capture output showing 1:1 binding model for **99** with Co^{2+} , using Thordarson's method.

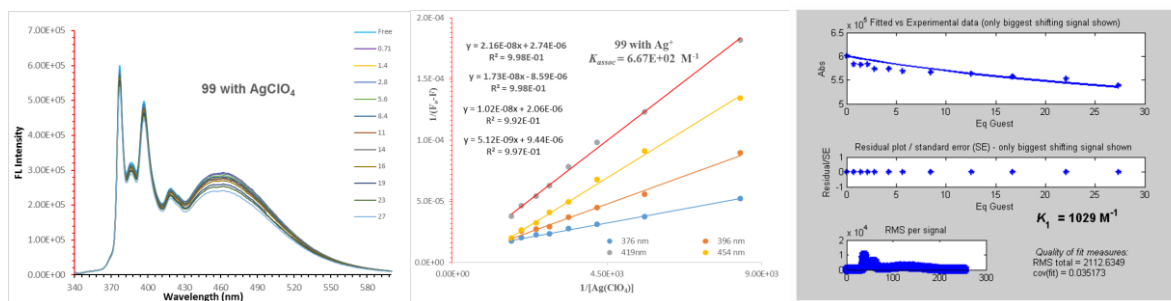
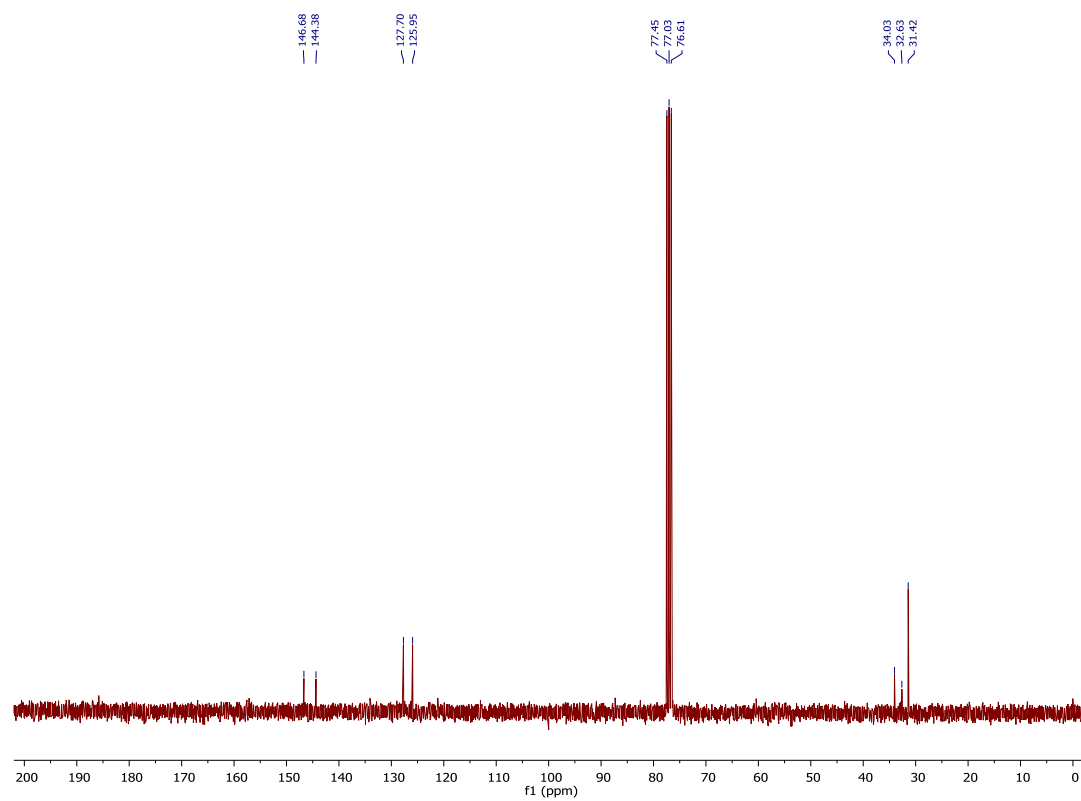
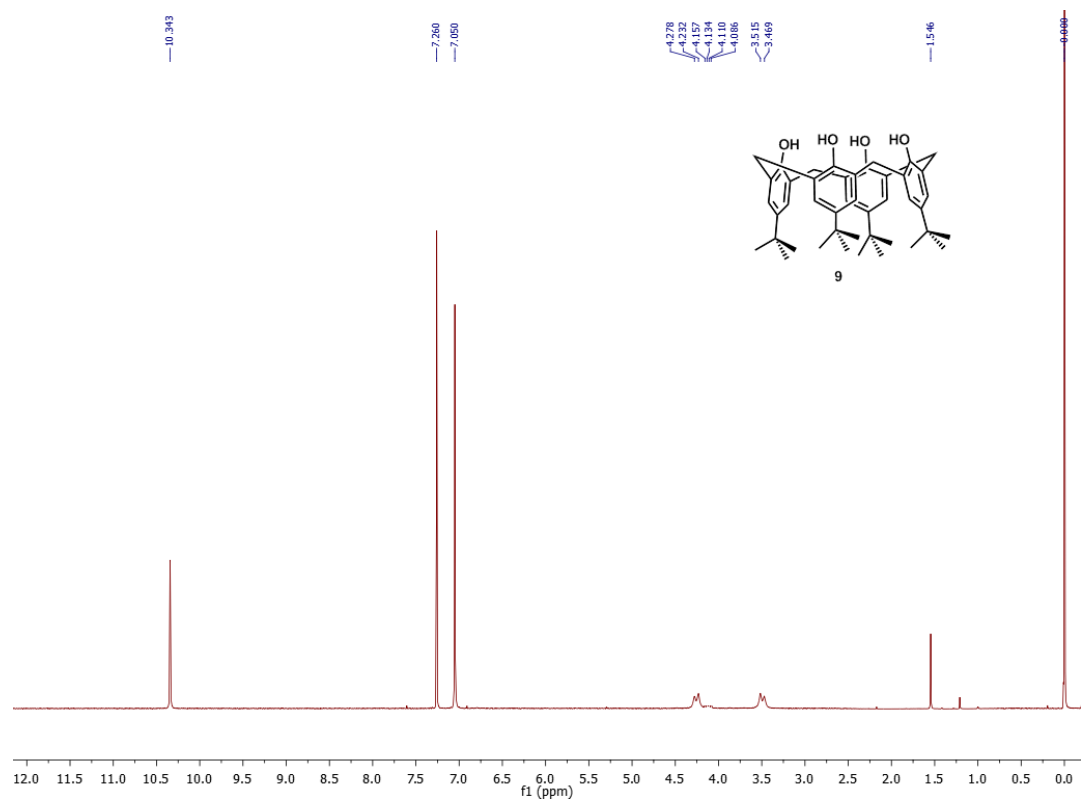


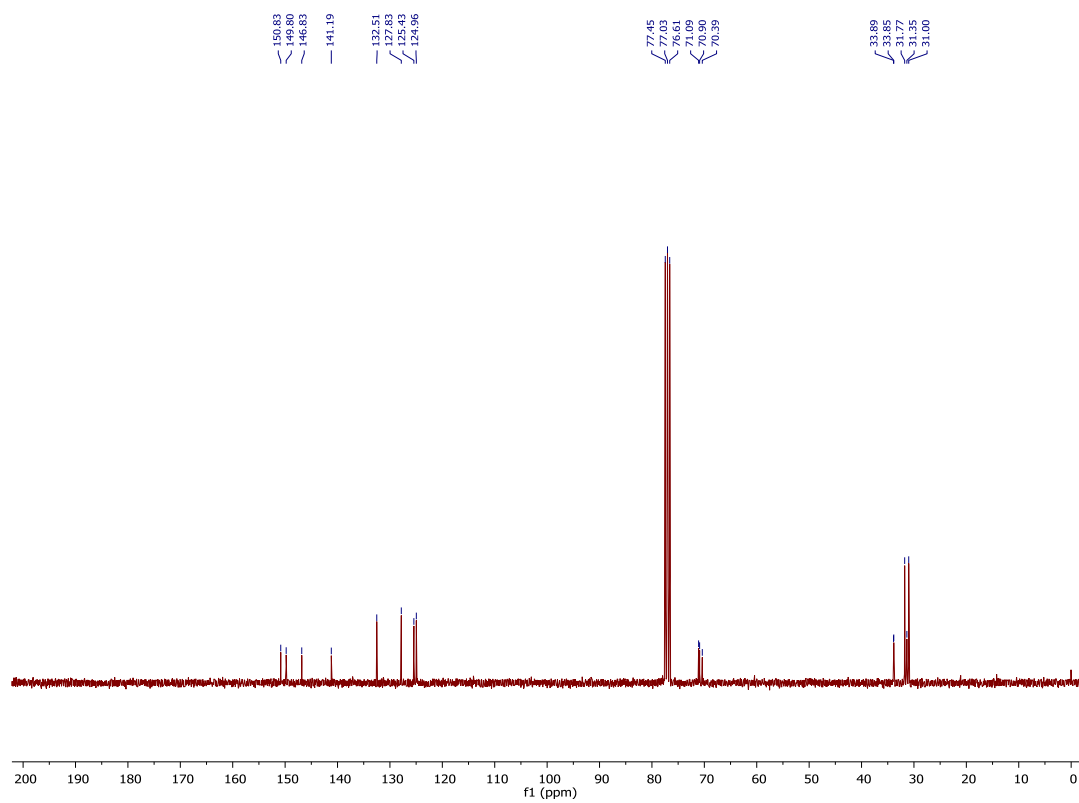
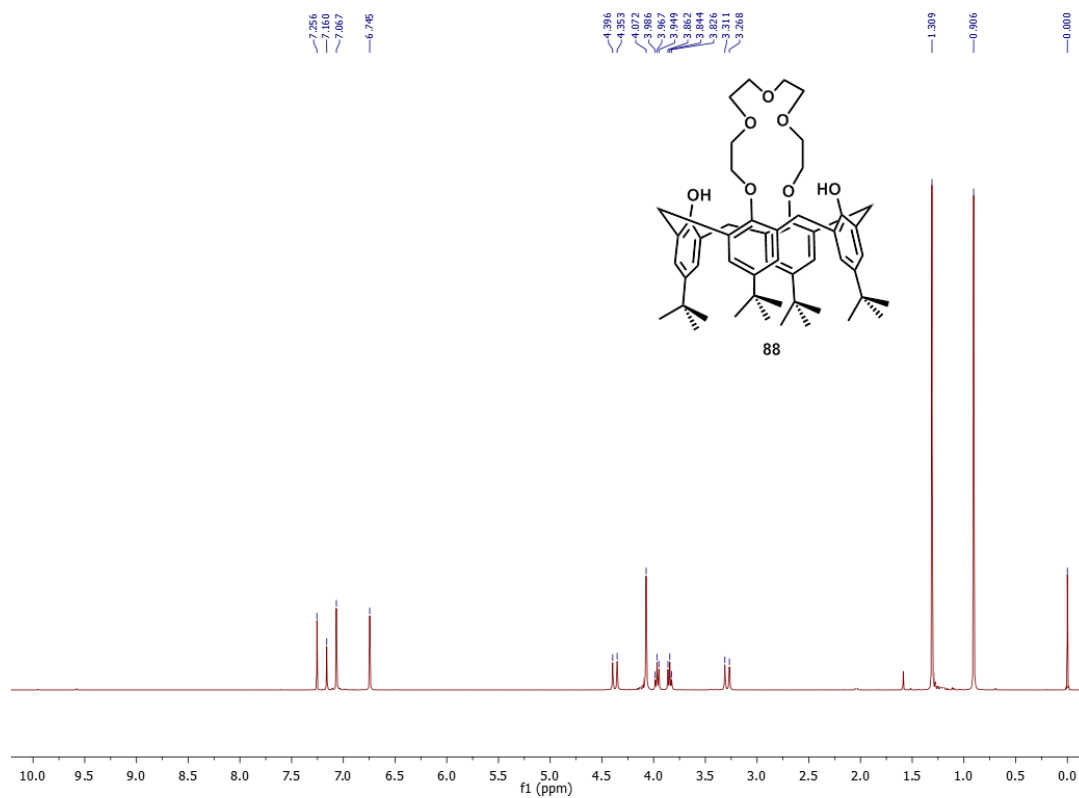
Figure 3.46 *Left*: Fluorescence spectra of **99** upon addition of Ag⁺ (0.71-27 eq) in acetonitrile/ chloroform (v/v= 9:1) solutions. $\lambda_{ex} = 330$ nm. *Middle*: Benesi-Hildebrand plot of $1/(F_0-F)$ versus $1/[Ag(ClO_4)]$ for **99** upon titration with Ag(ClO₄). The linear fit showed a 1:1 complexation between **99** and Ag⁺ ions. *Right*: Screen-capture output showing 1:1 binding model for **99** with Ag⁺, using Thordarson's method.

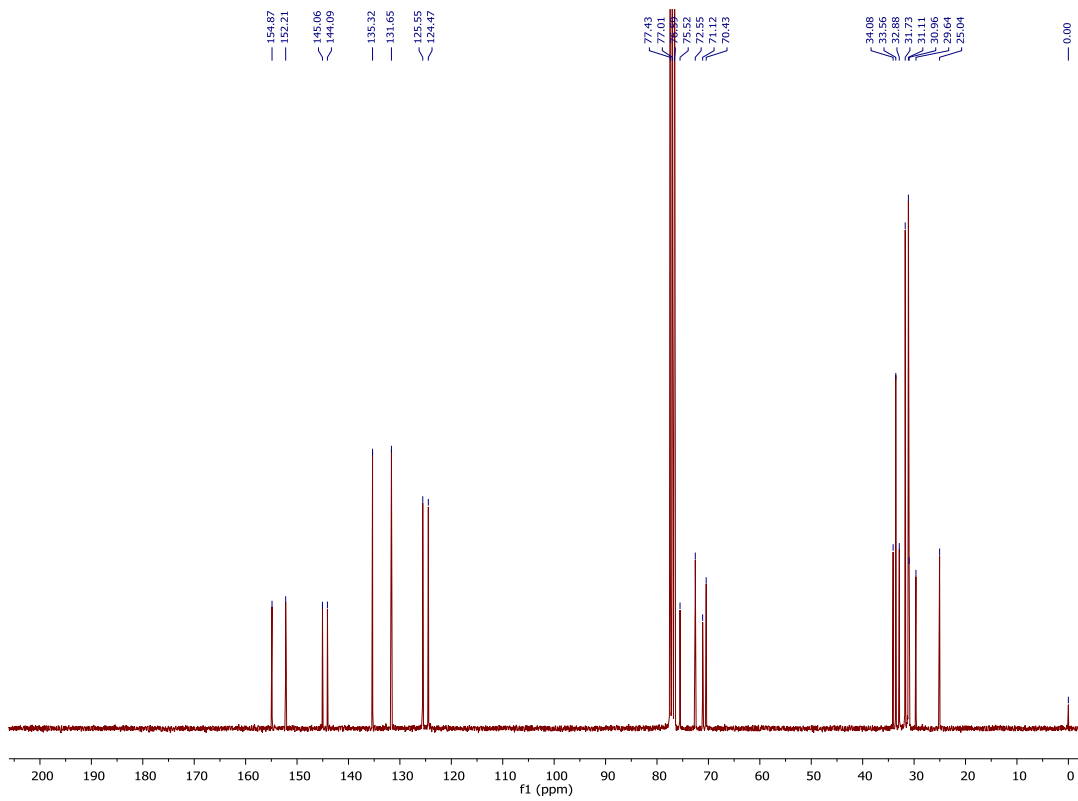
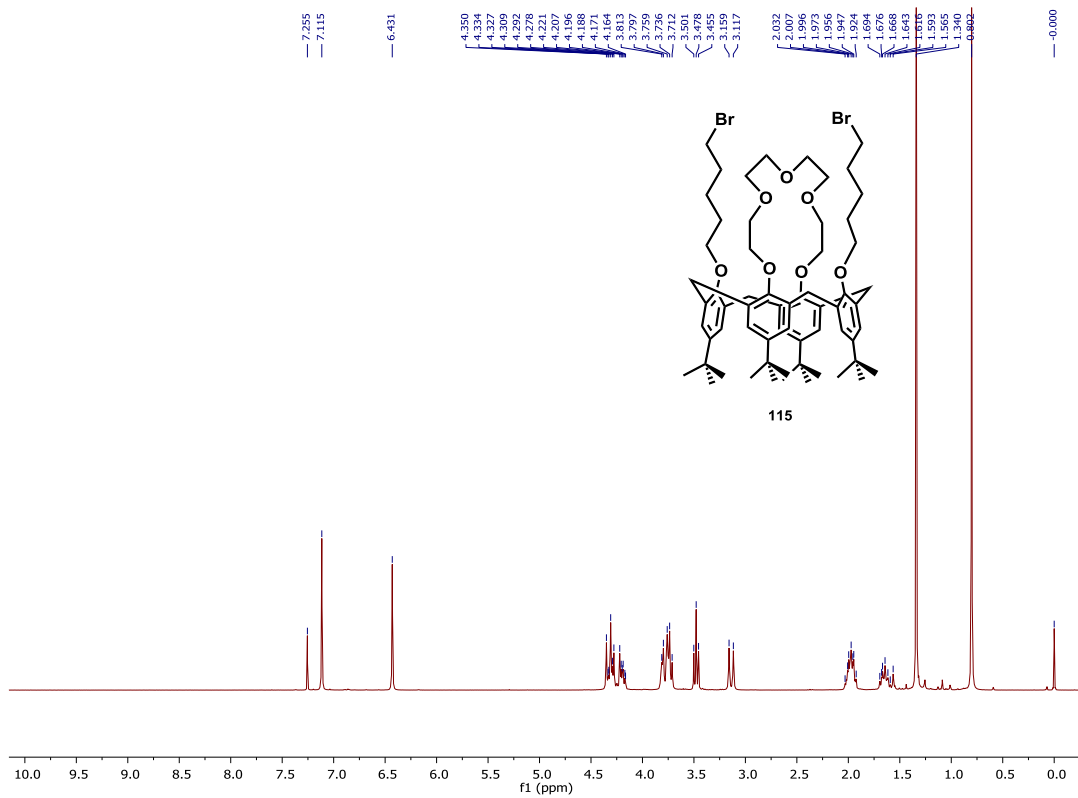
Appendix C

^1H - and ^{13}C -NMR spectra for compounds described in

Chapter 4







Appendix D

^1H - and ^{13}C -NMR spectra for compounds described in

Chapter 5

